University of Bath

UNIVERSITY OF BATH

PHD

Investigations into the well-controlled stereoselective ring-opening polymerisation of lactide

Frankis, Catherine

Award date:
2010

Awarding institution:
University of Bath

[Link to publication](#)

Investigations into the well-controlled stereoselective ring-opening polymerisation of lactide

Catherine J. Frankis

A thesis submitted for the degree of Doctor of Philosophy

Department of Chemistry

University of Bath

August 2010

This thesis is dedicated to my father, Eric,

and,

in memory of Mum.

Contents

Acknowledgements

Firstly, I would like to thank my supervisor Professor Matthew Davidson for giving me the opportunity to work on this project, and for his support, guidance and enthusiasm throughout the course of my PhD.

The University of Bath and the EPSRC are also gratefully acknowledged for their financial help.

Drs Mary Mahon and Gabriele Kociok-Kohn are thanked for their assistance with X-ray crystal structure determination, Dr John Lowe for his help with NMR spectroscopic experiments, and Dr Anneke Luben for her assistance with mass spectrometry. I would also like to thank Dr Matthew Jones for his long-standing patience, advice and friendship.

I also wish to thank all members of the Davidson and Jones research groups, past and present, for their friendship and high quality banter, with special mention to Dr Daniel Garcia, Kirsty Barber, Carlo Di Iulio and Emma Whitelaw. Many thanks also to my former MChem students, Gail Bance, Ant Thompson and Aled Lloyd, all of whom have contributed to the work described within this thesis.

And finally, thank you Malloy, for everything.

Abstract

Polylactide (PLA) is a biodegradable and biocompatible alternative to traditional petrochemical-based polymers. Synthesised by the ring-opening polymerisation of lactide (LA), the dehydrated form of lactic acid, PLA sits within a renewable cycle, and can be used in many commodity and biomedical applications. The intrinsic stereochemistry of LA can lead to a variety of polymer microstructures, and current industrially used initiators allow no control over this. Within this thesis a series of investigations into the use of amine tris(phenolate) metal complexes as stereoselective initiators for the ROP of LA are discussed.

Chapter 1 introduces the field of ring-opening polymerisation (ROP) via a coordination insertion mechanism, presents previously reported initiators, and examines the influence of stereocomplexation on the physical properties of PLA chains. This introductory chapter also includes an in-depth review of recent developments in poly(phenolate) complexes of Group 4 and rare earth metals.

Chapter 2 describes the synthesis of a series of isopropoxide and zwitterionic Group 4 complexes featuring the amine tris(phenolate) ligand motif, with emphasis on the effect of ligand variation on complex structure. The potential of the resulting complexes as initiators for the ROP of LA is also investigated, with in depth kinetic studies allowing for a proposed diastereoselective mechanism of stereocontrol.

Chapter 3 details the synthesis of a series of borohydride and amide Group 4 amine tris(phenolate) complexes, and investigates their potential as initiators for the ROP of *rac*-LA. Chain-end analysis and kinetic studies are included, providing the basis for mechanistic discussions.

Chapter 4 focuses on the synthesis of stereoblock PLA materials in a stereospecific manner, and co-block PLA-PEG materials by the reinitiation of short-chain macroinitiators. The effect of stereocomplexation on the thermal properties of these materials is investigated.

Chapter 5 concerns the synthesis of a series of isopropanol and zwitterionic rare earth complexes featuring the amine tris(phenolate) ligand motif. The potential of these complexes as initiators for the ROP of *rac*-LA is also investigated, but only slight stereocontrol was observed in selected cases.

Chapter 6 provides details of procedures employed in the synthesis of ligands, complexes and polymers within this thesis, as well as details of the analytical techniques used in their characterisation.

Chapter 1

Introduction

1.   Introduction

1.1.   Part One: Sustainable Plastics

Over recent years, a vast amount of interest has been generated by industry, governments and public opinion into the development of biodegradable polymers as a replacement for traditional petrochemical-based polymers, which have become unpopular over the last few decades due to their sourcing from non-renewable oil supplies and polluting effects on the environment as waste products[1-2].   Of the variety of biodegradable polymers known, aliphatic polyesters, especially those synthesised from naturally occurring lactic and glycolic acid, are the most commonly researched due to their good mechanical properties, hydrolyzability and biocompatibility.   Such properties lend these materials to biomedical and pharmaceutical applications as well as commodity uses, as they show resilience and strength on a short time-scale but break down into the simple non-toxic constituents carbon dioxide and water on a relatively long time-scale.[2] Variation of the stereochemistry and chemical composition of the polymer is used to tailor the resulting physical properties and decomposition profile of the polymer to the specific needs of each application.   For example, the use of the copolymer poly(glycolic-co-lactic acid) (PGLA) is popular for use as biomedical sutures and bone stints, and in the second case, where a higher degree of rigidity and longer life-time is required, the material will require a higher percentage of poly(lactic acid) (PLA).[3]   The demand for tailor-made polymers for such advanced applications requires a well-controlled reproducible method of synthesis.   Polycondensation of lactic and glycolic acid monomers forms an equilibrium, limiting the molecular weight of the resulting polymer.   Instead, the monomers are dehydrated to form the cyclic dimers lactide and glycolide, which in the presence of an initiator will ring-open to form linear aliphatic polyesters.
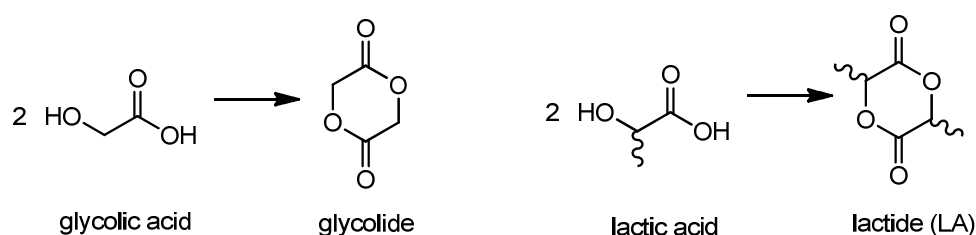
Figure 1.1: Dehydrated forms of glycolic and lactic acid.

Importantly, the production and disposal of PLA sits within a renewable cycle.[4]   Feedstocks such as corn starch and sugar beet are fermented and the resulting glucose is treated enzymatically to produce lactic acid.   Subsequent dehydration and ring-opening polymerisation then produces the commodity polymer.   Alternatively, the cyclic lactone may be indirectly produced by degradation of a pre-polymer resulting from the polycondensation of lactic acid.   After commercial use, the intrinsic sensitivity of the aliphatic backbone of PLA to hydrolytic attack allows the polymer to be broken down into oligomers of lactic acid, which can be used as compost in the growth of

further feedstocks. Alternatively, these oligomers can be broken down enzymatically to carbon dioxide and water, as would occur in vivo. The biggest worldwide producer of PLA is the Cargill subsidiary NatureWorks LLC, which was the first company to offer polymers derived from 100 % annually renewable resources. Opened in 2002, NatureWorks' main production facility at Blair, Nebraska in the USA now produces 140,000 metric tonnes of PLA every year.[5] The bio-derived plastics market as a whole is set to increase drastically over the next few years, due to environmental concern and the high price of oil, and as is the case in much industry, production looks set to move from the developed countries of the west to the developing countries of the east. A new lactide plant has recently been commissioned in Thailand with a capacity of 75,000 metric tonnes, to help meet the increasing demand for the monomer.[6]

1.1.1. Ring-Opening Polymerisation of lactide

1.1.1.1. *Coordination-insertion mechanism*

Although PLA can be obtained by direct polycondensation of lactic acid, ring-opening polymerisation (ROP) of the dehydrated cyclic dimer lactide (LA) allows for much higher control of the polymerisation and remains the more popular method. The process requires an appropriate initiator and metal-based systems have been the focus of considerable attention for many years, which have been shown to facilitate the three-step coordination insertion mechanism shown in Scheme 1.1.[7-8] Initially, coordination of the LA monomer to the Lewis-acidic metal centre brings the ketonic carbon into close proximity with the nucleophilic initiating group, allowing the insertion of the LA unit into the M-X bond via nucleophilic addition. Finally, ring-opening of the LA occurs via cleavage of the acyl-oxygen bond, and propagation of the polymer chain can occur by coordination of further LA monomers to the **LM** group situated at the growing end of the chain. The process is considered to be of a well-controlled nature as the degree of polymerisation is dependent on the monomer to initiator ratio, and although the process will cease when the favoured equilibrium between monomer and polymer has been reached (conversion dependent on temperature), further addition of monomer will restart the polymerisation process. Termination only occurs on hydrolysis of the M-O bond by the addition of H_2O or MeOH, which leads to the formation of a hydroxyl ω-chain end group. The end-group present at the α-chain end will depend on the choice of initiating group used.
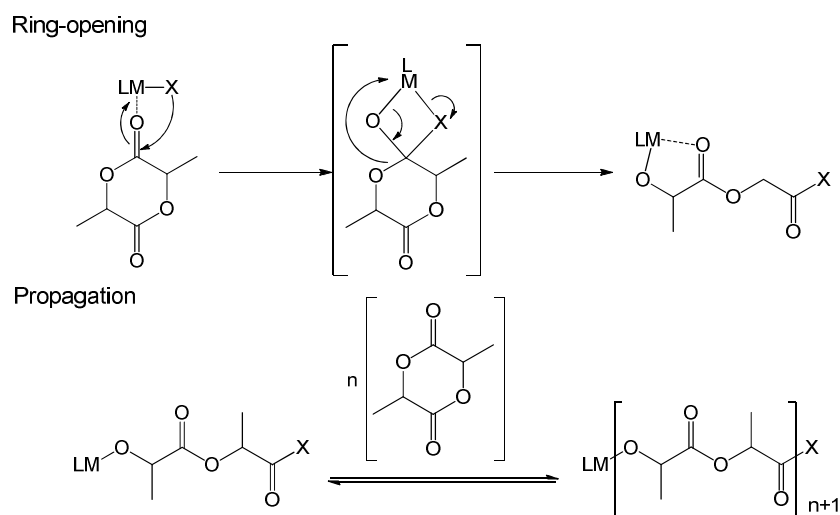
Scheme 1.1: Coordination insertion mechanism: ring-opening and propagation steps.[9]

The molecular weight control exhibited by a metal-initiated coordination insertion mechanism depends on the ratio $k_{propagation}/k_{initiation}$ (k_{prop}/k_{init}), which can vary significantly between metals, to be discussed in due course, and also between initiating groups. The effect of initiating group was investigated by Chisholm and co-workers within the series of compounds Ph_3SnX, and the rate of LA ring-opening was reported to follow the order $X = NMe_2 > OMe > O^iPr > O^tBu > OPh$.[10] If $k_{init} \gg k_{prop}$, polymer chain growth can occur simultaneously, resulting a narrow molecular weight distribution. In this case, molecular weights of resulting polymers should be close to theoretical values, calculated from the monomer to initiator ratio. Gel Permeation Chromaography (GPC) is a useful tool in determining the molecular weights of polymers, and also the polydispersity index (PDI), a measure of molecular weight distribution calculated from the ratio M_w/M_n. If a polymer has a low PDI (1.0 – 1.2), the polymerisation can be considered as well-controlled. On the other hand, if $k_{init} < k_{prop}$, polymer chains will grow over various timespans, albeit at the same rate, resulting in a broad molecular weight distribution. GPC analysis often shows these polymers to have molecular weights far higher than expected and high PDI values (> 1.5).

1.1.1.2.   Transesterification

The molecular weight control of the coordination-insertion mechanism also depends on the extent of transesterification side reations, which can occur both intermolecularly, resulting in chain redistributions, and intramolecularly, or 'back-biting', resulting in macrocycles (Figure 1.2).[2] Both will result in the broadening of the molecular weight distribution, and a higher value of PDI obtained from GPC analysis. The extent of transesterification is highly dependent on reaction conditions, tending to be more prolific at long reaction times or and at higher temperatures, but has also been found to depend strongly on the nature of the metal initiator and the following order has been observed in the case of alkoxide initiators: $Bu_2Sn(OR)_2 > Bu_3SnOR > Ti(OR)_4 >$

4

$Zn(OR)_2 > Al(OR)_3$.[1] The flexibility of the polymer chain has also been shown to effect the degree of transesterification, with a higher degree of side reactions seen in atactic PLA synthesised from *rac*-LA, which lacks the crystalline characteristics of isotactic PLA synthesised from enantiopure L- or D-LA.[11]
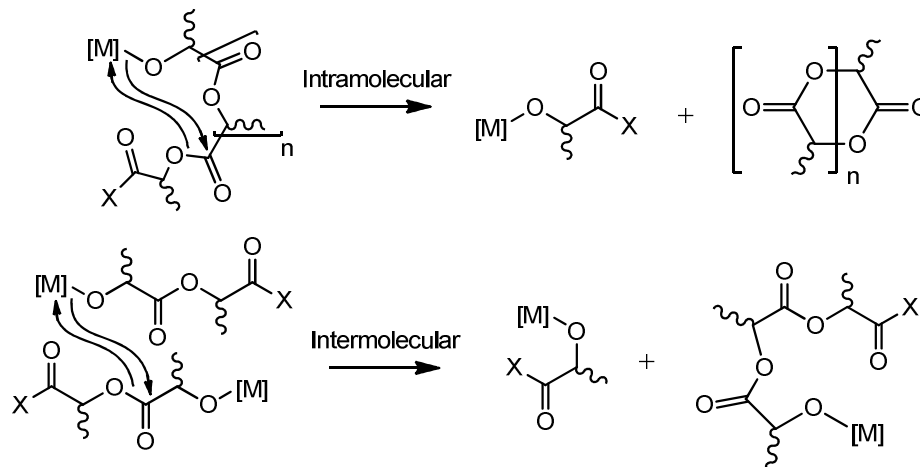
Figure 1.2: Intramolecular and intermolecular transesterification.

The occurrence of transesterification can be determined by Matrix Assisted Laser Desorption Time of Flight (MALDI-ToF) mass spectrometry analysis of the low molecular weight polymers. In the absence of transesterification, only one population will be observed in the mass spectrum, in which individual polymer species are separated by 144 mass units, the molecular weight of one LA monomer. The nucleophilic attack responsible for transesterification can occur at any ketonic carbon along the polymer chain, and as such a second population, in which individual polymer species are separated by 72 mass units, will also be observed.
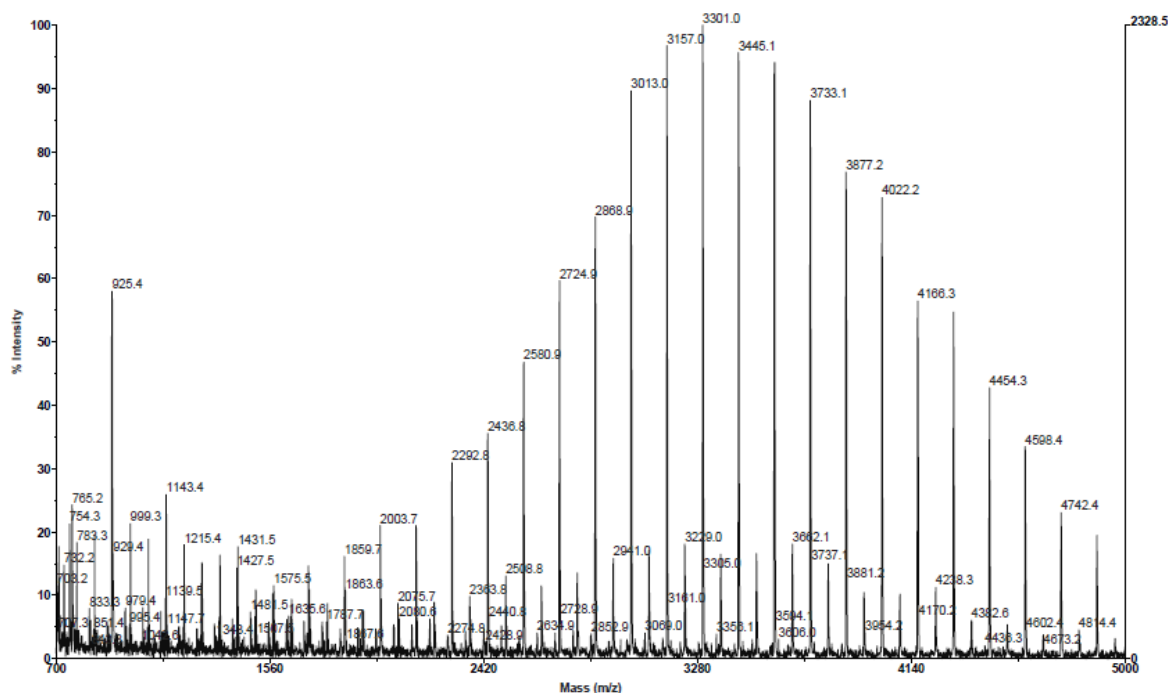
Figure 1.3: MALDI-ToF mass spectrum of PLA sample.

5

1.1.1.3. Stereochemical considerations

The two enantiomeric forms of the monomer, L-LA (*S,S*) and D-LA (*R,R*), lead to a variety of possible polymer microstructures, which can have an effect on the mechanical properties of the polymer.[12] Polymerisation of either enantiomer in its optically pure form will lead to isotactic PLA, where all stereocentres are identical, but the polymer microstructure arising from the polymerisation of a racemic mixture of the two (known as *rac*-LA) will depend on the stereoselectivity of the initiator used. A non-stereoselective catalyst, such as commercially popular tin(II) octanoate will produce atactic PLA, where there is no preference for the addition of either monomer, and so a random chain of L- and D- units is formed. This chain is not however random with respect to the individual stereocentres, as every two adjacent centres must be identical (e.g. *–RRSS-*) due to the internal stereochemical symmetry of the monomer. A stereoselective catalyst will either preferentially polymerise one of the monomers throughout the polymerisation, resulting in isotactically enriched or stereoblock PLA, or alternate preference between the monomers after each addition, forming heterotactically enriched PLA of the type [(*RR*)(*SS*)(*RR*)(*SS*)]$_n$.[13]
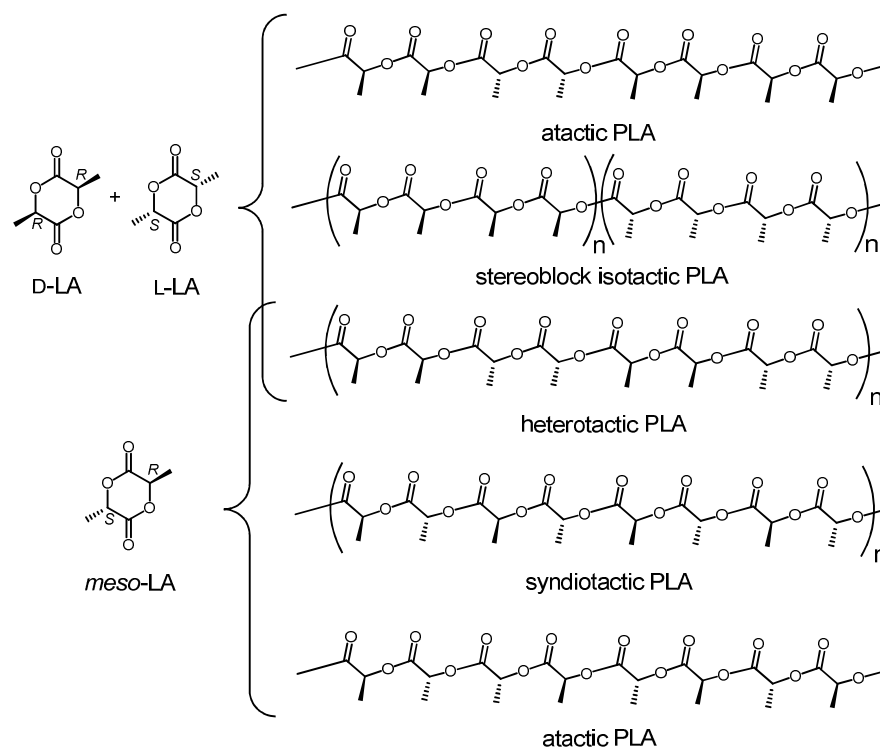
Figure 1.4: Possible microstructures of PLA from the polymerisation of *rac*- and *meso*-LA.

The polymerisation of *meso*-LA by a non-stereoselective initiator will again result in atactic PLA, although in this case the intrinsic stereochemical difference in the structure of the monomer means a series of three or more stereocentres can have alternate stereochemistries (e.g. *–RSR-*). If a stereoselective catalyst is employed, polymerisation can either result in heterotactically enriched

PLA if there is a selectivity for addition of a stereocentre identical to the chain end, or syndiotactic enriched PLA if the opposite case is preferred.[14]

Analysis of polymer microstructure by homonuclear ^{1}H NMR spectroscopy. The exact nature of the polymer microstructure present in a material can be determined by analysis of the ^{13}C{^{1}H} or ^{1}H homonuclear decoupled NMR spectra,[15-17] although the latter usually gives a superior signal-to-noise ratio. Here, each stereocentre along the length of the polymer chain is influenced by the nature of the stereochemical tetrad in which it resides. Given that adjacent centres with opposite stereochemistry are assigned the label *s* (syndio), while those with the same stereochemistry are labelled *i* (iso), each observed tetrad can be assigned. Isotactic PLA, synthesised from either pure D- or L-LA will always only contain the *iii* tetrad. Stereoblock PLA, synthesised using an isotactically selective initiator in the polymerisation of *rac*-LA, contains alternate blocks of PLLA and PDLA. The *iii* tetrad is therefore the most prominent however a small number of *isi*, *iis* and *sii* tetrads will be observed at the points where the blocks join. The prominence of peaks relating to the *isi*, *iis* and *sii* tetrads in the ^{1}H homonuclear decoupled spectrum depends on the frequency and length and the stereoblocks.
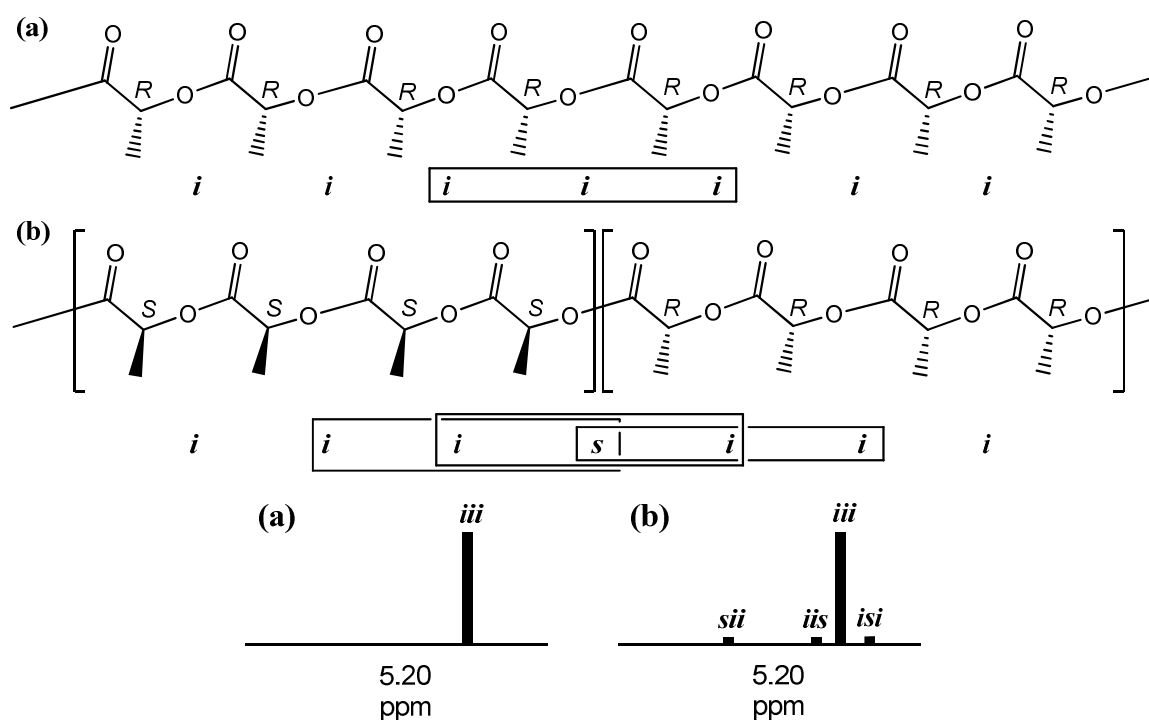
Figure 1.5: Schematic microstructures and ^{1}H stereosequence assignments for isotactic (a) and stereoblock (b) PLA synthesised from *rac*-LA.

The alternate nature of the monomers in heterotactic PLA synthesised from *rac*-LA mean only *isi* and *sis* tetrads are observed, and accordingly only two signals are present in the homonuclear decoupled spectrum. The random monomer addition in atactic PLA synthesised from *rac*-LA

7

allows all possible tetrads *isi*, *sis*, *iii*, *iis* and *sii* (Figure 1.6), observed as five separate peaks in the ratio 1:1:1:3:2. These relative intensities are dictated by Bernoullian statistics, and illustrate that whilst monomer addition in atactic polymerisation is random, the resulting microstructure does have a bias towards isotactic character. Due to the stereochemical symmetry of its components, the tetrads *sss*, *ssi* and *iss* are not found in any polymer synthesised from *rac*-LA, in the absence of transesterification reactions.
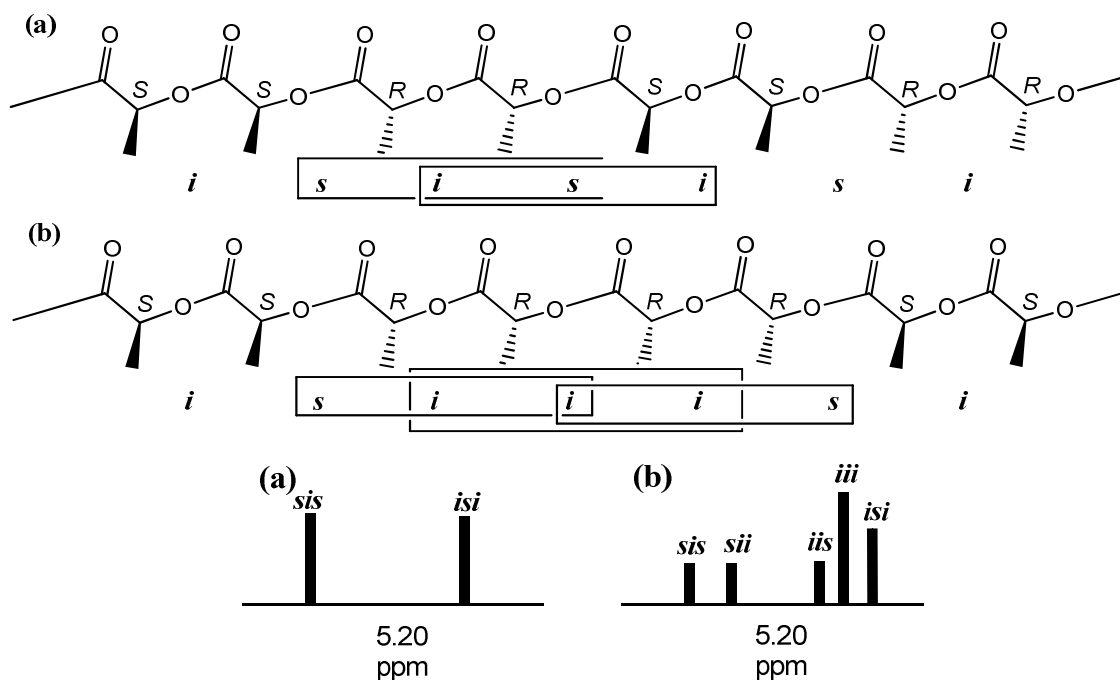
Figure 1.6: Schematic microstructures and ^{1}H stereosequence assignments for heterotactic (a) and atactic (b) PLA synthesised from *rac*-LA.

ROP of *meso*-LA will lead to a slightly different set of stereochemical tetrads along the polymer chain, due to the inherent unsymmetrical nature of the monomer. The polymer chain resulting from the random addition of monomers, although still considered atactic, consists of the five tetrads *sis*, *ssi*, *iss*, *sss* and *isi*. However, due to overlapping chemical shifts and the degeneracy of the *iss* and *ssi* tetrads, often only two signals are observed in the ^{1}H homonuclear decoupled spectrum, the prominent *sss* signal hiding all but the *sis* signal. The employment of stereoselective initiators will either result in syndiotactic PLA, exhibiting only an *sss* tetrad, or heterotactic PLA, exhibiting the same tetrads to that synthesised from *rac*-LA, *isi* and *sis*. The theoretical ^{1}H homonuclear decoupled spectra of heterotactic PLA should be identical, irrespective of the synthetic route, but it is worth noting that in practice, additional peaks arising from stereoirregularities in the chain will be different in nature depending on whether *rac*- or *meso*-LA was used.
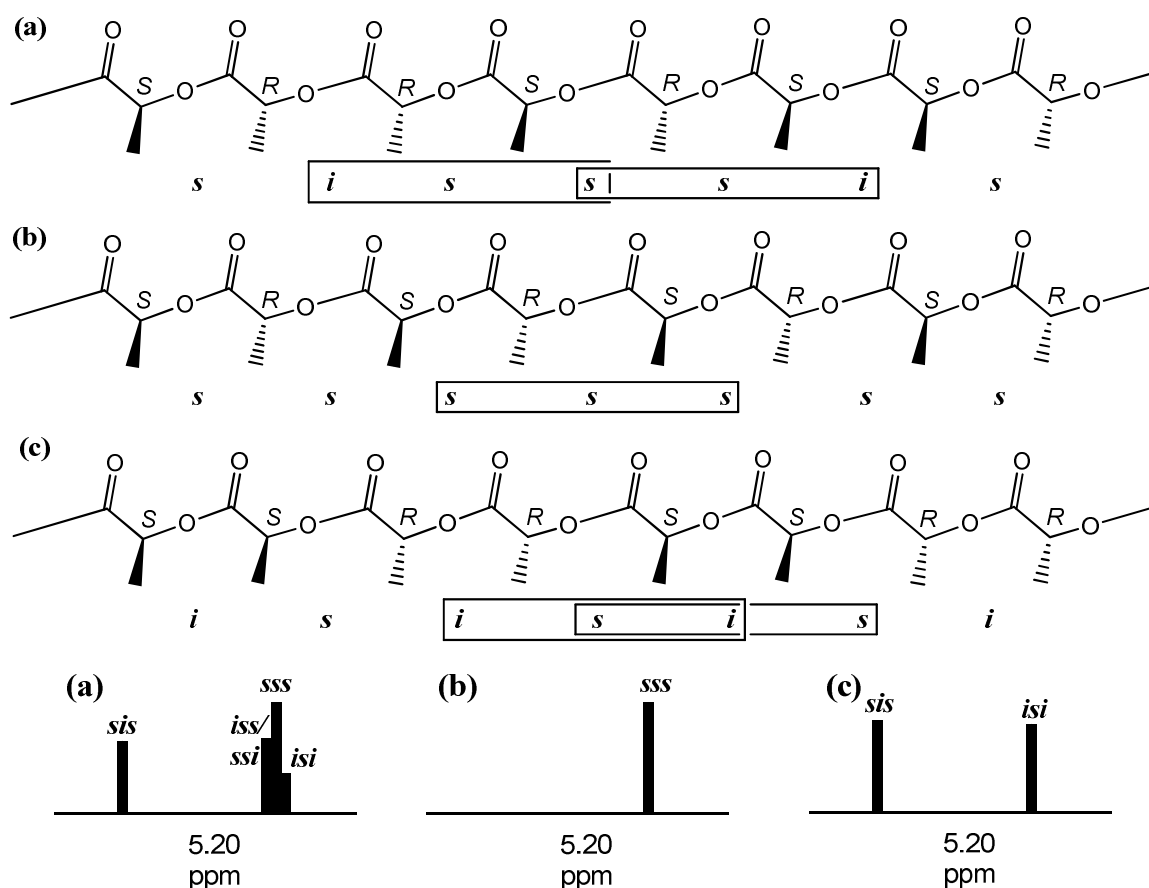
Figure 1.7: Schematic microstructures and ^{1}H stereosequence assignments for atactic (a), syndiotactic (b) and heterotactic (c) PLA synthesised from *meso*-LA.

Quantifying polymer microstructure. As mentioned above, in practice, the ROP of *rac*- or *meso*-LA using a stereoselective initiator will not result in 100% heterotactic or syndiotactic PLA, but will instead produce an enrichment of that character within the polymer chain. In order to quantify this, the probabilities of syndio linkages (P_s) and iso linkages (P_i) between any two monomers in a chain can be calculated from the relative intensity of the *sis* signal in the ^{1}H homonuclear decoupled spectrum. In the case of *rac*-LA, according to Bernoullian statistics, P_s is related to the relative intensity of the *sis* peak via:[13]

$$P_s^2/2 = [sis] \qquad [1]$$

In this case, if $P_s > 0.5$, the polymer can be considered heterotactically enriched, and if $P_s > 0.75$, it can be considered strongly heterotactic. Conversely, if $P_s < 0.5$, the polymer can be considered isotactically enhanced. If this is the case, a value of P_i is more commonly quoted, easily obtained by the following relationship, which holds if Bernoullian statistics are assumed:[18]

$$P_s + P_i = 1 \qquad [2]$$

tetrad	Probability	
	rac-LA	*meso*-LA
[*iii*]	$P_i^2 + P_sP_i/2$	0
[*iis*]	$P_sP_i/2$	0
[*sii*]	$P_sP_i/2$	0
[*sis*]	$P_s^2/2$	$(P_i^2 + P_sP_i)/2$
[*sss*]	0	$P_s^2 + P_sP_i/2$
[*ssi*]	0	$P_sP_i/2$
[*iss*]	0	$P_sP_i/2$
[*isi*]	$(P_s^2 + P_sP_i)/2$	$P_i^2/2$

Table 1.1: Tetrad probabilities based on Bernoullian statistics.

In the case of *meso*-lactide, all but one tetrad (*sis*) overlay in the ^{1}H NMR homodecoupled spectrum. Therefore, assuming Bernoulian statistics, a value of P_i can be obtained from the relative intensity of [*sis*], as follows:

$$[sis] = (P_i^2 + P_sP_i)/2 \qquad [3]$$

Substituting in [2], and rearranging, gives:

$$[sis] = P_i/2 \qquad [4]$$

P_s can then be simply determined using [2]. In the case of *meso*-LA, if $P_s > 0.5$, the polymer can be considered syndiotactically enriched, but if $P_s < 0.5$, it can be considered heterotactically enriched.

1.1.2.   Initiators for the ring-opening polymerisation of lactide

1.1.2.1.   *Non-stereoselective initiators*

For many years, the most widely used catalytic system for the preparation of PLA has undoubtedly been tin(II) bis(2-ethylhexanoate), also known as tin(II) octanoate (SnOct$_2$) (Figure 1.8), due to its commercial availablity, ease of handling and high activity in the solution or bulk ROP of LA. There have been numerous investigations into the mechanism of ring-opening undertaken by SnOct$_2$, and the increase in molecular weight control and activity exhibited by the system on the addition of a protic reagent (e.g. alcohol), indicates that a co-initiator is required. On addition of alcohol, two possible reaction pathways have been proposed depending on reaction conditions, both of which are based on the coordination-insertion mechanism of ring-opening polymerisation.[1] In the first, the alcohol reacts with SnOct$_2$ to form a tin alkoxide complex, which initiates ROP and results in the liberation of octanoic acid.[19] In the activated monomer mechanism, the monomer instead coordinates to SnOct$_2$ and is then activated by the alcohol, so no liberation of octanoic acid is observed.[20] The addition of excess alcohol to a polymerisation will promote chain transfer reactions, limiting the molecular weight and increasing the PDI of the resulting polymer, and so optimisation of the correct ROH/SnOct$_2$ ratio

is critical. In the absence of protic additives, it is thought impurities in the monomer, such as lactic acid or water, would also act as co-initiators.[21]
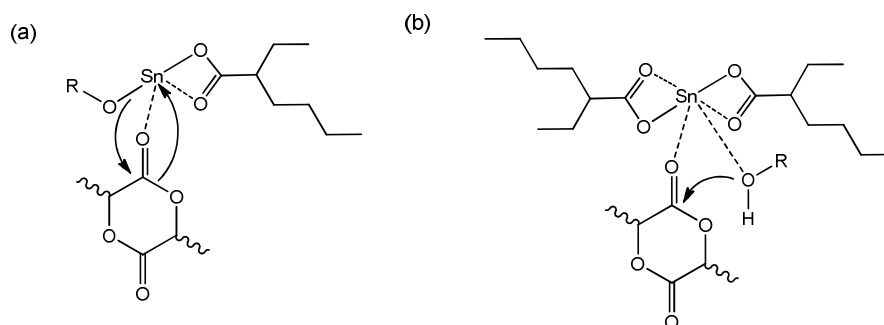
Figure 1.8: SnOct₂ initiated ROP via (a) tin alkoxide complex and (b) activated monomer mechanism.

Although SnOct$_2$ has been approved as a food additive in numerous countries, the toxicity associated with many tin compounds means PLA produced in this way is not suitable for biomedial applications.[22] Crucially, SnOct$_2$ also displays no stereoselectivity in the polymerisation of *rac*-LA. With these considerations in mind, research into complexes of various different metals as possible initiating systems has been undertaken. Primarily, alumiunium and zinc alkoxides were investigated but, despite providing superior control of molecular weight, were found to be far less active than the tin system, and so subsequent research interests appear to have diversified into Group 2 metals and Group 4 transition metals, the majority of which have the advantage of being non-toxic and present in the human metabolism. In recent years, a series of lanthanide complexes have also been considered with regard to their ROP catalytic ability, as will be discussed in due course. In all but a handful of cases,[23] it has been noted that structurally simple ligands allow no control over polymer microstructure, which in turn limits control over physical, mechanical and degradation properties of the resulting PLA.

1.1.2.2. Stereoselective initiators

Since the turn of the century, there has been a distinct move towards structurally more diverse ligand systems in initiator design in an attempt to gain increased stereocontrol over the polymer produced. The nature of the ligand system will often determine the mechanism of stereocontrol employed by the initiator. If a chiral ligand is involved, the stereochemistry at the metal centre is responsible for the monomer preference in chain formation via an enantiomorphic site control mechanism. On the other hand, an initiator based on an achiral ligand system can also influence microstructure via a chain-end control mechanism.[24] A wealth of different metals have been tested for their reactivity and control, resulting in a wide range of reported complexes that show promise, the most prominent of which will be discussed herein.

Early Zn, Mg and Ca initiators. The first significant results to be published in this area arose from the pioneering work of Coates and co-workers in the development of β-diiminate (BDI) coordinated Zn and Mg systems.[13] In dichloromethane solution, complex **1** was found to give 90% heterotactically enriched polymer from *rac*-LA and high conversions after 20 minutes. The Mg analogue of this system was found to be more reactive (complete conversion in only 2 minutes), attributed to the increased polarisation of the M-OR bond, but at the expense of molecular weight and stereocontrol. Chisholm et al went on to isolate the monomeric THF adduct of the system, **2**, and reported an interesting solvent dependence with respect to stereocontrol, whereby heterotactically enriched PLA was obtained when the polymerisation was carried out in THF.[25] Chisholm also reported that the Ca analogue of this complex, although highly active, produced atactic polymer exclusively.[26] It was believed that the larger Ca metal required greater steric protection to influence stereocontrol, and so a move towards the bulkier tris(pyrazolyl)borate ligands was undertaken. At the time of publishing, complex **3** was one of the most reactive and stereoselective initiators reported, undergoing 90% monomer conversion in under 1 minute at room temperature and affording > 90% heterotactic PLA.[27] The achiral nature of these systems indicate a chain end control mechanism is responsible for the stereocontrol exhibited in the aforementioned cases.
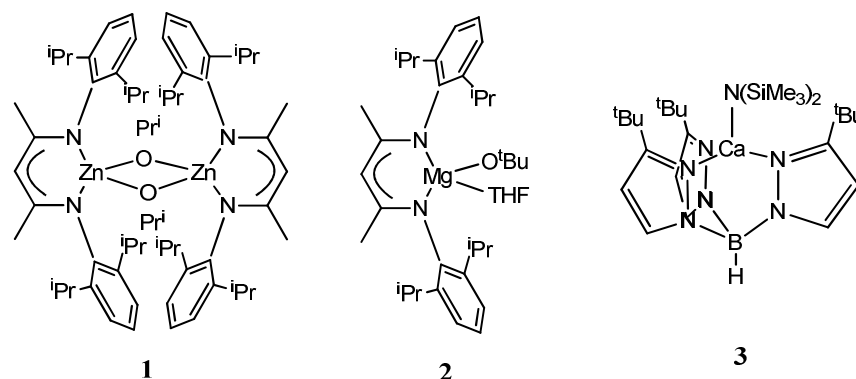
Figure 1.9: Early Zn, Mg and Ca initiators.

Salen- and salan-based Al initiators. The original Al salen complex **4** and the binaphthalene-substituted enantiopure derivative (-)-**5** were reported in the late 1990s by Spassky and co-workers, who found both complexes polymerised *rac*-LA with an isotactic bias to afford a tapered stereo co-block polymer.[28-29] Shortly afterwards, Coates and co-workers reported the synthesis of syndiotactic PLA from *meso*-LA using (-)-**5**, and isotactic stereoblock PLA of the type [(*RR*)$_n$(*SS*)$_m$] was afforded from *rac*-LA using (±)-**5**.[14, 30] In the latter case, each enantiomer of the initiator preferentially consumes either D-LA or L-LA until exchange of the propagating chains occurs between Al centres of opposing chirality. Feijen and co-workers reported in 2002 that complex **6** afforded isotactically enriched polymer from *rac*-LA, crucially under industry preferred solvent-free conditions,[31-32] and in the same year Nomura et al reported the same degree

of selectivity using the achiral complex **7**, the first example of such stereocontrol exhibited by a chain end control mechanism.[33-34]
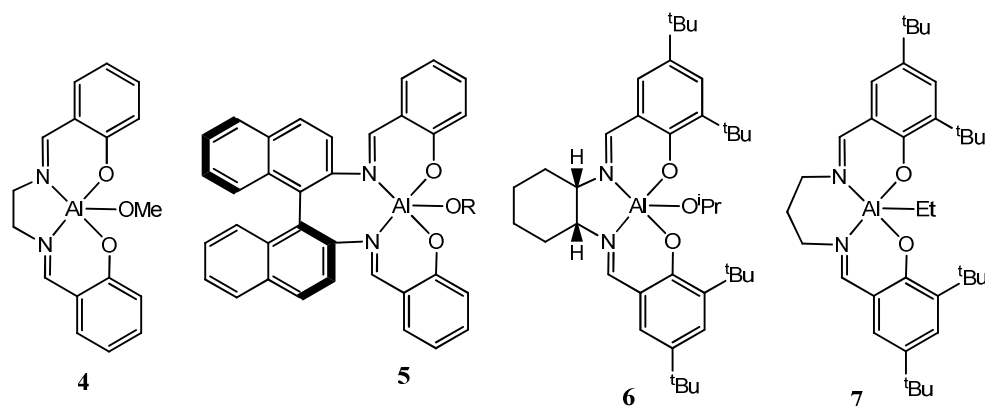
Figure 1.10: Salen-based Al initiators.

In 2004, Gibson and co-workers published a series of Al complexes containing the saturated salan ligands. Remarkedly, ROP of *rac*-LA by these complexes was found to result in either isotactically or heterotactically enriched polymer, depending only on the nature of the R groups (**8**: R = H, P_i = 79%; R = Cl, P_s = 96%).[35]
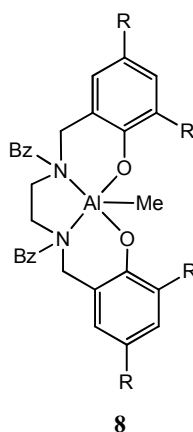
Figure 1.11: Al-salan initiator.

1.1.2.3.   Group 4 initiators

The similarity in electronic configuration between Sn and Ti, coupled with the biocompatibility of the latter, makes the Group 4 metals an ideal choice of research avenue. At the beginning of the last decade, reports were made of a series of Ti complexes featuring chalogen-bridged bis(phenolate) ligands as ROP initiators. Following initial reports by Takeuchi and co-workers that showed the isopropoxide analogues to undertake the ROP of ε-caprolactone,[36] Nakamura, Harada and co-workers investigated the use of complexes **9** and **10** as ROP initiators, the latter containing the sulphur-bridged ligand.[37] Analysis of the crystal structures of these analogous methylene and sulphur-bridged titanium complexes illustrated a clear change in the coordination environment at the titanium centre from tetrahedral to trigonal and previous reports had observed

13

a higher activity for **10** with respect to the polymerisation of olefins, attributed to the coordination of the sulphur atom to the metal.[38] In this report however, the methylene-bridged complex **9** was found to be the more active for the ROP of ε-caprolactone (91% in 8 hrs in toluene solution at 100 °C), but at the expense of molecular control, as the afforded polymer displayed a molecular weight twice the theoretical value and a relatively broad PDI of 1.60.[37] Although less active, **10** afforded polymer with molecular weights close to theoretical values and lower values of PDI, both in the case of ROP of ε-caprolactone (90% in 32 hrs) and that of L-LA (90% in 120 hrs), where the linear increase of molecular weight with polymer yield indicated a well-controlled polymerisation. Concurrent investigations showed that despite exhibiting moderate activities (high conversions only after 40 hrs), the dimeric chloro substituted complex **11** displayed good molecular control and a lack of transesterification reactions (PDI = 1.13).[39]
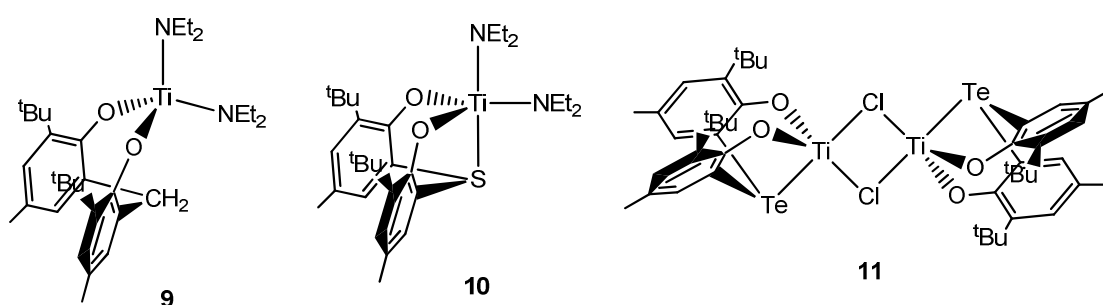
Figure 1.12: Ti initiators featuring methylene-, thio- and tellurium-bridged bis(phenolate) ligands.

Ligands of a similar scaffold, but including a third phenolate group attached in a linear fashion, were reacted with titanium isopropoxide by Hofmeister and co-workers, and resulted in the dimeric complexes **12a** and **12b**.[40] These complexes were found to be active for the ROP of LA and analysis of the resulting polymer showed low PDI's and isopropyl end groups, indicating that polymer chains grow from both Ti centres in a living manner. Significantly, the polymerisation of *rac*-LA afforded heterotactically enriched polymer (79% in dichloromethane at 80 °C), which at the time was the greatest degree of stereocontrol in the ROP of *rac*-LA reported for Ti initiators.[41] The kinetics of these polymerisations were investigated and although both proceeded at a similar rate (k_{app}: **12a** = 0.52 h^{-1}, **12b** = 0.53 h^{-1}), **12a** exhibited a 30 minute induction period, attributed to a steric hinderance to conformational change by the seemingly non-consequential bulky *para*-substituent.
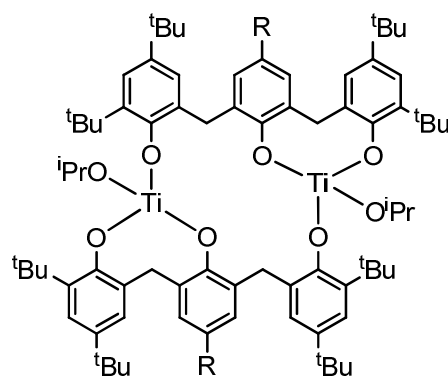
12a: R = ᵗBu
12b: R = Me

Figure 1.13: Ti intiators featuring tris(phenolate) ligands.

Ti complexes of the salen-type ligands were published in 2006 by Gibson et al and activity was found to be highly dependent on the nature of the phenol *para*-substituents.[42] Contrary to previous reports in the case of Al where halogen substituents were seen to improve activity,[43] in this case the inclusion of chloro and iodo substituents had a detrimental effect. Kinetic investigations were undertaken of the most active complexes and **13** was found to be more active (k_{app} = 6.17 x 10^{-5} s^{-1}) than the previously reported linear tris(phenolate) titanium complexes, **12a** and **12b**, described above. However, none of the salen-based Ti complexes exhibited any degree of stereocontrol.
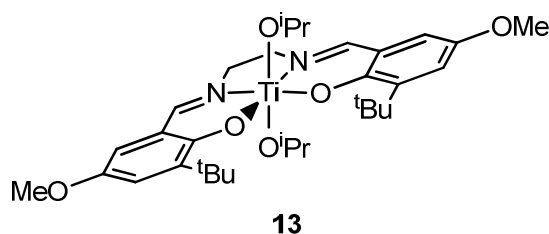
13

Figure 1.14: Ti-salen initiator.

Titanium and zirconium complexes of amine bis(phenolate) ligands were reported by Goldschmidt, Kol and co-workers from as early as 1999, many of which showed activity for the polymerisation of 1-hexene.[44-47] However, it was not until 2006 that their full potential as ROP initiators for LA was realised, following publications by the research groups of Kol and Davidson. The bis alkoxide Ti complex **14**, which includes a non-coordinating alkyl group as the third ligand arm, was shown to be active for the ROP of ε-caprolactone,[48] but a move to a coordinative ligand arm had a more profound effect on complex activity with respect to ROP of LA. Amongst others, the Zr complex **16** was examined and found to be 200 times more active than its Ti analogue **15**.[49] At the time, this was the first comparative study between analogous Ti and Zr complexes, and the remarkable difference between the activities was attributed to the sterically less crowded environment at the larger Zr metal centre. A further investigation

capitalised on the use of a pyridine group in the third ligand arm to obtain mono-substituted Group 4 complexes,[50] and the Zr complex **17a** was shown to be active for the ROP of *rac*-LA both in solution at 110 °C and under solvent-free conditions at 130 °C. **17a** also exhibited a moderate stereoselectivity in the ROP of *rac*-LA, resulting in isotactic enhancement of the resulting polymer chain ($P_s = 0.4$). The sterically unhindered complex of **17a** was also shown to be far more active than its tertiary butyl substituted analogue **17b**, and it was suggested that increased steric hindrance, disrupting the monomer path of approach, were responsible. Remarkably, **17a** facilitated the synthesis of a PCL-PLA co-block polymer by sequentially undertaking the ROP of ε-caprolactone followed by L-LA, however the co-block was not produced when the process was reversed.
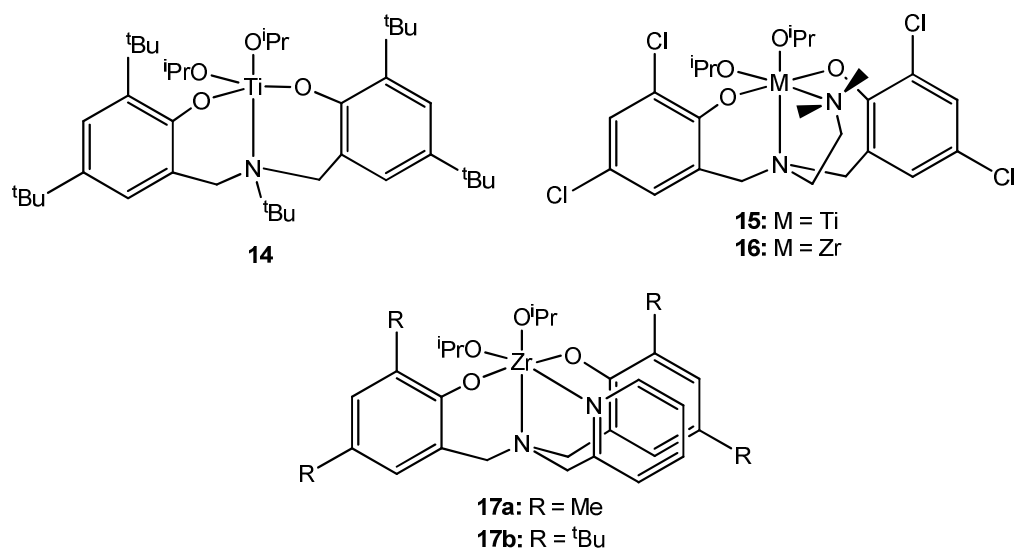
Figure 1.15: Ti and Zr initiators featuring amine bis(phenolate) ligands.

The reports published by the research groups of Kol and Davidson also investigated a series of Group 4 complexes containing the related *N,N'*-dimethyltetrahydrosalan ligands. These bind to Group 4 metals in a C_2- symmetric manner, as opposed to the C_s-symmetric coordination undertaken by the amine bis(phenolate) ligands. As with the bis(phenolate) complexes, Kol reported by far the highest activity for the ROP of L-LA with the Zr analogue of **18c**.[49] Studies by the Davidson group into the use of complexes **18a** and **18b** for the ROP of *rac*-LA in solvent-free conditions, showed less of a difference in activities between these and their Ti analogues, but more interestingly, an isotactic enhancement when **18a** was used ($P_s = 0.3$, solvent-free conditions; $P_s = 0.25$ in toluene).[50]
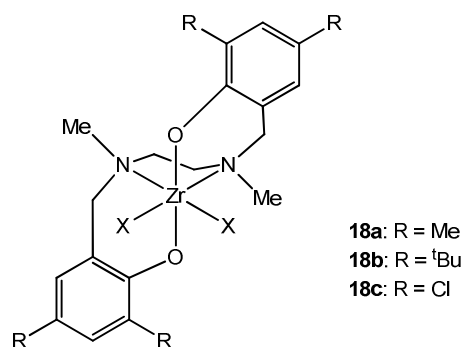
Figure 1.16: Zr initiators featuring *N,N'*-dimethyltetrahydrosalan ligands.

18a: R = Me
18b: R = ^tBu
18c: R = Cl

Meanwhile, the work of Verkade and co-workers has concentrated on the use of C_3-symmetric ligands in the synthesis of Group 4 complexes which exhibit activity for ROP.[51-54] A series of dimeric titanatranes of the type **19** were synthesised from the coordination of triethanolamine to Ti,[55] and the tetrameric complex **20** was synthesised from reaction with the tris(hydroxymethyl)ethane ligand.[56] Both were shown to be active for ROP of L- and *rac*-LA both in solution and bulk conditions, although longer polymerisation times often led to larger PDI's, indicating the occurrence of transesterification, and no stereocontrol was observed.
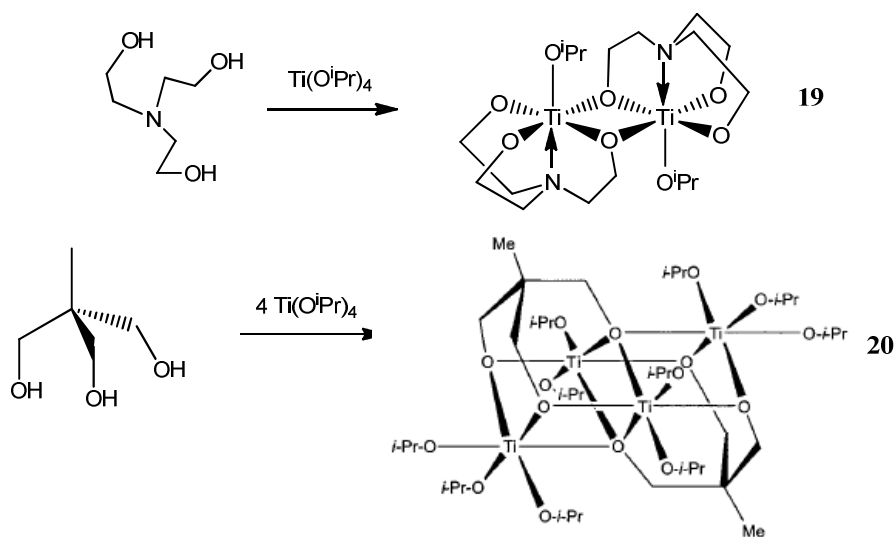
Figure 1.17: Ti initiators featuring C_3-symmetric ligands reported by Verkade and co-workers.

Coordination of the C_3-symmetric amine tris(phenolate) ligand to Ti was first reported by Kol et al in 2001[57], but it was Verkade who first realised the potential of these complexes as ROP initiators when in 2003 he reported the high activity of **21a** under solvent-free conditions.[53] However, no polymerisation was seen of either L- or *rac*-LA in solution and once again, no stereocontrol was observed. Kol et al returned to this class of compound in their 2006 publication, in which they reported the synthesis of **21b** as well as the Zr complex **22a**.[49] Within the study, it was reported that the Group 4 amine tris(phenolate) complexes were found to be the

17

most active of the three ligand systems investigated, and in keeping with the rest of the study, **22a** and **22b** were found to be more active than their Ti equivalents.
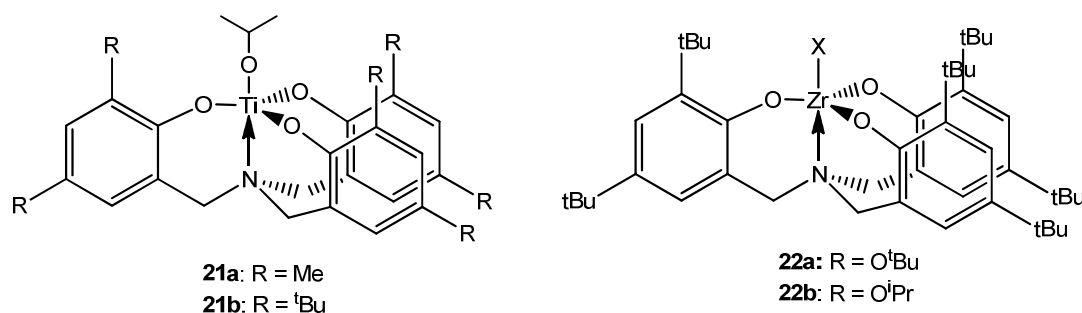
Figure 1.18: Ti and Zr initiators featuring amine tris(phenolate) ligands.

Soon after, Davidson and co-workers published the remarkable combination of stereo- and molecular weight control that is afforded by the Zr isopropoxide complex **22b** and its Hf analogue.[58] Using these initiators, high conversions were achieved in < 0.5 hrs in bulk conditions and in < 2 hrs in toluene solution at 100 °C. The resulting polymer molecular weights were close to theoretical values and the PDI's were low. These initiators also afforded highly heterotactically enriched PLA from the ROP of *rac*-LA (P_s = 0.96 for Zr; P_s = 0.88 for Hf), whilst the Ti analogue showed a lack in stereocontrol.

1.1.2.4. *Rare earth initiators*

Initial research into rare earth alkoxide complexes as potential initiators for ROP of cyclic esters began in the early 1990's when McLain et al first reported the catalytic activity of Y and La alkoxides.[59] The high reactivity of rare earth complexes have been shown to allow the initiation step in a polymerisation to occur rapidly, promoting well-controlled chain growth in a 'living' manner.

Rare earth initiators bearing simple monodentate ligands. Following pioneering work in this area by McLain et al, Stevels and co-workers reported the activity of commercially available yttrium oxo isopropoxide[60-61], shown previously to be the pentanuclear cluster $[Y_5(\mu\text{-}O)(O^iPr)_{13}]$ including both bridging and terminal isopropoxide groups (Figure 1.19).[62] Spassky et al continued this research by investigating the series of lanthanide oxo alkoxide clusters $[Ln_5(\mu\text{-}O)(O^iPr)_{13}]$ (Ln = La, Sm, and Yb), in which reactivity was seen to decrease across the series as the ionic radii of the lanthanides decrease (La > Sm > Yb).[63] Despite exhibiting the highest activity, the PDI of the polymer produced using the La catalyst was found to increase with conversion and the occurrence of transesterification reactions was observed even after a very short polymerisation time. The Sm and Yb clusters on the other hand, although less active, produced polymer with narrow PDIs until high conversions were reached. Analysis of the

polymers by ^{1}H NMR spectroscopy calculated the number of polymer chains growing per metal atom to be 2.0 – 2.6, indicating that the polymerisation process is living.
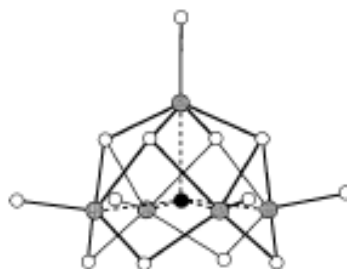
Figure 1.19: Structure of $[Ln_5(\mu\text{-}O)(O^iPr)_{13}]$.

Spassky and co-workers also reported the in-situ generation of $Y(O^iPr)_3$ from the equilibrium mixture of yttrium tris(2,6-di-tert-butylphenolate) and isopropanol (Scheme 1.2). Despite the requirement of this additional step in the polymerisation process, ROP of L-LA occurred at a faster rate than with the commercial yttrium oxo isopropoxide, indicating the detrimental effect of the bridging oxide group.
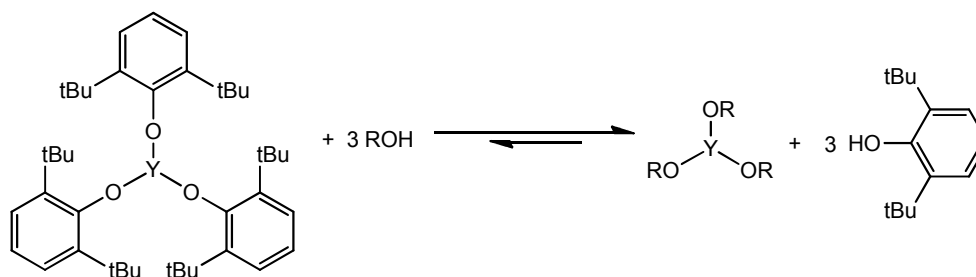
Scheme 1.2: In-situ generation of $Y(O^iPr)_3$.

More recently, a series of lanthanide tris(2,4,6-trimethylphenolate)s, $Ln(OMP)_3$ (Ln = La, Nd, Sm, Gd, Er) have been reported by Shen and co-workers to show activity for both the homopolymerisation of L-LA and the sequential copolymerisation of ε-caprolactone and L-LA without the need for an alcohol co-initiator.[64] As before, activity was found to decrease across the group, as the lanthanide ions get smaller and it becomes more difficult for monomers to coordinate. $La(OMP)_3$ produced high conversions of L-LA in solution conditions (1000 eq, 40 mins, 80 °C), but prolonged polymerisation runs and high monomer concentrations resulted in an increase in PDI.

Rare earth initiators including mulitidentate ligands. As with Group 4 initiators, there has been a drive towards the use of more complicated multidentate ligand systems in the synthesis of rare earth initators to promote the isolation of monomeric complexes with well-defined initiating groups. As such, a series of aryl amidinate coordinated Y complexes reported in 2001 by Hillmyer and co-workers were found to be monomeric in nature and highly active for the ROP of *rac*-LA at room temperature.[65] Complex **23** was found to be most active (1000 eq, 1 hr), but required the addition of 1 equiv BnOH as a co-initiator to produce narrow PDI's. In 2001, Arnold

and co-workers utilised a guanidinate-type ligand to synthesis the related complex **24**, which was shown to give moderate control over the ROP of LA at low molar ratios. However, transesterification was observed at higher catalyst loadings, resulting in high values of PDI and low molecular weights. This type of ligand was returned to more recently by Trifonov and co-workers when they reported the series of bis(guanidinate) alkoxide lanthanide complexes, **25**.[66] As had been observed in previous studies, the reactivity series Nd ~ Sm > Y ~ Lu was observed with respect to the ROP of LA, and despite exhibiting a syndiotactic enhancement in the ROP of β-butyrolactone, no such stereocontrol was observed in the case of *rac*-LA.
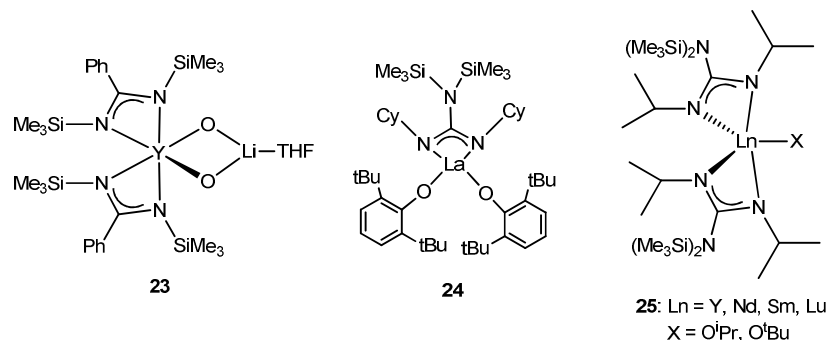
Figure 1.20: Rare earth initiators featuring bidentate ligands.

A series of Y bis(phosphinic) complexes reported by Williams and co-workers, clearly demonstrate the effect complex nuclearity can have on polymerisation behaviour.[67-69] Despite being shown to undertake ROP of *rac*-LA at comparative rates, the dimeric complex **26** was found to result in predominantly atactic PLA (P_s = 0.62), while the monomeric isopropoxide complex **27** resulted in strongly heterotactically enriched PLA (P_s = 0.85).[67] Interestingly, this degree of stereocontrol was seen to drop when the polymerisation was carried out in DCM (P_s = 0.62) instead of THF, indicating that the coordinated THF molecule in **26** is crucial in achieving heterotactic polymer growth. It has been proposed that, within the propagation step, the mononuclear structure of **26**, in conjunction with the steric bulk of the ligand, promotes LA coordination from one side of the complex only. There is thought to be a steric hinderance between the methyl groups of the last inserted LA monomer and the coordinated LA monomer, so that the opposite enantiomer is favoured via a chain-end control mechanism.[67]
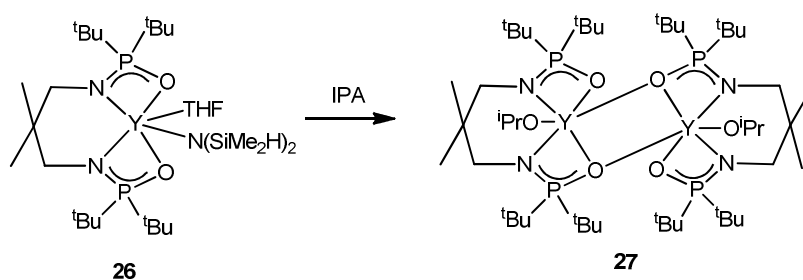
Scheme 1.3: Monomeric and dimeric Y initiators featuring bis(phosphinic) ligands.

Rare earth initiators including chiral ligand systems. Several research groups have investigated the effect of chiral ligands on the stereocontrol exhibited by the resulting lanthanide complexes. An early report was made by Coates and co-workers in which the same binol-substituted Salen ligand investigated previously with Al, was used in the synthesis of the dimeric Y complex, **28**.[30] The Y compound was found to be more active for the ROP of *rac*-LA in solution at 70 °C than the Al derivative (100 eq, 14 hrs vs 40 hrs for Al), but no stereocontrol was observed. In 2007, Carpentier and co-workers reported a series of chiral tetradentate diamine-diamido lanthanide complexes of the type **29**, the Y analogue of which was found to initiate ROP of *rac*-LA at room temperature (200 eq, 15 mins).[70] In addition, the resulting polymer was found to be moderately isotactically enhanced ($P_i = 0.66$), but was also observed to have relatively high PDI's and higher molecular weights than expected. This was attributed to a slow initiation process brought about by the use of the less nucleophilic amido group as an initiator as opposed to the more commonly used alkoxide groups.[71-72] Arnold and co-workers recently utilised a chiral bidentate ligand to synthesis a racemic mixture of two homochiral C_3-symmetric complexes, **30**, upon lanthanide complexation.[73] When applied to the ROP of *rac*-LA, each enantiomer of the complex *rac*-[YL$_3$] exhibited a strong preference for only one enantiomeric form of LA, resulting in a strong isotactic enhancement ($P_i = 0.75 - 0.83$). Mass spectroscopy confirmed the polymer was terminated by a ligand, L, molecule, and polymerisation was thought to proceed via the displacement of one ligand and the formation of an [L$_2$Y-O-polymer-L] propagating species. Mixing of the two enantiomerically opposite enriched PLA chains would lead to stereocomplexation.
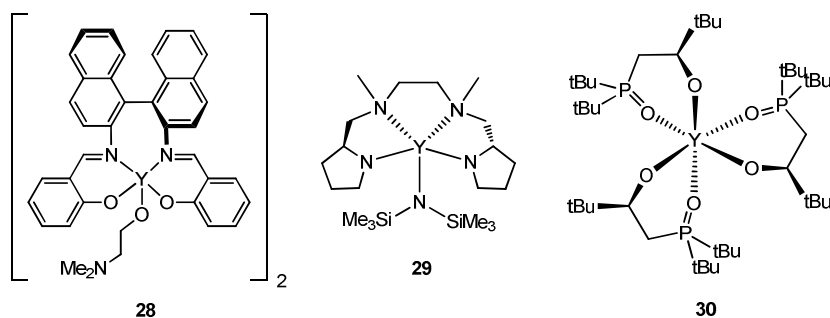
Figure 1.21: Rare earth initiators featuring chiral initiators.

Rare earth initiators including poly(phenolate) ligands. Following the success of multidentate poly(phenolate) ligands in the synthesis of stereoselective Group 4 ROP initiators, great attention has been paid to applying these types of ligands to the search for rare earth initiators. In 2003, Okuda and Ma[74] first reported their investigations into the catalytic activity of a series of 1,ω-dithiaalkanediyl-bridged bis(phenolato) ligated lanthanide complexes of the type **31** and **32**, amongst others. All complexes in the series were found to be active for the ROP of L-LA in solution at room tempertaure, although those of the type **31** were found to be more so (300 eq, 5 mins for Lu). For any given ligand, the reactivity was found to follow the series Lu > Y >> Sc.

Both these trends were explained by a steric hinderance to monomer approach created by a smaller ionic radius or overcrowding at the rare earth metal, which could occur when a longer ligand backbone "wraps around" the metal. It is these cases however, where the most stereocontrol has been observed. Initially, the ROP of *rac*-LA carried out using the Y analogue of **32** (R = ^{t}Bu) afforded PLA with a moderate 70% heterotactic enrichment, and subsequent publications from the group report that the Sc analogue (R = Me) exhibited a substantial heterotactic selectivity, resulting in values of P_s as high as 0.96.[75] These selectivities were, however, much reduced if the polymerisations were carried out in non-polar toluene, as opposed to THF. In the case of the BDI coordinated Zn complexes, this phenomenon has been reasoned by computational analysis carried out by Rzepa et al, who reported on the key role that the solvent plays to entropically balance the system.[76] In an attempt to improve the molecular weight control of this initiator system, isopropanol was added to generate a metal alkoxide in situ. Monitoring of this reaction by ^{1}H NMR studies led Okuda to propose the formation of a dimeric structure, which would initiate the ROP of LA very slowly, resulting in high values of PDI.[72]
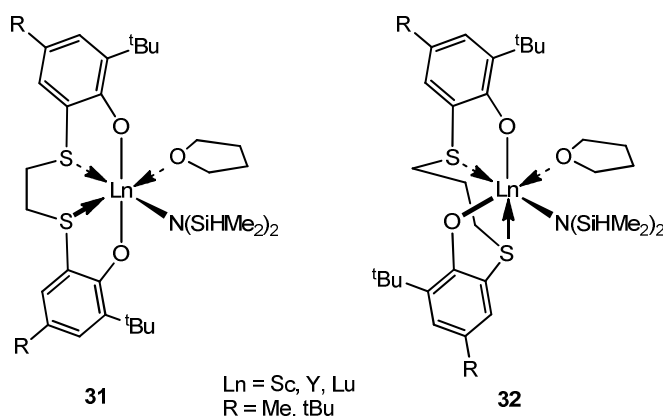
Figure 1.22: Rare earth initiators featuring 1,ω-dithiaalkanediyl-bridged bis(phenolate) ligands.

Carpentier and co-workers have made several reports concerning the activity and selectivity afforded by the series of rare earth complexes featuring amine bis(phenolate) ligands, shown below. Initial reports of the complex **33a** noted good activity for the ROP of *rac*-LA (500 eq, 1 hr, RT) coupled with a selectivity for heterotactic addition (P_s = 0.80) when the polymerisation was carried out in THF, but again this was seen to reduce when carried out in toluene (P_s = 0.60).[77] The stereoselectivity of this system was also seen to decrease when the Y metal is replaced by La (P_s = 0.64) or Nd (P_s = 0.49), and it is believed the increase in ionic radius or a resulting conformation change of the ligand could be responsible. Variation of the phenol substituents had little effect on the stereoselectivity of the initiator system, with the exception of the cumyl (α,α-dimethylbenzyl) substituted complex, **33b**. In this case, even higher heterotactic selectivity was observed for ROP of *rac*-LA (P_s = 0.90) and a syndiotactic enrichment was shown in ROP of *meso*-LA. In this case, reaction of complexes **33a** and **33b** with isopropanol did not result in dimeric structures, but instead remained monomeric in nature. Direct comparisons

between the amido and alkoxo initiators showed no change in stereoselectivity, but a reduction in PDI values, and in the case of complex **33a**, an increase in activity (1000 eq, 40 mins).[71]

33a: R = ^{t}Bu
33b: R = cumyl
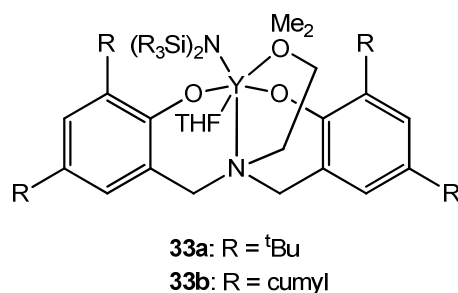
Figure 1.23: Y amido initiators featuring amine bis(phenolate) ligands.

Mountford and co-workers have concentrated on bis(phenolate) coordinated complexes and their application for the polymerisation of 1-hexene and methyl methacrylate (MMA) for some years. But, in 2005 the group published a series of dimeric rare earth borohydride compounds of the type **34**, and reported their ROP activities for ε-caprolactone, L- and *rac*-LA, the first use of a rare-earth borohydride initiator in the production of PLA.[78]   **34** was shown to have the highest activity of the investigated series in both toluene and THF solutions, and resulted in polymer molecular weights close to calculated values, due to the faster rates of initiation present in this system that keep chain transfer to a minimum.   Kinetic studies of **34** showed the rate of polymerisation in THF for *rac*-LA (9.96 x 10^{-4} s^{-1}) to be approximately double that of L-LA (4.96 x 10^{-4} s^{-1}), and displayed first-order dependence on the monomer concentration.   The microstructure of polymers resulting from ROP of *rac*-LA by all these complexes were analysed and were found to be heterotactically enriched by up to 87%.   The living nature of the system also allowed the synthesis of the PCL-PLA co-block copolymer sequentially.   Recently, the group reported the synthesis of a series of zwitterionic complexes of the type **35**,[79-80] a bi-product of Carpentier's initiator **33a**.   Complexes of the type **35** were found to efficiently undertake ROP of *rac*-LA, and resulted in heterotactic enrichment of up to 96%.

34

35a: R = OMe
35b: R = NMe
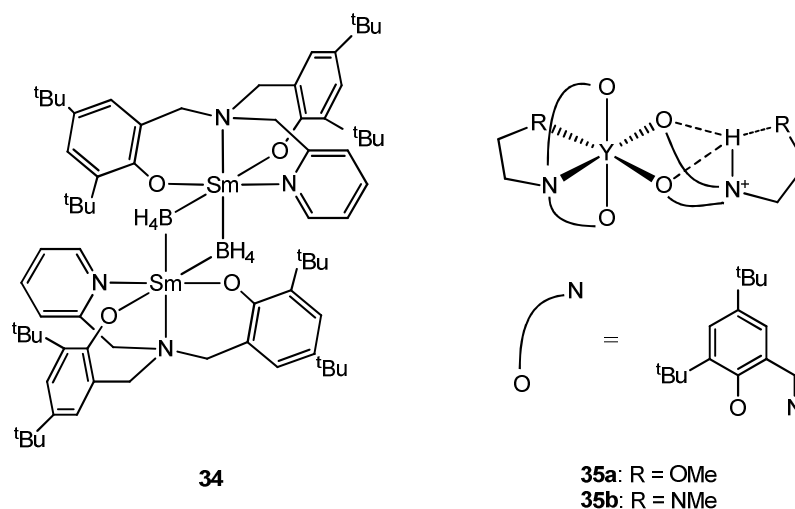
Figure 1.24: Rare earth borohydride and zwitterionic initiators featuring amine bis(phenolate) ligands.

1.1.3. Stereocomplexes and block-copolymers

1.1.3.1. *Stereocomplexation*

A significant hinderance to the widespread industrial use of PLA is the relatively low melting temperature displayed by the material. However, in 1987, Ishida and co-workers first reported strong interactions between chains of enantiomerically opposite PLLA and PDLA, synthesised by the ROP of enantiomerically pure L-LA and D-LA respectively.[81] Known as stereocomplexation, the interactions involved take place between the left and right-handed helices of adjacent macromolecular chains of PLLA and PDLA (Figure 1.25) through specific $CH_3 \cdots O=C$ and $C_\alpha H \cdots O=C$ H-bonding forces.[82] This results in a significant increase in both melting temperature (T_m) and glass transition temperature (T_g) of the materials (Table 1.2), which can be followed using differential scanning calorimetry (DSC), due to their highly crystalline nature.
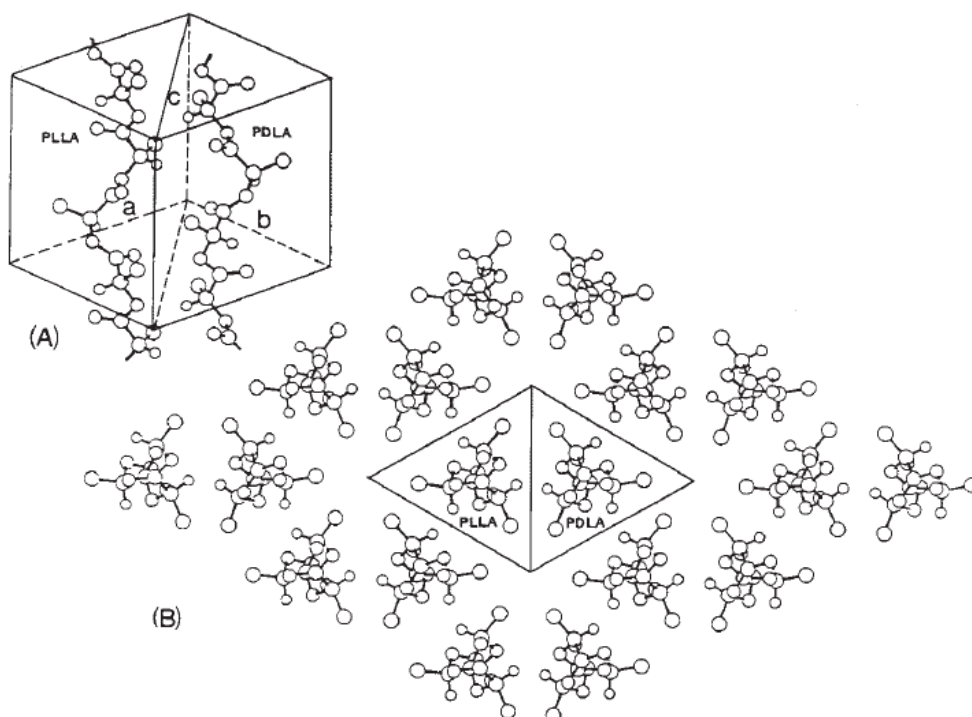
Figure 1.25: Crystal structure of stereocomplex PLA, taken from ref. [83].

	T_m (°C)	T_g (° C)
PLLA	170 – 190	50 – 65
heterotactic PLA	-	< 45
atactic PLA	-	45 – 55
syndiotactic PLA	151	34
sc-PLA	220 - 240	65 – 72

Table 1.2: Thermal properties of various forms of PLA.[68-69]

Stereocomplex PLA (**sc**-PLA) can be synthesised in solution, and extracted via precipitation, film casting or fibre spinning, or in the melt, to which crystal nucleators can be added to promote stereocomplex formation and suppress crystallisation of single polymer crystals.[83-84] In both

cases, an exact 1:1 ratio of PLLA and PDLA proves the most favourable in the formation of **sc**-PLA, although stereocomplexation was shown to be the predominant process in mixtures from 40/60 to 60/40.[81] It is possible to differentiate between crystalline regions arising from homopolymer interactions and those arising from **sc**-PLA using wide-angle X-ray diffraction (WAXD), as the process of stereocomplexation induces a significant effect on the crystal structure of the polymer chains, and a different set of peaks are observed in the WAXD pattern (Figure 1.26). Morphological differences are also apparent between the two types of crystallites, as **sc**-PLA exhibits a triangular morphology, while a hexagonal form is often seen in crystals of PLLA.
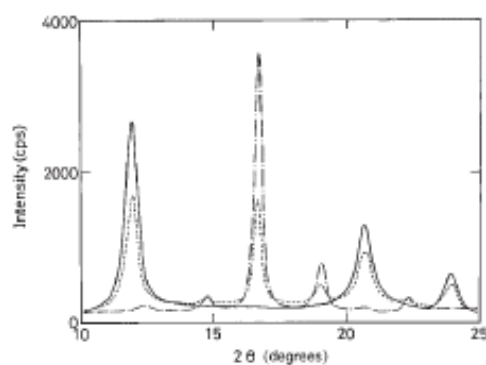
Figure 1.26: WAXS profiles of PDLA/PLLA blends: 50/50 (solid); 75/25 (dash); 100/0 (dash/single dot). Taken from ref. [81].

1.1.3.2. *Stereoblock PLA*

A convenient path to stereocomplex PLA is the synthesis of stereoblock PLA, which undergoes stereocomplexation in situ, and results in little homopolymer crystallisation, due to the enhanced interaction that occurs between neighbouring blocks. This method was first reported by Yui and co-workers who reported stereocomplexation of di-stereoblock PLA of the type PLLA-*b*-PDLA, synthesised in a step-wise manner.[85] The same phenomenon was observed in multi-stereoblock PLA consisting of relatively short PLLA and PDLA segments, arising from the isoselective ROP of *rac*-LA.[86] The **sc**-PLA produced in this manner tends to exhibit T_m values ranging from 180 to 230 °C depending on the block length, which is lower than **sc**-PLA synthesised from traditional PLLA/PDLA mixtures, as shown by the comparable DSC thermograms in Figure 1.27. Here, the stereoblock PLA (top) exhibits only one endotherm at ~ 200 °C, whereas two endotherms are shown for a mixture of PLLA and PDLA; one at ~ 220 °C from **sc**-PLA and one at ~ 175 °C from homopolymer crystallites.
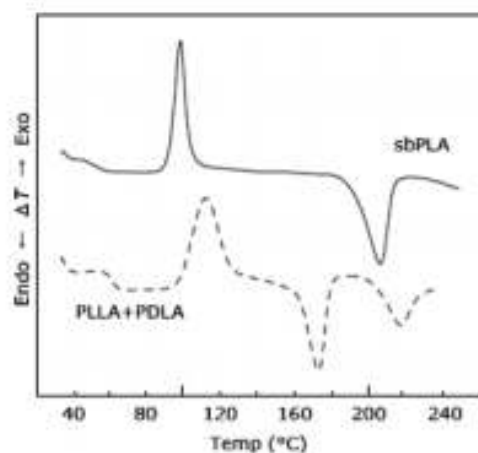
Figure 1.27: DSC curves after melt quenching of stereoblock PLA and a PLLA/PDLA polymer blend, taken from ref. [84].

1.1.3.3.   *Block co-polymers*

In order to tailor the properties of the resulting material, LA is often co-polymerised with a second monomer, but in the majority of cases, concurrent polymerisation of both monomers in a one-pot fashion will result in random co-polymers with poorly defined microstructures (Figure 1.28). One noteworthy exception was recently reported by Thomas and co-workers, in which an Y initiator showing syndiotactic selectivity in the ROP of β-butyrolactone facilitated the alternate co-polymerisation of two different enantiopure β-lactones.[87] A large difference in the rates of initiation and propagation between the two monomer types could lead to a block co-polymer of the type AB, but these are more commonly synthesised by the sequential addition of the second monomer once polymerisation of the first has reached completion, provided the polymerisation is living.[88] Reinitiation of a short-chain macroinitiator also acts as an alternative route to AB di-blocks, but also allows the synthesis of ABA tri-blocks.[89]

As well as exhibiting homocrystallisation singularly, block co-polymers containing enantiopure PLLA or PDLA have been shown to undergo stereocomplexation on mixing with their enantiomerically opposite equivalents (Figure 1.29). For example, both di-blocks (AB) and tri-blocks (ABA), where A represents PLLA or PDLA and B represents either polyethylene glycol (PEG) or polycaprolactone (PCL) undergo stereocomplexation, resulting in an increase in T_m of the PLA segment by 50 – 60 °C.[90] The effect of stereocomplexation on the T_m of the B block (PCL or PEG) within the tri-block ABA is dependent on the relative lengths of the blocks. In some instances, when A and B are of equal length, a decrease in melting point of the B block by 30 - 40 °C has been observed[91-92], whereas a significantly longer B block results in no change in melting point of the B block. In cases where the A block (PLA) is significantly longer, **sc**-PLA crystallites dominate the system, and no thermodynamic information about the B block can be

26

obtained from the DSC thermogram. Equally, a minimum amount of around 20% PLA by weight is required in these tri-block systems to allow crystallisation of the A block to occur.[92-93]
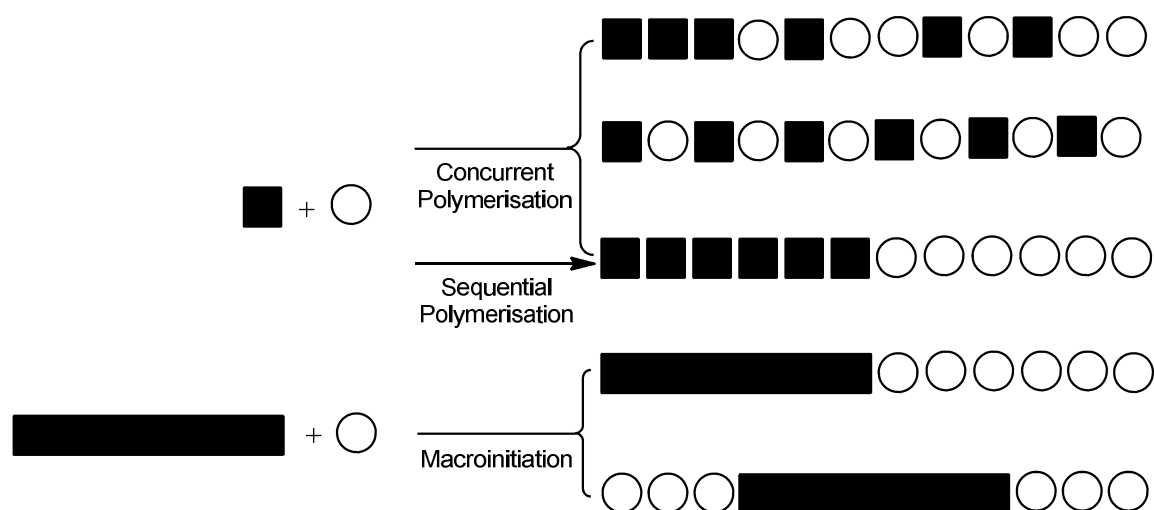
Figure 1.28: Possible structures of copolymers shown schematically.
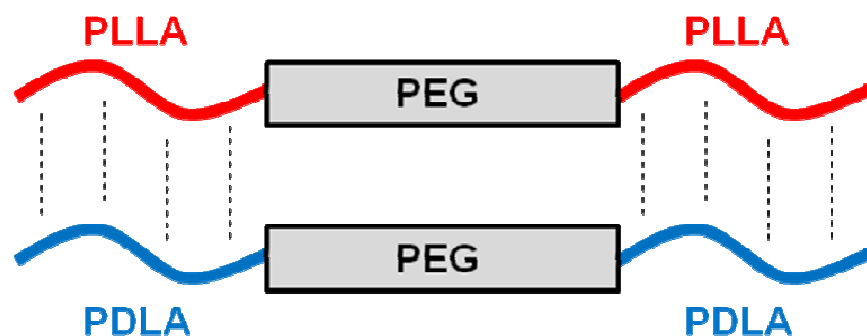
Figure 1.29: Stereocomplexation of block-copolymers containing enantiopure PLLA and PDLA blocks.

Self-assembly of block co-polymers. Reports of self-assembly driven by interactions between blocks of PLLA and PDLA within both PCL and PEG co-polymers have been made. Enantiomeric polymer pairs of PLA-PCL di-blocks were shown to form aggregates with hydrodynamic radii of 200 nm by dynamic light scattering (DLS), in THF after 10 days at high concentrations (10 g/L).[94] After this point, the rate of aggregation dropped considerably at high concentrations, while lower concentrations (1 g/L) underwent self-assembly at a slower rate over 6 months. This considerable difference indicates that at high concentrations, stereocomplexation is in competition with a solvophobically driven aggregation process.[95] The hydrophilic nature of PEG, coupled with the hydrophobic nature of PLA, causes stereocomplexed copolymers of the type AB, ABA and BAB to form core-shell type micelles in water (Figure 1.30). Mixing of ABA copolymers, PLLA-PEG-PLLA and PDLA-PEG-PDLA, results in an irreversible gel formation at 37 °C, which was shown to be attributed to the formation of **sc**-PLA by WAXD analysis.[96] In the

reverse case, mixing of BAB copolymers results in gel formation at room temperature, but turns to solution on heating. This process was shown to be reversible, as cooling of the sample once again results in gel formation, and is thought to be due to stereointeractions between helical PEG chains, induced by the helices of the PLLA and PDLA blocks.[97] Subsequent studies into similar micelles formed by the stereocomplexation of PLA-PEG di-blocks observed them to be highly stable. Micelles of this form were shown to be spherical in shape, via atomic force microscopy, and that their size (30 – 60 nm) was directly related to the proportion of LA units in the polymer chain.[98-99] So strong are the interactions in **sc**-PLA that they can be utilised to overcome repulsions between two differing hydrophilic blocks, PEG and poly(N-isopropylacrylamide) (PNIPAAM), in micelle formation of AB di-block copolymers PLLA-PNIPAAM and PDLA-PEG.[100]
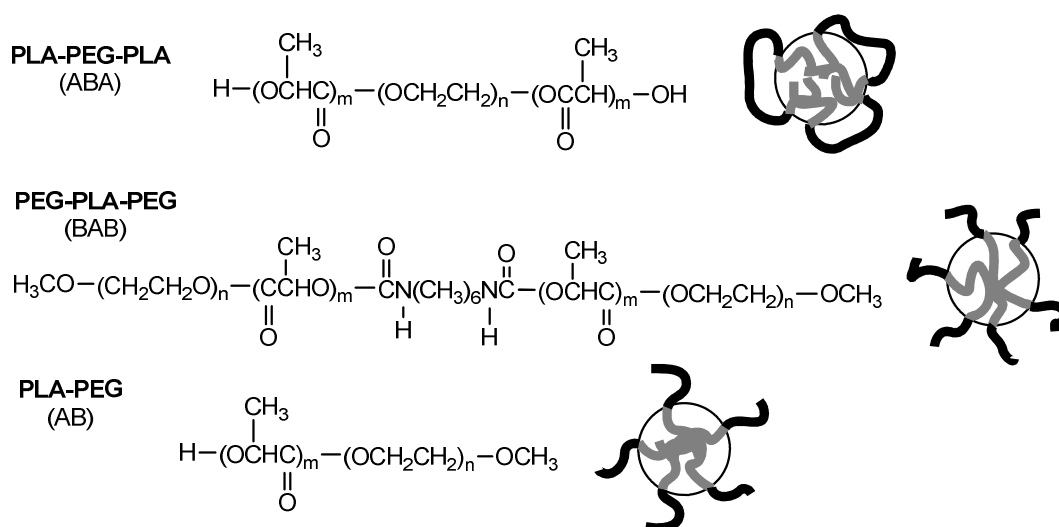
Figure 1.30: Formation of core-shell type micelles via stereocomplexation.

1.2. Part Two: Recent developments in poly(phenolate) complexes of Group 4 and rare earth metals

It is clear that multidentate ligands with structures containing numerous linked phenolate groups are a popular choice in the search for effective single-site initators for the ROP of cyclic esters, and several specific studies have already been described within the previous section. The more general field of the coordination chemistry of these ligands to early transition metals and *f*-block elements was comprehensibly reviewed in 2004 by Kawaguchi and Matsuo[101], but since then considerate progress has been made in the area, which stands to influence the design of future ROP initiators of this type. In the second part of this introductory chapter, the coordination chemistry of several types of poly(phenolate) ligands to Group 4 and rare earth metals, reported over the last 6 years, shall be summarised, with special attention paid to reports of stereoselective catalysis that has been attributed to the molecular structure.

28

1.2.1. Bis(phenolate) ligands

1.2.1.1.   Bis(phenolate) ligands linked by a single atom

H_2L^1: E = CH_2; R^1 = ^tBu; R^2 = Me
H_2L^2: E = CHPh; R^1 = R^2 = ^tBu
H_2L^3: E = S; R^1 = ^tBu; R^2 = Me
H_2L^4: E = S; R^1 = H; R^2 = $CMe_2CH_2CMe_3$
H_2L^5: E = S; R^1 = ^tBu; R^2 =

H_2L^6: E = PPh; R^1 = R^2 = H
H_2L^7: E = PPh; R^1 = ^tBu; R^2 = Me
H_2L^8: E = PPh; R^1 = R^2 = ^tBu
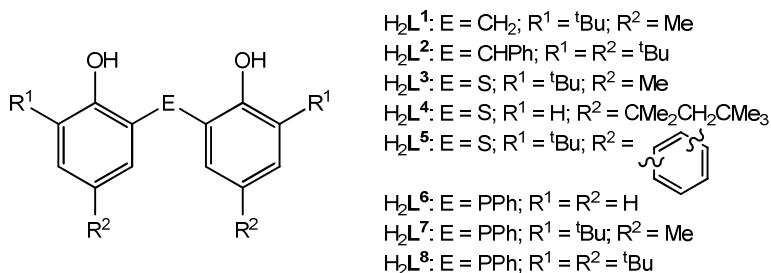
Figure 1.31: Bis(phenolate) variations discussed in this section.

Bis(phenolate) ligands bridged by the carbon atom. As described previously, the reaction of the bidentate ligand 2,2'-methylene-bis(phenol) with Ti(IV) precursors results in monomeric mono-ligand complexes, from which alkylated derivatives can be prepared using standard procedures.[101] In 2007, Zhang reported a propensity to dimer formation when the complex **36** undergoes reaction with $AlMe_3$, PhLi in ether, and ^tBu-N_3, resulting in **37**, **38** and **39** respectively.[102-103] Zhang also reported the addition of alkali metals to **36** resulting in binuclear Ti-alkali metal complexes of the type **40**, the exact nature of which depends on the alkali metal and solvent used.[103]
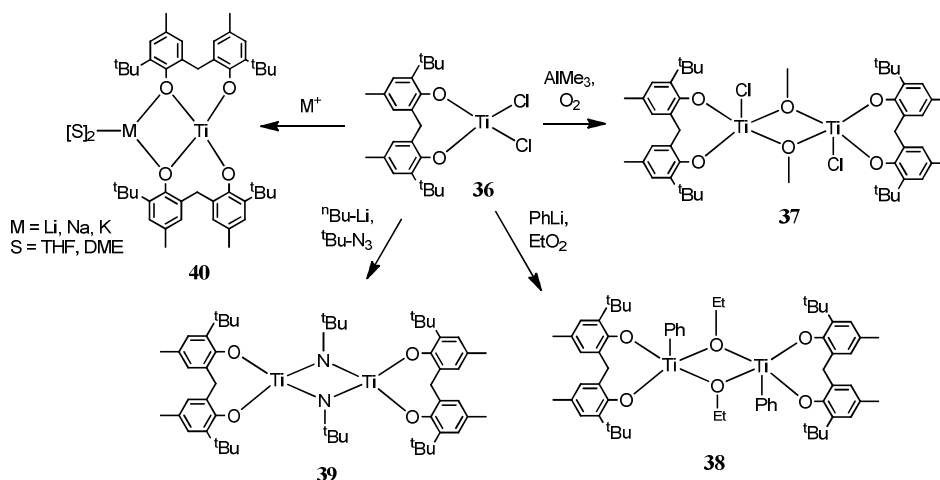
Scheme 1.4: Reactions of 36 resulting in binuclear complexes.

Shen and co-workers reported similar behaviour when the sodiated ligand precursor was reacted with various lanthanide(III) chlorides, resulting in binuclear lanthanide-sodium complexes of the type **41**.[104-105] Reaction instead with lanthanide tris(cyclopentadiene) resulted in monomeric complexes of the type **42** and subsequent addition of alcohol afforded the dimeric complexes **43**, which were found to be active for ROP of ε-caprolactone.[106-108] Addition of a second equivalent of the ligand to **42** resulted in an unsymmetrical dimeric complex **44** in the case of La, and the bis-ligated complex **45** in the cases of Y and Yb, as a result in the difference in ionic radii. One

phenolate group acts only as a neutral donor in **45**, resulting in one substantially longer Ln-O bond length in the crystal structures.[109]
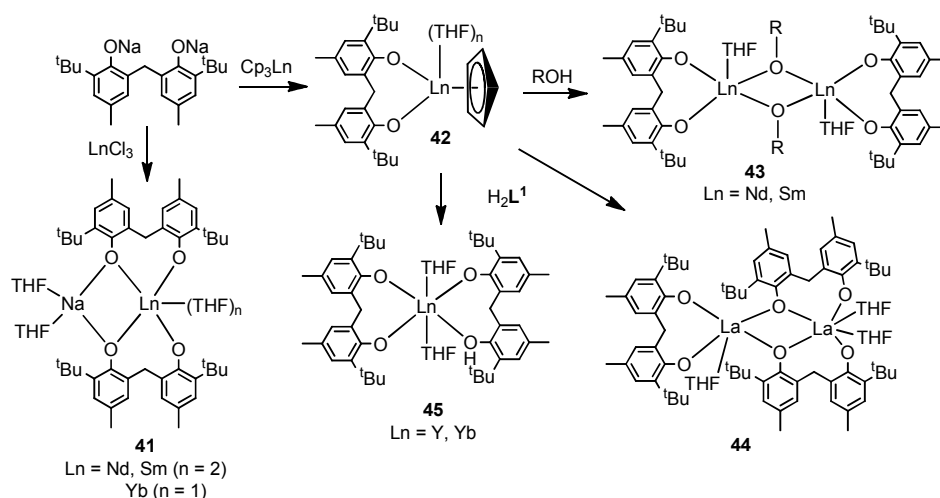
Scheme 1.5: Reactions of Na$_2$L^1 with Ln(III).

Reaction of the same ligand with [Ln{N(TMS)$_2$}$_2$Cl(THF)$_2$] results in two products depending on the conditions of the synthesis – the dimeric complex **46** under mild conditions and the monomeric 'ate' complex **47** using BuLi at -10 °C. Reaction of **46** with alkali metal silyl amides provided a pathway to the neutral monomer **48**.[110] All monomeric complexes from this study were found to be active for the ROP of ε-caprolactone, with those anionic in nature being more so, and as before, complexes of the larger metal Nd, were found to more active than those of Yb.
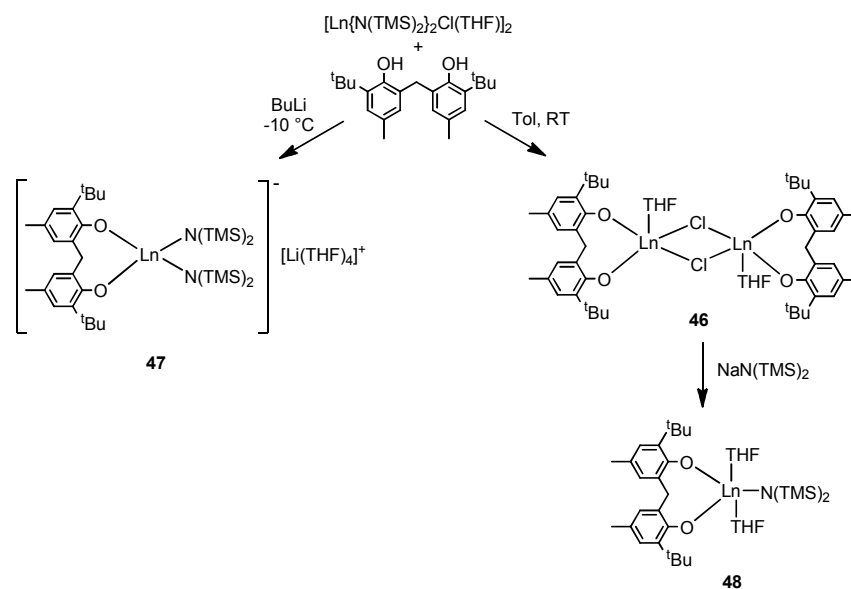
Scheme 1.6: Reactions of H$_2$L^1 **with Ln(II).**

The binding strength of this type of ligand was shown by Brown and co-workers, who reported that the addition of the ligand H$_2$L^2 to triethanolamine coordinated Ti resulted in the formation of a fully metalated cyclic octatitantiun complex **49**, comprising of four dimeric Ti repeat units.[111]

This structure is a result of the unprecedented 'slippage' of the triethanolamine ligands from their stable titranocene coordinated form, in which the favourable 8-membered ring created by coordination of the bis(phenolate) ligand pushes both triethanolamine ligands onto only one Ti centre.
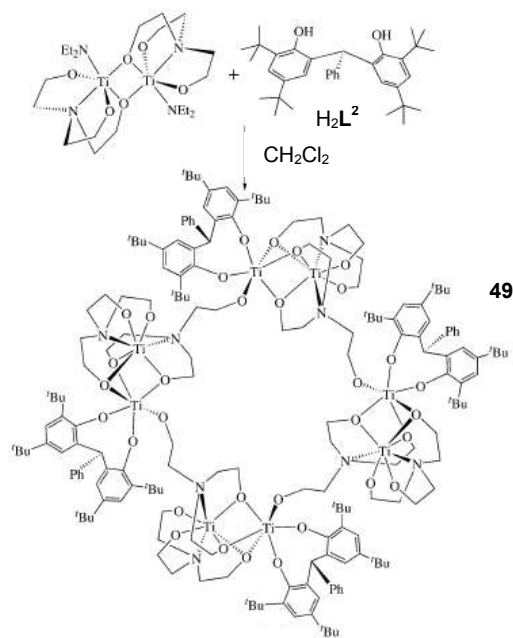
Scheme 1.7: Synthesis of metalated cyclic octatitanium complex reported by Brown et al, taken from ref. [111].

Bis(phenolate) ligands linked by a single heteroatom (S or P). Kakugo and co-workers first described the coordination of Group 4 metals by a sulphur-bridged bis(phenolate) ligand in 1989.[112] A higher activity with respect to the polymerisation of olefins has subsequently been observed, attributed to the coordination of the sulphur atom to the metal.[39] As described earlier, Takashima applied these principles to his search for effective initiators for the ROP of cyclic esters, and despite reporting a decrease in activity, the polymerisations initiated by the sulphur-bridged Ti complex were more living in nature. Okuda and co-workers have recently gone on to use the ligand H$_2$L^3 to isolate alkyl (**50**), and the subsequent alkoxide (**51**) and hydride (**52**), lanthanide complexes from [Ln(CH$_2$SiMe$_3$)$_3$(THF)$_n$].[113-114] The isopropoxide complex **51** exhibited activity for ROP of L-LA (88 %, [M]/[I] = 200, 24 hrs at 298 K), and in the presence of excess isopropanol, demonstrated good molecular weight control and a low polydispersitiy.[113]
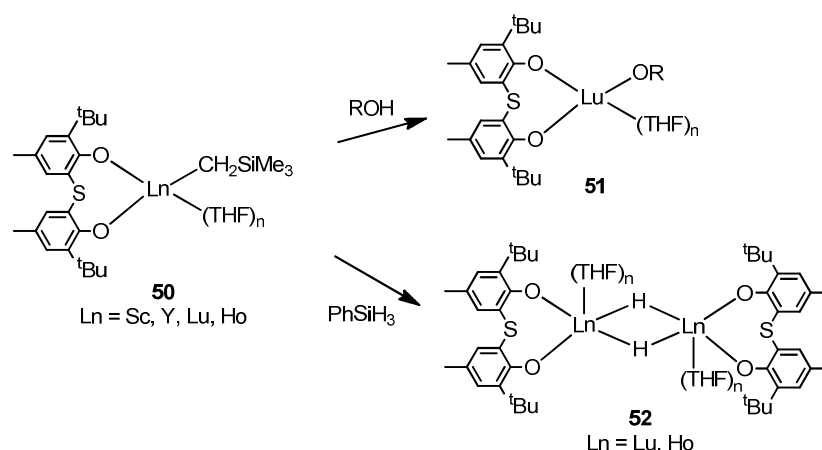
Scheme 1.8: Synthesis of rare earth hydride and alkoxide complexes featuring H₂L³.

Sobota and co-workers amended the ligand system by removing the ortho substituents and increasing the sterics of the para substituents. As would be expected, this was shown to promote the formation of dimeric complexes (**53**) on the coordination of the ligand to Group 4 metals. On reaction with Ti(OR)₄, bridging occurs through the alkoxide groups, allowing rearrangement and further aggregation to the tetrameric complex on the addition of water (**54**).[115]
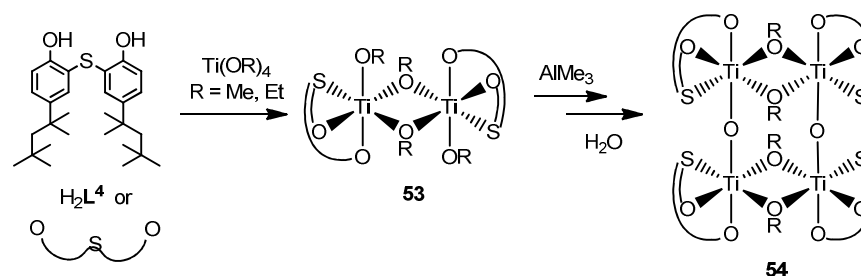
Scheme 1.9: Reaction of H₂L⁴ with Ti(IV) alkoxides.

Reaction of the above ligand H₂**L⁴** with TiCl₄ led to dimeric complexes in which bridging occurs via the phenolate groups (**55**), and if the stoichiometry of the reaction is altered, a third ligand molecule is included, binding only in a bidentate manner (**56**).[116] The 1:1 reaction of the ligand with zirconium and hafnium chlorides also result in phenolate bridged dimers (**57**), but the ligand does not bind in the usual *fac* manner, instead occupying the apical sites.[117] These observations are in contrast to dimeric complexes of ligand **L³** in which the ortho positioned tertiary butyl substituents prevent bridging via the phenolate groups.[112] Once again, increasing the stoichiometry of the ligand in the reaction has a profound effect, and bis-ligand complexes of the type **58** were isolated as a result.[118] The titanium analogue of **58** could be isolated from 2:1 reaction of the ligand with Ti(NEt₂)₄ instead.[116] Interestingly, this series of bis-ligand complexes undergo reaction with AlMe₃ to form the trinuclear mixed metal methylated compound **59**.[118]
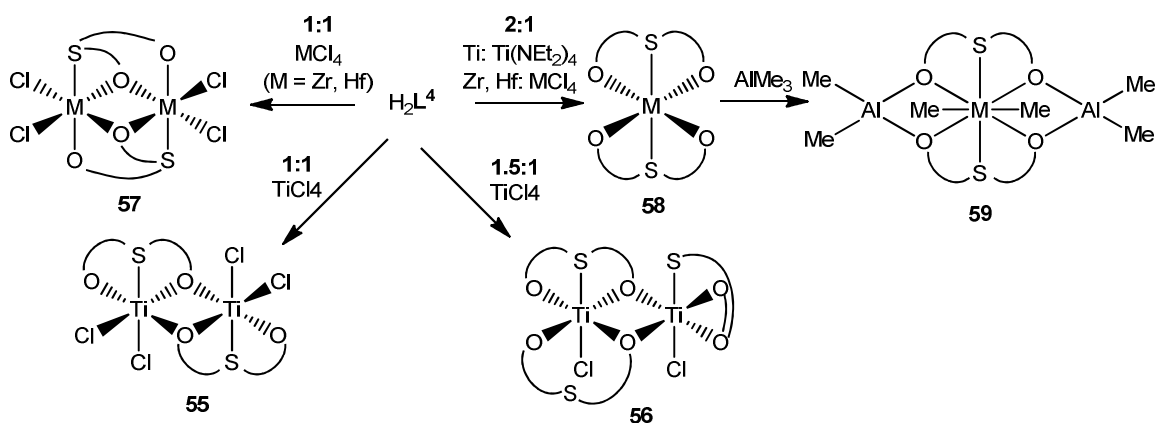
Scheme 1.10: Reaction of H₂L⁴ with Group 4 chlorides.

Weinstein, Arnold and co-workers have concentrated their investigations on the binaphtholate ligand H_2L^5 and resulting Group 4 and lanthanide complexes. The stoichiometry of the reaction was again found to influence the resulting complex – a 2:1 reaction of the ligand with TiCl₄ led to the bis-ligand monomeric structure **60**, while a 1:1 reaction resulted in a chloro-bridged dimer **61**.[119] Unlike in the examples described by Janas, the increased sterics and rigidity of the ligand prevents bridging through the naphtholate groups. Due to the larger ionic radius of Zr, the stoichiometric reaction of the ligand with ZrCl₄(THF)₂ results in the mono-ligated monomeric complex **62** and addition of a second equivalent of the ligand led to a bis-ligand complex of the type **60** (Scheme 1.11).
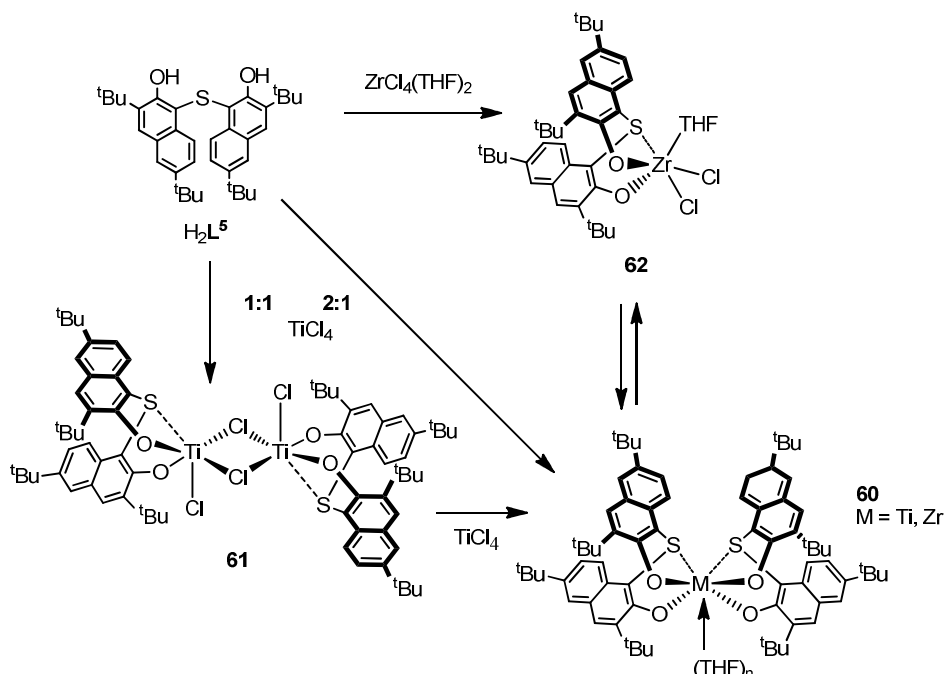
Scheme 1.11: Reaction of H₂L⁵ with Group 4 metals.

Bridging via the naphtholate groups was, however, observed in the dimeric complex (**63**) resulting from the reaction of the same ligand with Sm[N(SiMe₃)₃], but tritruation with THF afforded the monomeric complex **64**. Addition of the lithiated form of ligand Li_2L^5 to a series of

33

lanthanide (III) silyl amides resulted in the tris-ligated lithium coordinated propeller complexes **65**.[120] Interactions of a similar nature were observed when Li_2L^5 was instead reacted with a series of lanthanide tris di-tert-butyl β-diketonates (thd) resulting in complexes of the type **66**, although in this case the degree of ligand substitution could be controlled stoichiometrically.[121]
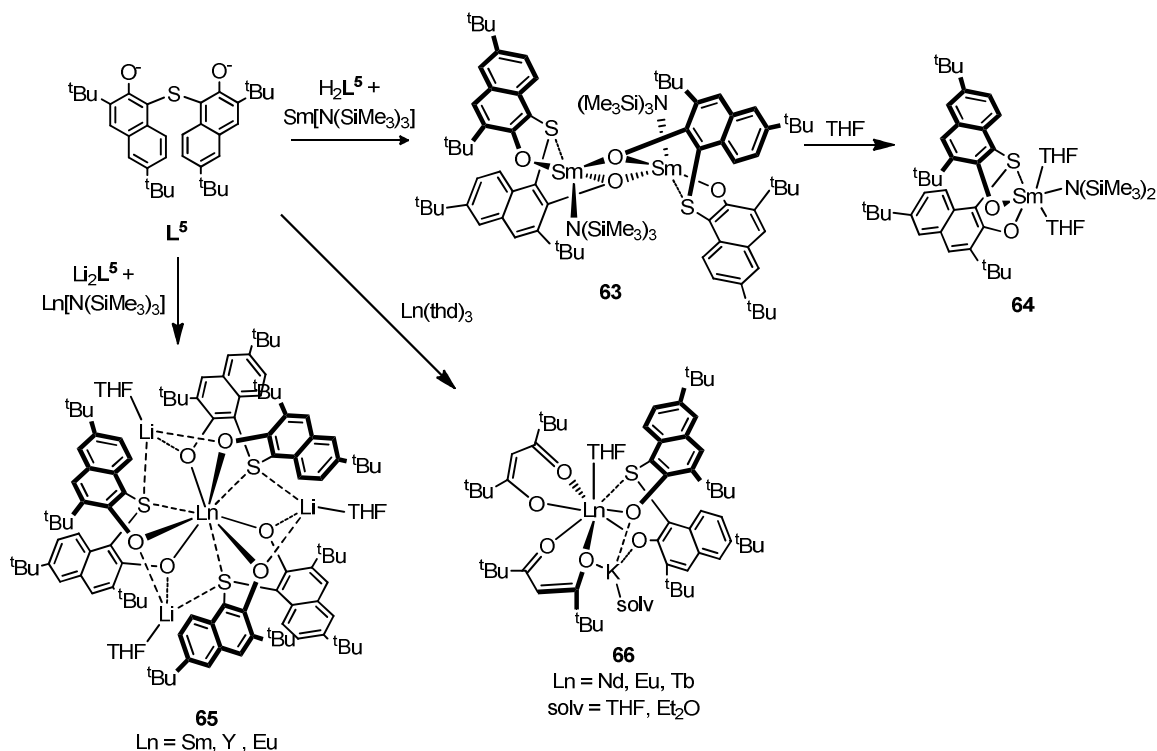
Scheme 1.12: Reaction of L^5 with rare earth metals.

Interest has also been paid in recent years to bis(phenolate) ligands linked by the phosphorous atom for much the same reasons. In 2004, Balakrishna and co-workers published a tetrameric Ti structure (**67**) based on the sterically unhindered ligand L^6,[122] but subsequent work by the research groups of Liang and Oda have concentrated on promoting the formation of monomeric complexes and the exploration of their catalytic potential. Whilst the reaction of sterically more hindered H_2L^7.HCl with $TiCl_4(THF)_2$ by Oda and co-workers resulted in the monomeric complex **68** directly,[123] Liang and co-workers reported a mixture of products in the case of L^8. They instead progressed via the bis-ligand complex **69** that was reported from reaction of H_2L^8 with titanium(IV) alkoxides, regardless of the reaction stoichiometry.[124] Comproportiation of **69** with $TiCl_4(THF)_2$ resulted in the monomeric complex **70**, analogous to the structure by Oda (**68**) and exhibiting the same octahedral structure, in which the ligand coordinates in a *fac* manner. The Ti–P bond distances in **68** and **70** were reported as 2.620 Å[123] and 2.596 Å[124] respectively, significantly shorter than Ti-S bond distances in sulphur-bridged bis(phenolate) analogues. This indicates that despite the increased atomic radius of phosphorous, the bonding interaction with titanium is stronger than is the case with sulphur. In an attempt to isolate the THF-free complex, Oda and co-workers reacted the ligand precursor $(MeOMe)_2L^7$ with $TiCl_4$, the resultant product

34

of which was shown to be formally $\mathbf{L^7TiCl_2}$, but is thought to have a dimeric structure.[123] On the other hand, Liang and co-workers reported that fluxionality between the C_1-symmetric complex **70** and the C_s-symmetric complex **71** takes place on the NMR timescale and cooling of the sample to -50 °C allowed resolution of the two sets of resonances. Liang and co-workers also reported the synthesis of the bis-ligand water coordinated analogues of the type **72** (M = Zr, Hf) from $MCl_2[N(SiMe_3)_2]_2$, irrespective of stoichiometry.[124]
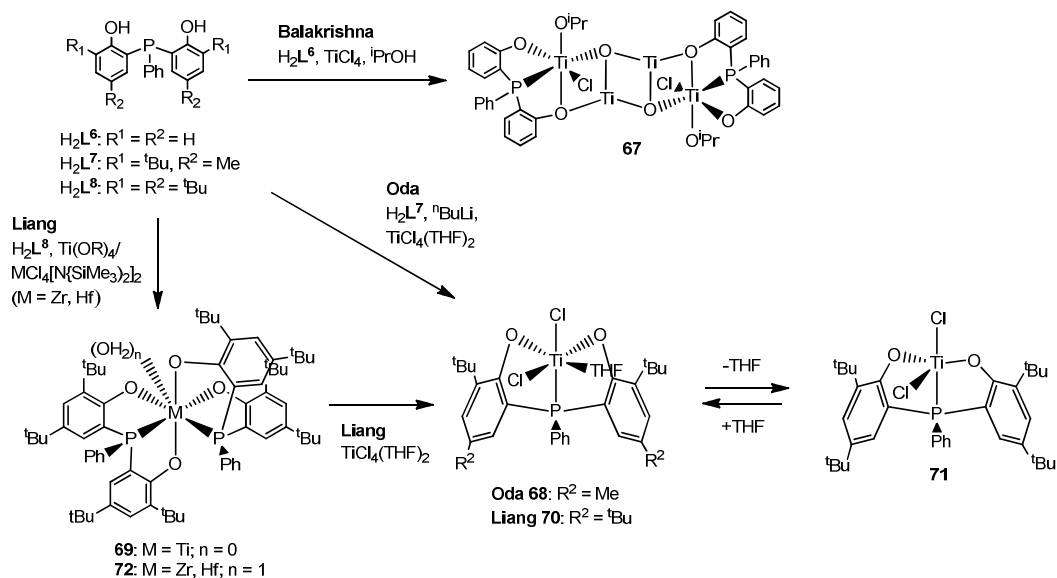
Scheme 1.13: Coordination chemistry of Group 4 metals by H_2L^{6-8}.

1.2.1.2. Bis(phenolate) ligands linked by a chain

Bis(phenolate) ligands linked by heteroatoms (S or P) within a carbon chain. Attempts have been made to combine the catalytic activity arising from the weak coordination of soft S or P donors to hard metals with a mechanism of stereoselectivity, and as such, Okuda and co-workers have investigated the Group 4 and rare earth metal complexes of tetradentate bis(aryloxide) ligands linked through a dithiaalkane-bridge, $\mathbf{L^{9-11}}$.[74, 125-129] Within this series of complexes, the nature of conformation taken on by the ligand, and the subsequent stability of this conformation in terms of its stereorigidity, was found to be inherent to the nature of ligand backbone and substituents of the phenolate moieties. Reaction of the ligand H_2L^9 with the appropriate titanium starting materials afforded C_2-symmetric *cis*-α conformation (*trans*-O,O *cis*-S,S *cis*-Cl,Cl) complexes of the type **73**. When the phenolate ortho substituent is bulky ($R^1 \geq {}^tBu$), the Λ-**73** isomer is observed exclusively at temperatures up to 100 °C, while in cases where these substituents are smaller, rapid enantiomerisation between the isomers Λ-**73** and Δ-**73** was shown to occur in solution at room temperature.[125] Reaction of the racemic form of the chiral ligand H_2L^{10} affords only the two diastereomers (Λ,R,R)-**74** and (Δ,S,S)-**74**, each enantiomer of ligand favouring only one conformation and no fluxionality being observed.[126] In contrast, coordination of $\mathbf{L^9}$ to Ti(R-BINOL) afforded both (Λ,R)-**75** and (Δ,R)-**75** enantiomers, but interestingly,

subsequent reaction with trace amounts of H_2O stereoselectively produced a homochiral dinuclear oxo-bridged (Λ,R,Λ) complex.[128] Benzylation of the stereorigid complexes Λ-**73**, (Λ,R,R)-**74** and (Δ,S,S)-**74** afforded stable, non-fluxional benzylated complexes, which when activated led to the isospecific polymerisation of styrene.[129] The Zr and Hf analogues of these complexes were reported to influence regioselectivity in the polymerisation of 1-hexene, switching from a 1,2-insertion in the case of Ti to a 2,1-insertion with Zr and Hf.[127] The increased flexibility of the trimethylene ligand H_2L^{11} results in further fluxionality on complexation to Ti, between *cis*-α-**76** and the C_1-symmetric *cis*-β-**76** (*cis*-O,O *cis*-S,S) conformations in solution,[125] however the solid state structure of the isopropoxide analogue of **76** ($R^1 = R^2 = {}^tBu$) was confirmed to be *cis*-α by X-ray diffraction.
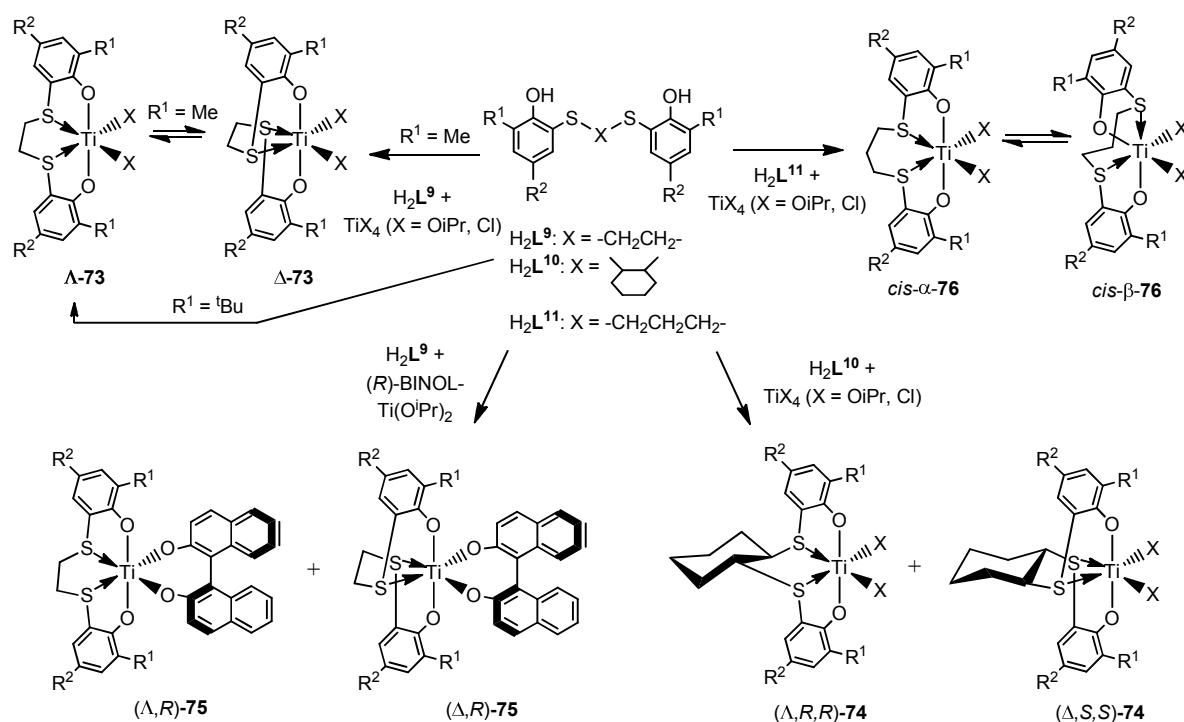
Scheme 1.14: Coordination of Group 4 metals by H_2L^{9-11}.

As well as benzyl groups, the monodentate ligands of the complexes **73** can be substituted for a series of other groups via methylation with $AlMe_3$ and the subsequent reaction with lithium isopropylisobutyrate. The resulting Ti ester enolate complex has been reacted with alcohols to give alkoxy complexes.[130] Amido (**77**) and imido (**78**) complexes of this type have also been reported by Okuda et al. via the reaction of the ligand, either in its protio or lithiated form, with [$Ti(NMe_2)_4$] or the imido precursor [$Ti(NR)-Cl_2(NC_5H_5)_3$] respectively.[131]
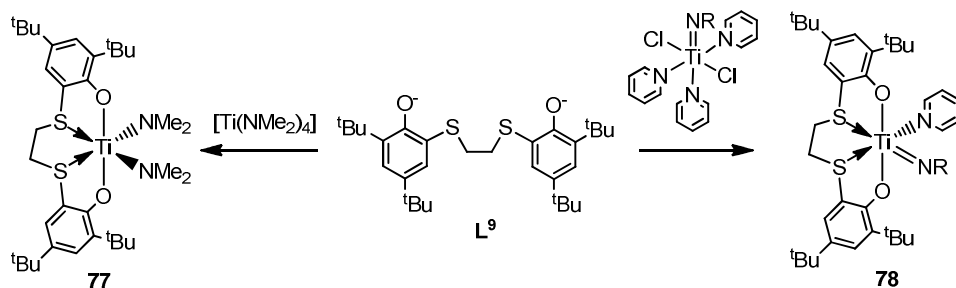
Scheme 1.15: Synthesis of titanium amido and imido complexes featuring L⁹.

As mentioned in an earlier section of this introduction, this ligand system has also been employed in the synthesis of a series of rare earth metal silyl amide complexes (Ln = Sc, Y, Lu), displaying high activity as initiators for the ROP of cyclic esters. X-ray crystal structures of selected complexes infer those containing the ligand **L⁹** take a *cis*-α conformation (**79**), while those containing the ligand **L¹¹** take either a *cis*-α-**80** or *cis*-β-**80** conformation depending on the ionic radius of the metal.[74] These rare earth complexes also exhibited fluxionality, attributed primarily to the rapid dissociation of the THF moiety on the NMR timescale. However, Okuda and co-workers have proposed that fluxionality between the *cis*-α and *cis*-β conformations occurs in the complex *cis*-α-**80**, providing the origin of the highly heterotactic stereocontrol exhibited by this complex in the ROP of *rac*-LA (P_s = 0.96).[75] As with the OSO ligand motif **L³**, H_2L^9 could be reacted with $[Ln(CH_2SiMe_3)_3(THF)_n]$ leading to alkyl, and subsequent hydride complexes, although in this case, a change in the reaction stoichiometry resulted in the ligand-bridged dinuclear complex **81**.[113-114]

79: X = -CH₂CH₂-; Ln = Sc, Y, Lu
cis-α-**80**: X = -CH₂CH₂CH₂-; Ln = Sc   *cis*-β-**80**: Ln = Y, Lu   **81**
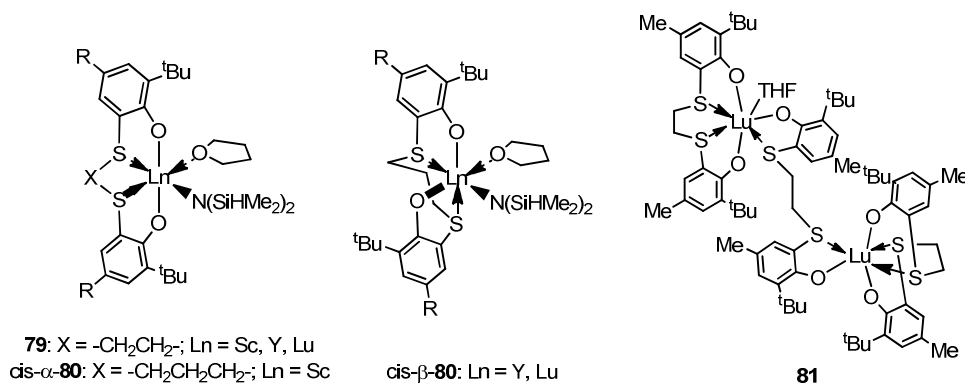
Scheme 1.16: Rare earth complexes of L⁹,¹¹.

Coordination of the analogous phosphoro bridged ligands H_2L^{12} to Zr exhibited clear dependence on the chirality of the ligand. *Rac*-**L¹²** was seen to adopt the *cis*-α coordination mode in both solid and solution states of the dichloro and dibenzyl complexes (**82**). On the other hand, the coordination of *meso*-**L¹²** resulted in the C_i-symmetric dinuclear dichloro complex **83** in the solid state, in which the ligand is seen to adopt the *cis*-β coordination mode at both Zr centres. However, in solution this species was shown to exist in equilibrium between the dimeric and monomeric states. The dibenzyl analogue was shown to be fluxional at room temperature but

adopts the *cis-β* conformation at low temperatures. The retention of ligand stereochemistry on coordination to Zr was attributed to a large barrier to inversion at the tertiary phosphorous groups.[132]

82: X = Cl, Bn

83
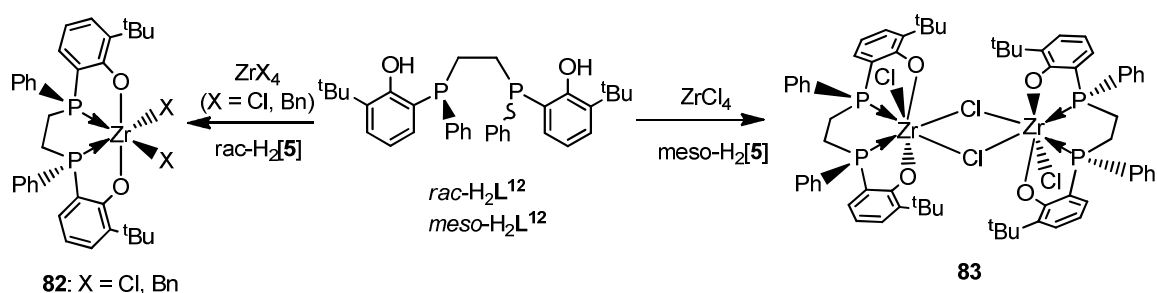
Scheme 1.17: Coordination of zirconium by *rac-* and *meso-*H₂L[12].

Bis(phenolate) ligands linked by N atoms within a carbon chain. In the last year, Okuda and co-workers have applied their structural knowledge of the sulphur-bridged ligands to systems where either one or both sulphur atoms are replaced by harder amine donors. The coordination of the unsubstituted diamine bis(phenolate) ligand H_2L^{13} to the Group 4 metals resulted only in complexes of the *cis-α* conformation (**84**), irrespective of other ligands present.[133] On the other hand, resultant products from the coordination of the methyl substituted ligand H_2L^{14} were shown to depend on the nature of the surrounding ligands. The isopropoxide complex occupies the *cis-α* conformation, as was seen in the case of the OSSO ligands[125], but a mixture of the two conformers *cis-α*-**85** and *cis-β*-**85** were initially observed for the dichloride complex.[133] Heating of this mixture eventually afforded the *cis-α*-**85** conformer exclusively. In the case of the mixed donor ligands $H_2L^{15,16}$, there is a rise in possible coordination geometries on coordination to Ti due to the unsymmetrical nature of the ligand, but in spite of this, only two were observed.[134] The dichloro complexes, in which the ligand amine group remains unsubstituted, favoured the *cis-β* conformation (**86**), while those containing a methyl group or larger on the ligand amine group (**87**) and all isopropoxide complexes (**88**) take on the *cis-α* conformation. This is in contrast with initial studies of the OSSO ligand system and the complexes of the ONNO ligands described above.
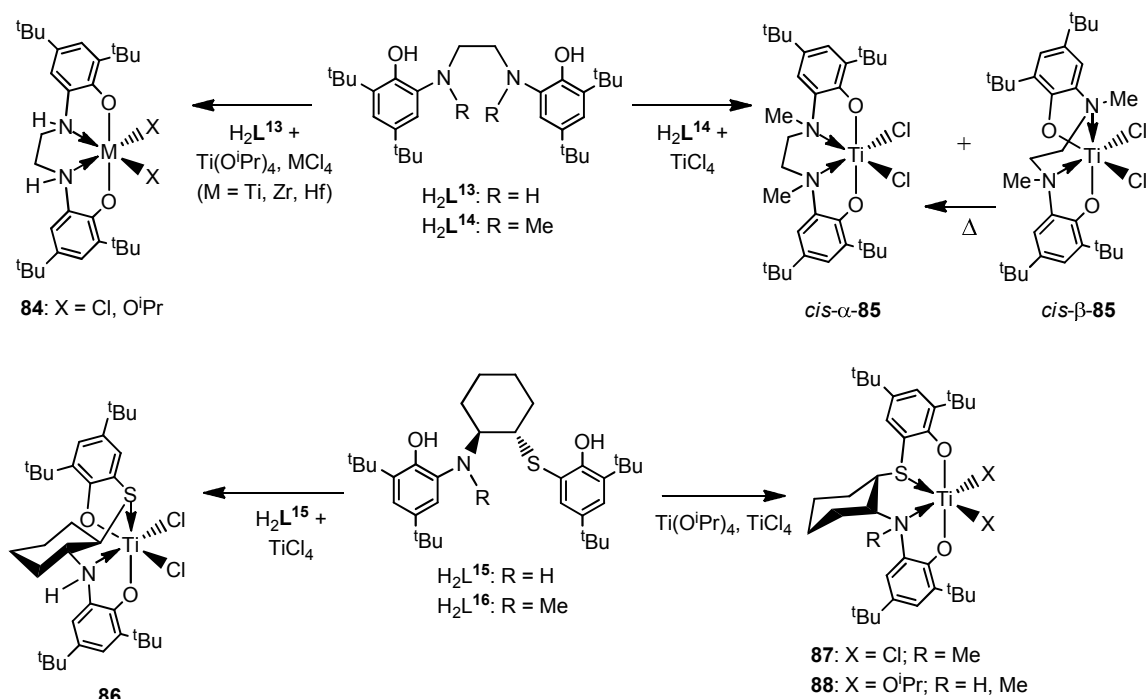
Scheme 1.18: Coordination of Group 4 metals by the ligands L[13-16].

Introduction of methylene linkers between the amine and phenolate moieties creates the diamine bis(phenolate) ligands H_2L^{17-20}. The longer backbone of this ligand system almost exclusively promotes the *trans*-O,O conformation on coordination with Group 4 metals, in which steric hinderance between the bulky phenolate groups is minimised.[49-50, 135] In an octahedral environment, ligands of this type can also be described as adopting a *fac,fac* coordination mode, in which the ligand backbone can twist to cover two faces of the octahedron. As was the case with other ONNO, OSSO and OSNO ligands described previously, a strong preference for monomeric complexes has been observed with the diamine bis(phenolate) ligands, making these complexes ideal candidates for catalytic applications. Indeed, the C_2-symmetry present in the Zr dibenzyl analogue of **89** promotes a high degree of isotactic stereocontrol in the polymerisation of 1-hexene, dependent on the presence of bulky tertiary butyl phenolate substituents.[136] Once again, the coordination of a chiral form of the ligand based around a *trans*-1,2-diaminocyclohexane bridge to the Group 4 metals was investigated. In the case of Ti, the presence of amine substituents within the ligand resulted in a mixture of two major products [(Λ,*R*,*R*)-**90** and (Δ,*R*,*R*)-**90**] and two minor products, whilst reaction of the unsubstituted ligands led to the isolation of only the Δ-(*R*,*R*) diastereomer (**91**).[137] In the case of Zr, this steric issue was not critical and the Δ-(*R*,*R*) diastereomer (**92**) was isolated from reaction of every ligand studied.[138] Reaction of two equivalents of H_2L^{18} with Zr(IV) sec-butoxide led to the isolation of the eight-coordinated bis-ligand complex **93**, in which each ligand retains the *trans*-O,O coordination mode, but binds the metal in a *trans mer,mer* fashion with all four donor atoms lying in a near-plane.[139] One exception to the common *trans*-O,O coordination mode was reported by

Tshuva and co-workers, in which reaction of the Ti isopropoxide analogue of **89** with one equivalent of ortho-catechol results in the complex **94**, in which the ligand motif coordinates in a *cis*-O,O manner.[140] Another example was reported by Tinoco and co-workers, in which the carboxylate groups were substituted onto the amine moieties creating a hexadentate ligand that wraps around the entire metal centre. In this way, the phenolate oxygens are forced to occupy positions *cis* to each other in the complex **95**.[141]
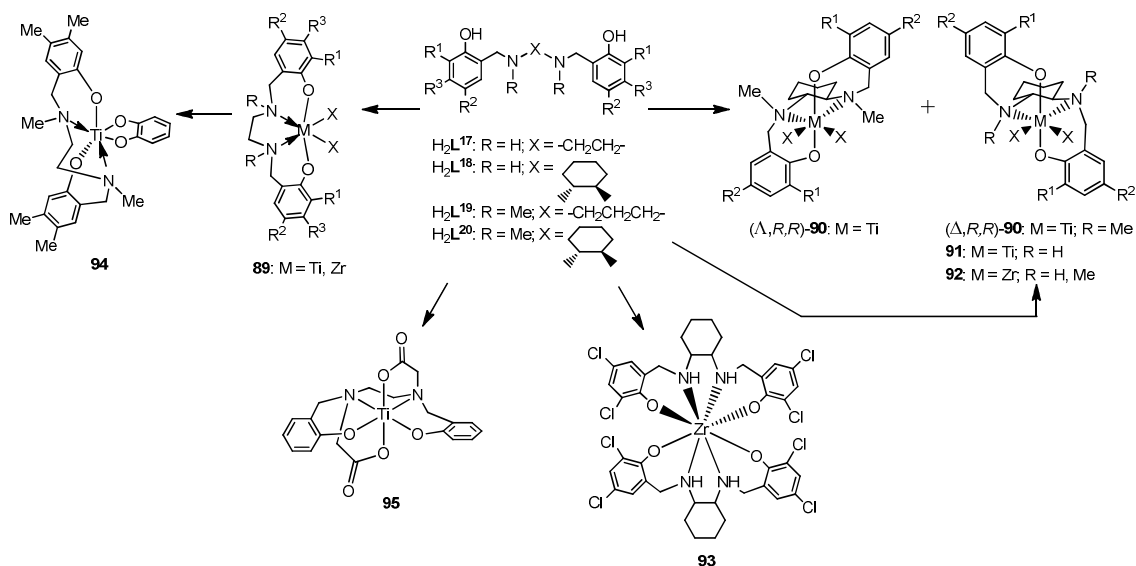
Scheme 1.19: Coordination of Group 4 metals by the diamine bis(phenolate) ligands L[17-20].

Reports of mulitnuclear Group 4 complexes involving the diamine bis(phenolate) ligands are limited, and involve reaction of monomeric complexes of the type **89** with controlled amounts of H_2O, forming oxo-bridged complexes. A distinct change in the coordination mode of the ligands from *trans*-O,O to *cis*-O,O was reported in the dinuclear complex (*R,R*)-**96**, reported by Sawada and co-workers within an investigation of asymmetric epoxidation of unfunctionalised olefins using aqueous hydrogen peroxide.[142] In addition, two of the three Ti centres in the trinuclear complex, **97**, reported as part of a study into the effect of structural parameters on cytotoxic activity of Ti complexes, adopted the new geometry.[140] The preference for di- or tri- nuclear complex formation is most likely dictated by the difference in ligand backbone and phenolate substituents.
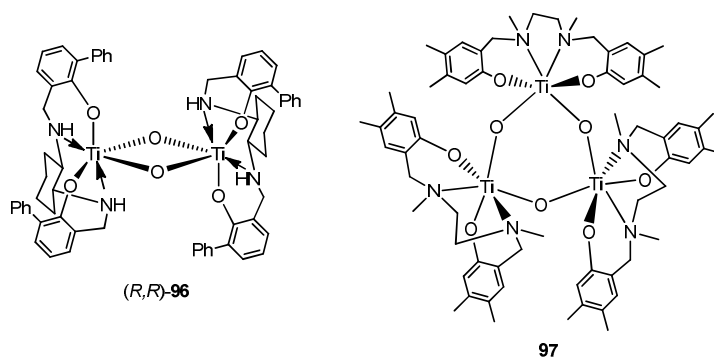
Scheme 1.20: Examples of multinuclear titanium complexes featuring the diamine bis(phenolate) ligands L[18,19].

Coordination of the diamine bis(phenolate) ligands L[17,19] to rare earth metals has been reported by various research groups, but structural information is limited and to date only one solid-state structure of a monomeric mono-ligand rare earth complex has been reported. Contrary to previous reports,[143] the ligand in the reported Y complex of the type **98** was shown to coordinate in a *cis*-O,O manner, and included no coordinated solvent molecules.[87] Addition of stoichiometric amounts of IPA, oxygen or water to monomeric complexes of the type **98** leads to the isolation of Y dimeric complexes of the type **99,** and the Lu dinuclear complex **100**, the X-ray crystal structures of which show the ligand motif remains coordinated in the sterically unfavourable *cis*-O,O manner.[144] Several interesting bis-ligand mononuclear rare earth complexes have also been reported in which the ligand motif adopts the more common *trans*-O,O coordination mode and binds in a *trans mer,mer* fashion (**101**).[145-146] In the cases involving Ln[3+], the non-bonding character of one phenolate group is actually shared between two adjacent ligand arms, resulting formally in half a proton at each site (**102**).[147-149]
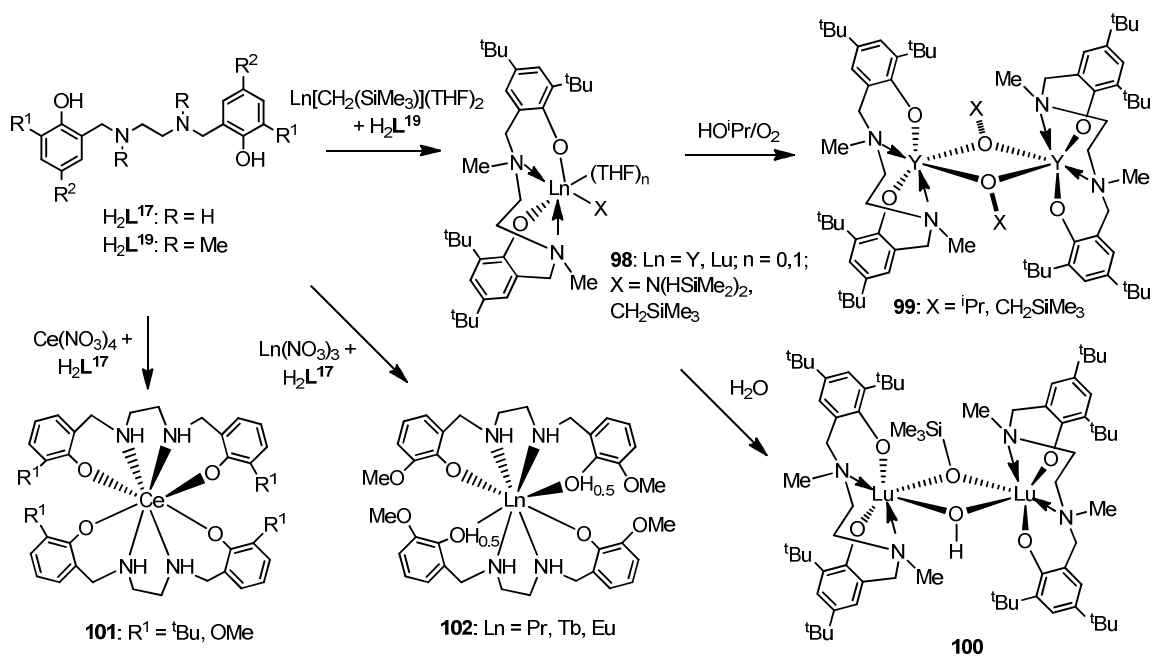
Scheme 1.21: Rare earth complexes featuring the diamine bis(phenolate) ligands L[17,19].

Bis(phenolate) ligands linked by a conjugated group in the carbon chain. The presence of a rigid conjugated group in the ligand backbone has been found to interfere with conventional modes of coordination. This is most commonly observed in the coordination of planar Salen-type ligands, described earlier in this chapter with respect to the use of their Al derivatives as stereoselective ROP initiators. Due to this, and a wealth of other potential applications, this is a very popular area of coordination chemistry that has been reviewed at length and therefore will not be included in this review.[150-152] A more relevant example is the ligand set H_2L^{21-23}, in which the two phenolate groups are linked by a pyridine, thiophene or furan group respectively.

Stoichiometric reaction of these ligands with tetrabenzyl Ti and Zr resulted in C_{2v}-symmetric 5-coordinate complexes of the type **103**, in which the tridentate ligand binds in a *mer* fashion.[153] In the case of the pyridine-linked ligand $\mathbf{L^{21}}$, increasing the stoichiometry of the ligand and the reaction time, results in bisligated octahedral complexes of type **104**, in which the two ligands bind in a *trans mer,mer* fashion.
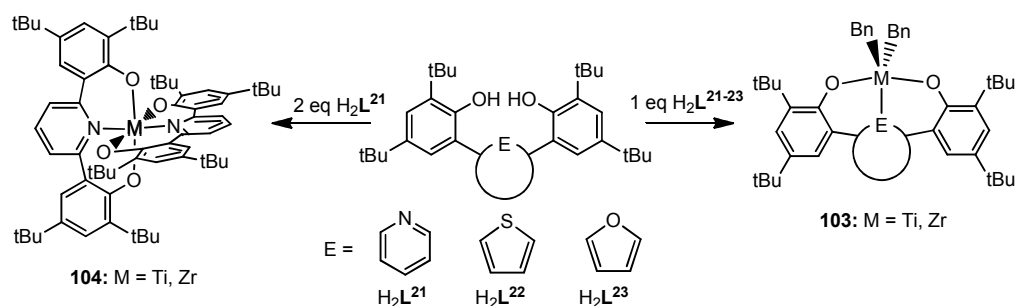
Scheme 1.22: Coordination of Group 4 metals with $\mathbf{L^{21-23}}$.

Inclusion of methylene or amine linkers do allow a degree of flexibility, as despite conformational strain arising from the backbone phenyl group, coordination of the ligand $\mathbf{H_2L^{24}}$ to Ti results in the C_2-symmetric *cis-α* coordinated titanium complex **105**.[154] Unlike, complexes of previously described diamine ligands, **105** was shown to be fluxional between the Δ and Λ forms on the NMR timescale at room temperature, and addition of a second equivalent of Ti(O^{i}Pr)$_4$ readily facilitated a transformation into the dinuclear complex **106**. Interestingly, this transformation was seen to be reversible, dependent on the addition of a further equivalent of ligand. These observations indicate that the formation of mononuclear complexes is not exceptionally favourable in the case of this ligand system.
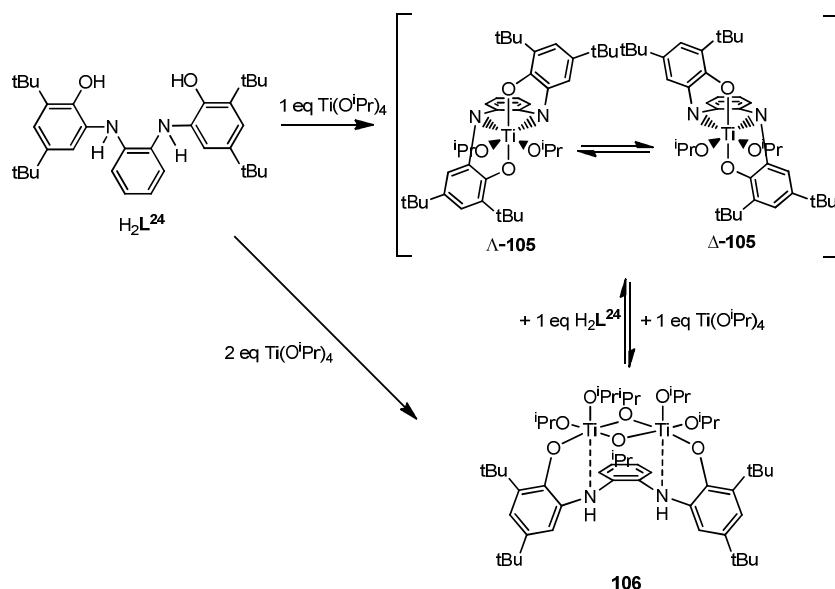
Scheme 1.23: Coordination of Group 4 metals by $\mathbf{L^{24}}$.

1.2.1.3. Tripod amine bis(phenolate) ligands

The coordination mode adopted by tripod amine bis(phenolate)s on binding to a Group 4 metal centre depends on the nature of the sidearm and the size of the ligand substituents. A non-bonding alkyl or aryl sidearm on a sterically unhindered ligand (H_2L^{25}: R^1 =Me) will lead to a bis-ligand complex of the type **107**, in which two ligand molecules bind in a *mer* fashion, creating an octahedral environment at the metal centre.[44, 48] An increase in sterics of the sidearm (H_2L^{26}) or phenolate arm (R^1 = ^tBu) will often result in a mono-ligand complex of the type **108**, which commonly adopts a distorted trigonal bypyramid environment, the exact nature of which depends on the other coordinating ligands present. Interestingly, addition of one equivalent of a sterically less demanding ligand to the stable penta-coordinate Ti isopropoxide analogue of **107** results in the isolation of the bis-ligand 'heteroleptic' Ti complex **109**, indicating that an octahedral environment is preferred to trigonal bipyramid, where sterics allow.[155] If the sidearm is substituted with a donor group (H_2L^{28-30}), the ligand becomes tetradentate in nature and adopts either a *trans*-O,O or *cis*-O,O conformation within an octahedral coordination sphere on complexation to Ti (**110**).[44-47, 50, 156-158] Although the majority of these complexes favour the *trans*-O,O ligand environment, reaction of the ligand H_2L^{30} with $Ti(NMe_2)_2Cl_2$ yields the Ti chlorinated analogue of *cis*-O,O-**110**.[159] Subsequent alkylation with MeMgBr was accompanied by a reversion in coordination mode to the *trans*-O,O methylated complex. Increasing the length of the donor terminated sidearm can have a detrimental effect on metal coordination, as binding does not occur through the $-CH_2CH_2CH_2NMe_2$ sidearm and a trigonal bypyramidal environment was again observed.[160]

H_2L^{25}: R^2 = Me
H_2L^{26}: R^2 = ^nPr
H_2L^{27}: R^2 = ^nBu
H_2L^{28}: R^2 = CH_2CH_2NMe
H_2L^{29}: R^2 = CH_2CH_2OMe
H_2L^{30}: R^2 = CH_2pyr

107: R^2 = Me
109: R^2 = ^nPr

trans-O,O-**110**

108

cis-O,O-**110**
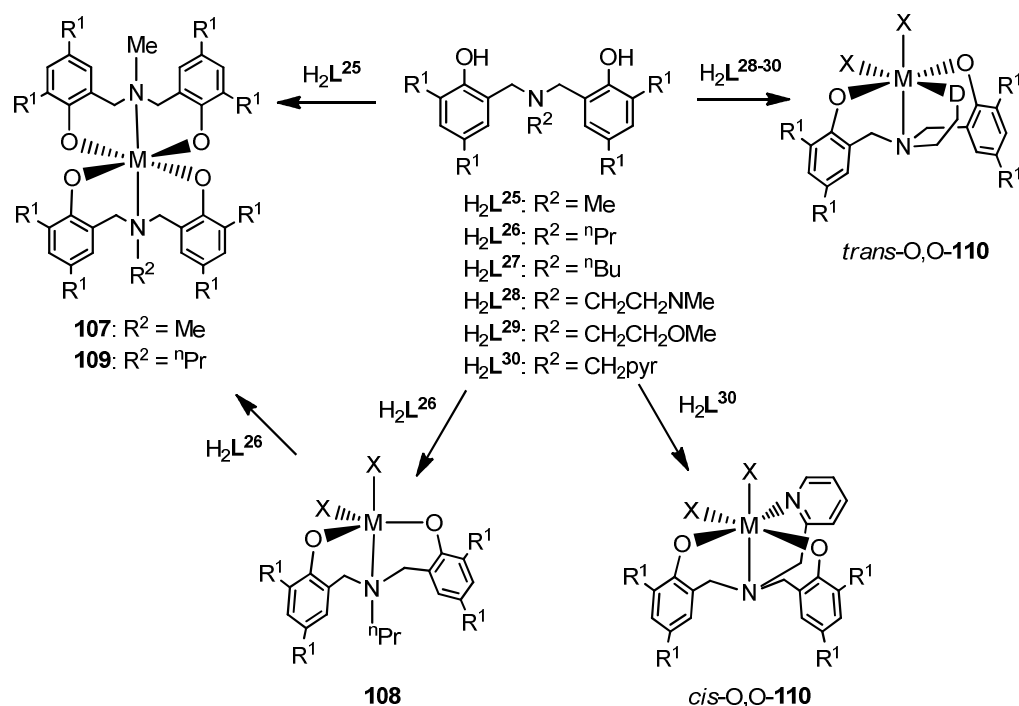
Scheme 1.24: Coordination of Group 4 metals by amine bis(phenolate) ligands.

43

The formation of dinuclear Ti complexes containing tripod amine bis(phenolate) ligands is relatively rare, but a number of examples have been reported in recent years. The oxo-bridged dinuclear complex **111**, in which both ligand molecules adopt a *cis*-O,O conformation results from reaction of a ligated Ti imine complex with CO_2.[159] Recent attempts to synthesise the dimethyl hydrazine analogue from the reaction of the ligated dimethyl amide complex with Me_2NNH_2 resulted instead in crystals of the unsymmetrical dinuclear complex **112**, in which one pyridal ligand sidearm decoordinates from a sterically crowded Ti centre.[161] Substitution of ligand sidearm from electronically neutral to anionic in nature, has also been shown to promote dimer formation. Reaction of the sterically unhindered ligand H_3L^{31} (R^1 = Me) with $Ti(OR)_4$ resulted in dimeric structures of the type **113**, within which both *cis*-O,O and *trans*-O,O coordination modes of the ligand were observed. The desired monomeric alkoxide complexes in this study were eventually obtained using a sterically more hindered ligand (R^1 = ^tBu).[162] A dinuclear Ti(III) complex containing an alkali metal (**114**) has also been reported from the reaction of the titanium isopropoxide analogue of **110** with sodium amalgam.[163]
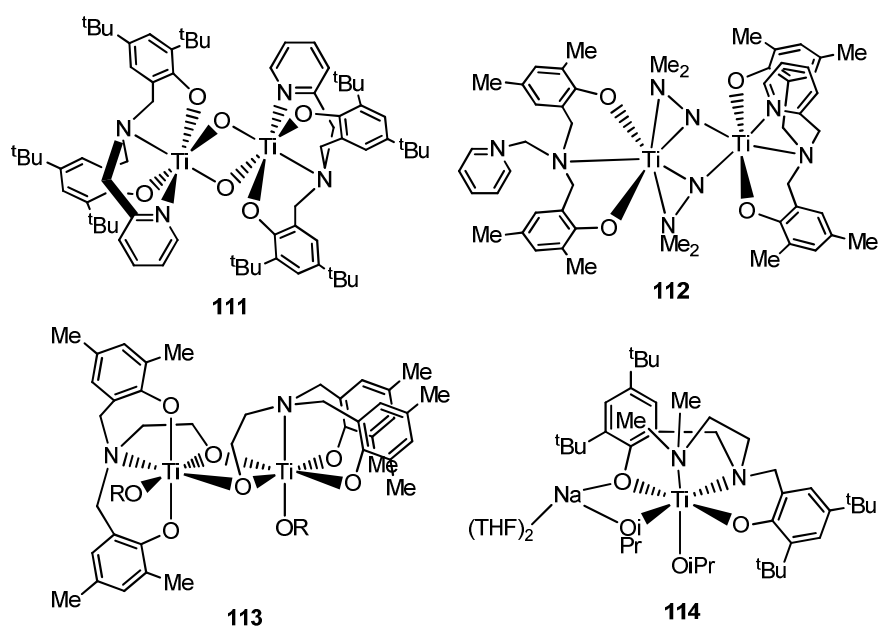
Scheme 1.25: Examples of dinuclear titanium complexes featuring tripod amine bis(phenolates).

Coordination modes in rare earth complexes of tripod amine bis(phenolates) are less dependent on the nature of the ligand sidearm, due to the tendency of rare earth metals towards highly saturated coordination spheres. This is well illustrated by the similarity in structures of the monomeric Yb(II) amine bis(phenolate) complexes **115** and **116**, both of which exhibit an octahedral environment at the metal centre despite the difference in binding tendency of the ligand sidearm.[164-165] However, an analogous synthetic procedure in which recrystallisation occurs from hexane instead of THF, yielded dimeric Yb(II) complexes of the type **117**.[166] Due to their increased ionic radii, dinuclear structures are more common in rare earth complexes of these ligands than is seen for Group 4 metals, and an analogous dimeric structure has been reported for

the Eu(II) complex.[165] However, no corresponding monomeric complex has been reported for Eu(II), arguably due to the increased ionic radius of Eu(II) compared to that of Yb(II). Reaction of the ligand H_2L^{27} with $Sm[N(SiMe_3)]_2(THF)_2$ resulted in the trinuclear mixed valent complex **118**, attributed to the lower oxidation potential of the Sm(II)/Sm(III) couple compared to the oxidation potential of the Yb(II)/Yb(III) couple.[165]
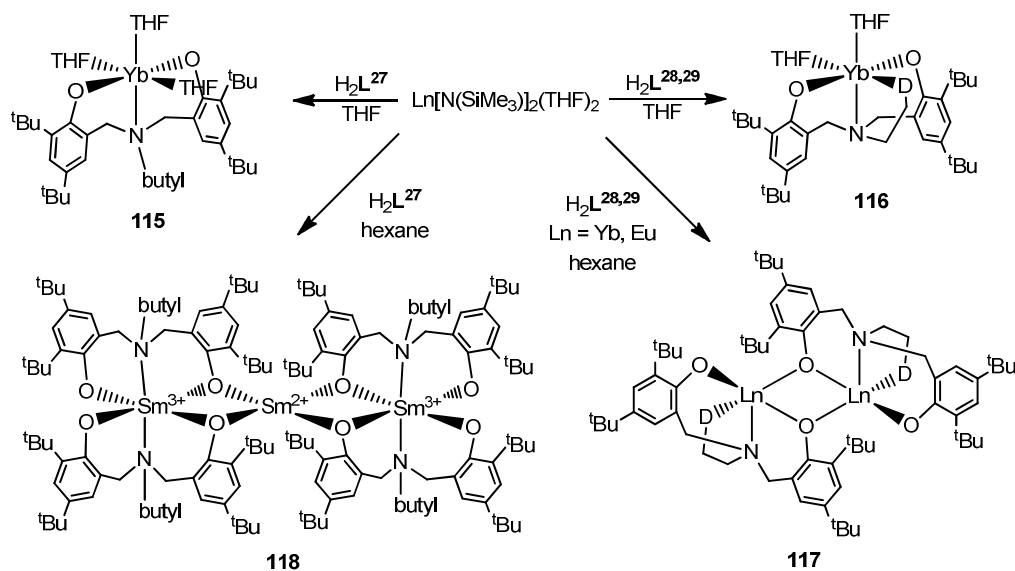
Scheme 1.26: Coordination of Ln^{2+} metals with amine bis(phenolates).

Trivalent rare earth complexes can be achieved by either the in-situ oxidation of the previously described dimers of the type **117**,[166] or by reaction of these ligands with trivalent rare earth starting materials. Several monomeric silyl amide and alkyl rare earth complexes have been reported both with and without coordinating solvent molecules, depending on the ionic radius of the rare earth metal and the solvent nature (**119**).[71, 77, 143, 166-167] On the other hand, the reaction of the ligands H_2L^{28-30} with rare earth tris-chlorides or borohydrides exhibits a strong tendency towards the formation of dimeric complexes.[78, 159, 168] In the majority of these cases, bridging occurs through the chloride or borohydride groups as occurs in complexes **120** and **121**, but in the case of Sc, bridging occurs through one phenolate arm of the ligand (**122**). The small ionic radius of Sc also allowed the pyridine-coordinated monomeric chloride complex of the type **123** to be isolated by direct protonolysis. Analogous monomeric complexes of larger rare earth metals can be synthesised by either salt elimination (Ln = Yb, Er)[169] or via the polymeric lithium precursor Li_2L^{28} (Ln = Y, Sm).[170-171] Dinuclear rare earth complexes containing alkali metals can be synthesised in a similar way via the reaction of Yb(III) chloride with the alkali metallated ligand precursor M_2L^{28} to form a series of bis-ligand monomeric complexes of the type **124**.[166, 172] One study worthy of particular mention was that of Mountford and co-workers, in which reaction of the ligands $H_2L^{26,28,29}$ with Sm resulted in the isolation of a bis-ligand rare earth complex **125**, in which the second ligand moiety is bound via a zwitterionic interaction.[79]
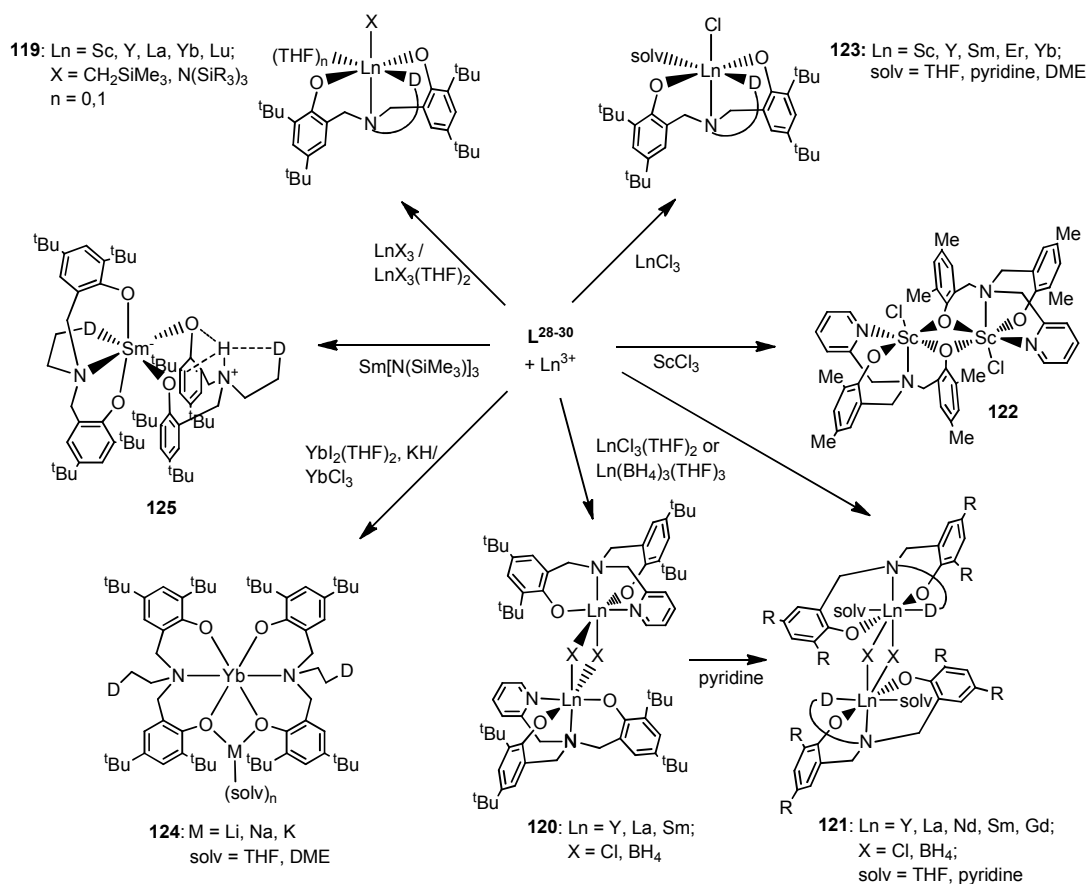
Scheme 1.27: Coordination of Ln^{3+} metals with amine bis(phenolates).

1.2.2. Tris(phenolate) ligands

The addition of a third phenolate group to the ligand structure either onto the *ortho*-position of a pre-existing group, leading to the open-chain tris(phenolate) ligands **L$^{31-32}$**, or via the linking moiety, leading to the tripod tris(phenolate) ligands, will now be discussed.

1.2.2.1.　　　*Open-chain tris(phenolate) ligands*

The coordination chemistry of Group 4 complexes of open-chain tris(phenolate) ligands H$_3$**L^{31}**, such as the Ti isopropoxide complexes **12a** and **12b** described in section 1.1.2.3., first reported by Hofmeister and co-workers, has recently been investigated in more detail by Kawaguchi and co-workers. Particular attention has been paid to the coordinative differences between the trianionic ligand H$_3$**L^{31}** and its selectively methylated dianionic counterpart H$_2$**L^{32}**. Reaction of **L^{32}** with ZrCl$_4$ in the presence of THF led to the isolation of the monomeric complex **127,**[173] in which the ligand adopts a U-conformation and binds in a *fac* manner, similar behaviour to the coordination of **L^{31}** to Ti (**126**).[174] In both cases, a dynamic equilibrium has been observed in the solution state between the monomeric and dimeric forms, dependent on the coordination of the THF moieties. The ligand motif has been shown to adopt the strained S-conformation in both the dinuclear complexes **128** and **129**, but the increased number of chloride ligands in the latter complex, as

46

well as the increased ionic radius of Zr, allows a (μ-Cl)$_2$ bridge to form between the metal centres. Reaction of **127** with LiBHEt$_3$ resulted in the identical tri-hydride dimeric complex, **130**, as had previously been isolated by reaction of the Zr analogue of **126**,[173, 175] in which both ligands revert back to the U-conformation. Benzylation of **127** results in the useful precursor **131**, which on reaction with H$_2$, forms the dinuclear complex **132** in quantitative yield – the first step in a Fischer-Tropsch cycle.[176]
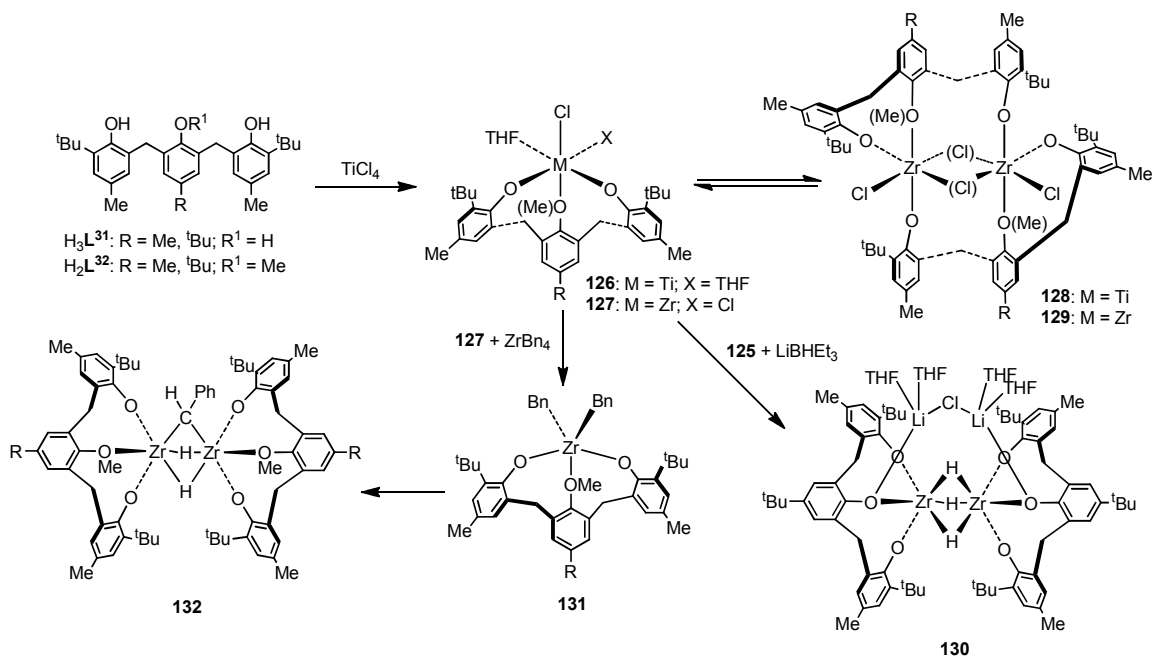
Scheme 1.28: Reaction of open-chain tris(phenolate) ligands.

1.2.2.2. Tripod tris(phenolate) ligands

The addition of a third phenolate group onto the bridging carbon of the ligand H$_2$**L**^{1} or the substitution of the sidearm of the amine bis(phenolate) ligands H$_2$**L**$^{25-30}$, leads to the tripodal trianionic tris(phenolate) ligands. Coordination of H$_3$**L**^{33} to Group 4 metals can occur in a number of ways, all of which have been exemplified by Kawaguchi and co-workers.[177] Amine elimination of Ti(NEt$_2$)$_4$ with H$_3$**L**^{33} leads to the isolation of *syn*-**133**, in which the methine proton interacts agnostically with the Ti centre. Heating of this complex resulted in conversion to *anti*-**133**, in which the proton is directed away from the titanium centre, indicating this to be the thermodynamically favoured product. Subsequent reaction with Me$_3$SiCl and PhCH$_2$MgCl led to the chloro and benzyl substituted analogues, both of which exhibit anti-geometry. However, reaction of H$_3$**L**^{33} with Zr(CH$_2$Ph)$_4$ in toluene/THF resulted in a mixture of *syn*-**134** and **135**, formation of the latter occurring via intramolecular C-H activation and the elimination of toluene. Modification of one phenolate arm to include an aryl imine group in the ortho position can alter the mode of coordination significantly, resulting in the zwitterionic Ti and Zr complexes **136**, in which each ligand binds through only two phenolate groups.[178] Substitution of the central

methine group in H_3L^{33} for an amine moiety produces the simplest amine tris(phenolate) H_3L^{35}. Coordination to titanium results in a five-membered ring titanotrane, most recently illustrated by the synthesis of the pentamethylcyclopentadienyl (Cp*) complex, **137**.[179] The interaction between the amine moiety and Ti in these complexes provides a barrier to inversion, and the distorted tetrahedral environment shown is always observed.
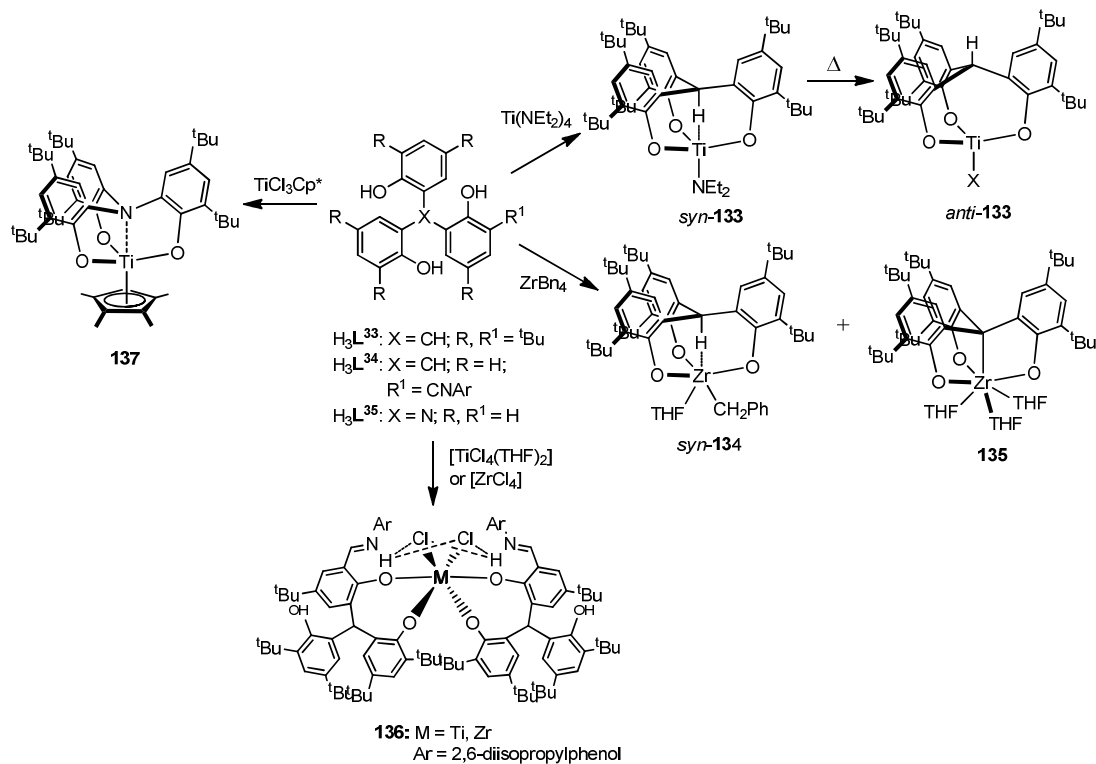
Scheme 1.29: Coordination of Group 4 metals by simple tris(phenolate) ligands.

1.2.2.3.   Amine tris(phenolate) ligands

Substitution of the sidearm of the tripodal amine bis(phenolate) ligands with a directly connected third phenolate group leads to the C_2-symmetric amine tris(phenolate) H_3L^{36}. Reaction of this ligand with Group 4 isopropoxides resulted in a series of monomeric Ti complexes **138**, and dimeric Zr complexes **139**, attributed to the larger ionic radius of Zr(IV).
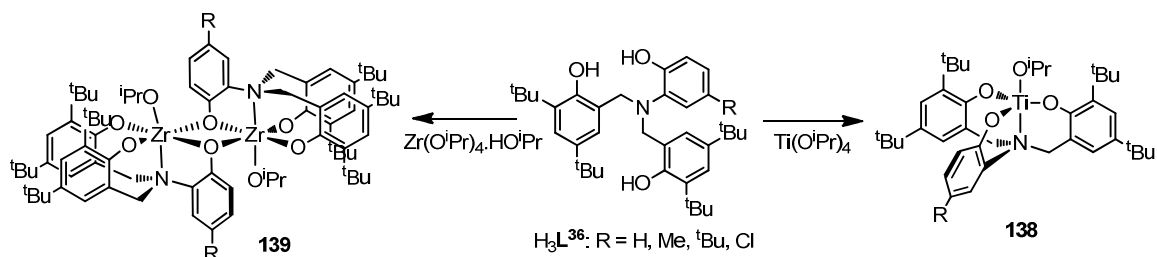
Scheme 1.30: Coordination of Group 4 metals by C_2-symmetric amine tris(phenolate) ligands.

C_3-symmetric amine tris(phenolate) ligands with a methylene linker between the amine and each phenolate group, H_3L^{37-42}, have received much more attention over recent years, and whilst only

their coordination to Group 4 metals will be covered here, a more comprehensive review has recently been published by Licini et al.[180] Reaction of H_3L^{37-42} with a number of Group 4 alkoxides yields a five-coordinate metallotrane featuring six-membered rings, the increased flexibility of which allows a 3-bladed propeller C_3-symmetric structure to be adopted. High barriers to inversion were observed between the enantiomeric forms P-**140** and M-**140** for Ti,[51, 57] while the Zr and Hf analogues exhibited fluxionality in solution at room temperature.[58, 181] Although no preference is shown between these two enantiomeric forms, the addition of a methyl group in the (R)-position of one methylene carbon forces this 'pseudo' C_3-symmetric complex to take the form (R,M)-**140**, in which the methyl group is axially positioned.[182] Coordination of sterically unhindered ligands of this nature (R^1, R^2 = Me) to Zr result in the bis-ligand zwitterionic complexes, **142**, in which each amine moiety becomes protonated and involved in trifuricated hydrogen bonding interactions with neighbouring phenolate groups.[181, 183-184] Sterically more hindered ligands ($R \geq {}^tBu$) are therefore required to isolate the mono-ligand Zr and Hf alkoxide complexes, in which a trigonal bipyramidal environment is observed at the metal centre.[58, 181]
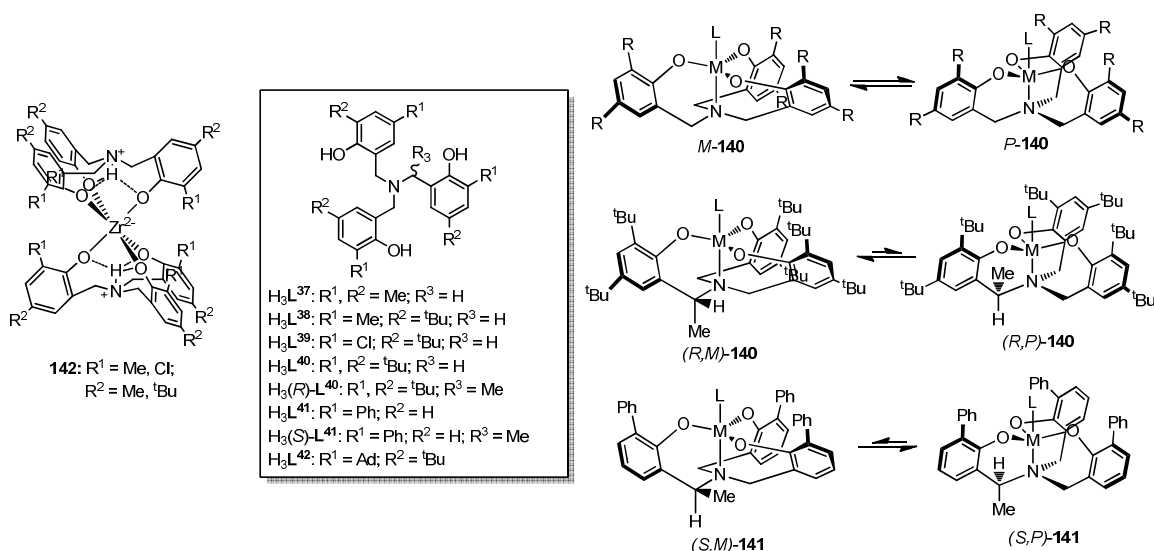
Scheme 1.31: Coordination of Group 4 metals by L^{37} - L^{42}.

Mono-ligand complexes with alternative apical groups can be achieved either by reaction of the ligand with alternative starting materials, such as $Ti(O^iPr)_3Cl$[185] and $TiCl_4(THF)_2$,[186] or by the subsequent reaction of the isopropoxide amine tris(phenolate) complex **143** with a more acidic reagent such as CF_3CO_2H,[187] $CF_3SO_3SiMe_3$.[188] Substitution of the apical alkoxide group in **143** with a number of bidentate, monoanionic ligands occurs readily to form octahedral, six-coordinate complexes **144**, in which inversion between the P and M enantiomers occurs more rapidly than is the case in five-coordinate complexes.[189] Substitution of the alkoxide has also been reported by a borohydride moiety to form **145**, in which the BH_4 group binds to Ti in a (μ-H_3) manner and subsequent reaction of **145** with PMe_3 resulted in the Ti(III) dimeric complex

146.[190] Other examples of Ti dinuclear complexes involving the amine tris(phenolate) motif have been reported, the most common being the oxo-bridged complexes **147**, a decomposition product of **143** in the presence of H_2O.[185, 188] There is little difference in these structures with the exception of a notably larger Ti-O-Ti bond angle in the sterically more hindered complex [Ti-O-Ti: 155.5(1)° (R^1 = ^tBu); 147.5(1)° (R^1 = Me)]. Indeed, the oxo-bridge in the complex featuring the phenyl-substituted ligand, **L⁴¹**, was shown to be linear, and the steric hindrance so great that only opposite enantiomeric forms of the monomer can be connected in such a fashion. Use of the enantiopure ligand $H_2(S)$-**L⁴¹** resulted in an enantiomerically pure monomeric complex which was shown to be stable to the reaction of water.[191] Also worthy of mention is the dinuclear Ti complex **148** formed from the reaction of **143** with dibenzyl phosphate, different from other dinuclear Ti complexes containing the amine tris(phenolate) ligand motif, as a pseudo C_3-symmetric conformation of the ligand is not observed.[189] Instead, both phenolate ligand arms adjacent to the phosphate groups are folded back, away from the bridging groups.
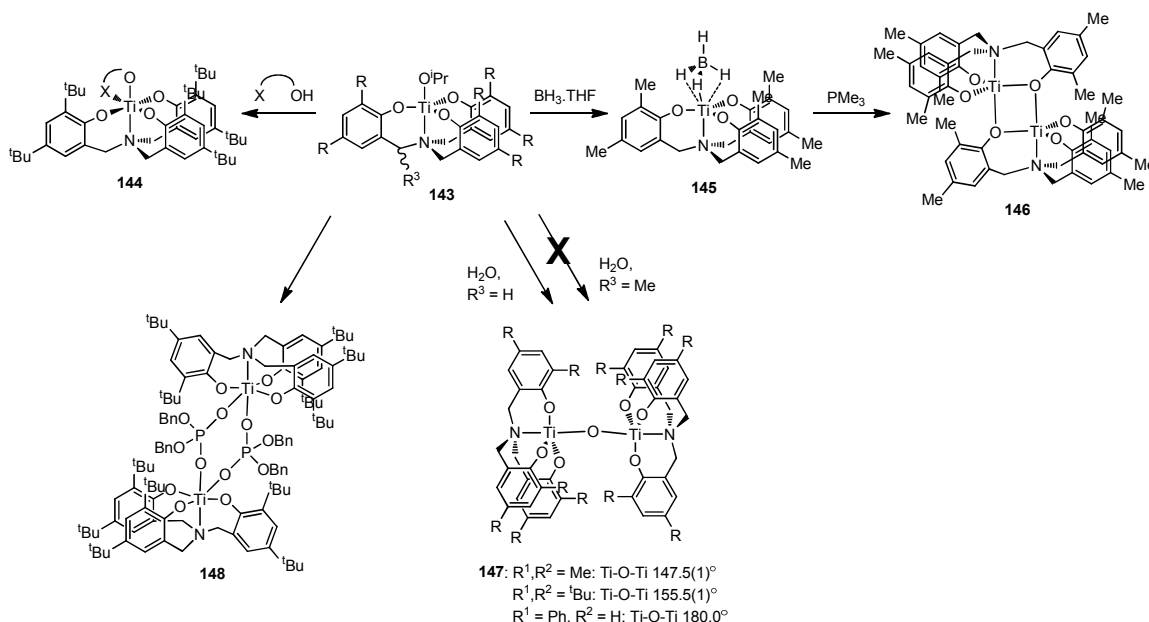
Scheme 1.32: Formation of dinuclear Ti complexes featuring the amine tris(phenolate) ligand.

1.2.3. Outlook

Recent developments in the coordination chemistry of poly(phenolate) ligands to Group 4 and rare earth metals have been rapid and plentiful, particularly in the search for olefin polymerisation catalysts and initiators for the ROP of cyclic esters, but also in more specialised applications, such as anti-cancer agents and redox-active systems. However, this area of coordination chemistry is still in its relative infancy, and several key areas are yet to be explored, most notably the coordination of amine tris(phenolate) ligands to the rare earth metals.

1.3. Research aims

Due to its renewable sourcing and eventual complete non-toxic degradation, the popularity of PLA has spread from commodity items to specialist biomedical applications, requiring a range of specific properties. In order to meet these requirements, there is a need for a synthetic route demonstrating consistent control of molecular weight and stereoselectivity, which can be easily integrated into current large-scale PLA production. The development of a well defined, non-toxic, single site initiator, capable of such high control is therefore required. Alternatively, in the case of isotactic or stereoblock PLA, or PLA copolymers, properties can be tailored post-synthesis via stereocomplexation, resulting in improved thermal and mechanical performance. The aim of the work reported within this thesis can therefore be described as multifold:

(i) Following recent success in this field from the use of a number of Group 4 complexes featuring various poly(phenolate) ligand motifs, our investigations will begin by elaborating on recent reports of the remarkable combination of activity, molecular weight and stereocontrol afforded by the amine tris(phenolate) coordinated Zr and Hf initiators.[58] The effect of variation of ligand substituents, on both complex structure and resulting control of ROP, will be investigated, followed by variation of the initiating group present. It is hoped that the latter factor will open this system up to new polymer applications, including the use of these initiators in the macroinitiation of short-chain polymers in the synthesis of block co-polymers.

(ii) The use of these initiators in the production of well-defined biodegradable polymers which can be further manipulated via stereocomplexation to match the desired properties of a specific application will also be investigated. This will include a novel one-pot method of stereo multi-block synthesis, capitalising on the unprecedented kinetic and stereoselective properties of this initiator system.

(iii) Following the recent interest in rare earth metals in initiator design, it is somewhat surprising that the coordination of this series of ligands to Group 3 metals and lanthanides has not been documented. Straightforward complexation of these trianionic ligands to Ln^{3+} would result in a lack of initiating group, but recent literature has shown how diverse the coordination chemistry of the rare earth metals can be. The presence of coordinating solvents and formation of dinuclear and zwitterionic complexes have all recently been reported and, in this instance, could lead to potential ROP initiators.

1.4. References

1.   Albertsson, A. C.; Varma, I. K., *Biomacromolecules* **2003,** *4* (6), 1466-1486.
2.   Dechy-Cabaret, O.; Martin-Vaca, B.; Bourissou, D., *Chem. Rev.* **2004,** *104* (12), 6147-6176.
3.   Athanasiou, K. A.; Niederauer, G. G.; Agrawal, C. M., *Biomaterials* **1996,** *17* (2), 93-102.
4.   Williams, C. K.; Hillmyer, M. A., *Polym. Rev.* **2008,** *48* (1), 1-10.
5.   NatureWorks LLC. http://www.natureworksllc.com/news-and-events/press-releases/2009/07-07-09-capacity-expansion.aspx (accessed August 24 2010).
6.   Purac. http://www.purac.com/EN/About_us/News/Press-release-Purac-to-build-new-lactide-plant.aspx (accessed August 24 2010).
7.   Schwach, G.; Coudane, J.; Engel, R.; Vert, M., *J. Polym. Sci., Part A: Polym. Chem.* **1997,** *35* (16), 3431-3440.
8.   Kricheldorf, H. R.; Kreisersaunders, I.; Boettcher, C., *Polymer* **1995,** *36* (6), 1253-1259.
9.   Chisholm, M. H.; Zhou, Z. P., *J. Mater. Chem.* **2004,** *14* (21), 3081-3092.
10.   Chisholm, M. H.; Delbridge, E. E., *New J. Chem.* **2003,** *27* (8), 1167-1176.
11.   Bero, M.; Kasperczyk, J., *Macromol. Chem. Phys.* **1996,** *197* (10), 3251-3258.
12.   Dove, A. P., *Chem. Commun.* **2008,** (48), 6446-6470.
13.   Chamberlain, B. M.; Cheng, M.; Moore, D. R.; Ovitt, T. M.; Lobkovsky, E. B.; Coates, G. W., *J. Am. Chem. Soc.* **2001,** *123* (14), 3229-3238.
14.   Ovitt, T. M.; Coates, G. W., *J. Am. Chem. Soc.* **1999,** *121* (16), 4072-4073.
15.   Chisholm, M. H.; Iyer, S. S.; Matison, M. E.; McCollum, D. G.; Pagel, M., *Chemical Communications* **1997,** (20), 1999-2000.
16.   Thakur, K. A. M.; Kean, R. T.; Zell, M. T.; Padden, B. E.; Munson, E. J., *Chemical Communications* **1998,** (17), 1913-1914.
17.   Zell, M. T.; Padden, B. E.; Paterick, A. J.; Thakur, K. A. M.; Kean, R. T.; Hillmyer, M. A.; Munson, E. J., *Macromolecules* **2002,** *35* (20), 7700-7707.
18.   Bovey, F. A., *NMR of Polymers*. Academic Press, Inc.: 1996.
19.   Kowalski, A.; Duda, A.; Penczek, S., *Macromol. Rapid Commun.* **1998,** *19* (11), 567-572.
20.   Nijenhuis, A. J.; Grijpma, D. W.; Pennings, A. J., *Macromolecules* **1992,** *25* (24), 6419-6424.
21.   Rafler, G.; Dahlmann, J., *Acta Polym.* **1992,** *43* (2), 91-95.
22.   Platel, R. H.; Hodgson, L. M.; Williams, C. K., *Polym. Rev.* **2008,** *48* (1), 11-63.
23.   Pietrangelo, A.; Hillmyer, M. A.; Tolman, W. B., *Chem. Commun.* **2009,** (19), 2736-2737.
24.   Stanford, M. J.; Dove, A. P., *Chem. Soc. Rev.* **2010,** *39* (2), 486-494.
25.   Chisholm, M. H.; Gallucci, J.; Phomphrai, K., *Inorg. Chem.* **2002,** *41* (10), 2785-2794.
26.   Chisholm, M. H.; Gallucci, J.; Phomphrai, K., *Chem. Commun.* **2003,** (1), 48-49.
27.   Chisholm, M. H.; Gallucci, J. C.; Phomphrai, K., *Inorg. Chem.* **2004,** *43* (21), 6717-6725.
28.   Spassky, N.; Wisniewski, M.; Pluta, C.; LeBorgne, A., *Macromol. Chem. Phys.* **1996,** *197* (9), 2627-2637.
29.   Wisniewski, M.; LeBorgne, A.; Spassky, N., *Macromol. Chem. Phys.* **1997,** *198* (4), 1227-1238.
30.   Ovitt, T. M.; Coates, G. W., *J. Am. Chem. Soc.* **2002,** *124* (7), 1316-1326.
31.   Zhong, Z. Y.; Dijkstra, P. J.; Feijen, J., *Angew. Chem., Int. Ed.* **2002,** *41* (23), 4510-4513.
32.   Chisholm, M. H.; Gallucci, J. C.; Quisenberry, K. T.; Zhou, Z. P., *Inorg. Chem.* **2008,** *47* (7), 2613-2624.
33.   Nomura, N.; Ishii, R.; Akakura, M.; Aoi, K., *J. Am. Chem. Soc.* **2002,** *124* (21), 5938-5939.
34.   Nomura, N.; Ishii, R.; Yamamoto, Y.; Kondo, T., *Chem.--Eur. J.* **2007,** *13* (16), 4433-4451.
35.   Hormnirun, P.; Marshall, E. L.; Gibson, V. C.; White, A. J. P.; Williams, D. J., *J. Am. Chem. Soc.* **2004,** *126* (9), 2688-2689.

36.   Takeuchi, D.; Nakamura, T.; Aida, T., *Macromolecules* **2000,** *33* (3), 725-729.

37.   Takashima, Y.; Nakayama, Y.; Hirao, T.; Yasuda, H.; Harada, A., *J. Organomet. Chem.* **2004,** *689* (3), 612-619.

38.   Nakayama, Y.; Watanabe, K.; Ueyama, N.; Nakamura, A.; Harada, A.; Okuda, J., *Organometallics* **2000,** *19* (13), 2498-2503.

39.   Takashima, Y.; Nakayama, Y.; Watanabe, K.; Itono, T.; Ueyama, N.; Nakamura, A.; Yasuda, H.; Harada, A.; Okuda, J., *Macromolecules* **2002,** *35* (20), 7538-7544.

40.   Appiah, W. O.; DeGreef, A. D.; Razidlo, G. L.; Spessard, S. J.; Pink, M.; Young, V. G., Jr; Hofmeister, G. E., *Inorganic Chemistry* **2002,** (41), 3656-3667.

41.   Russell, S. K.; Gamble, C. L.; Gibbins, K. J.; Juhl, K. C. S.; Mitchell, W. S.; Tumas, A. J.; Hofmeister, G. E., *Macromolecules* **2005,** *38* (24), 10336-10340.

42.   Gregson, C. K. A.; Blackmore, I. J.; Gibson, V. C.; Long, N. J.; Marshall, E. L.; White, A. J. P., *Dalton Trans.* **2006,** (25), 3134-3140.

43.   Cameron, P. A.; Jhurry, D.; Gibson, V. C.; White, A. J. P.; Williams, D. J.; Williams, S., *Macromol. Rapid Commun.* **1999,** *20* (12), 616-618.

44.   Tshuva, E. Y.; Versano, M.; Goldberg, I.; Kol, M.; Weitman, H.; Goldschmidt, Z., *Inorg. Chem. Commun.* **1999,** *2* (8), 371-373.

45.   Tshuva, E. Y.; Goldberg, I.; Kol, M.; Goldschmidt, Z., *Inorg. Chem. Commun.* **2000,** *3* (11), 611-614.

46.   Tshuva, E. Y.; Goldberg, I.; Kol, M.; Weitman, H.; Goldschmidt, Z., *Chem. Commun.* **2000,** (5), 379-380.

47.   Groysman, S.; Goldberg, I.; Kol, M.; Genizi, E.; Goldschmidt, Z., *Inorg. Chim. Acta* **2003,** *345*, 137-144.

48.   Chmura, A. J.; Davidson, M. G.; Jones, M. D.; Lunn, M. D.; Mahon, M. F., *Dalton Trans.* **2006,** (7), 887-889.

49.   Gendler, S.; Segal, S.; Goldberg, I.; Goldschmidt, Z.; Kol, M., *Inorg. Chem.* **2006,** *45* (12), 4783-4790.

50.   Chmura, A. J.; Davidson, M. G.; Jones, M. D.; Lunn, M. D.; Mahon, M. F.; Johnson, A. F.; Khunkamchoo, P.; Roberts, S. L.; Wong, S. S. F., *Macromolecules* **2006,** *39* (21), 7250-7257.

51.   Kim, Y.; Verkade, J. G., *Organometallics* **2002,** *21* (12), 2395-2399.

52.   Kim, Y. J.; Verkade, J. G., *Macromol. Rapid Commun.* **2002,** *23* (15), 917-921.

53.   Kim, Y.; Jnaneshwara, G. K.; Verkade, J. G., *Inorg. Chem.* **2003,** *42* (5), 1437-1447.

54.   Kim, Y.; Verkade, J. G., *Macromol. Symp.* **2005,** *224*, 105-117.

55.   Naiini, A. A.; Ringrose, S. L.; Su, Y.; Jacobson, R. A.; Verkade, J. G., *Inorg. Chem.* **1993,** *32* (7), 1290-1296.

56.   Boyle, T. J.; Schwartz, R. W.; Doedens, R. J.; Ziller, J. W., *Inorg. Chem.* **1995,** *34* (5), 1110-1120.

57.   Kol, M.; Shamis, M.; Goldberg, I.; Goldschmidt, Z.; Alfi, S.; Hayut-Salant, E., *Inorg. Chem. Commun.* **2001,** *4* (4), 177-179.

58.   Chmura, A. J.; Davidson, M. G.; Frankis, C. J.; Jones, M. D.; Lunn, M. D., *Chem. Commun.* **2008,** (11), 1293-1295.

59.   McLain, S. J.; Ford, T. M.; Drysdale, N. E., *Polym. Prepr. (Am. Chem. Soc., Div. Polym. Chem.)* **1992,** *33*, 463.

60.   Stevels, W. M.; Ankone, M. J. K.; Dijkstra, P. J.; Feijen, J., *Macromolecules* **1996,** *29* (9), 3332-3333.

61.   Stevels, W. M.; Ankone, M. J. K.; Dijkstra, P. J.; Feijen, J., *Macromolecules* **1996,** *29* (19), 6132-6138.

62.   Poncelet, O.; Sartain, W. J.; Hubertpfalzgraf, L. G.; Folting, K.; Caulton, K. G., *Inorg. Chem.* **1989,** *28* (2), 263-267.

63.   Simic, V.; Spassky, N.; HubertPfalzgraf, L. G., *Macromolecules* **1997,** *30* (23), 7338-7340.

64.   Fan, L.; Xiong, Y. B.; Xu, H.; Shen, Z. Q., *Eur. Polym. J.* **2005,** *41* (7), 1647-1653.

65.   Aubrecht, K. B.; Chang, K.; Hillmyer, M. A.; Tolman, W. B., *J. Polym. Sci., Part A: Polym. Chem.* **2001,** *39* (2), 284-293.

66.   Ajellal, N.; Lyubov, D. M.; Sinenkov, M. A.; Fukin, G. K.; Cherkasov, A. V.; Thomas, C. M.; Carpentier, J. F.; Trifonov, A. A., *Chem.--Eur. J.* **2008,** *14* (18), 5440-5448.

67.   Platel, R. H.; White, A. J. P.; Williams, C. K., *Chem. Commun.* **2009,** (27), 4115-4117.

68.   Platel, R. H.; White, A. J. P.; Williams, C. K., *Inorg. Chem.* **2008,** *47* (15), 6840-6849.

69.   Platel, R. H.; Hodgson, L. M.; White, A. J. P.; Williams, C. K., *Organometallics* **2007,** *26* (20), 4955-4963.

70.   Heck, R.; Schulz, E.; Collin, J.; Carpentier, J. F., *J. Mol. Catal. A: Chem.* **2007,** *268* (1-2), 163-168.

71.   Amgoune, A.; Thomas, C. M.; Roisnel, T.; Carpentier, J. F., *Chem.--Eur. J.* **2006,** *12* (1), 169-179.

72.   Ma, H. Y.; Okuda, J., *Macromolecules* **2005,** *38* (7), 2665-2673.

73.   Arnold, P. L.; Buffet, J. C.; Blaudeck, R. P.; Sujecki, S.; Blake, A. J.; Wilson, C., *Angew. Chem., Int. Ed.* **2008,** *47* (32), 6033-6036.

74.   Ma, H. Y.; Spaniol, T. P.; Okuda, J., *Dalton Trans.* **2003,** (24), 4770-4780.

75.   Ma, H. Y.; Spaniol, T. P.; Okuda, J., *Angew. Chem., Int. Ed.* **2006,** *45* (46), 7818-7821.

76.   Marshall, E. L.; Gibson, V. C.; Rzepa, H. S., *J. Am. Chem. Soc.* **2005,** *127* (16), 6048-6051.

77.   Cai, C. X.; Amgoune, A.; Lehmann, C. W.; Carpentier, J. F., *Chem. Commun.* **2004,** (3), 330-331.

78.   Bonnet, F.; Cowley, A. R.; Mountford, P., *Inorg. Chem.* **2005,** *44* (24), 9046-9055.

79.   Dyer, H. E.; Huijser, S.; Schwarz, A. D.; Wang, C.; Duchateau, R.; Mountford, P., *Dalton Trans.* **2008,** (1), 32-35.

80.   Clark, L.; Cushion, M. G.; Dyer, H. E.; Schwarz, A. D.; Duchateau, R.; Mountford, P., *Chem. Commun.* **2010,** *46* (2), 273-275.

81.   Ikada, Y.; Jamshidi, K.; Tsuji, H.; Hyon, S. H., *Macromolecules* **1987,** *20* (4), 904-906.

82.   Sarasua, J. R.; Rodriguez, N. L.; Arraiza, A. L.; Meaurio, E., *Macromolecules* **2005,** *38* (20), 8362-8371.

83.   Tsuji, H., *Macromol. Biosci.* **2005,** *5* (7), 569-597.

84.   Fukushima, K.; Kimura, Y., *Polym. Int.* **2006,** *55* (6), 626-642.

85.   Yui, N.; Dijkstra, P. J.; Feijen, J., *Makromol. Chem., Macromol. Chem. Phys.* **1990,** *191* (3), 481-488.

86.   Radano, C. P.; Baker, G. L.; Smith, M. R., *J. Am. Chem. Soc.* **2000,** *122* (7), 1552-1553.

87.   Kramer, J. W.; Treitler, D. S.; Dunn, E. W.; Castro, P. M.; Roisnel, T.; Thomas, C. M.; Coates, G. W., *J. Am. Chem. Soc.* **2009,** *131* (44), 16042-+.

88.   Muller, A. H. E.; Matyjaszewski, K., *Controlled and Living Polymerisations: From Mechanisms to Applications*. Wiley: Weinham, Germany, 2009.

89.   Hadjichristidis, N.; Pispas, S.; Floudas, G. A., *Block Copolymers: Synthetic Strategies, Physical Properties, and Applications*. Wiley: Hoboken, New Jersey, 2003.

90.   Pensec, S.; Leroy, M.; Akkouche, H.; Spassky, N., *Polym. Bull.* **2000,** *45* (4-5), 373-380.

91.   Kricheldorf, H. R.; Rost, S.; Wutz, C.; Domb, A., *Macromolecules* **2005,** *38* (16), 7018-7025.

92.   Stevels, W. M.; Ankone, M. J. K.; Dijkstra, P. J.; Feijen, J., *Macromol. Chem. Phys.* **1995,** *196* (11), 3687-3694.

93.   Stevels, W. M.; Ankone, M. J. K.; Dijkstra, P. J.; Feijen, J., *Macromol. Symp.* **1996,** *102*, 107-113.

94.   Portinha, D.; Belleney, J.; Bouteiller, L.; Pensec, S.; Spassky, N.; Chassenieux, C., *Macromolecules* **2002,** *35* (5), 1484-1486.

95.   Portinha, D.; Bouteiller, L.; Pensec, S.; Richez, A.; Chassenieux, C., *Macromolecules* **2004,** *37* (9), 3401-3406.

96.   Fujiwara, T.; Mukose, T.; Yamaoka, T.; Yamane, H.; Sakurai, S.; Kimura, Y., *Macromol. Biosci.* **2001,** *1* (5), 204-208.

97.   Mukose, T.; Fujiwara, T.; Nakano, J.; Taniguchi, I.; Miyamoto, M.; Kimura, Y.; Teraoka, I.; Lee, C. W., *Macromol. Biosci.* **2004,** *4* (3), 361-367.

98.   Riley, T.; Stolnik, S.; Heald, C. R.; Xiong, C. D.; Garnett, M. C.; Illum, L.; Davis, S. S.; Purkiss, S. C.; Barlow, R. J.; Gellert, P. R., *Langmuir* **2001,** *17* (11), 3168-3174.

99.   Kang, N.; Perron, M. E.; Prud'homme, R. E.; Zhang, Y. B.; Gaucher, G.; Leroux, J. C., *Nano Lett.* **2005,** *5* (2), 315-319.

100.   Kim, S. H.; Tan, J. P. K.; Nederberg, F.; Fukushima, K.; Yang, Y. Y.; Waymouth, R. M.; Hedrick, J. L., *Macromolecules* **2009,** *42* (1), 25-29.

101.   Kawaguchi, H.; Matsuo, T., *J. Organomet. Chem.* **2004,** *689* (24), 4228-4243.

102.   Zhang, D., *Eur. J. Inorg. Chem.* **2007,** (19), 3077-3082.

103.   Zhang, D., *Organometallics* **2007,** *26* (16), 4072-4075.

104.   Xu, X. P.; Ma, M. T.; Yao, Y. M.; Zhang, Y.; Shen, Q., *J. Mol. Struct.* **2005,** *743* (1-3), 163-168.

105.   Xu, X. P.; Ma, M. T.; Yao, Y. M.; Zhang, Y.; Shen, Q., *Eur. J. Inorg. Chem.* **2005,** (4), 676-684.

106.   Yao, Y. M.; Xu, X. P.; Liu, B.; Zhang, Y.; Shen, Q.; Wong, W. T., *Inorg. Chem.* **2005,** *44* (14), 5133-5140.

107.   Xu, X. P.; Yao, Y. M.; Hu, M. Y.; Zhang, Y.; Shen, Q., *J. Polym. Sci., Part A: Polym. Chem.* **2006,** *44* (15), 4409-4419.

108.   Xu, X. P.; Hu, M. Y.; Yao, Y. M.; Qi, R. P.; Zhang, Y.; Shen, Q., *J. Mol. Struct.* **2007,** *829* (1-3), 189-194.

109.   Qi, R. P.; Liu, B.; Xu, X. P.; Yang, Z. J.; Yao, Y. M.; Zhang, Y.; Shen, Q., *Dalton Trans.* **2008,** (37), 5016-5024.

110.   Xu, X. P.; Zhang, Z. J.; Yao, Y. M.; Zhang, Y.; Shen, Q., *Inorg. Chem.* **2007,** *46* (22), 9379-9388.

111.   Maestri, A. G.; Brown, S. N., *Inorg. Chem.* **2004,** *43* (22), 6995-7004.

112.   Miyatake, T.; Mizunuma, K.; Seki, Y.; Kakugo, M., *Makromol. Chem., Rapid Commun.* **1989,** *10* (7), 349-352.

113.   Konkol, M.; Spaniol, T. P.; Kondracka, M.; Okuda, J., *Dalton Trans.* **2007,** (36), 4095-4102.

114.   Konkol, M.; Kondracka, M.; Voth, P.; Spaniol, T. P.; Okuda, J., *Organometallics* **2008,** *27* (15), 3774-3784.

115.   Janas, Z.; Jerzykiewicz, L. B.; Przybylak, K.; Sobota, P.; Szczegot, K., *Eur. J. Inorg. Chem.* **2004,** (8), 1639-1645.

116.   Janas, Z.; Jerzykiewicz, L. B.; Przybylak, K.; Sobota, P.; Szczegot, K.; Wisniewska, D., *Eur. J. Inorg. Chem.* **2005,** (6), 1063-1070.

117.   Janas, Z.; Godbole, D.; Nerkowski, T.; Szczegot, K., *Dalton Trans.* **2009,** (41), 8846-8853.

118.   Wisniewska, D.; Janas, Z.; Sobota, P.; Jerzykiewicz, L. B., *Organometallics* **2006,** *25* (26), 6166-6169.

119.   Natrajan, L. S.; Wilson, C.; Okuda, J.; Arnold, P. L., *Eur. J. Inorg. Chem.* **2004,** (18), 3724-3732.

120.   Natrajan, L. S.; Blake, A. J.; Wilson, C.; Weinstein, J. A.; Arnold, P. L., *Dalton Trans.* **2004,** (21), 3748-3755.

121.   Natrajan, L. S.; Blake, A. J.; Wilson, C.; Weinstein, J. A.; Arnold, P. L., *Dalton Trans.* **2006,** (37), 4465-4473.

122.   Priya, S.; Balakrishna, M. S.; Mague, J. T., *Chem. Lett.* **2004,** *33* (3), 308-309.

123.   Hanaoka, H.; Imamoto, Y.; Hino, T.; Oda, Y., *J. Organomet. Chem.* **2006,** *691* (23), 4968-4974.

124.   Liang, L. C.; Chang, Y. N.; Lee, H. M., *Inorg. Chem.* **2007,** *46* (7), 2666-2673.

125.   Capacchione, C.; Manivannan, R.; Barone, M.; Beckerle, K.; Centore, R.; Oliva, L.; Proto, A.; Tuzi, A.; Spaniol, T. P.; Okuda, J., *Organometallics* **2005,** *24* (12), 2971-2982.

126.   Beckerle, K.; Manivannan, R.; Lian, B.; Meppelder, G. J. M.; Raabe, G.; Spaniol, T. R.; Ebeling, H.; Pelascini, F.; Mulhaupt, R.; Okuda, J., *Angew. Chem., Int. Ed.* **2007,** *46* (25), 4790-4793.

127.   Lian, B.; Beckerle, K.; Spaniol, T. P.; Okuda, J., *Angew. Chem., Int. Ed.* **2007,** *46*, 8507-8510.

128.   Meppelder, G. J. M.; Spaniol, T. P.; Okuda, J., *J. Organomet. Chem.* **2006,** *691* (14), 3206-3211.

129.   Beckerle, K.; Manivannan, R.; Spaniol, T. P.; Okuda, J., *Organometallics* **2006,** *25* (12), 3019-3026.
130.   Lian, B.; Spaniol, T. P.; Okuda, J., *Organometallics* **2007,** *26* (26), 6653-6660.
131.   Lian, B.; Spaniol, T. P.; Horrillo-Martinez, P.; Hultzsch, K. C.; Okuda, J., *Eur. J. Inorg. Chem.* **2009,** (3), 429-434.
132.   Long, R. J.; Jones, D. J.; Gibson, V. C.; White, A. J. P., *Organometallics* **2008,** *27* (22), 5960-5967.
133.   Meppelder, G. J. M.; Fan, H. T.; Spaniol, T. P.; Okuda, J., *Organometallics* **2009,** *28* (17), 5159-5165.
134.   Meppelder, G. J. M.; Fan, H. T.; Spaniol, T. P.; Okuda, J., *Inorg. Chem.* **2009,** *48* (15), 7378-7388.
135.   Shavit, M.; Peri, D.; Manna, C. M.; Alexander, J. S.; Tshuva, E. Y., *J. Am. Chem. Soc.* **2007,** *129* (40), 12098-+.
136.   Segal, S.; Goldberg, I.; Kol, M., *Organometallics* **2005,** *24* (2), 200-202.
137.   Yeori, A.; Groysman, S.; Goldberg, I.; Kol, M., *Inorg. Chem.* **2005,** *44* (13), 4466-4468.
138.   Yeori, A.; Goldberg, I.; Shuster, M.; Kol, M., *J. Am. Chem. Soc.* **2006,** *128* (40), 13062-13063.
139.   Shalumova, T.; Tanski, J. M., *Acta Crystallogr., Sect. E: Struct. Rep. Online* **2008,** *E64*, m1029-m1030.
140.   Peri, D.; Meker, S.; Shavit, M.; Tshuva, E. Y., *Chem.--Eur. J.* **2009,** *15* (10), 2403-2415.
141.   Tinoco, A. D.; Incarvito, C. D.; Valentine, A. M., *J. Am. Chem. Soc.* **2007,** *129* (11), 3444-3454.
142.   Sawada, Y.; Matsumoto, K.; Kondo, S.; Watanabe, H.; Ozawa, T.; Suzuki, K.; Saito, B.; Katsuki, T., *Angew. Chem., Int. Ed.* **2006,** *45* (21), 3478-3480.
143.   Liu, X. L.; Shang, X. M.; Tang, T.; Hu, N. H.; Pei, F. K.; Cui, D. M.; Chen, X. S.; Jing, X. B., *Organometallics* **2007,** *26* (10), 2747-2757.
144.   Liu, X. L.; Cui, D. M., *Dalton Trans.* **2008,** (28), 3747-3752.
145.   Liu, Y. F.; Xia, H. T.; Wang, D. Q.; Yang, S. P., *Acta Crystallogr., Sect. E: Struct. Rep. Online* **2007,** *63*, M484-M486.
146.   Yang, S. P.; Han, L. J.; Wang, D. Q.; Wang, B., *Acta Crystallogr., Sect. E: Struct. Rep. Online* **2007,** *63*, M2777-U1351.
147.   Xia, H. T.; Liu, Y. F.; Yang, S. P.; Wang, D. Q., *Acta Crystallogr., Sect. E: Struct. Rep. Online* **2009,** *65*, M200-U765.
148.   Xia, H. T.; Liu, Y. F.; Yang, S. P.; Wang, D. Q., *Acta Crystallogr., Sect. E: Struct. Rep. Online* **2009,** *65*, M201-U776.
149.   Xia, H. T.; Rong, D. F.; Zhang, Y. Y.; Yang, S. P.; Wang, D. Q., *Acta Crystallogr., Sect. E: Struct. Rep. Online* **2009,** *65*, M198-U754.
150.   Kleij, A. W., *Eur. J. Inorg. Chem.* **2009,** (2), 193-205.
151.   Miyasaka, H.; Saitoh, A.; Abe, S., *Coord. Chem. Rev.* **2007,** *251* (21-24), 2622-2664.
152.   Flanagan, S. P.; Guiry, P. J., *J. Organomet. Chem.* **2006,** *691* (10), 2125-2154.
153.   Agapie, T.; Henling, L. M.; DiPasquale, A. G.; Rheingold, A. L.; Bercaw, J. E., *Organometallics* **2008,** *27* (23), 6245-6256.
154.   Zelikoff, A. L.; Kopilov, J.; Goldberg, I.; Coates, G. W.; Kol, M., *Chem. Commun.* **2009**, 6804-6806.
155.   Tshuva, E. Y.; Goldberg, I.; Kol, M.; Goldschmidt, Z., *Inorg. Chem.* **2001,** *40* (17), 4263-4270.
156.   Tshuva, E. Y.; Goldberg, I.; Kol, M.; Goldschmidt, Z., *Chem. Commun.* **2001,** (20), 2120-2121.
157.   Tshuva, E. Y.; Groysman, S.; Goldberg, I.; Kol, M.; Goldschmidt, Z., *Organometallics* **2002,** *21* (4), 662-670.
158.   Groysman, S.; Tshuva, E. Y.; Goldberg, I.; Kol, M.; Goldschmidt, Z.; Shuster, M., *Organometallics* **2004,** *23* (22), 5291-5299.
159.   Boyd, C. L.; Toupance, T.; Tyrrell, B. R.; Ward, B. D.; Wilson, C. R.; Cowley, A. R.; Mountford, P., *Organometallics* **2005,** *24* (2), 309-330.

160.   Tshuva, E. Y.; Goldberg, I.; Kol, M.; Goldschmidt, Z., *Organometallics* **2001,** *20* (14), 3017-3028.
161.   Selby, J. D.; Manley, C. D.; Schwarz, A. D.; Clot, E.; Mountford, P., *Organometallics* **2008,** *27* (24), 6479-6494.
162.   Padmanabhan, S.; Katao, S.; Nomura, K., *Organometallics* **2007,** *26* (7), 1616-1626.
163.   Sarazin, Y.; Howard, R. H.; Hughes, D. L.; Humphrey, S. M.; Bochmann, M., *Dalton Trans.* **2006,** (2), 340-350.
164.   Zhou, H.; Guo, H. D.; Yao, Y. M.; Zhou, L. Y.; Sun, H. M.; Sheng, H. T.; Zhang, Y.; Shen, Q., *Inorg. Chem.* **2007,** *46* (3), 958-964.
165.   Guo, H. D.; Zhou, H.; Yao, Y. M.; Zhang, Y.; Shen, Q., *Dalton Trans.* **2007,** (32), 3555-3561.
166.   Delbridge, E. E.; Dugah, D. T.; Nelson, C. R.; Skelton, B. W.; White, A. H., *Dalton Trans.* **2007,** (1), 143-153.
167.   Amgoune, A.; Thomas, C. M.; Ilinca, S.; Roisnel, T.; Carpentier, J. F., *Angew. Chem., Int. Ed.* **2006,** *45* (17), 2782-2784.
168.   Kerton, F. M.; Whitwood, A. C.; Willans, C. E., *Dalton Trans.* **2004,** (15), 2237-2244.
169.   Yao, Y. M.; Ma, M. T.; Xu, X. P.; Zhang, Y.; Shen, Q.; Wong, W. T., *Organometallics* **2005,** *24* (16), 4014-4020.
170.   Kerton, F. M.; Kozak, C. M.; Luttgen, K.; Willans, C. E.; Webster, R. J.; Whitwood, A. C., *Inorg. Chim. Acta* **2006,** *359* (9), 2819-2825.
171.   Willans, C. E.; Sinenkov, M. A.; Fukin, G. K.; Sheridan, K.; Lynam, J. M.; Trifonov, A. A.; Kerton, F. M., *Dalton Trans.* **2008,** (27), 3592-3598.
172.   Ma, M. T.; Xu, X. P.; Yao, Y. M.; Zhang, Y.; Shen, Q., *J. Mol. Struct.* **2005,** *740* (1-3), 69-74.
173.   Matsuo, T.; Kawaguchi, H., *Inorg. Chem.* **2007,** *46* (20), 8426-8434.
174.   Matsuo, T.; Kawaguchi, H.; Sakai, M., *J. Chem. Soc., Dalton Trans.* **2002,** (12), 2536-2540.
175.   Matsuo, T.; Kawaguchi, H., *Organometallics* **2003,** *22* (26), 5379-5381.
176.   Matsuo, T.; Kawaguchi, H., *J. Am. Chem. Soc.* **2005,** *127* (49), 17198-17199.
177.   Akagi, F.; Matsuo, T.; Kawaguchi, H., *J. Am. Chem. Soc.* **2005,** *127* (34), 11936-11937.
178.   Homden, D.; Redshaw, C.; Wright, J. A.; Hughes, D. L.; Elsegood, M. R. J., *Inorg. Chem.* **2008,** *47* (13), 5799-5814.
179.   Lee, J.; Hong, Y.; Kim, J. H.; Kim, S. H.; Do, Y.; Shin, Y. K.; Kim, Y., *J. Organomet. Chem.* **2008,** *693* (25), 3715-3721.
180.   Licini, G.; Mba, M.; Zonta, C., *Dalton Trans.* **2009,** (27), 5265-5277.
181.   Davidson, M. G.; Doherty, C. L.; Johnson, A. L.; Mahon, M. F., *Chem. Commun.* **2003,** (15), 1832-1833.
182.   Axe, P.; Bull, S. D.; Davidson, M. G.; Gilfillan, C. J.; Jones, M. D.; Robinson, D.; Turner, L. E.; Mitchell, W. L., *Org. Lett.* **2007,** *9* (2), 223-226.
183.   Chartres, J. D.; Dahir, A.; Tasker, P. A.; White, F. J., *Inorg. Chem. Commun.* **2007,** *10* (10), 1154-1158.
184.   Nielson, A. J.; Shen, C. H.; Waters, J. M., *Acta Crystallographica Section C-Crystal Structure Communications* **2003,** *59*, M494-M496.
185.   Nielson, A. J.; Shen, C. H.; Waters, J. M., *Polyhedron* **2006,** *25* (10), 2039-2054.
186.   Cortes, S. A.; Hernandez, M. A. M.; Nakai, H.; Castro-Rodriguez, I.; Meyer, K.; Fout, A. R.; Miller, D. L.; Huffman, J. C.; Mindiola, D. J., *Inorg. Chem. Commun.* **2005,** *8* (10), 903-907.
187.   Bull, S. D.; Davidson, M. G.; Johnson, A. L.; Robinson, D.; Mahon, M. F., *Chem. Commun.* **2003,** (14), 1750-1751.
188.   Ugrinova, V.; Ellis, G. A.; Brown, S. N., *Chem. Commun.* **2004,** (4), 468-469.
189.   Fortner, K. C.; Bigi, J. P.; Brown, S. N., *Inorg. Chem.* **2005,** *44* (8), 2803-2814.
190.   Johnson, A. L.; Davidson, M. G.; Mahon, M. F., *Dalton Trans.* **2007,** (46), 5405-5411.
191.   Bernardinelli, G.; Seidel, T. M.; Kundig, E. P.; Prins, L. J.; Kolarvoic, A.; Mba, M.; Pontini, M.; Licini, G., *Dalton Trans.* **2007,** (16), 1573-1576.

Chapter 2

Group 4 complexes of amine tris(phenolates) as initiators for ROP of lactide:

Effect of ligand variation

2. Group 4 complexes of amine tris(phenolates) as initiators for ROP of lactide: Effect of ligand variation

2.1. Preamble

As has been discussed in Chapter 1, initial interest into the use of amine tris(phenolate) coordinated Group 4 complexes as initiators for the ROP of LA has been demonstrated most successfully by the research groups of Kol and Verkade.[1-3] In recent years, the Davidson research group has further probed the coordination chemistry of this class of ligand to Group 4 metals amongst others, and has reported that the observed coordination mode with respect to the larger metals, such as zirconium and tin, depends on the nature of the phenol substituents of the ligand.[4] Preliminary investigations have shown that the isopropoxide complexes **L^{tBu}Zr(O^{i}Pr)** and **L^{tBu}Hf(O^{i}Pr)** not only undertake rapid well-controlled ROP of LA, but also exhibit a significant degree of heterotactic stereocontrol.[5]

Within this chapter, the effect of altering the substitutents of the tris(phenolate) ligand, both sterically and electronically, shall be investigated, with respect to coordination of Group 4 metals. The potential of the resulting complexes as initiators for the ROP of LA will then be discussed with particular attention being paid to activity, molecular weight control and stereocontrol. A series of kinetic experiments will also be described, from which a great deal of information can be obtained about the mechanism of polymerisation and remarkable stereocontrol that selected complexes described herein afford.

2.2. Synthesis of ligands

The series of tris(phenolate) ligands described above and discussed here on in, are given the notation H$_3$L^R and were synthesised via two modified versions of the Mannich reaction, depending on the nature of their substituents.

H$_3$L^{Me}: R = CH$_3$
H$_3$L^{tBu}: R = C(CH$_3$)$_3$
H$_3$L^{Np}: R = C(CH$_3$)$_2$CH$_2$CH$_3$
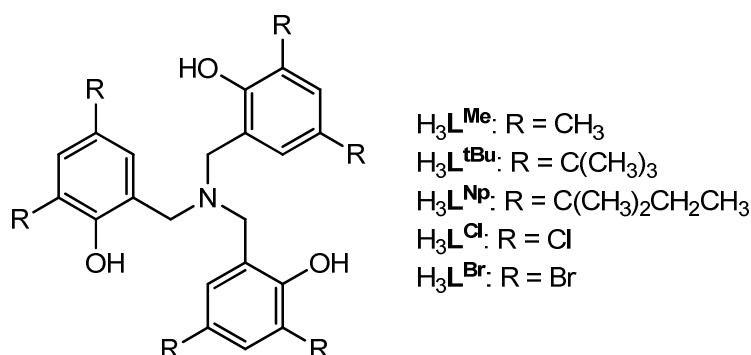H$_3$L^{Cl}: R = Cl
H$_3$L^{Br}: R = Br

Figure 2.1: Ligands synthesised in this chapter.

2.2.1. Alkyl substituted ligands

The ligands H_3L^{Me} and H_3L^{tBu} were synthesised by following previously reported methods, and the new ligand H_3L^{Np} was synthesised in an analogous manner.[6] These syntheses involved heating an excess of the respective phenol starting material with hexamethylenetetramine (HMTA) and formaldehyde solution in a solvent-free environment, as shown in Scheme 2.1. In the case of H_3L^{tBu} and H_3L^{Np}, an intermediate 'ring-closed' bis(phenolate), HL'^{R}, was formed primarily, however in the case of H_3L^{tBu}, prolonged reaction over several days with periodical additions of extra equivalents of phenol yielded the desired ligand after washing with methanol. In the synthesis of H_3L^{Np}, these measures resulted in a mixture of the 'ring-closed' product and tris(phenolate) ligand, separation of which was only possible via fractional crystallization from ethanol solutions. To the best of our knowledge H_3L^{Np} has not previously been reported in the literature. All three ligands synthesised in this manner were characterised by ^1H and $^{13}C\{^1H\}$ NMR spectroscopy, and in the case of H_3L^{Np}, mass spectrometry, elemental analysis and X-ray crystallographic analysis were carried out on crystals grown from methanol solutions.
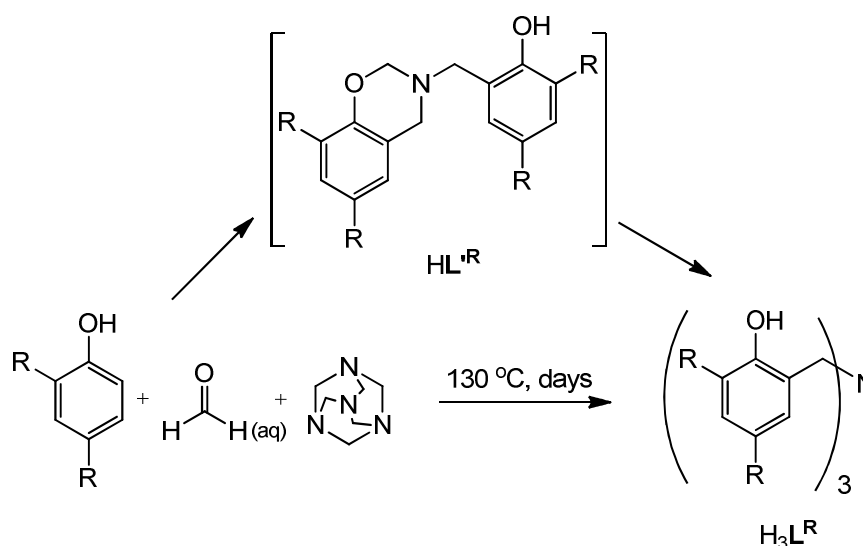
Scheme 2.1: Synthesis of H_3L^{R} **(R = Me, ^{t}Bu, Np).**

Previous reports of these ligands have shown the sterics of the ligand substituents to have an effect on the molecule packing in the crystal structures. Despite appearing C_3-symmetric in solution on the NMR timescale, the methyl substituted ligand H_3L^{Me} was shown not to adopt a C_3-symmetric structure in the solid state.[7] Two hydroxyl groups are directed toward the tertiary amine, whereas the third is involved in intermolecular hydrogen bonding with a phenolate arm in an adjacent molecule, forming a one-dimensional hydrogen-bonded network. The phenolate arms of the bulky ligand H_3L^{tBu} were all seen to be involved in intramolecular hydrogen bonding with the amine, forming no such network, and a C_3-symmetric structure was observed in the solid

state.[8] Unsurprisingly, the new ligand H_3L^{Np}, with even bulkier substituents, was found to take on a similar C_3-symmetric structure to H_3L^{tBu} with all three phenolic alcohol groups orientated in the same direction. Trifurcated $N \cdots (HO)_3$ hydrogen bonding occurs intramolecularly between the phenolic alcohol groups and the amine, as shown in Figure 2.2. Three carbons in the *para*-neopentyl group on one arm were each found to be disordered over two sites, which was modeled successfully.
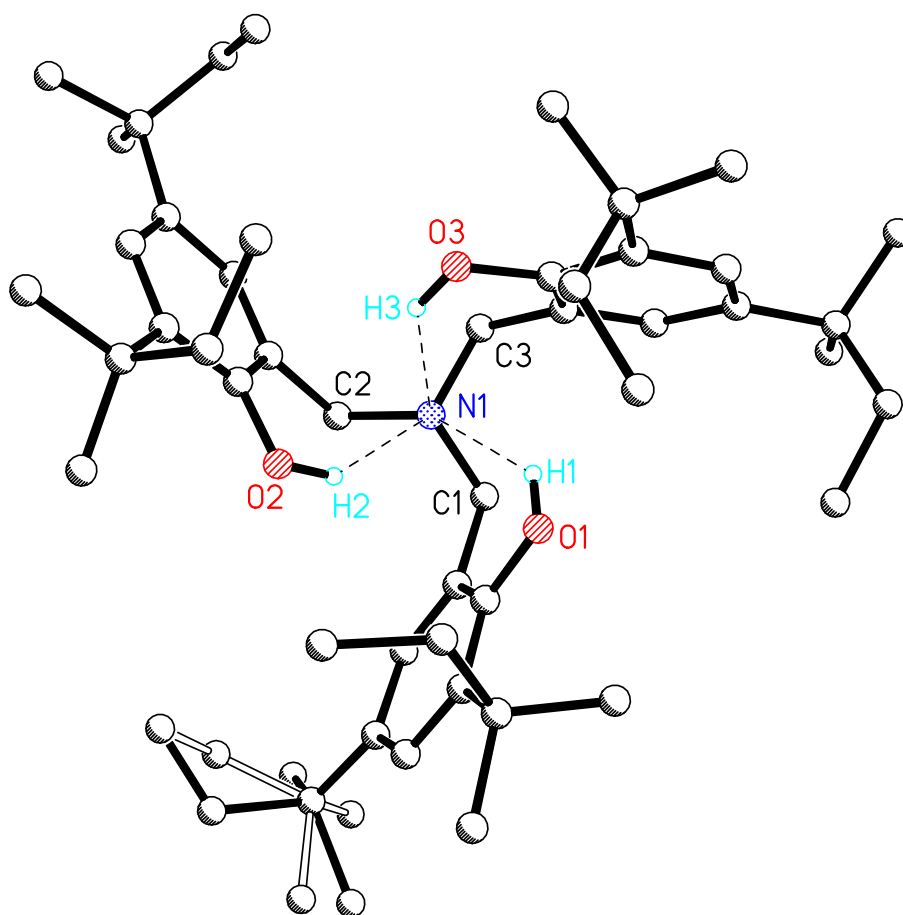
Figure 2.2: Structure of H_3L^{Np} as determined by X-ray crystallography. With the exception of H1, H2 and H3, hydrogen atoms have been omitted for clarity.

2.2.2. Halo substituted ligands

H_3L^{Cl} was prepared using the synthesis previously described by Kol and co-workers, where three equivalents of 2,4-dichlorophenol were reacted with HMTA.[9] The reaction was monitored by ^1H NMR spectroscopy, and once again the 'ring-closed' bis(phenolate) HL'^R is formed primarily,

61

shown in Scheme 2.2. An extra equivalent of phenol is then added to promote the continued reaction on to the tris(phenolate), H_3L^R. This gives rise to a 1:1 hydrogen bonded adduct of ligand and HMTA, $H_3L^R \cdot HMTA$, the exact nature of which will be explained in due course using X-ray crystallographic analysis. Column chromatography (silica, $CHCl_3$) was required to remove the HMTA molecule from the ligand. Synthesis of H_3L^{Br} was undertaken analogously using instead 2,4-dibromophenol, and to the best of our knowledge has not been previously reported in the literature. Elemental analysis, ^1H and $^{13}C\{^1H\}$ NMR were used to fully charaterise both the ligands and their HMTA adducts, and in addition, mass spectrometry was carried out on the purified ligands H_3L^{Cl} and H_3L^{Br}. Crystals suitable for X-ray crystallographic analysis were grown of H_3L^{Cl} from chloroform solutions, and of the adducts $H_3L^{Cl} \cdot HMTA$ and $H_3L^{Br} \cdot HMTA$, from ethyl acetate solutions.
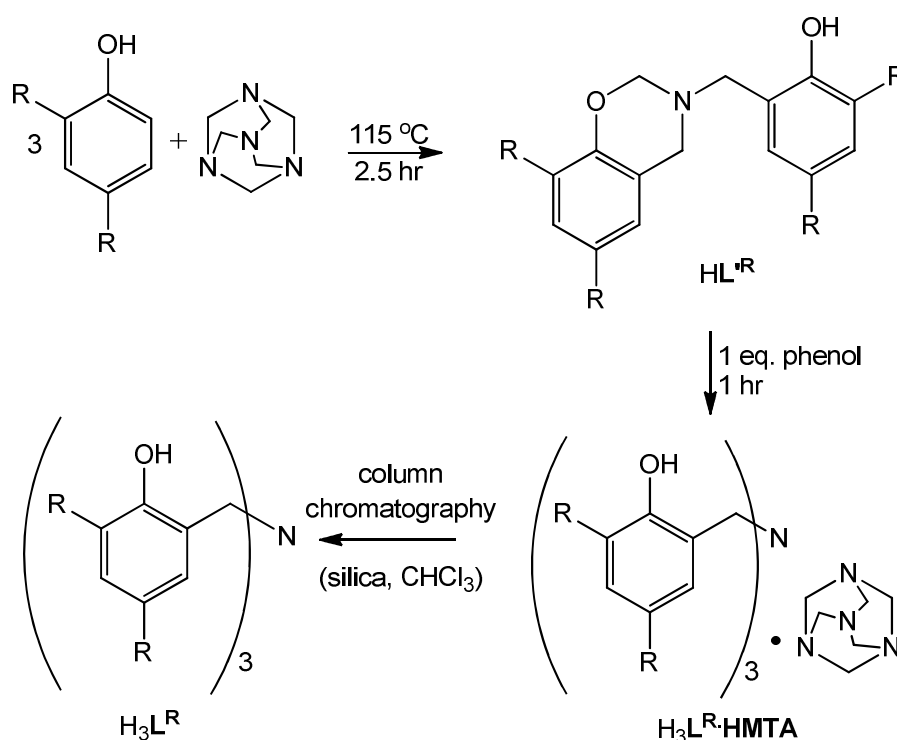
Scheme 2.2: Synthesis of H_3L^R (R = Cl, Br).

The resolved structures of $H_3L^{Cl} \cdot HMTA$ and $H_3L^{Br} \cdot HMTA$ are shown in Figures 2.4 and 2.5. These adducts are held together by two intermolecular hydrogen bonds between phenolate alcohol groups and HMTA amines, O3-H3···N2 and O1-H1···N5, to form a one-dimensional hydrogen-bonded network (Figure 2.3). In both adducts the remaining phenolic alcohol group interacts intramolecularly with the tris(phenolate) amine. These interactions mean that despite the tripodal nature of the ligand, it is unable to take on the familiar propeller structure, and in both

adducts the O3 phenolate arm is bent in the opposite direction to the O1 and O2 arms. $H_3L^{Cl}\cdot HMTA$ was also found to include a weak intramolecular interaction between the phenolic alcohol group and the ortho-positioned chlorine of the same arm, O3-H3···Cl31.
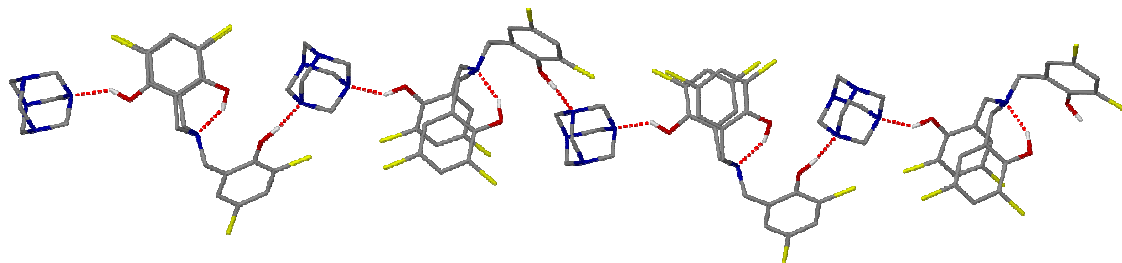
**Figure 2.3: One-dimensional hydrogen bonded network within $H_3L^{Cl}\cdot HMTA$.**
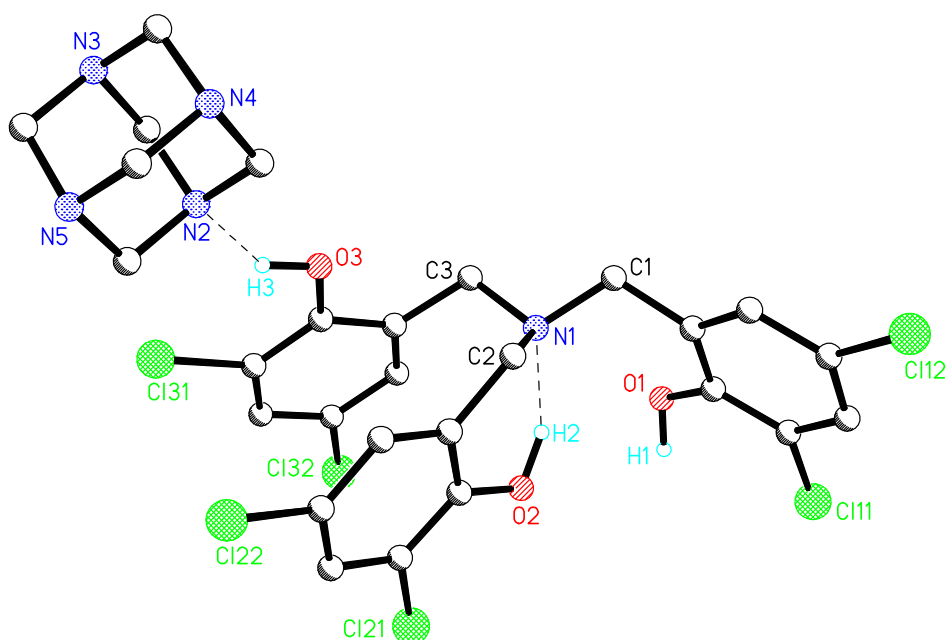
Figure 2.4: Structure of $H_3L^{Cl}\cdot HMTA$ as determined by X-ray crystallography. With the exception of H1, H2 and H3, hydrogen atoms have been omitted for clarity.

H-bond	D-H (Å)	H···A (Å)	D···A (Å)	D-H-A (°)
O1-H1···N5	0.93(4)	1.70(4)	2.598(3)	160(3)
O2-H2···N1	0.92(4)	1.86(4)	2.666(2)	145(4)
O2-H2···O1	0.92(4)	2.33(4)	2.974(2)	127(4)
O3-H3···N2	0.88(4)	1.89(4)	2.675(3)	148(3)
O3-H3···Cl31	0.88(4)	2.61(3)	3.040(2)	112(3)

Table 2.1: Hydrogen bond distances and angles in $H_3L^{Cl}\cdot HMTA$.
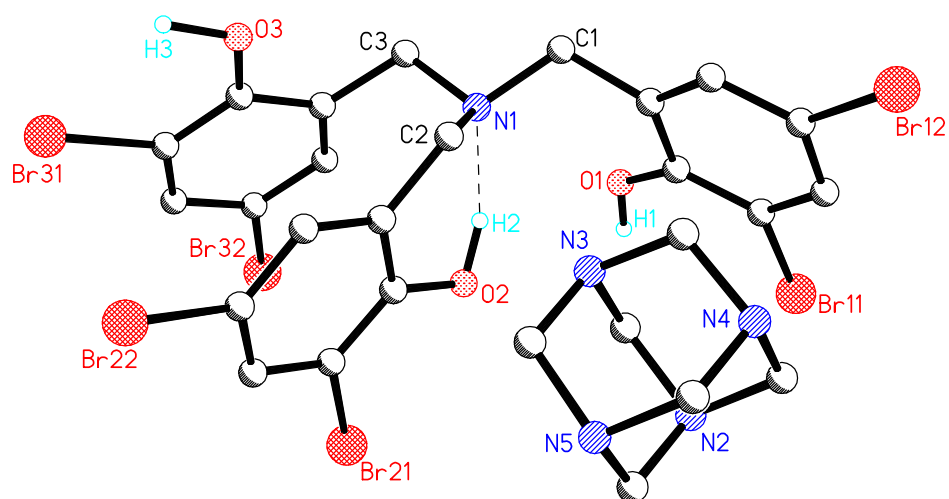
Figure 2.5: Structure of $H_3L^{Br} \cdot HMTA$ **as determined by X-ray crystallography. With the exception of H1, H2 and H3, hydrogen atoms have been omitted for clarity**

H-bond	D-H (Å)	H···A (Å)	D···A (Å)	D-H-A (°)
O1-H1···N5	1.00(2)	1.64(3)	2.623(6)	165(10)
O3-H3···N2	1.16(13)	1.67(13)	2.674(6)	142(10
O2-H2···N1	0.96(7)	1.73(7)	2.652(6)	160(6)
O2-H2···O1	0.96(7)	2.49(6)	2.999(5)	113(4)

Table 2.2: Hydrogen bond distances and angles in $H_3L^{Br} \cdot HMTA$**.**

Following removal of HMTA, crystals of $H_3\mathbf{L}^{Cl}$ were grown from chloroform solutions and the resolved structure is shown in Figure 2.6. Without the HMTA present the ligand is free to take on a propellor structure, but has only pseudo C_3-symmetry as was previously reported in the case of $H_3\mathbf{L}^{Me}$.[7] In this structure there is once again an intermolecular hydrogen bond between molecules (O1-H1···O2' 2.706(5) Å), but only one hydroxyl group undergoing intramolecular hydrogen bonding with the amine moiety (O2-H2···N1 2.616(5) Å). The closely related ligand recently reported by Chartres et al,[10] in which the *para*-substituents have been replaced with tertiary butyl groups, was found to have a similar solid state structure with only small differences in hydrogen bond lengths (O-H···O' 2.766 Å; O-H···N 2.634 Å).
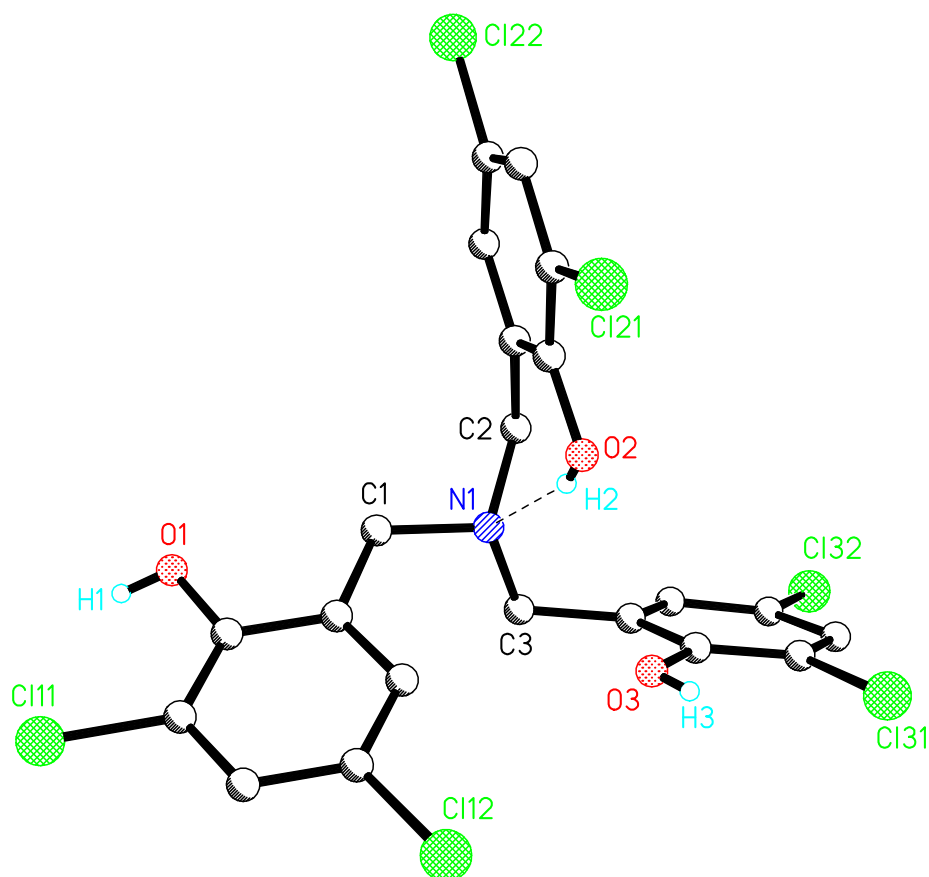
Figure 2.6: Structure of H$_3$L^{Cl} as determined by X-ray crystallography. With the exception of H1, H2 and H3, hydrogen atoms have been omitted for clarity.

2.3. Synthesis of Group 4 isopropoxide complexes

Following the synthesis of these ligands, the manner of their coordination to Group 4 metals was investigated. Novel complexes arising from this research are summarised in Scheme 2.3 and can be loosely collated into three groups, each of which will be discussed in turn: alkyl substituted alkoxide complexes {**L^{Np}Ti(O^{i}Pr)**, **L^{Np}Zr(O^{i}Pr)(IPA)**, **L^{Np}Hf(O^{i}Pr)(IPA)**}, halo substituted alkoxide complexes {**L^{Cl}Ti$_2$(O^{i}Pr)$_5$**, **L^{Cl}$_2$Ti$_3$(O)(O^{i}Pr)$_4$**} and zwitterionic complexes {**[HL^{Me}]$_2$Hf**, **[HL^{Cl}]$_2$Zr**]}.

L^{Cl}Ti$_2$(O^{i}Pr)$_5$

L^{Np}Ti(O^{i}Pr)

L^{Np}Zr(O^{i}Pr)(IPA)

H$_3$L^R

L$^{Cl}_2$Ti$_3$(O)(O^{i}Pr)$_4$

L^{Np}Hf(O^{i}Pr)(IPA)

[HL^{Cl}]$_2$Zr

[HL^{Me}]$_2$Hf
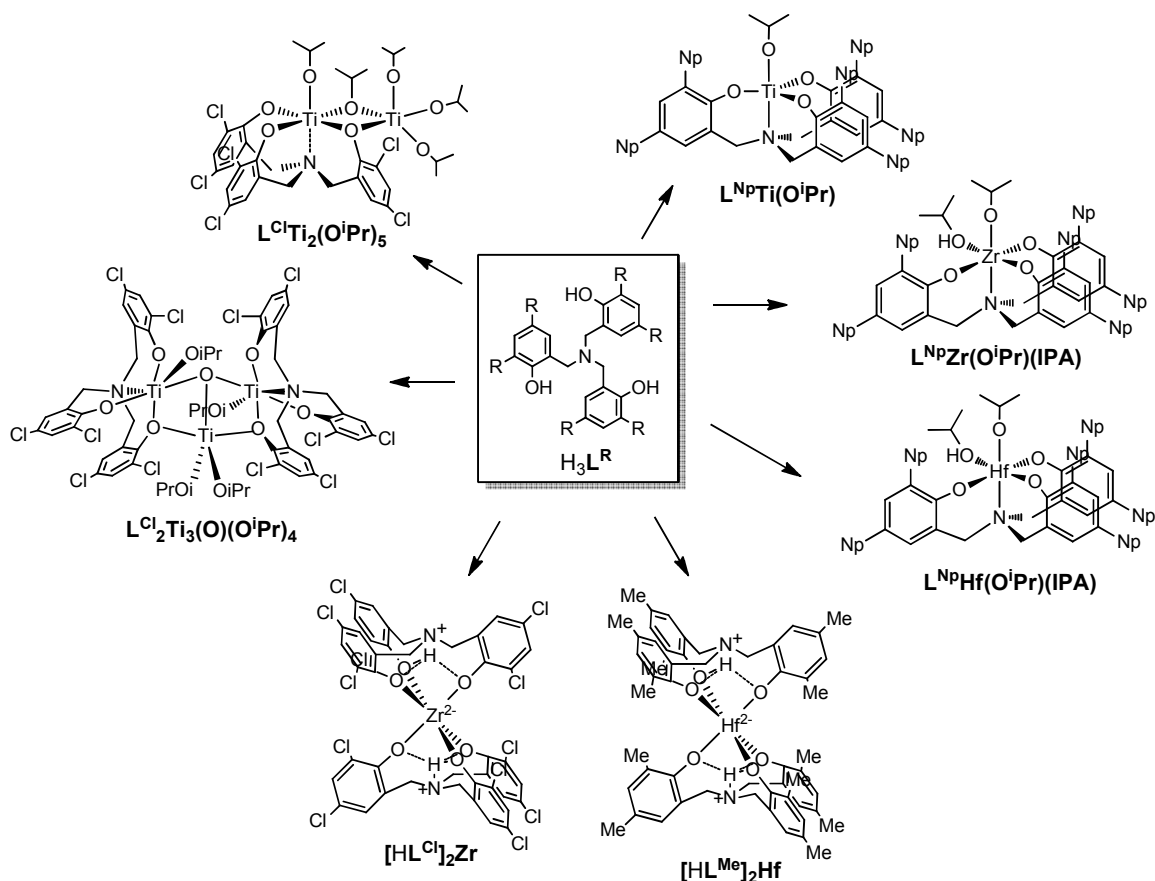
Scheme 2.3: Novel complexes reported in this chapter.

2.3.1. Alkyl-substituted amine(trisphenolate) isopropoxide complexes

Previous work has shown that in the majority of cases, reaction of the ligands H$_3$L^{Me} and H$_3$L^{tBu} to Group 4 isopropoxides results in monoligated C_3-symmetric isopropoxide complexes of the type **L^{R}M(O^{i}Pr)**, via simple ligand substitution driven by the stabilizing chelate effect of the tetradentate ligands.[4, 6] It was therefore expected that coordination of the new ligand H$_3$L^{Np} to Ti(IV), Zr(IV) and Hf(IV) would proceed in a similar manner, and the same reaction conditions were used (toluene, 2 hrs, ambient temperature). Amongst other techniques, ^{1}H NMR spectroscopy was used to charaterise the novel complexes, and the full annotated spectrum of **L^{Np}Ti(O^{i}Pr)** is shown in Figure 2.7. Although absent from the Ti complex, ^{1}H NMR spectroscopy also showed the presence of a coordinated molecule of isopropanol in the cases of **L^{Np}Zr(O^{i}Pr)(IPA)** and **L^{Np}Hf(O^{i}Pr)(IPA)** that remained even after prolonged exposure to vacuum.
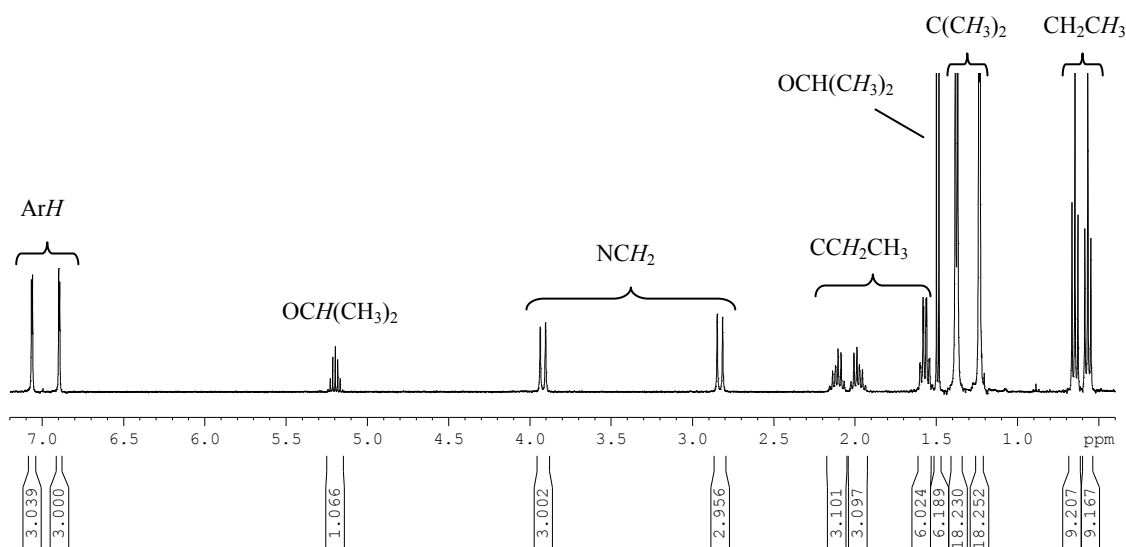
Figure 2.7: Annotated ^{1}H NMR spectrum of $L^{Np}Ti(O^iPr)$.

C_3-symmetric complexes encompassing the amine tris(phenolate) ligand such as those described here, can have two enantiomeric forms, *P* and *M* (Figure 2.8). As such, the two protons on each methylene arm of the tris(phenolate) ligand become diastereotopic as they take on either axial or equatorial positions. The magnetic inequivalence of these protons results in two doublets in the methylene region of the ^{1}H NMR spectrum, as is shown in Figure 2.8 for the case of **$L^{Np}Ti(O^iPr)$**.
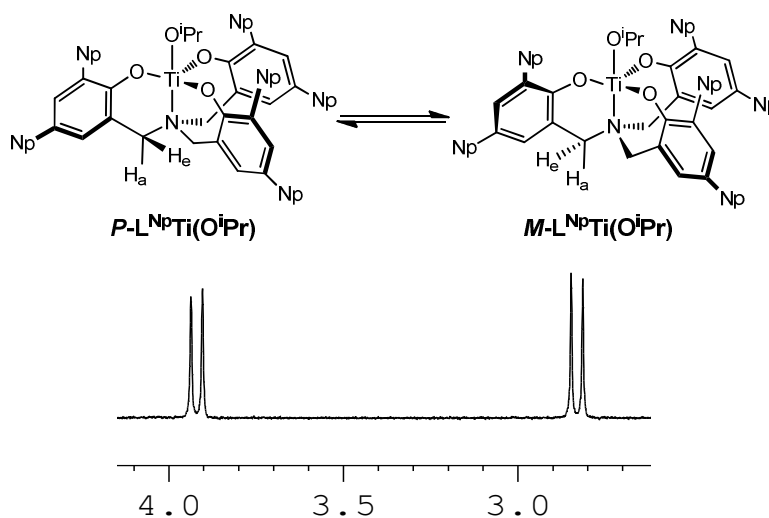
Figure 2.8: Methylene proton environments within the *P* and *M* enantiomers of $L^{Np}Ti(O^iPr)$ (above) and close-up of methylene region of ^{1}H NMR spectrum (below).

In the cases of Zr and Hf, ^{1}H NMR studies at 298 K does not resolve the doublets and a broad singlet is instead observed. This is indicative of the rapid inversion between the *P* and *M* enantiomers on the NMR timescale. A series of variable temperature ^{1}H NMR experiments were undertaken on the complexes **$L^{Np}Zr(O^iPr)(IPA)$** (Figure 2.9) and **$L^{Np}Hf(O^iPr)(IPA)$**. As the sample is cooled to 248 K, the arms of the ligand become locked, and the broad singlet at δ 3.40 starts to resolve into two signals at δ 2.85 and δ 4.10. However, further cooling of the sample to

67

228 K reveals the true C_i-symmetric nature of the complex, due to the presence of the coordinated IPA molecule, and separate signals for each methylene environment start to resolve.[11] No exchange was observed between the alcohol and alkoxide groups (observed in Figure 2.9 at δ 3.95 and δ 4.60 respectively) in either complex at temperatures up to 75 °C, but the signals were shown to broaden and exchange could occur at higher temperatures.
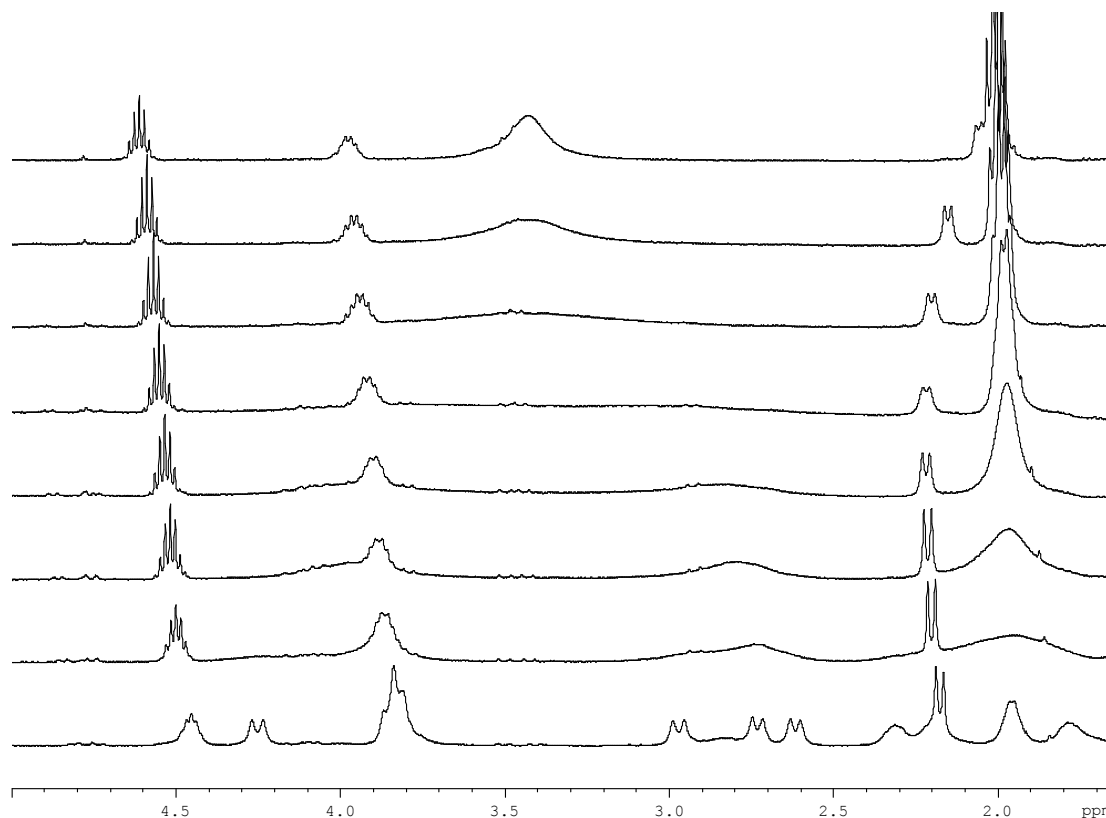
Figure 2.9: VT ^{1}H NMR spectra of $L^{Np}Zr(O^iPr)(IPA)$ between 228 K (bottom) – 298 K (top) in CD_2Cl_2.

Heating of $L^{Np}Hf(O^iPr)(IPA)$ at 180 °C under reduced pressure for 2 hours was required to remove the coordinated molecule of IPA. For comparison, VT ^{1}H NMR spectra for $L^{Np}Hf(O^iPr)$ are shown in Figure 2.10 (VT ^{1}H NMR spectra for $L^{Np}Hf(O^iPr)(IPA)$ and $L^{Np}Zr(O^iPr)(IPA)$ were found to be similar). At 298 K, the broad multiplet at δ 4.00 and doublet at δ 2.10, corresponding to the methine and alcoholic protons respectively, are absent, indicating the loss of the coordinated IPA. $L^{Np}Hf(O^iPr)$ also appears to be less fluxional at 298 K, as the methylene protons are observed as two very broad signals, rather than a broad singlet, as was observed $L^{Np}Hf(O^iPr)(IPA)$. Crucially, on cooling of the sample to 258 K the methylene signals were found to resolve to a pair of doublets, as would be expected in a C_3-symmetric complex (the minor set of doublets positioned slightly upfield are due to a degradation product, thought to be resulting from the extreme conditions required for removal of IPA).
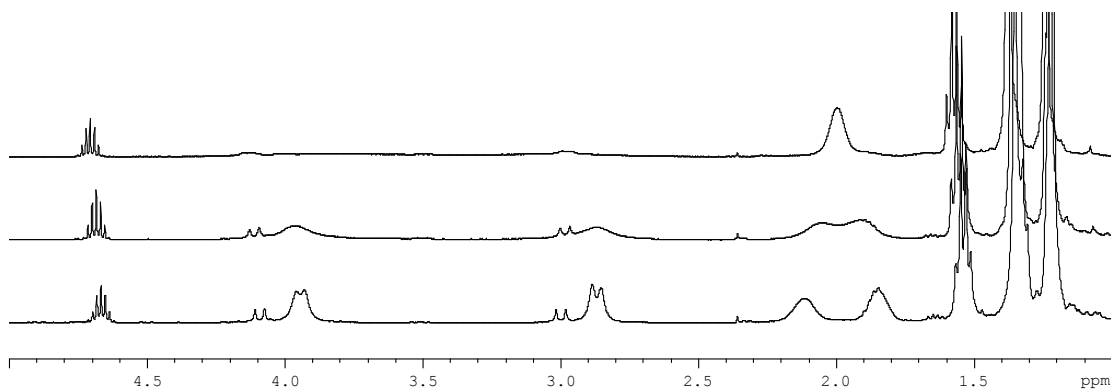
Figure 2.10: VT ^{1}H NMR spectra of $L^{Np}Hf(O^iPr)$ between 258 K (bottom) and 298 K (top) in CDCl$_3$.

Mass Spectrometry of $L^{Np}Ti(O^iPr)$, $L^{Np}Zr(O^iPr).IPA$ and $L^{Np}Hf(O^iPr).IPA$ was possible by Electrospray Ionisation (ESI) with addition of NaCl as a charge enhancer. Where present, the coordinated molecule of IPA was lost and in all cases a chloride ion was gained, leading to the observed negatively charged ion $[L^{Np}M(O^iPr)+Cl]$-.

The majority of structures of Group 4 isopropoxide complexes containing the ligands L^{Me} and L^{tBu}, as determined by X-ray crystallography, have been previously reported by us and others.[4-6] Due to the increased hydrocarbon content, complexes of the ligand L^{Np} were found to be highly soluble in hexane and pentane, but despite this, high quality crystals of $L^{Np}Ti(O^iPr)$ were successfully grown. Two forms of disorder were found to be present in this structure; chemical disorder of the flexible neopentyl substituents and crystallographic disorder of the two enantiomeric *P* and *M* forms of the complex. Crystallographic disorder of this description has been observed in other complexes of the series, and arises when there is no preference between the enantiomers during the crystallisation process and subsequently, a single crystal of the compound will contain both enantiomers.[4-5] The only significant difference in structural parameters between this structure and that of $L^{tBu}Ti(O^iPr)$, published in 2001 by Kol and co-workers,[6] is the increase in N(1)-Ti(1)-O(4) bond angle (179.82(19)° for $L^{Np}Ti(O^iPr)$ cf. 164.4(6)° for $L^{tBu}Ti(O^iPr)$), presumably caused by the increase in sterics of the phenolate *ortho*-substituents.
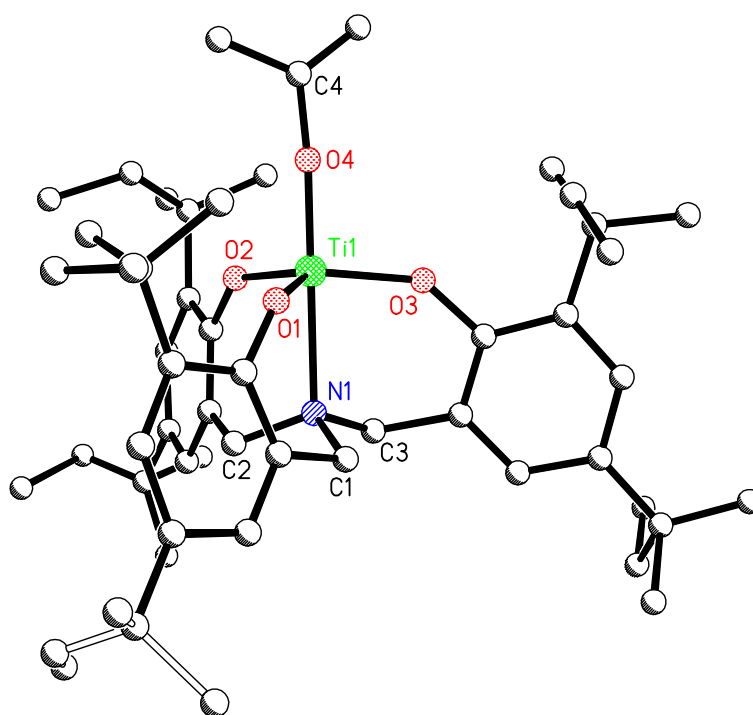
Figure 2.11: Structure of L^{Np}Ti(O^{i}Pr) as determined by X-ray crystallography. Hydrogen atoms have been omitted for clarity. Selected bond lengths [Å] and angles [°]: Ti(1)-O(1) 1.791(5), Ti(1)-O(2) 1.860(9), Ti(1)-O(3) 1.891(5), Ti(1)-O(4) 1.778(3), Ti(1)-N(1) 2.298(3), C(4)-O(4)-Ti(1) 175.4(7),O(4)-Ti(1)-N(1) 179.82(19), O(1)-Ti(1)-O(2) 117.9(3).

Crystals of **L^{Np}Zr(O^{i}Pr)(IPA)** grown from diethyl ether solutions over several weeks were of insufficient quality to resolve a full structure of the complex, but could be used to determine a framework of the structure (Figure 2.12), confirming the presence of a coordinated molecule of IPA. Previous unpublished work within the group leads us to believe that the isoproxide group resides in the *trans* position to the amine. This was confirmed by visual inspection of bond angles as the C(4)-O(4)-Zr(1) bond angle was observed to be closer to 180° than the C(5)-O(5)-Zr(1) bond angle and therefore the latter was attributed to the coordinated isopropanol molecule, although location of the alcoholic proton was not possible. This is contrary to the previously reported isopropanol coordinated complex **L^{Me}Ge(O^{i}Pr).IPA**, in which the isopropanol occupies the secondary coordination sphere through hydrogen bonding to the isopropoxide ligand (Figure 2.13).[12]
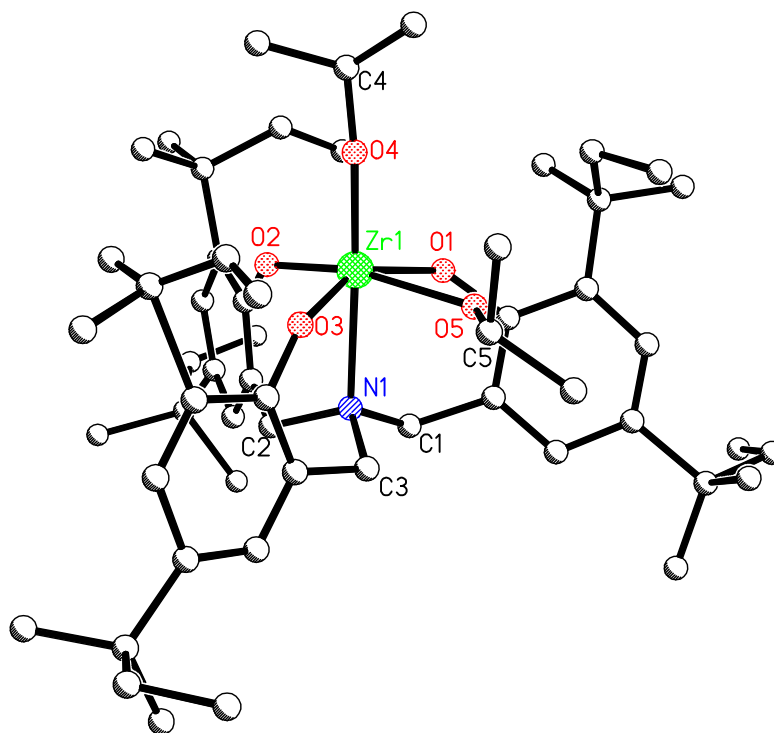
Figure 2.12: Isotropic framework structure of $L^{Np}Zr(O^iPr)(IPA)$ as determined by X-ray crystallography. Hydrogen atoms have been omitted for clarity.
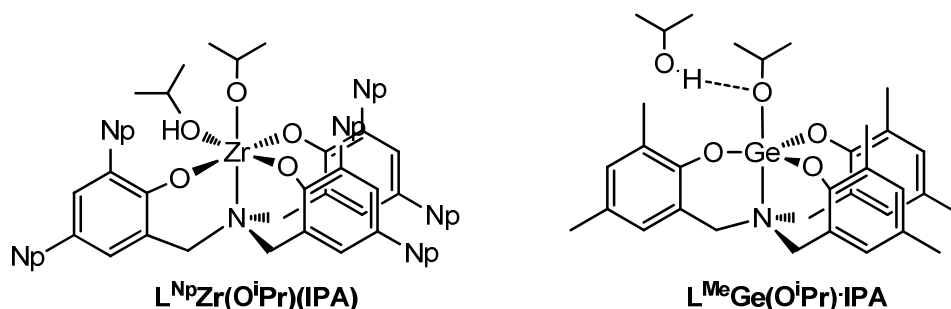
Figure 2.13: Representations of different IPA coordination modes observed.

2.3.2. Halo-substituted amine(trisphenolate) isopropoxide complexes

Following the procedure published by Kol et al, reaction of H_3L^{Cl} with titanium(IV) ispropoxide was expected to yield a 1:1 complex, as has been previously reported.[3] However, the reaction yielded a mixture of products, from which the dinuclear complex, $L^{Cl}Ti_2(O^iPr)_5$, could be isolated by washing and recrystallisation. Increasing the stoichiometry of the reaction to 1:2 ratio of H_3L^{Cl} with $Ti(O^iPr)_4$ resulted in an increased yield of $L^{Cl}Ti_2(O^iPr)_5$. Investigation was carried out as to whether an analogous dinuclear complex could be isolated from the reaction of H_3L^{Me} with Ti(IV) in a 1:2 ratio, but only the monomeric complex $L^{Me}Ti(O^iPr)$ resulted. As a methyl group and a chlorine atom are of similar size, it was noted that this difference in coordination behaviour is likely to be due to electronic factors. Crystals of the complex $L^{Cl}Ti_2(O^iPr)_5$ were

71

grown from the toluene/hexane washings of the crude reaction residue and the determined structure is shown in Figure 2.14. The complex contains two titanium metal centres linked via bridging phenolate and isopropoxide groups. Inspection of the bond angles showed that Ti1 has a distorted octahedral geometry and that Ti2 has a distorted trigonal bipyramid geometry. The absence of oxo- or hydroxyl- bridging groups between the metals indicate that this is not a degradation product of the previously reported monomeric complex $\mathbf{L^{Cl}Ti(O^iPr)_3}$ or another unknown product.
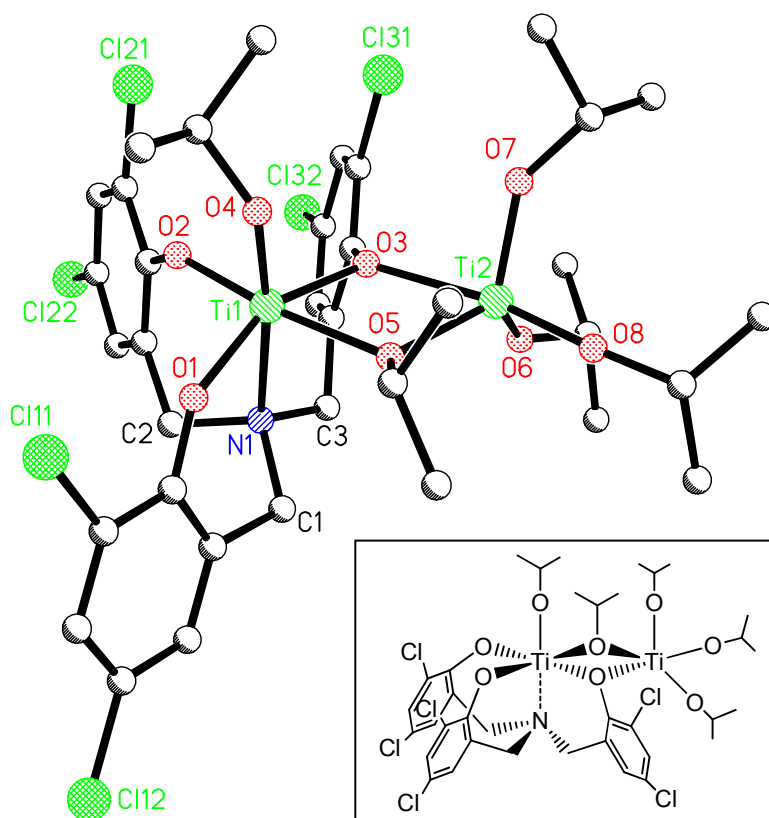
Figure 2.14: Structure of $\mathbf{L^{Cl}Ti_2(O^iPr)_5}$ as determined by X-ray crystallography and schematic diagram (inset). Hydrogen atoms have been omitted for clarity. Selected bond lengths [Å] and angles [°]: Ti(1)-O(1) 1.8969(11), Ti(1)-O(2) 1.8839(12), Ti(1)-O(3) 1.9921(11), Ti(2)-O(3) 2.1795(11), Ti(1)-O(5) 2.0490(11), Ti(2)-O(5) 2.0170(11), Ti(1)-O(4) 1.7698(12), Ti(2)-O(6) 1.8008(13), Ti(1)-N(1) 2.4045(14), O(1)-Ti(1)-O(2) 100.12(5), O(4)-Ti(1)-N(1) 172.76(5).

The dinuclear complex $\mathbf{L^{Cl}Ti_2(O^iPr)_5}$ was characterised by elemental analysis, ^{1}H and ^{13}C{^{1}H} NMR. ^{1}H NMR at 298 K gave a series of very broad undefined peaks, but cooling of the sample to 258 K gave a far cleaner NMR spectrum that could be assigned fully (Figure 2.15). Due to the lack of symmetry in the coordination of the ligand in this complex, six separate doublets were seen in the region δ 7.4 – 6.3, each corresponding to a different aryl-hydrogen environment. The same is true of the six doublets in the region δ 4.2 – 2.2, corresponding to the methylene protons. Three septets were observed for the isopropoxide groups at chemical shifts of δ 5.5, 4.9 and 4.6,

corresponding to the bridging, Ti1 bound, and Ti2 bound groups respectively in a 1:1:3 ratio. Integration of the alkyl region of the spectrum confirmed the presence of three different isopropoxide environments.
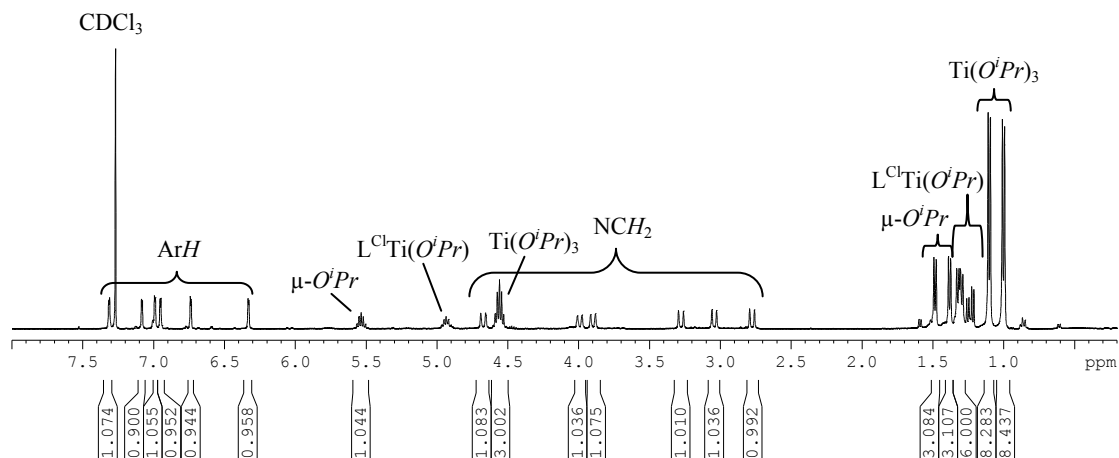
Figure 2.15: ^{1}H NMR spectrum of $\mathbf{L^{Cl}Ti_2(O^iPr)_5}$ at 258 K in CDCl₃.

Dinuclear structures are not unknown within Group 4 bis and tris(phenolate) coordination chemistry, but usually they are symmetrical and dimeric by virtue of the size of the metal centre (e.g. found for Zr, but not Ti).[13] As was described in Chapter 1, Jones and co-workers recently reported an example of this, where a series of ligands gave rise to monomeric titanium complexes, but when reacted with zirconium, led instead to dimeric complexes.[14] In cases such as this, the dimeric structures are symmetrical, and still consist of a 1:1 metal to ligand ratio with one phenolate arm of each ligand acting as a bridge. However, a low-symmetry dinuclear Ti complex of a tetradentate phenylenediamine bis(phenolate), in which binding occurs in a 2:1 metal to ligand ratio, has recently been published by Kol and co-workers.[15] In this case, bridging between the Ti centres occurs directly through isopropoxide groups rather than through the ligand phenolate groups. The dinuclear complex $\mathbf{L^{Cl}Ti_2(O^iPr)_5}$ described here is unusual in the fact that bridging occurs via both OPh and O^{i}Pr groups.
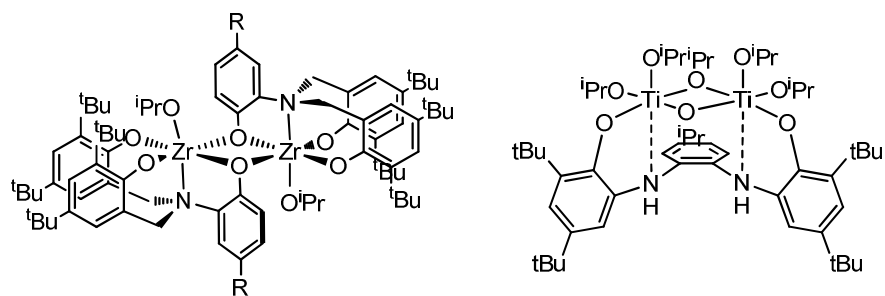
Figure 2.16: Examples of symmetrical (left)[14] and unsymmetrical (right)[15] dinuclear Group 4 complexes featuring bis- or tris(phenolate) ligands.

After standing for several weeks, a second set of signals began to appear in the ^{1}H NMR spectrum. These were attributed to the hydrolysis degradation of the dinuclear complex and the formation of the trinuclear 'oxo' complex **L$^{Cl}_2$Ti$_3$(O)(O^{i}Pr)$_4$** (Scheme 2.4), which can be thought of as a dimeric complex including a 'trapped' (RO)$_2$Ti-O unit.
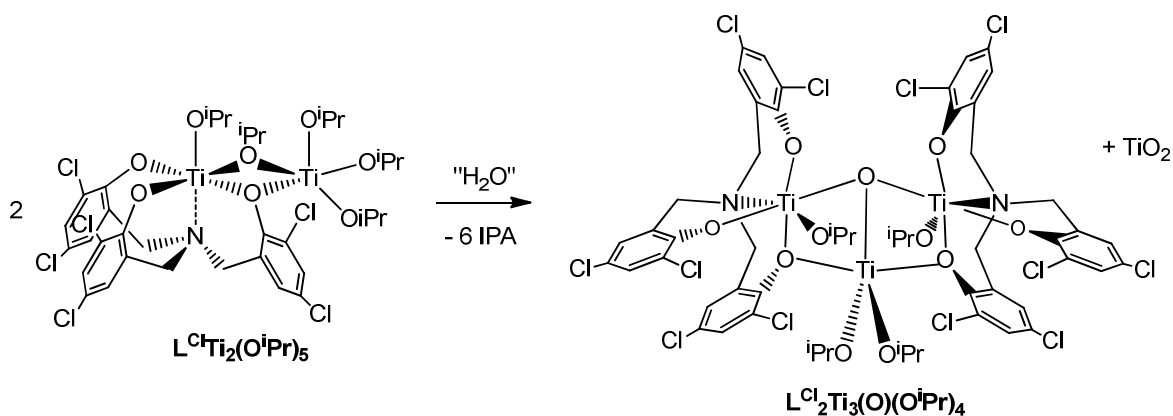
Scheme 2.4: Hydrolysis degradation of L^{Cl}Ti$_2$(O^{i}Pr)$_5$ to form L$^{Cl}_2$Ti$_3$(O)(O^{i}Pr)$_4$.

X-ray diffraction of **L$^{Cl}_2$Ti$_3$(O)(O^{i}Pr)$_4$** confirms the complex structure, although the collected data was of poor quality, limiting the information that can be taken from it. The three titanium metal centres are arranged in a ladder, in which the oxo-bridge binds to all three titanium centres in a μ^3 manner. Ti1 was shown to exhibit a distorted trigonal bipyramid coordination environment, while Ti2 and Ti3 display distorted octahedral geometries; the core structure of **L$^{Cl}_2$Ti$_3$(O)(O^{i}Pr)$_4$** is shown in Figure 2.18.
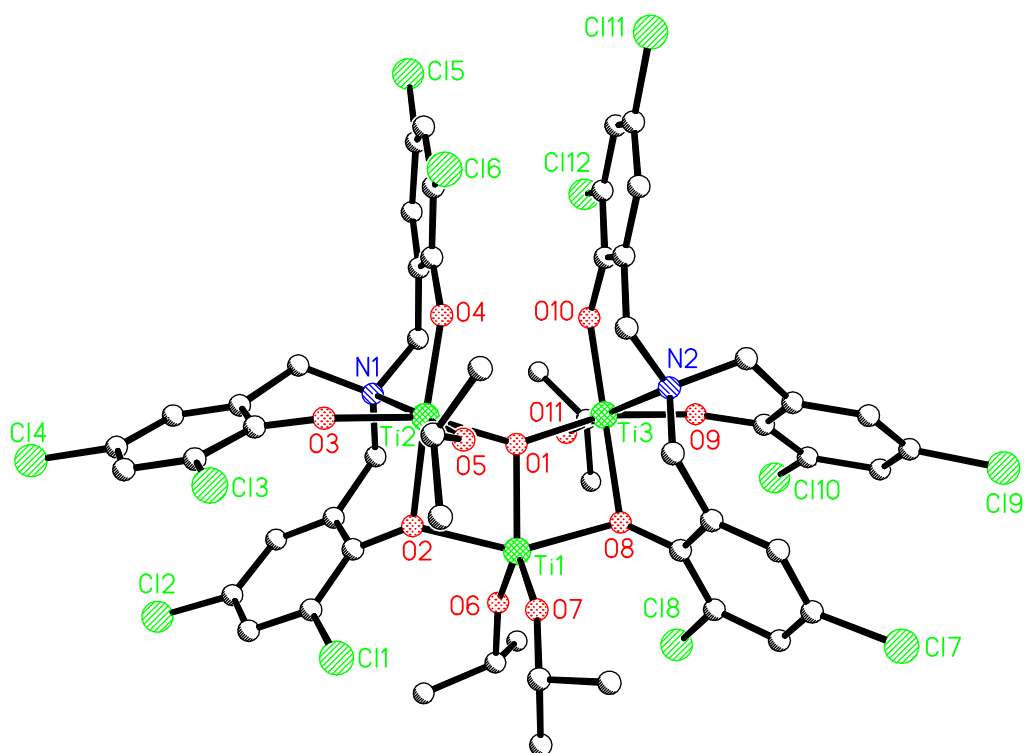
Figure 2.17: Structure of $L^{Cl}_2Ti_3(O)(O^iPr)_4$ as determined by X-ray crystallography. Hydrogen atoms are omitted for clarity. Selected bond lengths [Å] and angles [°]: Ti(1)-O(1) 1.976(6), Ti(1)-O(2) 1.996(6), Ti(2)-O(1) 1.974(6), Ti(2)-O(2) 2.101(7), Ti(2)-O(3) 1.877(6), Ti(2)-O(4) 1.865(7), Ti(2)-O(5) 1.791(6), Ti(1)-O(6) 1.760(8), Ti(2)-N(1) 2.370(8), O(3)-Ti(2)-O(4) 98.8(3).
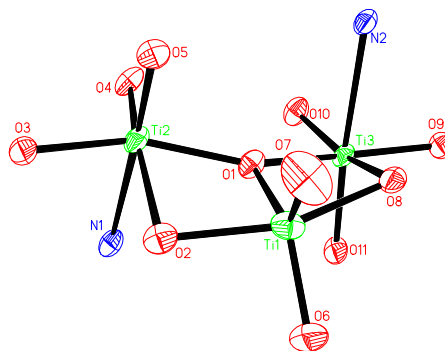
Figure 2.18: Core structure of $L^{Cl}_2Ti_3(O)(O^iPr)_4$. All carbon and hydrogen atoms are omitted.

^{1}H NMR analysis suggests that this complex retains its pseudo C_2-symmtery in solution (Figure 2.19). Each tris(phenolate) ligand is bound to the metal centres in an unsymmetrical manner, as six separate environments are observed for the methylene protons. However, the overall C_2-symmetry of the compound in solution means only one set of peaks are seen for the tris(phenolate) ligands and only two septets are observed for the isopropoxide ligands.
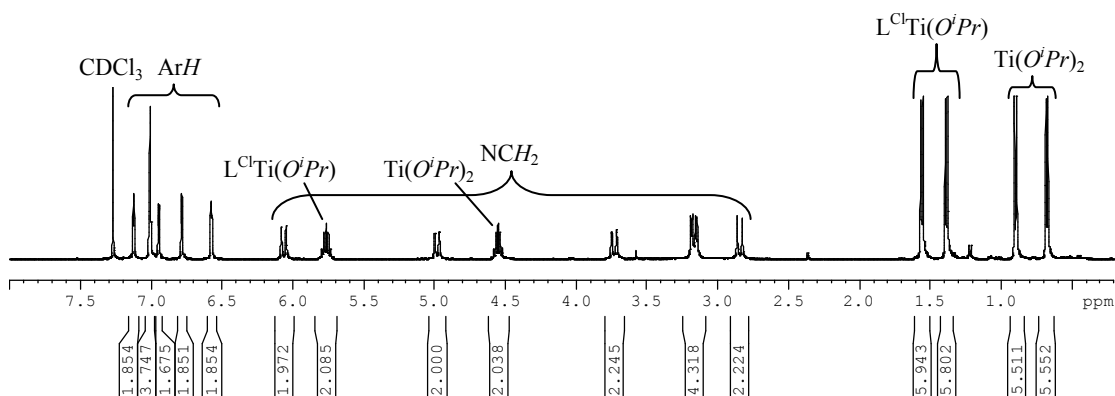
Figure 2.19: ^{1}H NMR spectrum of $L^{Cl}_2Ti_3(O)(O^iPr)_4$ at 298 K in CDCl$_3$.

2.4. Synthesis of Group 4 zwitterionic complexes

As discussed in Chapter 1 of this thesis, the Davidson group has previously reported the synthesis of the zwitterionic complex **[HL^{Me}]$_2$Zr** from the reaction of the sterically unhindered ligand H$_3$L^{Me} with zirconium(IV) isopropoxide.[4] Reaction of the same ligand with hafnium(IV) isopropoxide resulted in isolation of the isomorphous complex **[HL^{Me}]$_2$Hf**, as shown in Scheme 2.5.
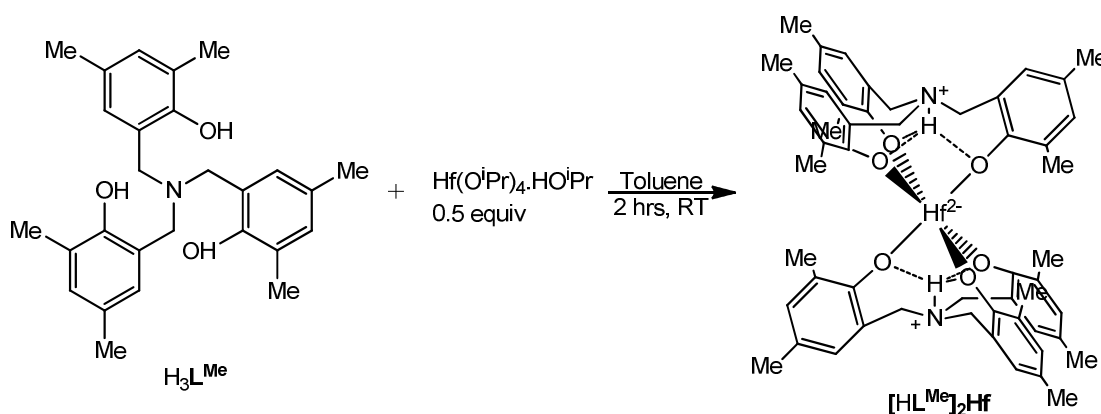
Scheme 2.5: Synthesis of zwitterionic complex [HL^{Me}]$_2$Hf.

X-ray crystallographic analysis has shown this C_3-symmetric complex to contain two formally trianionic **L^{Me}** motifs bound to a central 6-coordinate octahedral Hf centre, resulting in a formal dianionic charge at the metal centre.[16] This charge is balanced by the protonation of both nitrogen atoms to form acidic cationic ammonium centres,[17] which are involved in unusual trifurcated N$\cdots$(HO)$_3$ hydrogen bonding (N1$\cdots$O1 2.872(4) Å, N1-H1-O1 129(3)° for **[HL^{Me}]$_2$Hf**). ^{1}H NMR spectroscopy shows a broad singlet at δ 11.8 corresponding to the N-H protons in both complexes. Two chemical shifts were observed corresponding to the methylene protons of the ligand as broad singlets at δ 4.79 and δ 3.31 for **[HL^{Me}]$_2$Hf**, indicating that fluxionality will occur between the two enantomeric forms of these complex in solution at temperatures above room

76

temperature. Variable temperature ^{1}H NMR studies (Figure 2.20) confirmed that the slow exchange limit for **[HL^{Me}]$_2$Hf** occurs just above 318 K, while the fast exchange limit occurs between 258 K and 278 K. At this point, two sets of doublets are resolved for the downfield signal, as the axial positioned protons are further split by the N-H proton to a greater degree than the equatorial positioned protons, as dictated by the Karplus-Conroy curve.[18]
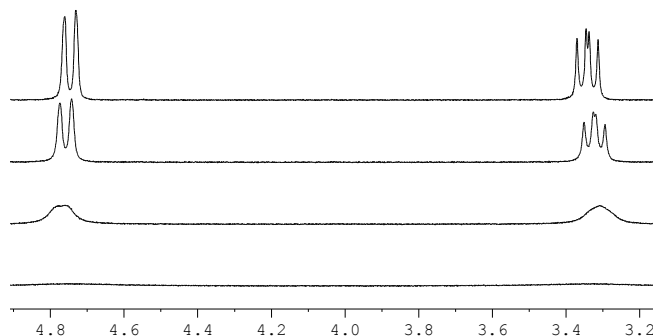
Figure 2.20: ^{1}H NMR spectra of [HL^{Me}]$_2$Hf at 318 K, 298 K, 278 K, 258 K (bottom to top).

Reaction of the chloro-substituted ligand H$_3$L^{Cl} with Zr(IV) yielded a mixture of unidentified compounds in the crude reaction mixture. Washing of this mixture with toluene led to growth of crystals suitable for X-ray crystallography, and an analogous zwitterionic structure was observed, as shown in Figure 2.21. Despite the major electronic change to the ligand there are very few differences between the observed bond angles and bond lengths of this complex and those containing the methyl-substituted ligand. The only point worthy of mention is a more symmetrical trifurcated H-bonding observed in the chloro complex **[HL^{Cl}]$_2$Zr** when compared to **[HL^{Me}]$_2$Hf** (Table 2.3). The zwitterionic nature of these three complexes meant they could be easily observed using mass spectrometry.

H bond	D···A (Å)		
	[HL^{Me}]$_2$Hf	[HL^{Me}]$_2$Zr[4]	[HL^{Cl}]$_2$Zr
N1-H1···O1	2.872(4)	2.868(2)	2.847(2)
N1-H1···O2	2.906(4)	2.920(2)	2.847(2)
N1-H1···O3	2.830(4)	2.834(2)	2.862(2)

Table 2.3: Trifurcated H-bond lengths in zwitterionic complexes.

77
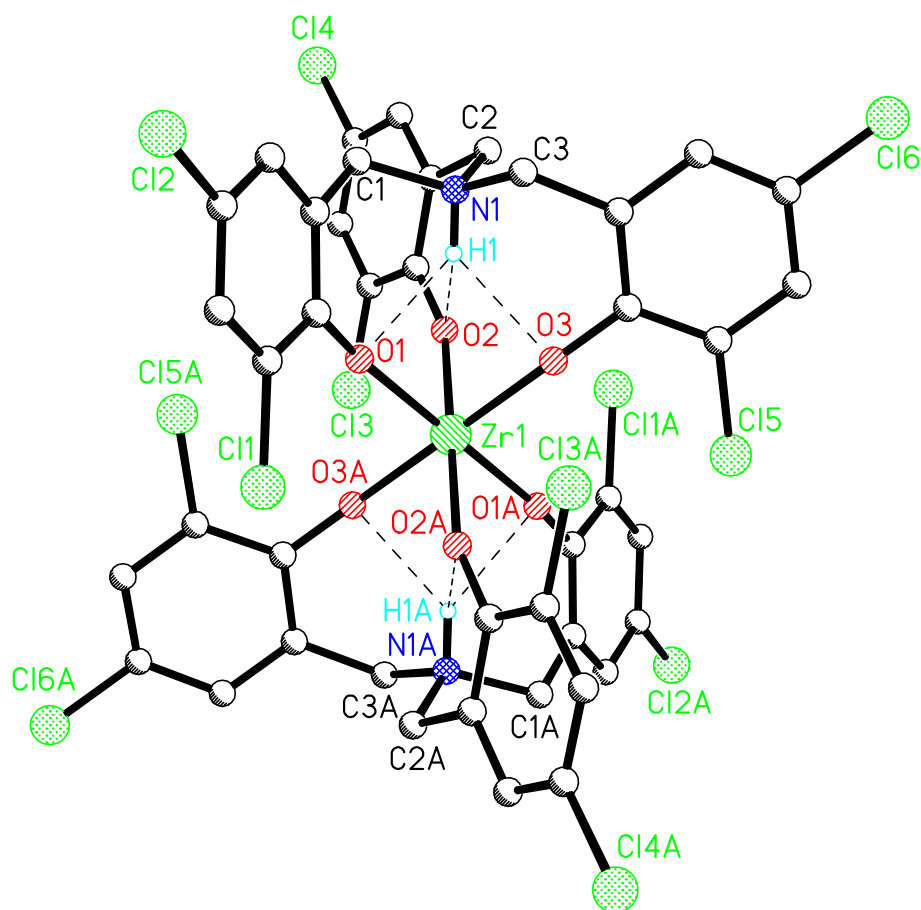
Figure 2.21: Structure of [HL^{Cl}]$_2$Zr as determined by X-ray crystallography. Selected bond lengths [Å]: Zr(1)-O(1) 2.0600(12), Zr(1)-O(2) 2.0555(12), Zr(1)-O(3) 2.0504(12), Zr(1)-N(1) 3.264.

2.5. Ring-opening polymerisation of lactide

All novel Group 4 complexes discussed above were investigated for their potential as initiators for ROP of *rac*-LA. Selected previously reported isopropoxide initiators have also been returned to in order that a better understanding of the mechanism involved can be obtained.[5] Investigations were carried out under the industrially favoured solvent-free conditions, and also in solutions of toluene and chlorinated solvents. Although, less suitable for industrial scale-up, solution studies allow for in-depth investigations into the kinetics of the polymerisation, shedding light on the possible mechanisms of stereocontrol. Preliminary investigations show the zwitterionic complexes **[HL^{Me}]$_2$Zr** and **[HL^{Me}]$_2$Hf** are active for ROP of *rac*-LA in solvent-free conditions, however the absence of a classical initiating group indicates a complex mechanism, to be discussed in due course.

78

Polymer conversions can be conveniently monitored by the relative integrals of the methine signals of the monomer and polymer, which undergoes a downfield shift during the ROP process. In addition, the microstructure of the PLA chain formed will have a profound effect on the nature of the methine signal, transforming from a simple quartet in the case of the *rac*-LA monomer, to a more complex overlay of multiple quartets, each representing a separate stereochemical tetrad. This is clearly seen in the case of heterotactically enriched PLA, obtained from the ROP of *rac*-LA using **L^{tBu}Zr(O^{i}Pr)** (Figure 2.22(c)), in which two quartets are prominent, corresponding to the *sis* and *isi* tetrads. Syndiotactically enriched PLA, obtained from the polymerisation of *meso*-LA using **L^{tBu}Zr(O^{i}Pr)** as initiator, contains only one prominent quartet corresponding to the *sss* tetrad (Figure 2.22(d)).
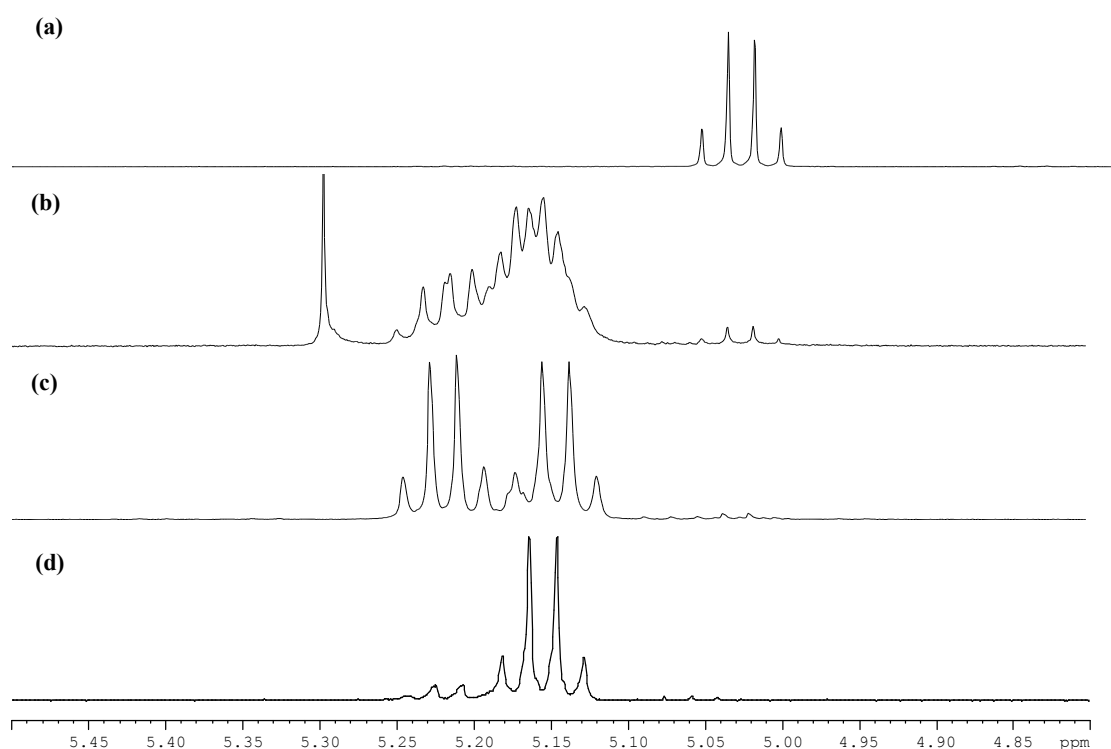
Figure 2.22: Example ^{1}H NMR spectra: (a) LA, (b) atactic PLA from *rac*-LA (Table 2.4, Entry 9) (peak at δ 5.30 due to dichloromethane), (c) heterotactic PLA from *rac*-LA (Table 2.5, Entry 1) and (d) syndiotactic PLA from *meso*-LA (Table 2.5, Entry 2).

As described in Chapter 1, in such cases, homonuclear decoupled ^{1}H spectroscopy can be employed to determine quantatively the degree of stereoselectivity present in the system. A sample of polymer dissolved in CDCl$_3$ (10 mg in 1 ml) was excited at the resonance frequency of methyl CH$_3$ protons. This allows a clear spectrum of the different tetrad signals present to be observed at approx δ 5.2 – 5.3. As shown in Figure 2.23, purely heterotactic PLA from *rac*-LA would exhibit only peaks corresponding to the *isi* and *sis* tetrads, while atactic PLA from *rac*-LA would exhibit the five peaks shown in the ratio 1:1:1:3:2 from left to right.
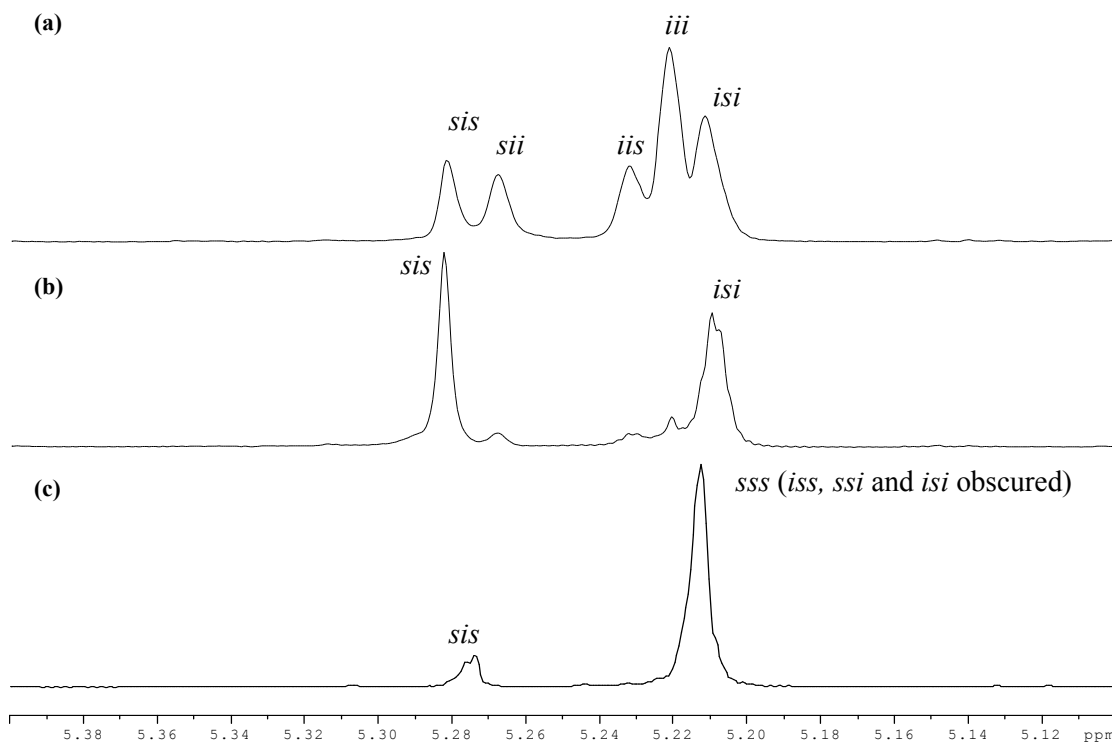
Figure 2.23: Example homodecoupled ^{1}H NMR spectra: (a) atactic PLA from *rac*-LA (Table 2.4, Entry 9), (b) heterotactic PLA from *rac*-LA (Table 2.5, Entry 1) and (a) syndiotactic PLA from *meso*-LA (Table 2.5, Entry 2).

Polymer end-group charaterisation has been previously performed on PLA synthesised using **L^{tBu}Zr(O^{i}Pr)** and **L^{tBu}Hf(O^{i}Pr)**.[5] In both cases, MALDI-ToF mass spectra indicate an isopropoxide group at one end, confirming the initiating nature of this group, and a hydroxyl group at the other chain end, created when the polymerisation is quenched with methanol.[5]

2.5.1. Group 4 isopropoxide initiators

2.5.1.1. Solvent-free ROP

All synthesised isopropoxide complexes have shown activity for the ROP of *rac*-LA in industrially favoured solvent-free conditions with high conversions and molecular weights, summarised in Table 2.4. All mono-nuclear complexes led to the production of PLA exhibiting molecular weights close to the calculated value of M_n = 43,300, with the exception of **L^{Np}Hf(O^{i}Pr)** where the coordinated IPA had been removed by heating (Entry 8). In this case, the polymer was found to possess a much higher molecular weight than the calculated value, and it is possible that decomposition of a significant proportion of the catalyst is taking place during the removal of IPA. The multi-nuclear complexes **L^{Cl}Ti$_2$(O^{i}Pr)$_5$** and **L$^{Cl}_2$Ti$_3$(O)(O^{i}Pr)$_4$** gave rise to lower molecular weight polymer, approximately half the calculated value of M_n, indicating that in both cases polymer chains are growing from more than one Ti centre (Entries 9 and 10). Generally, Ti complexes resulted in polymers with higher values of PDI than was the case with Zr

and Hf complexes, indicating that Ti complexes promote transesterifcation reactions. Mononuclear Ti complexes were also shown to be generally less active for the ROP of *rac*-LA than their Zr and Hf analogues; high conversions were reached after 24 hrs with $\mathbf{L^{Np}Ti(O^iPr)}$ (Entry 5), as opposed to 20 mins in the cases of $\mathbf{L^{Np}Zr(O^iPr)(IPA)}$ (Entry 6) and $\mathbf{L^{Np}Hf(O^iPr)(IPA)}$ (Entry 7). An interesting comparison can be made between $\mathbf{L^{tBu}Zr(O^iPr)}$, reported previously by the Davidson group,[5] and $\mathbf{L^{tBu}Zr(O^tBu)}$, reported by Kol and co-workers,[3] in which the former complex is far more active towards ROP of *rac*-LA (Entry 3: 78% yield, 5 mins) than the latter towards ROP of L-LA (50 % yield, 3 hrs). Although the presence of the bulkier tert-butoxide initiating group will affect activity, there is an apparent difference in the kinetics of the polymerisation of L- and *rac*-LA using this system of initiator, which will be discussed further in a later section of this chapter. Remarkably, Zr and Hf were found to produce polymer with high values of P_s, up to 0.98 in the case of $\mathbf{L^{Np}Zr(O^iPr)(IPA)}$ (Entry 6), indicating a high heterotactic stereoselectivity. However, such high stereocontrol was not observed in polymers initiated by Ti complexes, which resulted in atactic PLA in every case. ROP of *meso*-LA was also undertaken using $\mathbf{L^{tBu}Zr(O^iPr)}$, and as in the case of *rac*-LA, high conversions were observed after only 5 minutes, and resulted in polymer with a molecular weight close to the theoretical value and a narrow polydispersity. A P_s value of 0.70 in the polymerisation of *meso*-LA shows a significant syndiotactic enrichment of the polymer (Entry 11).

Entry	Complex	Time	Conv. (%)	Yield (%)	M_n	PDI	P_s	Ref.
1	$\mathbf{L^{Me}Ti(O^iPr)}$	4 hrs	-	53	51400	1.35	-	[2]
2	$\mathbf{L^{tBu}Ti(O^iPr)}$	30 min	-	50	37100	1.38	0.50	[5]
3	$\mathbf{L^{tBu}Zr(O^iPr)}$	5 min	-	78	32300	1.22	0.96	[5]
4	$\mathbf{L^{tBu}Hf(O^iPr)}$	30 min	-	95	71150	1.19	0.88	[5]
5	$\mathbf{L^{Np}Ti(O^iPr)}$	24 hrs	91	88	51800	1.59	0.55	This work
6	$\mathbf{L^{Np}Zr(O^iPr)(IPA)}$	20 min	93	83	50100	1.20	0.98	"
7	$\mathbf{L^{Np}Hf(O^iPr)(IPA)}$	20 min	94	82	52450	1.15	0.88	"
8	$\mathbf{L^{Np}Hf(O^iPr)}$	20 min	93	90	147300	1.33	0.97	"
9	$\mathbf{L^{Cl}Ti_2(O^iPr)_5}$	20 min	96	83	17350	1.41	0.55	"
10	$\mathbf{L^{Cl}_2Ti_3(O)(O^iPr)_4}$	20 min	72	43	20950	1.19	0.55	"
11	$\mathbf{L^{tBu}Zr(O^iPr)}$	5 min	96	84	54550	1.22	0.70	This work

Table 2.4: ROP of LA. 2.0 g of *rac*-LA (Entries 1 – 10) or *meso*-LA (Entry 11) in the absence of solvent at 130 °C, [LA]/[cat] = 300. M_w, M_n and PDI determined by GPC in THF, relative to polystyrene standards. Conversion as determined via ^{1}H NMR. P_s calculated from the ^{1}H homodecoupled NMR (CDCl$_3$) analysis.

2.5.1.2.   *Solution ROP*

As has been previously reported by Verkade and co-workers[2], mononuclear Ti complexes of this type were found to be inactive towards ROP of *rac*-LA in solution at high temperatures (80 – 130 °C). However, the Zr and Hf mononuclear complexes were found to be active in dichloromethane solutions at room temperature over 48 hours.[5] ROP in solution allows for a greater degree of stereocontrol and P_s values close to 1 were observed. Undertaking the

polymerisations in solution also allowed the kinetics of the reactions to be monitored accurately by ^{1}H NMR spectroscopy. To this end, comparative studies were undertaken using $\mathbf{L^{tBu}Zr(O^iPr)}$ as initiator in the polymerisations of *rac*-, *meso*-, L- and D-LA. Also investigated was the effect of an increase in the sterics of the ligand between the tert-butyl groups of $\mathbf{L^{tBu}}$ and the neo-pentyl groups of $\mathbf{L^{Np}}$.

Entry	Complex	Monomer	Time (hr)	Conv. (%)	M_n	PDI	P_s
1	$\mathbf{L^{tBu}Zr(O^iPr)}$	*rac*-LA	48	98	13400	1.16	0.99
2	$\mathbf{L^{tBu}Zr(O^iPr)}$	*meso*-LA	10	98	27750	1.16	0.78
3	$\mathbf{L^{tBu}Zr(O^iPr)}$	L-LA	168	97	13350	1.06	-
4	$\mathbf{L^{tBu}Zr(O^iPr)}$	D-LA	174	98	13500	1.18	-
5	$\mathbf{L^{Np}Zr(O^iPr).IPA}$	*rac*-LA	26	97	22250	1.14	0.99
6	$\mathbf{L^{Np}Zr(O^iPr).IPA}$	L-LA	142	94	17350	1.07	-

Table 2.5: Solution ROP of LA. [LA]/[cat] = 100, $CD_2Cl_2/CDCl_3$, RT. M_n and PDI determined by GPC in THF relative to polystyrene standards. Conversion as determined via ^{1}H NMR. P_s calculated from the ^{1}H homodecoupled NMR (CDCl$_3$) analysis.

2.5.1.3. *Kinetic studies*

The solution ROP of *rac*-, *meso*-, L- and D-LA using $\mathbf{L^{tBu}Zr(O^iPr)}$ were monitored by removal of aliquots and subsequent analysis by ^{1}H NMR spectroscopy. A conversion vs. time plot for the polymerisations clearly shows the ROP of *rac*- and *meso*-LA proceeding at a significantly faster rate than L- and D-LA (Figure 2.24). An induction period of approx. 30 mins was observed in the cases of *rac*- and *meso*-LA, however semilogarithmic plots show the polymerisations to be first order with respect to monomer concentration (Figure 2.25). Values for the apparent rate constant (k_{app}) of each polymerisation, shown in Table 2.7, can be obtained from the semilogarithmic plots of this data, direct comparison of which dictates that ROP of *rac*-LA using $\mathbf{L^{tBu}Zr(O^iPr)}$ proceeds seven times faster than ROP of either L- or D-LA, themselves shown to proceed at approximately the same rate. These observations are not entirely surprising, bearing in mind the strong heterotactic selectivity demonstrated by $\mathbf{L^{tBu}Zr(O^iPr)}$ in the ROP of *rac*-LA. ROP of *meso*-LA using $\mathbf{L^{tBu}Zr(O^iPr)}$ was found to progress at an even faster rate than *rac*-LA, by a factor of approximately 1.5. A move to a sterically more bulky ligand system, provided by the neo-pentyl substituted ligand $\mathbf{L^{Np}}$, has little effect on the rate constants for ROP of either *rac*-LA or L-LA by $\mathbf{L^{Np}Zr(O^iPr)(IPA)}$. In both cases, $\mathbf{L^{tBu}Zr(O^iPr)}$ was shown to undertake ROP at a slightly faster rate, and the difference between $k_{app(rac)}$ and $k_{app(L)}$, although still profound, was shown to be slightly reduced for $\mathbf{L^{Np}Zr(O^iPr)(IPA)}$ ($k_{app(rac)}/k_{app(L)}$ = 6.5). In a separate control experiment comparing the apparent rate constants for ROP using $\mathbf{L^{tBu}Zr(O^iPr)}$ and the isopropanol-coordinated analogue $\mathbf{L^{tBu}Zr(O^iPr)(IPA)}$, the presence of IPA was shown to have no effect.
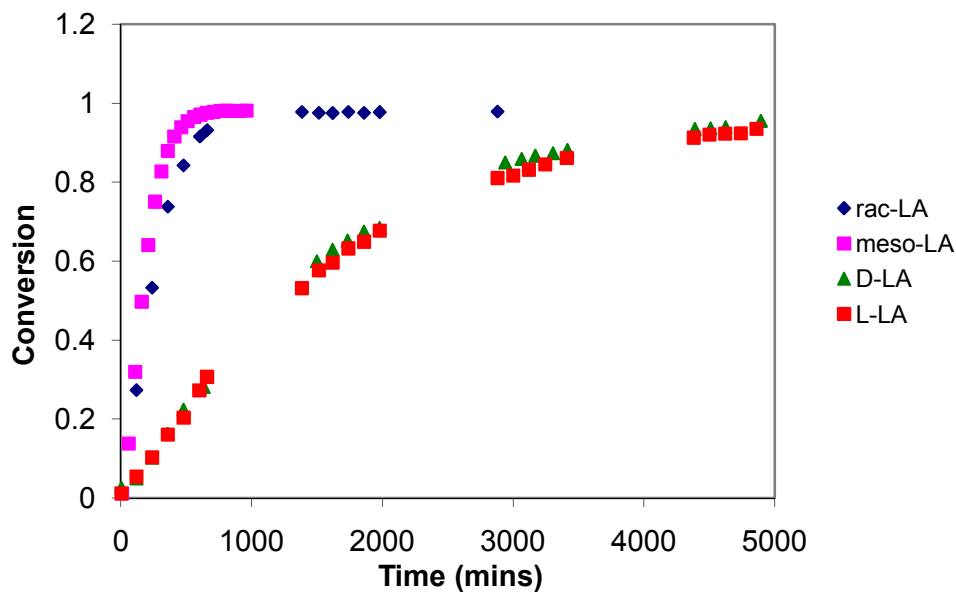
Figure 2.24: Conversion vs time plot for ROP of *rac*-, *meso*-, L- and D-LA using L^{tBu}Zr(O^{i}Pr).
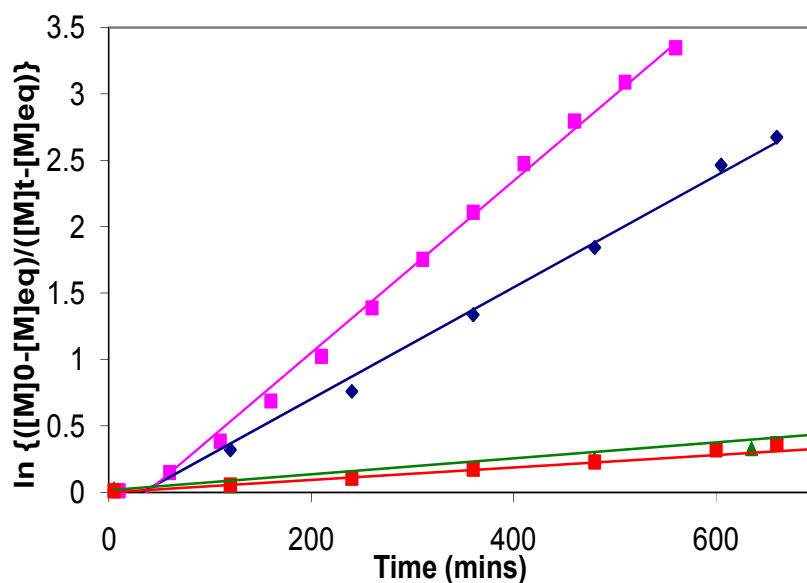
Figure 2.25: Semilogarithmic plot of ln{([M]$_0$-[M]$_{eq}$)/([M]$_t$-[M]$_{eq}$)} vs time.

Initiator	Monomer	k$_{app}$ (min^{-1})	R^2
L^{tBu}Zr(O^{i}Pr)	*rac*-LA	4.2 x 10^{-3}	0.9937
L^{tBu}Zr(O^{i}Pr)	*meso*-LA	6.5 x 10^{-3}	0.9949
L^{tBu}Zr(O^{i}Pr)	L-LA	0.6 x 10^{-3}	0.9991
L^{tBu}Zr(O^{i}Pr)	D-LA	0.6 x 10^{-3}	0.9983
L^{Np}Zr(O^{i}Pr)(IPA)	*rac*-LA	3.4 x 10^{-3}	0.9829
L^{Np}Zr(O^{i}Pr)(IPA)	L-LA	0.4 x 10^{-3}	0.9884

Table 2.7: Apparent rate constants (k$_{app}$) calculated from kinetic data. Calculated error < 1%.

Previous reports from the Nomura group have used the relative ROP rates of *rac*-LA and enantiomerically pure D- or L-LA to estimate the resulting degree of stereocontrol in the synthesis of isotactically enriched PLA using achiral salen-aluminium complexes.[19] As such, the following relationship was reported, where $k_{(rac)}$ is the rate of ROP of *rac*-LA, $k_{(D-L)}$ is the rate of inserting an L-LA unit into a D-chain end and $k_{(L-L)}$ is the rate of inserting an L-LA unit into an L-chain end:

$$k_{(rac)} = \tfrac{1}{2} \left(k_{(L-L)} + k_{(D-L)} \right) \qquad (1)$$

$$k_{(D-L)} = 2k_{(rac)} - k_{(L-L)} \qquad (2)$$

Given that, by definition[20]:

$$P_s = k_{(D-L)} / \left(k_{(D-L)} + k_{(L-L)} \right) \qquad (3)$$

Rearrangement and substitution give:

$$P_s = \left(2k_{(rac)} - k_{(L-L)} \right) / 2k_{(rac)} - k_{(L-L)} + k_{(L-L)} \qquad (4)$$

$$P_s = 1 - \tfrac{1}{2} \left(k_{(L-L)} / k_{(rac)} \right) \qquad (5)$$

Given that, $k_{app} = k[\text{Initiator}]_o^n$, and assuming that the concentration and order of initiator are constant for ROP of *rac*-, D- or L-LA:

$$k_{app(L-L)} / k_{app(rac)} = k_{(L-L)} / k_{(rac)} \qquad (6)$$

Combination of (5) and (6) gives:

$$P_s = 1 - \tfrac{1}{2} \left(k_{app(L-L)} / k_{app(rac)} \right) \qquad (7)$$

In the case of $\mathbf{L^{tBu}Zr(O^iPr)}$, $k_{app(rac)} / k_{app(L-L)} = 7$, therefore P_s can be calculated as 0.93. This is close to the experimentally determined value of $P_s = 0.99$, although it is proposed that in reality, monomer addition to a polymer chain is determined by more than one LA unit.

A plot of equation (7) allows P_s to be predicted for a range of $k_{app(rac)} / k_{app(L-L)}$ values (Figure 2.26). As such, it is clear that a difference in rates by any less than a factor of seven would have a profoundly detrimental effect on the P_s of the resulting polymer, whereas a significant increase in the difference in rates would increase P_s by only a small amount. A $k_{app(rac)} / k_{app(L-L)}$ value of seven is therefore optimal in the achievable synthesis of highly heterotactically enriched PLA.

$$P_s = 1 - \tfrac{1}{2}(k_{L-L}/k_{rac})$$
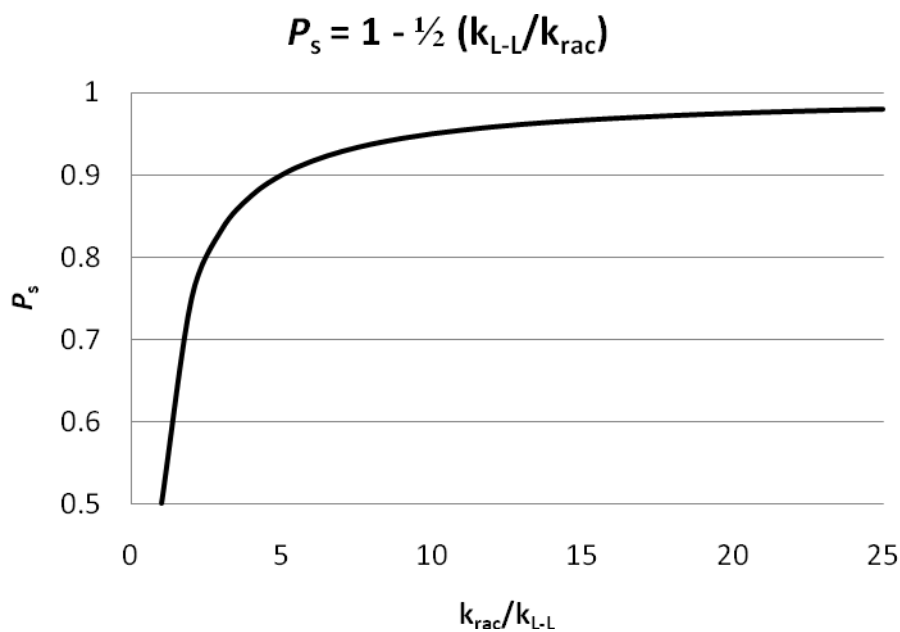
Figure 2.26: Plot of equation (7).

2.5.1.4.   *Mechanism of stereocontrol*

As described in the introductory chapter of this thesis, stereocontrol of an initiator commonly arises from one of two mechanisms.[21] A chain-end control mechanism (CEC) would selectively polymerise a LA monomer with the opposite stereochemistry to that which was subsequently polymerised, as shown in Scheme 2.6(i). On the other hand, in this case, an enantiomorphic site control mechanism (ESC) would selectively polymerise a LA monomer based on the dynamic chirality of the complex i.e. (*P*) or (*M*), as shown in Scheme 2.6(ii). Previous work by the Davidson group has postulated the mechanism of stereocontrol exhibited by this series of initiators to be dependent on aspects of both traditional mechanisms, and is termed 'enhanced chain end control'.[12]   Here, the correct combination of chain-end and complex chirality is required at each insertion step, shown in Scheme 2.6(iii).   The (*R,R*)-(*M*)-M enantiomer is selective towards L-LA insertion, while the (*S,S*)-(*P*)-M enantiomer is selective towards D-LA insertion. The fluxionality of the Zr and Hf systems allows ready interconversion between the two enantiomers formed after each monomer addition, and heterotactic propagation can occur.   It is possible that the absence of fluxionality in the Ti systems inhibits the path of selectivity, resulting in lower activities and atactic PLA. The profound differences in rate between ROP of *rac*- and enantiomerically pure L- or D-LA using Zr and Hf systems are also explained by this mechanism, as consecutive addition of identical monomers is unfavourable and so the polymerisation proceeds at a slower rate.

(R,**R**)-(P/M)-M $\xrightarrow{(S,S)\text{-LA}}$ (R,R)-(S,**S**)-(P/M)-M $\xrightarrow{(R,R)\text{-LA}}$ heterotactic propagation   **(i)**

(R,R)-(**P**)-M $\xrightarrow{(S,S)\text{-LA}}$ (R,R)-(S,S)-(**M**)-M $\xrightarrow{(R,R)\text{-LA}}$ heterotactic propagation   **(ii)**

(R,R)-(P)-M   (R,R)-(S,**S**)-(**P**)-M $\xrightarrow{(R,R)\text{-LA}}$ heterotactic propagation   **(iii)**

(R,**R**)-(**M**)-M $\xrightarrow{(S,S)\text{-LA}}$ (R,R)-(S,S)-(**M**)-M
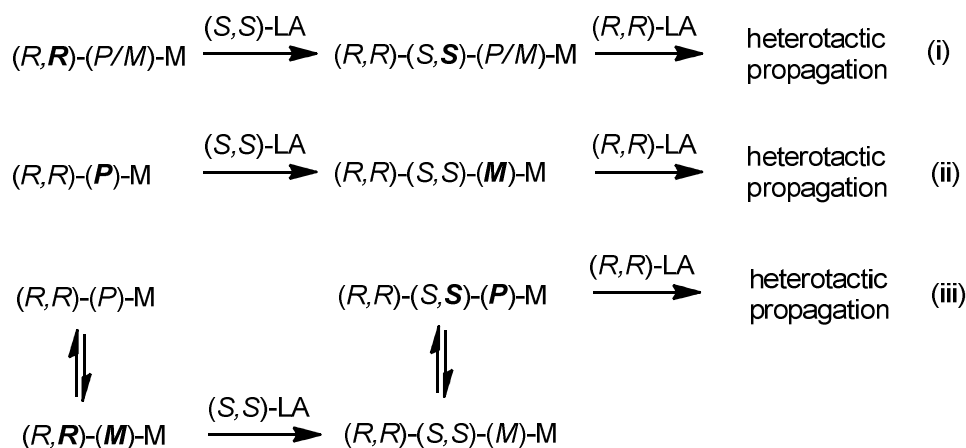
Scheme 2.6: Possible mechanisms of stereocontrol – (i) chain-end control, (ii) dynamic enantiomorphic site control, (iii) enhanced chain-end control.

In an effort to confirm the proposed mechanism, the previously synthesised and available chiral Zr complex ***L^{tBu}Zr(O^{i}Pr)** was utilised.[22] Synthesised from the chiral ligand (R)-H$_3$***L^{tBu}** reported by Bull, Davidson et al,[23] ***L^{tBu}Zr(O^{i}Pr)** includes a methyl group substituted onto one of the ligand methylene groups, resulting in the loss of C_3-symmetry (Scheme 2.7). Surprisingly, minimum fluxionality was observed between the (P) and (M) forms of ***L^{tBu}Zr(O^{i}Pr)** on the NMR timescale up to temperatures of 378 K, as determined by VT ^{1}H NMR spectroscopy. The **(R,M)-*L^{tBu}Zr(O^{i}Pr)** conformation, in which the methyl group is positioned axially, decreasing steric interactions, was found to be most favorable, the structure having been confirmed by X-ray crystallographic analysis.[22] As such, this system uniquely allows control of complex fluxionality with no change to electronics and only a small variation in sterics.
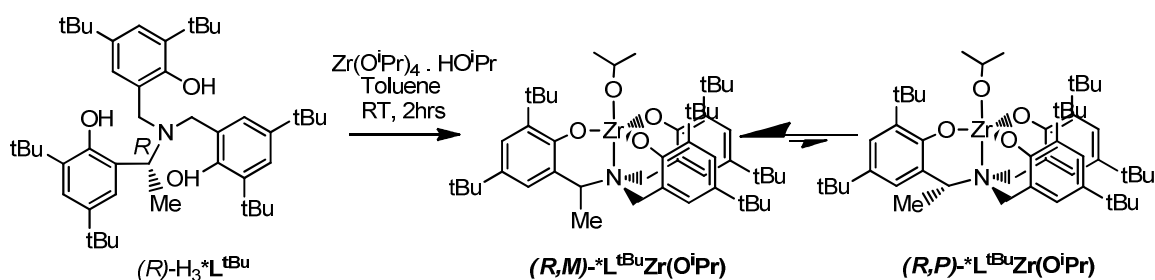
Scheme 2.7: Synthesis of chiral complex *L^{tBu}Zr(O^{i}Pr).

Kinetic investigations into the solution ROP of *rac-*, *meso-*, L- and D-LA using the chiral initiator ***L^{tBu}Zr(O^{i}Pr)** were undertaken on an NMR scale. The results of these experiments are therefore not directly comparable to those previously discussed undertaken on a larger scale, and so to allow comparison between the kinetics of **L^{tBu}Zr(O^{i}Pr)** and ***L^{tBu}Zr(O^{i}Pr)**, the polymerisation of *rac*-LA by achiral **L^{tBu}Zr(O^{i}Pr)** was repeated on the NMR scale. Selected semi-logarithmic plots of these experiments are shown in Figures 2.27-2.28 and the calculated values of k$_{app}$ in Table 2.8.
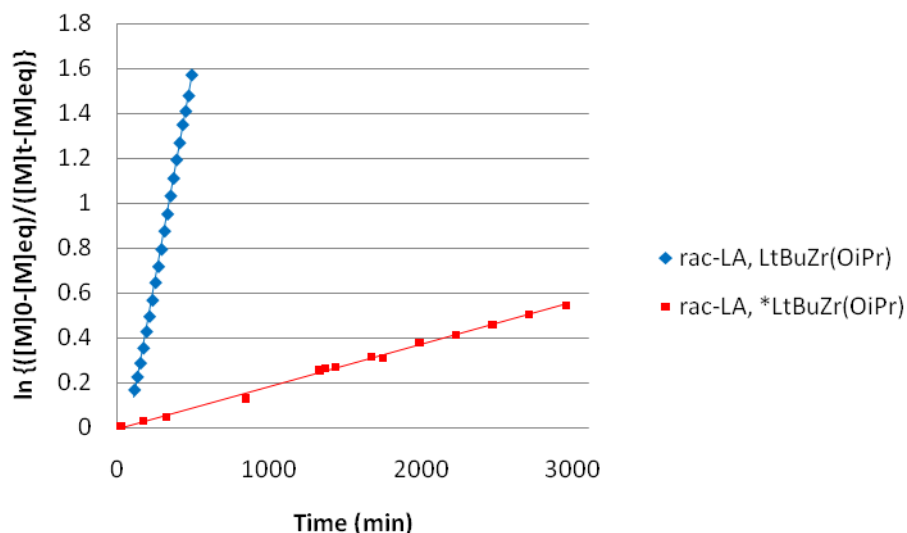
Figure 2.27: Semilogarithmic plots of *rac*-LA ROP by L^tBuZr(O^iPr) and *L^tBuZr(O^iPr).
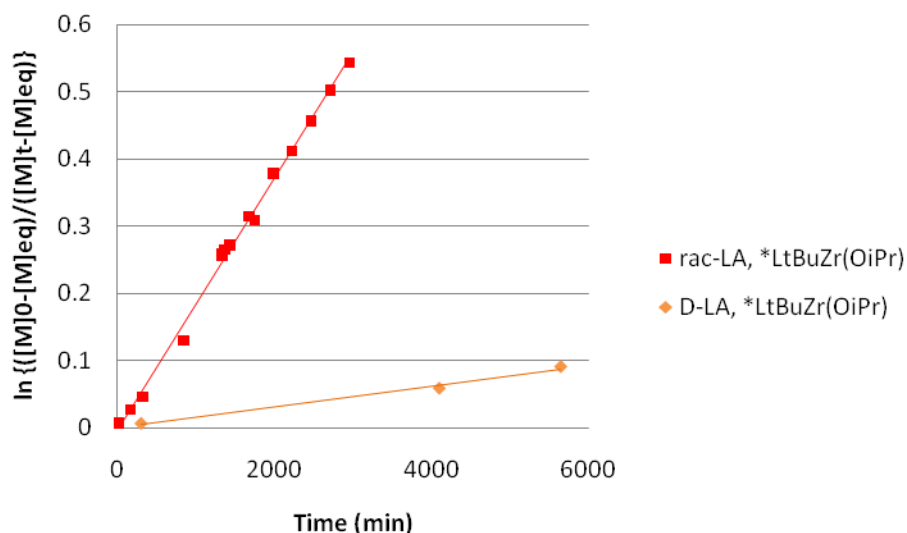
Figure 2.28: Semilogarithmic plots of *rac*-, D- and L-LA ROP by *L^tBuZr(O^iPr).

Initiator	Monomer	k_{app} (min^{-1})	R^2
L^tBuZr(O^iPr)	*rac*-LA	3.8×10^{-3}	0.9991
*L^tBuZr(O^iPr)	*rac*-LA	0.2×10^{-3}	0.9957
*L^tBuZr(O^iPr)	*meso*-LA	0.9×10^{-3}	0.9985
*L^tBuZr(O^iPr)	L-LA	No appreciable polymerisation	
*L^tBuZr(O^iPr)	D-LA	0.02×10^{-3}	0.9899

Table 2.8: Values of k_{app} for *L^tBuZr(O^iPr) calculated from kinetic data. Calculated error < 5%.

In the case of both the chiral and achiral initiator, k_{app} follows the order *meso-* > *rac-* > D-/L-LA, however $k_{app(rac)}$ was shown to be larger for **L^tBuZr(O^iPr)** than ***L^tBuZr(O^iPr)** by a factor of almost 20. This can be explained by the reduced fluxionality in the chiral complex, and so

interconversion between the *P* and *M* enantiomers of the complex does not occur so readily. In the ROP of *rac*-LA, this will have an adverse affect on the addition of every other monomer, however, crucially heterotactic addition is still observed, albeit at a decreased rate.

(R,R)-(R,P)-Zr $\quad\quad\quad$ (R,R)-$(S,\boldsymbol{S})$-$(R,\boldsymbol{P})$-Zr $\xrightarrow[slow]{(R,R)\text{-LA}}$ heterotactic propagation

$(R,\boldsymbol{R})$-$(R,\boldsymbol{M})$-Zr $\xrightarrow[fast]{(S,S)\text{-LA}}$ (R,R)-(S,S)-(R,M)-Zr
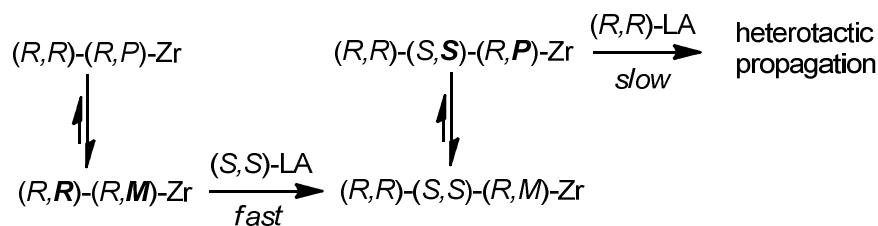
Scheme 2.8: Heterotactic propagation using *L^{tBu}Zr(O^{i}Pr) proceeding via enhanced chain-end control.

As was the case for the achiral catalyst, ***L^{tBu}Zr(O^{i}Pr)** was shown to undertake ROP of D-LA approximately an order of magnitude slower than *rac*-LA. However, unlike the achiral system, a significant difference was observed in the ROP of D- and L- LA by ***L^{tBu}Zr(O^{i}Pr)**. In the case of D-LA high conversions are eventually obtained after several weeks at room temperature, but no polymerisation of L-LA was observed under the same conditions. These observations can be tentatively attributed to the relative stability of the (R,M)-Zr form over the (R,P)-Zr form, allowing polymerisation of D-LA, however the diastereoselective control exhibited by this system results in a slow rate of polymerisation when the correct chain-end chirality is absent.[12] In the case of L-LA, an absence of both the correct chain-end chirality and the correct complex chirality at room temperature results in no appreciable polymerisation over the observed timescale.

(R,R)-(R,P)-Zr $\quad\quad\quad$ (R,R)-(R,R)-(R,P)-Zr

$(R,\boldsymbol{R})$-$(R,\boldsymbol{M})$-Zr $\xdashrightarrow{(R,R)\text{-LA}}$ (R,R)-$(R,\boldsymbol{R})$-$(R,\boldsymbol{M})$-Zr $\xdashrightarrow{(R,R)\text{-LA}}$ PDLA
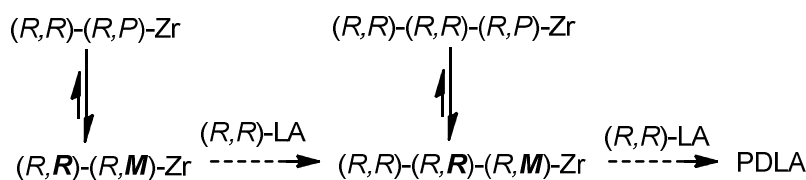
Scheme 2.9: ROP of D-LA by *L^{tBu}Zr(O^{i}Pr).

$(S,\boldsymbol{S})$-$(R,\boldsymbol{P})$-Zr $\xrightarrow{(S,S)\text{-LA}}\!\!\!\!\!\times$ (S,S)-$(S,\boldsymbol{S})$-$(R,\boldsymbol{P})$-Zr $\xrightarrow{(S,S)\text{-LA}}\!\!\!\!\!\times$ No appreciable polymerisation

(S,S)-(R,M)-Zr $\quad\quad\quad$ (S,S)-(S,S)-(R,M)-Zr
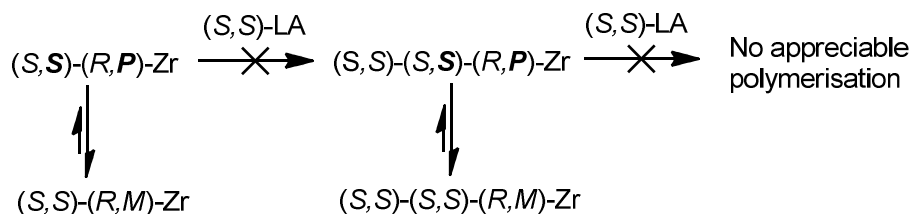
Scheme 2.10: No appreciable polymerisation of L-LA is observed by *L^{tBu}Zr(O^{i}Pr).

2.5.2. Group 4 zwitterionic initiators

The zwitterionic complexes $\mathbf{[HL^{Me}]_2Zr}$, reported in 2003, and $\mathbf{[HL^{Me}]_2Hf}$, reported in this thesis, have until now remained unexplored with respect to their ROP potential. Despite the absence of a classical initiating group, ROP of *rac*-LA was undertaken by these initiators to high conversions under solvent-free conditions, both with and without the addition of a co-initiator.

2.5.2.1.   Solvent-free ROP

Initial results under solvent-free conditions showed both complexes to be active and most remarkably, resulted in heterotactically enriched polymer. Considerably high molecular weights were observed after reaction times of 20 hrs, but these were seen to reduce, with conversion, when shorter reaction times were implicated. Increasing the monomer to initiator ratio from 300:1 to 150:1 did not result in a decrease in polymer molecular weight, as would be expected in well-controlled ROP.
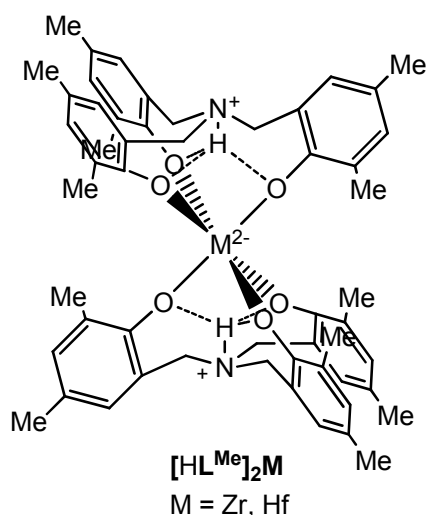
Figure 2.29: Structure of $[HL^{Me}]_2Zr$ and $[HL^{Me}]_2Hf$.

Entry	Initiator	Time	[M]/[I]	Conv. (%)[c]	M_n[d]	M_w[d]	PDI[d]	P_s[e]
1	$[HL^{Me}]_2Hf$[a]	20 hrs	300	77	266700	429850	1.61	0.83
2	$[HL^{Me}]_2Zr$[a]	20 hrs	300	69	653700	909100	1.39	0.84
3	$[HL^{Me}]_2Zr$[a]	6 hrs	300	58	306150	358300	1.17	0.78
4	$[HL^{Me}]_2Zr$[b]	4 hrs	300	10	69000	70200	1.02	0.79
5	$[HL^{Me}]_2Zr$[b]	2 hrs	300	5	21750	22150	1.02	0.80
6	$[HL^{Me}]_2Zr$[b]	30 mins	300	~ 0	-	-	-	-
7	$[HL^{Me}]_2Zr$[b]	2 hrs	150	6	31400	32750	1.04	0.79
8	$[HL^{Me}]_2Zr$[b]	1 hr	75	~ 0	-	-	-	-

Table 2.9: Solvent-free ROP of *rac*-LA by zwitterionic initiators. [a] 2.0 g or [b] 1.0 g of *rac*-LA in the absence of solvent at 130 °C. [c] Conv. (%) determined by ^{1}H NMR spectroscopy. [d] M_w, M_n and PDI determined by GPC in THF, relative to polystyrene standards. [e] P_s determined by homonuclear decoupled ^{1}H NMR spectroscopy.

2.5.2.2. *Proposed mechanism*

The observations indicate that the mechanism involved is not a conventional coordination-insertion type, resulting from a lack of formal initiating group. In such a circumstance, it is reasonable to believe that k_{init} is slow in comparison to k_{prop}, and so much larger molecular weights are observed than would be expected. It is thought that the ROP of LA by **[HL^{Me}]₂Zr** and **[HL^{Me}]₂Hf** depends on the presence of small amounts of protic impurities which act as a co-initiator. The stability given to these complexes by their zwitterionic nature makes the formation of an initiating complex, by direct reaction with an alcohol, unlikely. Instead, initiation is thought to proceed via an activated monomer mechanism, in which the monomer is activated by the protic impurity while coordinated to the metal centre. However, the sterically crowded nature of the metal centre, coupled with the small amounts of protic impurities present in the system, results in a slow initiation process ($k_{init} \lll k_{prop}$).
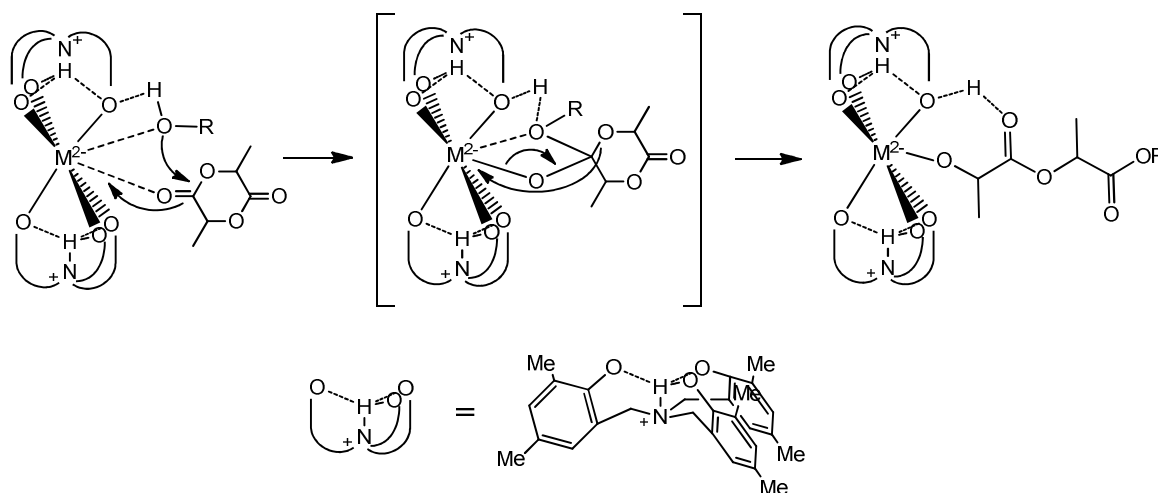
Scheme 2.11: Proposed mechanism of initiation in ROP of LA by [HL^{Me}]₂Zr and [HL^{Me}]₂Hf.

End-group analysis of the resulting polymers via MALDI-ToF Mass Spectrometry was not possible due to the lack of molecular weight control afforded by this class of initiator, however inspection of the ¹H NMR spectra of these polymers showed the retention of the zwitterionic complex within the polymer. It is unclear whether the complex forms part of a polymer end-group or is simply trapped within the matrix of the polymer, although quenching of the polymerisation by the addition of MeOH would most likely cleave the complex from the polymer chain-end.

2.5.2.3. *Addition of co-initiator*

The purposeful addition of 1 and 10 equivalents of a co-initiator, benzyl alcohol, to the solvent-free polymerisation of *rac*-LA by the zwitterionic complex **[HL^{Me}]$_2$Zr** resulted in a decrease in the molecular weight of polymers (Table 2.10). It is thought that the ready availability of co-initiator facilitates a more rapid initiation process, resulting in improved molecular weight control. Short-chain PLA synthesised in this manner (Table 2.10, Entry 2) was analysed by MALDI-ToF mass spectrometry, which confirmed that these polymers contain at –OBn end group (Figure 2.30). These zwitterionic initiators were found to be inactive towards ROP of LA in solution both with and without the addition of the co-initiator, benzyl alcohol, even at elevated temperatures

Entry	Initiator	Time	[BnOH]/[I]	Conv. (%)[a]	M_n[b]	M_w[b]	PDI[b]	P_s[c]
1	[HL^{Me}]$_2$Zr	20 hrs	1	74	166950	276100	1.65	0.77
2	[HL^{Me}]$_2$Zr	20 hrs	10	84	6300	6500	1.04	0.70

Table 2.10: Solvent-free ROP of *rac*-LA by zwitterionic initiators in the presence of a co-initiator. 2.0 g of *rac*-LA in the absence of solvent at 130 °C, [M]/[I] = 300. [a] Conv. (%) determined by ^{1}H NMR spectroscopy. [b] M_w, M_n and PDI determined by GPC in THF, relative to polystyrene standards. [c] P_s determined by homonuclear decoupled ^{1}H NMR spectroscopy.
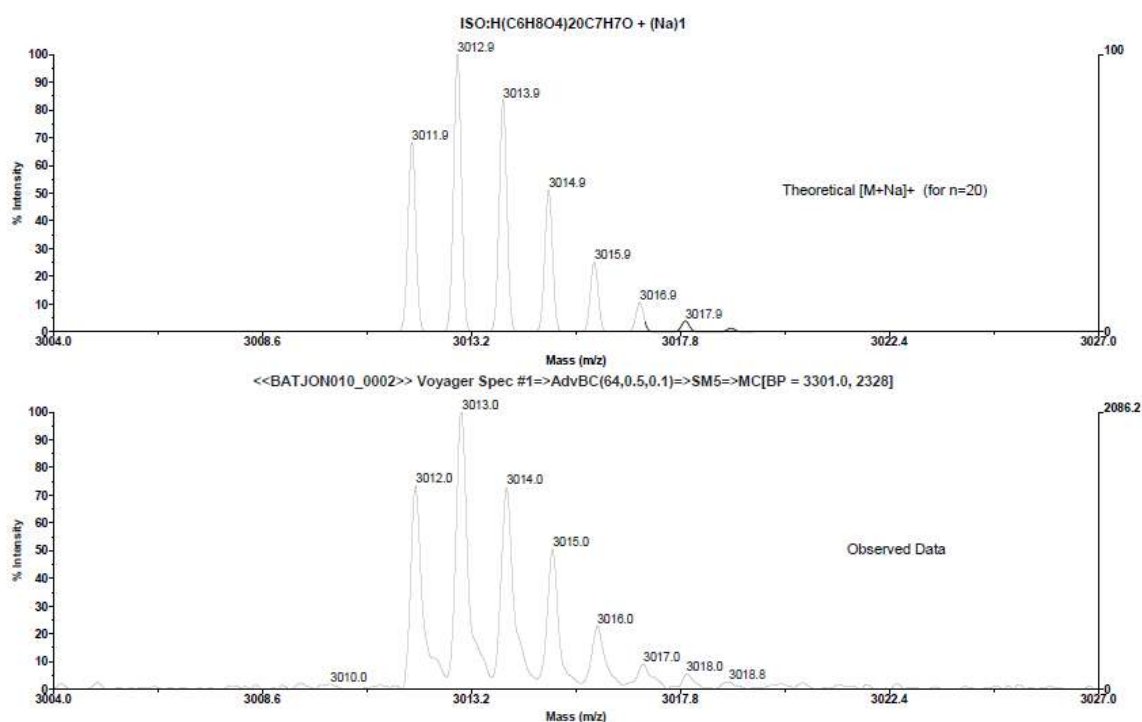
Figure 2.30: MALDI-ToF mass spectra of PLA synthesised with [HL^{Me}]$_2$Zr and 10 equiv. BnOH. Expansion of experimental spectrum (bottom) and calculated data for BnO-terminated PLA (top).

2.6. Summary

Within this chapter, the synthesis of a series of amine tris(phenolate) ligands was described, featuring either alkyl or halo substituents on the aryl rings, including two previously unreported ligands, H_3L^{Np} and H_3L^{Br}. Reaction of these ligands with Group 4 isopropoxides led to a variety of metal complexes, the nature of which have been fully investigated. In addition, their potential as initiators for the well-controlled stereoselective ROP of *rac*-LA and *meso*-LA has been examined.

$L^{Np}Ti(O^iPr)$ was found to possess the familiar five-coordinate tetradentate C_3-symmetric structure, while $L^{Np}Zr(O^iPr)(IPA)$ and $L^{Np}Hf(O^iPr)(IPA)$ were shown to adopt a six-coordinate pseudo C_3-symmetric structure due to the presence of a coordinated molecule of IPA. Well-controlled ROP of *rac*-LA was observed with these initiators under solvent-free conditions. In line with previous reports,[5] the Zr and Hf analogues showed a high degree of heterotactic selectivity, while $L^{Np}Ti(O^iPr)$ resulted only in atactic PLA. In contrast, reaction of H_3L^{Cl} with $Ti(O^iPr)_4$ yielded multinuclear complexes which were found to undergo ROP at multiple sites, and did not show any stereocontrol.

The initiator $L^{tBu}Zr(O^iPr)$, which was previously shown to give heterotactic selectivity in the ROP of *rac*-LA, has now been shown to exhibit a syndiotactic selectivity in the ROP of *meso*-LA. In-depth kinetic analysis of $L^{tBu}Zr(O^iPr)$ and the chiral initiator $*L^{tBu}Zr(O^iPr)$ suggest a diastereoselective mechanism of PLA stereocontrol, in which both the polymer chain end and the metal centre must possess the correct combination of stereochemistries.

The zwitterionic complexes, $[HL^{Me}]_2Zr$ and $[HL^{Me}]_2Hf$, were also shown to exhibit a strong heterotactic selectivity in the ROP of *rac*-LA, which is especially interesting considering their observed departure from the traditional initiator-led coordination insertion mechanism. Instead, in these cases, the well-controlled ROP of *rac*-LA was shown to depend on the presence of a co-initiator. When absent, it is proposed that initiation depends entirely on the presence of protic impurities within the monomer, resulting in long reaction times and high molecular weights.

2.7. References

1.   Kim, Y.; Verkade, J. G., *Organometallics* **2002,** *21* (12), 2395-2399.
2.   Kim, Y.; Jnaneshwara, G. K.; Verkade, J. G., *Inorg. Chem.* **2003,** *42* (5), 1437-1447.
3.   Gendler, S.; Segal, S.; Goldberg, I.; Goldschmidt, Z.; Kol, M., *Inorg. Chem.* **2006,** *45* (12), 4783-4790.
4.   Davidson, M. G.; Doherty, C. L.; Johnson, A. L.; Mahon, M. F., *Chem. Commun.* **2003,** (15), 1832-1833.

5.   Chmura, A. J.; Davidson, M. G.; Frankis, C. J.; Jones, M. D.; Lunn, M. D., *Chem. Commun.* **2008,** (11), 1293-1295.

6.   Kol, M.; Shamis, M.; Goldberg, I.; Goldschmidt, Z.; Alfi, S.; Hayut-Salant, E., *Inorg. Chem. Commun.* **2001,** *4* (4), 177-179.

7.   Kubono, K.; Hirayama, N.; Kokusen, H.; Yokoi, K., *Anal. Sci.* **2001,** *17* (7), 913-914.

8.   Kelly, B. V.; Weintrob, E. C.; Buccella, D.; Tanski, J. M.; Parkin, G., *Inorg. Chem. Commun.* **2007,** *10* (6), 699-704.

9.   Groysman, S.; Goldberg, I.; Kol, M.; Genizi, E.; Goldschmidt, Z., *Adv. Synth. Catal.* **2005,** *347* (2-3), 409-415.

10.   Chartres, J. D.; Dahir, A.; Tasker, P. A.; White, F. J., *Inorg. Chem. Commun.* **2007,** *10* (10), 1154-1158.

11.   Fortner, K. C.; Bigi, J. P.; Brown, S. N., *Inorg. Chem.* **2005,** *44* (8), 2803-2814.

12.   Chmura, A. J.; Chuck, C. J.; Davidson, M. G.; Jones, M. D.; Lunn, M. D.; Bull, S. D.; Mahon, M. F., *Angew. Chem., Int. Ed.* **2007,** *46* (13), 2280-2283.

13.   Kawaguchi, H.; Matsuo, T., *J. Organomet. Chem.* **2004,** *689* (24), 4228-4243.

14.   Whitelaw, E. L.; Jones, M. D.; Mahon, M. F.; Kociok-Kohn, G., *Dalton Trans.* **2009,** (41), 9020-9025.

15.   Zelikoff, A. L.; Kopilov, J.; Goldberg, I.; Coates, G. W.; Kol, M., *Chem. Commun.* **2009**, 6804-6806.

16.   Chauvin, R., *Eur. J. Inorg. Chem.* **2000,** (4), 577-591.

17.   Brammer, L.; Rivas, J. C. M.; Spilling, C. D., *J. Organomet. Chem.* **2000,** *609* (1-2), 36-43.

18.   Gunther, H., *NMR Spectroscopy - An Introduction*. John Wiley & Sons, Ltd.: 1980.

19.   Nomura, N.; Ishii, R.; Yamamoto, Y.; Kondo, T., *Chem.--Eur. J.* **2007,** *13* (16), 4433-4451.

20.   Bovey, F. A., *NMR of Polymers*. Academic Press, Inc.: 1996.

21.   Stanford, M. J.; Dove, A. P., *Chem. Soc. Rev.* **2010,** *39* (2), 486-494.

22.   Chmura, A. J. Group 4 Metal Alkoxide Complexes as Initiators for the Ring Opening Polymerisation of Cyclic Esters. University of Bath, Bath, United Kingdom, 2008.

23.   Axe, P.; Bull, S. D.; Davidson, M. G.; Gilfillan, C. J.; Jones, M. D.; Robinson, D.; Turner, L. E.; Mitchell, W. L., *Org. Lett.* **2007,** *9* (2), 223-226.

Chapter 3
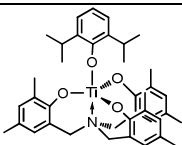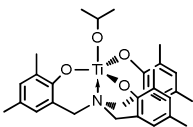
Group 4 complexes of amine tris(phenolates) as initiators for ROP of lactide:

Effect of initiating group variation

3. Group 4 complexes of amine tris(phenolates) as ROP initiators: Effect of initiating group variation

3.1. Preamble

Although less influential on stereocontrol, the nature of the initiating group present has been shown to have a profound effect on the activity of the initiator, as well as the molecular weight and polydispersity of the resulting polymer.[1] The majority of aryl and alkoxide initiators exhibit good polymer control, due to a fast rate of initiation compared to the rate of propagation. However, the sterics of these groups can also impinge on the overall rate of polymerisation, and so aryloxides and the bulkier alkoxides often require longer reaction times. This is demonstrated by results taken from two publications from the research group of Verkade, in which a Ti complex featuring the bulky diisopropylphenolate initiator was shown to be less active and resulted in broader polydispersities in comparison to $\mathbf{L^{Me}Ti(O^iPr)}$ (Table 3.1).[2-3]

Initiator	Monomer	Time (hr)	Yield (%)	M_w	M_n	PDI
	L-LA	24	69	29300	19400	1.51
	rac-LA	24	68	23000	16000	1.43
	L-LA	4	55	76100	52000	1.46
	rac-LA	4	53	51400	38000	1.32

Table 3.1: Selected bulk polymerisation data 130 °C, [LA]/[Ti] = 300, 2 g of LA.

Other initiating groups investigated over the years, with varying degrees of success, include alkyl, acetyl and amido, however all were reported as inferior compared to alkoxides. In 2001, Coates investigated the initiating groups –N(SiMe$_3$), -Et and –OAc within his series of zinc and magnesium β-diiminate complexes, reporting the detrimental effect on molecular weight control and activity resulting from these groups compared to –O^{i}Pr.[4] It was thought most likely that direct insertion of the group into the acyl-oxygen bond of the LA monomer does not occur, instead relying on impurities in the monomer as a co-initiator, as is also thought to be the case in the Sn(II)Oct$_2$ initiated system. This slows the rate of initiation with respect to the rate of propagation, and broad polydispersities often result. Similar findings were reported by Carpentier and co-workers within the scope of a series of lanthanide initiators.[5] Here, once again, lower values of PDI and higher activities were reported on switching from silyl amide to alkoxy initiating groups. However, Chisholm and co-workers reported that the use of sterically less

hindered dialkylamido initiating groups had the opposite effect on reactivity, and the complex Ph$_3$Sn(NMe$_2$) was found to have a higher activity than its isopropoxide analogue, Ph$_3$Sn(O^{i}Pr).[6] In cases such as this, it has been reasoned that the increased basicity is responsible for the increase in activity. However, in the silylamides, the lone pair on the nitrogen is sterically less accessible, and so does not react so rapidly.

More recently, increased attention has been paid to the use of borohydride groups as initiators for ROP of cyclic esters. Concentrating on ε-caprolactone, Guillaume and co-workers have investigated a series of both ligand supported, [Sm(η-C$_5$Me$_5$)$_2$(BH$_4$)(THF)], and non-supported, [Nd(BH$_4$)$_3$(THF)$_3$], rare earth borohydride complexes with respect to their activity and mechanism.[7-11] Mountford and co-workers were the first to report the borohydride-initiated ROP of LA using the amine bis(phenolate) coordinated rare earth complexes described previously in Chapter 1 and shown in Figure 3.1.[12]

Ln = Y, Sm, Nd (n = 0,1)
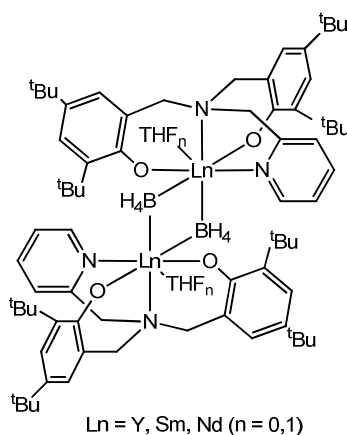
Figure 3.1: Borohydride rare earth initiators reported by Mountford and co-workers.

Therefore within this chapter, the effects of substituting the isopropoxide initiating group of the previously described series of Group 4 amine tris(phenolate) complexes with amide and borohydride groups on both the structural and catalytic behaviour will be investigated.

3.2. Synthesis of Group 4 borohydride complexes

Although reactions between transition metal alkoxides and boranes often result in reduction of the metal centre to a lower oxidation state, previous work in the group has shown that **L^{Me}Ti(O^{i}Pr)** can be reacted with BH$_3$-THF to synthesise the borohydride complex **L^{Me}Ti(BH$_4$)**.[13] Treatment of **L^{tBu}Ti(O^{i}Pr)**, **L^{tBu}Zr(O^{i}Pr)** and **L^{tBu}Hf(O^{i}Pr)** with BH$_3$-THF was also shown to result in the corresponding borohydride complexes **L^{tBu}Ti(BH$_4$)**, **L^{tBu}Zr(BH$_4$)** and **L^{tBu}Hf(BH$_4$)** (Scheme 3.1). A slight colour change was only observed in the case of **L^{tBu}Ti(BH$_4$)**, where the solution was seen to change from yellow to orange during the course of the reaction, indicating no

reduction of the metal had taken place. The Zr and Hf analogues were both found to be colourless.
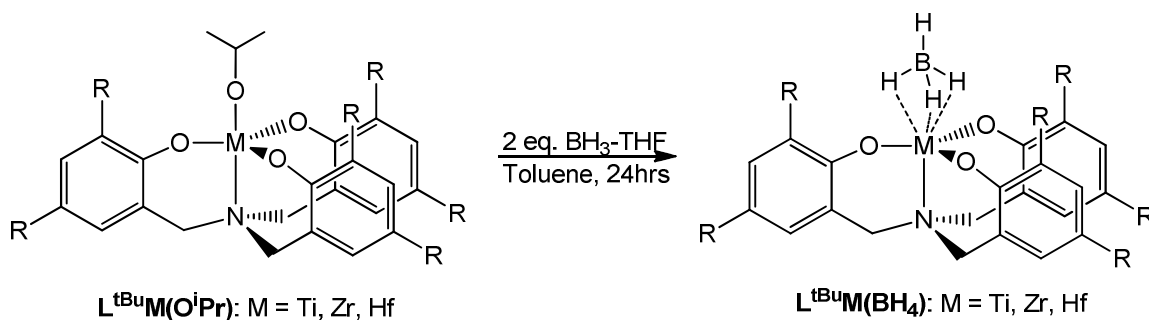
Scheme 3.1: Synthesis of Group 4 borohydride complexes.

A proposed mechanism for the ligand exchange is shown in Scheme 3.2.[13] The addition of BH_3 results in the formation of the borane adduct, H_2BO^iPr, facilitating the removal of the alkoxide ligand from the metal centre. The leaving borane is relatively stable and can be later removed from the reaction media by recrystallisation. During this process a single hydride is transferred to the metal centre. The resulting intermediate hydride species is highly unstable and quickly reacts with a secondary BH_3 group to form the BH_4 adduct, **L^{tBu}M(BH$_4$)**. This final step is thought to be in equilibrium due to the somewhat unstable nature of the BH_4 ligand, which can easily detach from the complex, re-forming the hydride species. However, the equilibrium lies far to the right, strongly favouring **L^{tBu}M(BH$_4$)** and allowing crystallisation from toluene solutions.
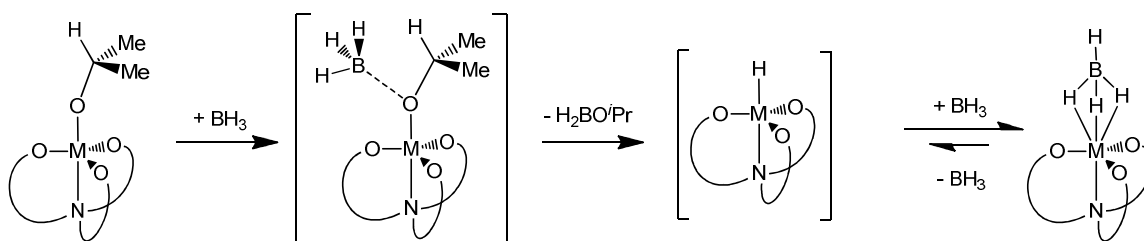
Scheme 3.2: Proposed mechanism for the ligand exchange leading to the formation of L^{tBu}M(BH$_4$). L^{tBu} motif is represented schematically for clarity.

The BH_4^- ligand can be observed by ^{1}H NMR spectroscopy as a broad signal, integrating to three protons, in the region δ 1.5 - 2.5. This corresponds to the bonding mode of the BH_4 ligand, in which three protons interact with the metal centre, while the fourth points away from the metal. A signal that corresponds to the apical B-H proton is not observed in the spectrum, presumably obscured by the alkyl region signals. The broadness of the BH_4 signals (both observed and hidden) in the ^{1}H NMR spectra is a result of the quadrupolar nature of the ^{11}B nucleus,[14] but is also indicative of a fluxional process, in which the ligand "rotates" on the NMR timescale, with the protons exchanging positions rapidly.[13] The fact that the BH_4 proton signals retain a 1:3 ratio

shows that this process of ligand exchange is not so rapid that the protons become equivalent on the NMR timescale. Cooling of the sample to 198 K showed a sharpening of the BH_4 signal in the region δ 1.5 - 2.5, but the apical proton remains unobserved. $^{11}B\{^1H\}$ NMR was also used to characterise the compounds, with a single resonance observed in the spectrum of each complex. This signal was observed to shift slightly upfield from δ -17 for the Ti species to around δ -21 for the Zr and Hf species.
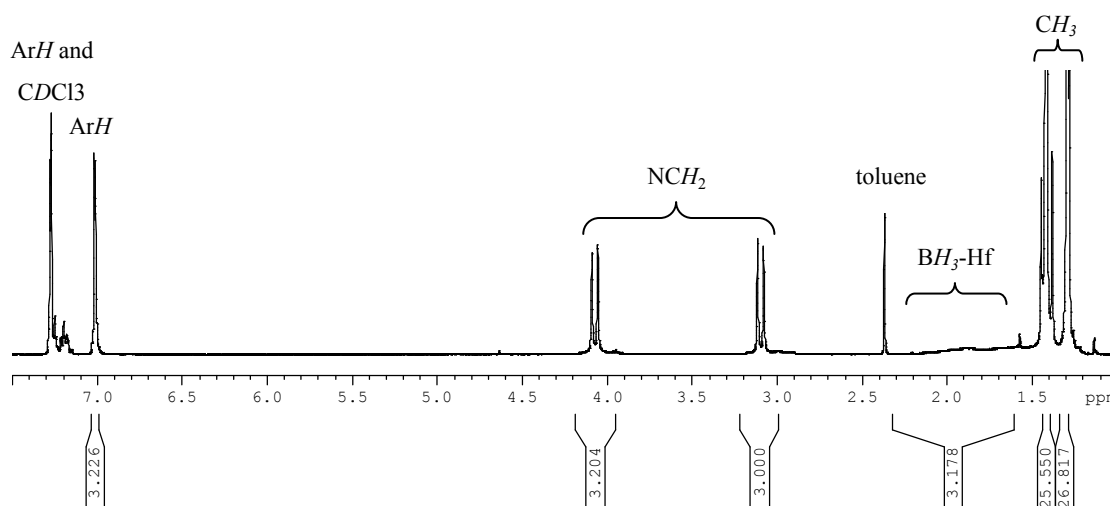
Figure 3.2: ^1H NMR spectrum of $L^{tBu}Hf(BH_4)$.

Another noteworthy feature of the NMR spectrum shown above are the sharp doublets corresponding to the methylene protons within $L^{tBu}Hf(BH_4)$, which are also observed in the ^1H NMR spectrum of the Zr complex, $L^{tBu}Zr(BH_4)$. This is distinctly different from the isopropoxide analogues of these complexes, in which the methylene signals are very broad at room temperature due to the inversion of the *P* and *M* forms of the complex, as was discussed in the previous chapter.

Crystallographic analyses of $L^{tBu}Ti(BH_4)$ and $L^{tBu}Hf(BH_4)$ showed the complexes to have similar structures, only that of $L^{tBu}Ti(BH_4)$ is shown in Figure 3.3, and key structural parameters of both structures are summarised in Table 3.2. Particular attention was paid to the M-B and M-N bond lengths, as it has been previously reported that a shorter M-N bond length may restrict fluxionality in the complex,[15] and indeed the fluxional complex $L^{tBu}Hf(O^iPr)$ exhibits a longer M-N bond (2.406(2) Å) than the non-fluxional $L^{tBu}Hf(BH_4)$ (2.386(3) Å), though the difference is small. As would be expected, the mode of bonding between the metal centre and the tetrahydroborate group results in a longer distance between the metal and the ligand than occurs in the respective isopropoxide complexes. Despite the apparent structural similarities between $L^{tBu}Ti(BH_4)$ and $L^{tBu}Hf(BH_4)$, the packing behaviour of the two complexes in the solid state is

98

somewhat different. Whilst only one enantiomer is observed in asymmetric unit of $\mathbf{L^{tBu}Ti(BH_4)}$, disorder between both enantiomers was observed in the asymmetric unit of $\mathbf{L^{tBu}Hf(O^iPr)}$ and was modelled successfully.
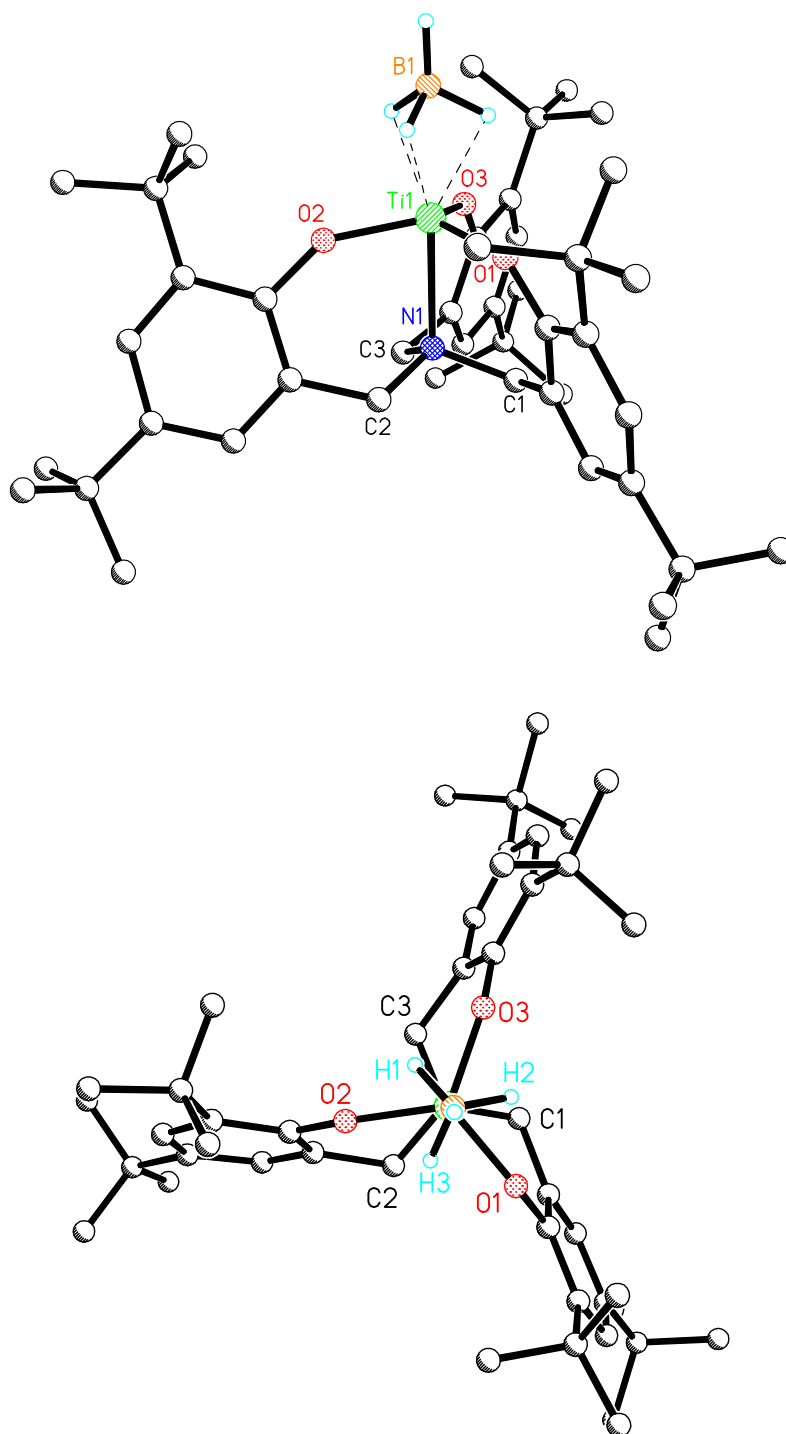
Figure 3.3: Structure of $\mathbf{L^{tBu}Ti(BH_4)}$ as determined by X-ray crystallography, side-view (top) and top-down view (bottom). With the exception of H1, H2, H3 and H4, hydrogen atoms have been omitted for clarity.

	$L^{tBu}Ti(BH_4)$	$L^{tBu}Hf(BH_4)$
M-N (Å)	2.263(3)	2.386(3)
M-B (Å)	2.223(5)	2.346(7)
M-O1 (Å)	1.823(2)	1.975(4)
M-O2 (Å)	1.808(2)	1.842(4)
M-O3 (Å)	1.816(2)	2.026(4)
M-(O1,O2,O3) (Å)	0.265	0.326

Table 3.2: Selected structural parameters of $L^{tBu}Ti(BH_4)$ and $L^{tBu}Hf(BH_4)$. (O1,O2,O3) represents the plane defined by the atoms O1, O2 and O3.

3.3. Synthesis of Group 4 amide complexes

One factor potentially governing a complex's ability to reinitiate polymerisation of a pre-existing short-chain polymer is the reactivity of the monodentate ligand in the complex. It was believed that by including a more labile ligand the catalytic system would be more reactive and thereby capable of initiating 'difficult' substrates such as macroinitiators (see Chapter 4). The series of dialkylamino zirconium tris(phenolate) complexes described below were identified as promising candidates, as they are sterically similar to, but more labile than isopropoxide ligands. Scheme 3.3 shows the synthesis of these compounds from the tetrakis(dialkylamido)zirconium(IV) starting materials.
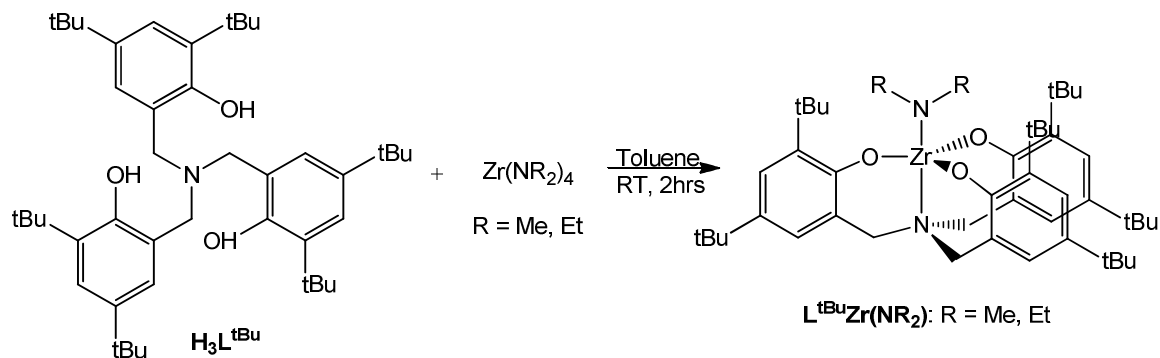
Scheme 3.3: Synthesis of zirconium(IV) amide complexes.

Variable-temperature ^{1}H NMR studies showed the slow exchange limit for the fluxional exchange between the *P* and *M* enantiomers of $L^{tBu}Zr(NMe_2)$ to be approximately 238 K (Figure 3.4), significantly lower than the slow exchange limit of 268 K reported for $L^{tBu}Zr(O^iPr)$.[16] This implies that the barrier to inversion occurs at a lower temperature for $L^{tBu}Zr(NMe_2)$, and thus the complex exhibits a higher degree of fluxionality at room temperature (Figure 3.4).
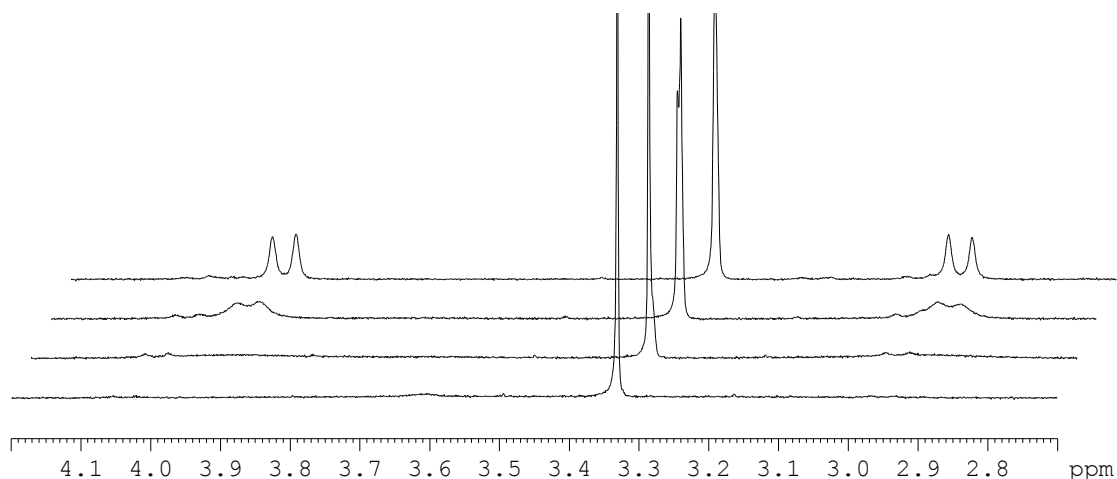
Figure 3.4: Expanded VT NMR spectra of L^{tBu}Zr(NMe$_2$) showing methylene region at 298 K, 278 K, 258 K and 238 K (bottom to top). Singlet at δ 3.6 due to the protons of the dimethyl amide group.

Despite a higher solubility and more sensitive nature than **L^{tBu}Zr(O^{i}Pr)**, high quality crystals of **L^{tBu}Zr(NMe)$_2$** were grown from toluene and analysed by X-ray crystallography. Figure 3.5 shows the structure of **L^{tBu}Zr(NMe)$_2$** to possess a similar geometry to previously described amine tris(phenolate) complexes and selected bond lengths are summarised in Table 3.3. The most significant difference in the bond lengths of these two structures is the difference in the bond length to the axial ligand, which is significantly longer in **L^{tBu}Zr(NMe$_2$)** compared to **L^{tBu}Zr(O^{i}Pr)**. This implies that the dimethyl amide group is bound less strongly to the zirconium centre in **L^{tBu}Zr(NMe$_2$)** than the axial isopropoxide group is in **L^{tBu}Zr(O^{i}Pr)**. This observation may also explain the difference in fluxional behaviour between the *P* and *M* enantiomers of the two complexes, as in this case there is no significant difference between the Zr-N1 bond lengths.

	L^{tBu}Zr(NMe)$_2$	L^{tBu}Zr(O^{i}Pr)
Zr-N1 (Å)	2.449(3)	2.442(3)
Zr-N2 (Å)	2.045(3)	-
Zr-O4 (Å)	-	1.916(3)
Zr-O1 (Å)	2.031(5)	1.967(2)
Zr-O2 (Å)	1.973(5)	1.949(2)
Zr-O3 (Å)	1.959(5)	1.993(2)

Table 3.3: Selected bond lengths for L^{tBu}Zr(NMe$_2$) and L^{tBu}Zr(O^{i}Pr).
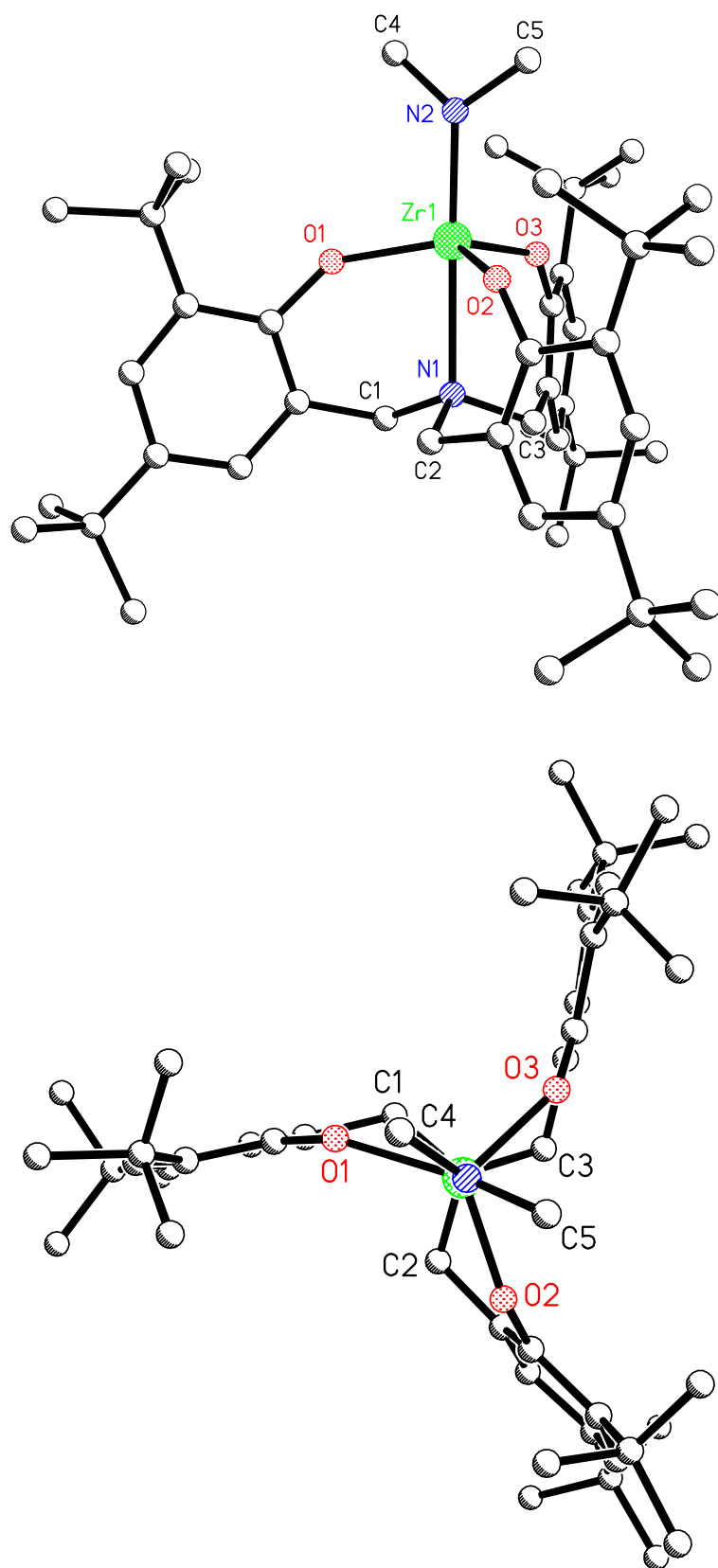
Figure 3.5: X-ray crystal structure of L^tBuZr(NMe₂), side-view (top) and top-down view (bottom). Hydrogen atoms have been omitted for clarity.

3.4. Ring-opening polymerisation of lactide

3.4.1. Group 4 borohydride initiators

As mentioned in the preamble to this chapter, the use of borohydride complexes as initiators for ROP of cyclic esters has received great attention in recent years. The Group 4 borohydride complexes synthesised here were therefore investigated as initiators for ROP of LA.

3.4.1.1.   Solvent –free ROP

The Group 4 borohydride initiators described above were shown to be active for the ROP of *rac*-LA under solvent-free conditions. Within the series of borohydride complexes, similar trends were observed as have been shown for the monomeric isopropoxide complexes discussed in Chapter 2. Specifically, the Zr and Hf complexes were considerably more active than their Ti counterpart, resulting in high conversions after 10 and 30 minutes, and the resulting polymer molecular weights were found to be close to calculated values. Surprisingly though, $L^{tBu}Ti(BH_4)$ gave rise to polymer with a PDI of 1.19, lower than the values observed for polymers initiated by $L^{tBu}Zr(BH_4)$ and $L^{tBu}Hf(BH_4)$. The Zr and Hf borohydride complexes also exhibited heterotactic stereoselectivity comparable to the previously discussed isopropoxide complexes, which is unsurprising given that the propagating species' within the two systems will be identical in nature.

Complex	Time	Conv. (%)	M_n	M_w	PDI	P_s
$L^{tBu}Ti(BH_4)$	24 hrs	57	23950	25600	1.19	0.56
$L^{tBu}Zr(BH_4)$	10 min	93	52600	69500	1.32	0.83
$L^{tBu}Hf(BH_4)$	30 min	94	49000	68500	1.40	0.89

Table 3.4: Solvent-free ROP of *rac*-LA by borohydride initiators. 2.0 g of *rac*-LA in the absence of solvent at 130 °C, [LA]/[cat] = 300. M_w, M_n and PDI determined by GPC in THF, relative to polystyrene standards.

3.4.1.2.   Solution ROP

As was the case with the isopropoxide complexes,[17] ROP of *rac*- and L-LA could be undertaken using the borohydride initiators, $L^{tBu}Zr(BH_4)$ and $L^{tBu}Hf(BH_4)$, over several hours at 100 °C in toluene or over several days at room temperature in chlorinated solvents. Once again, the resulting PLA from the ROP of *rac*-LA was found to by heterotactically enriched.

Determination of polymer end-group. Previous reports by Guillaume and co-workers have shown the ROP of ε-caprolactone initiated by rare earth borohydride complexes, both supported and unsupported by ancillary ligand systems, results in PCL exhibiting CH_2OH chain ends.[7-8] In such cases, the mechanism for ring-opening has been proposed as analogous to the coordination insertion mechanism (Scheme 3.4). One significant difference between this mechanism and the commonly accepted model for alkoxide-initiated ROP, is the instability of the ring-opened intermediate, which is immediately reduced by BH_3 resulting in the alkoxyborane propogation

species. Quenching of the system, usually by the addition of a few drops of protic solvent, leads to hydrogen transfer and results in α,ω-telechelic PCL diols.
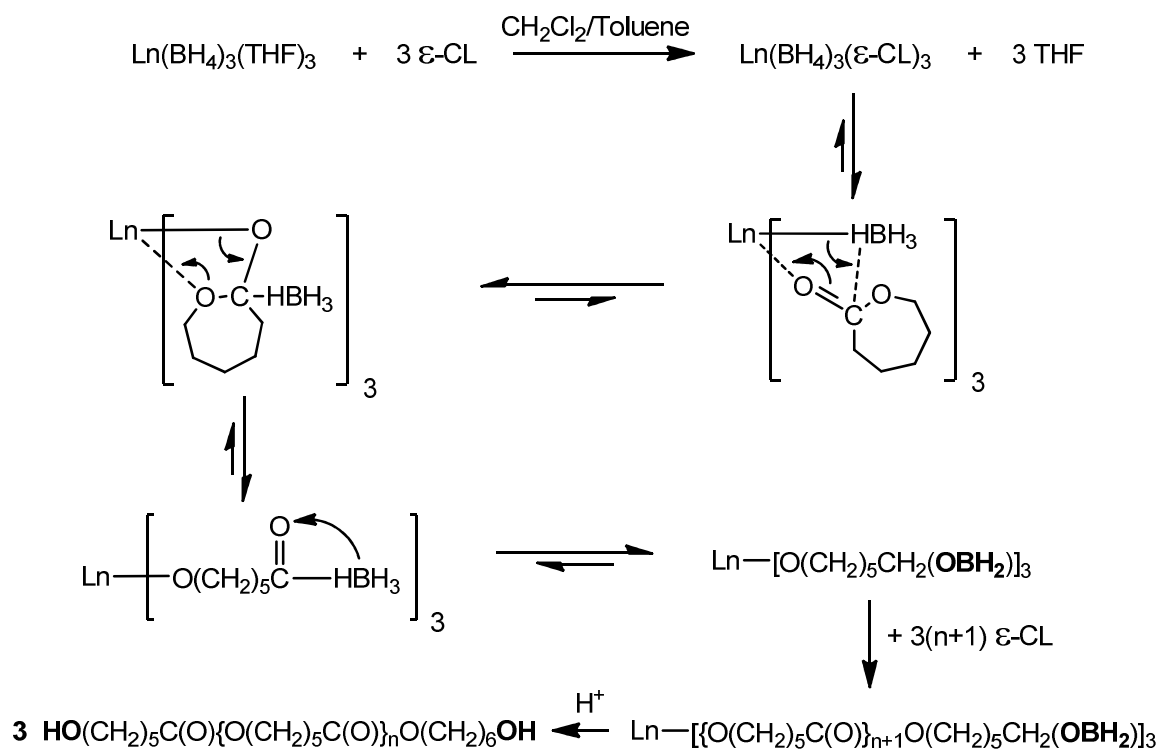
Scheme 3.4: ROP of ε-caprolactone using rare earth borohydride initiators, proposed by Guillaume and co-workers.[7]

Subsequent work by the group of Mountford et al in the use of rare earth borohydride initiators for the ROP of *rac*-LA observed an analogous process resulting in CH_2OH terminated PLA chains. In addition they noted the presence of aldehydic terminated chains and proposed that end groups of this nature are the result of BH_3 liberation after coordination of the monomer to the metal centre.[18] In this case, ring-opening will result in an aldehydic propagating species, which does not undergo hydrogen transfer so easily on quenching of the polymerisation, and so an aldehyde group remains at the chain-end (Scheme 3.5).

Short chain PLLA (M_n = 10800, PDI = 1.20) was synthesised using **L^{tBu}Zr(BH$_4$)** (toluene, 100 °C, 2 hrs) and analysed via MALDI-ToF mass spectrometry. Comparision of the experimental spectra with calculated data (Figure 3.4) showed a clear correlation to the aldehyde-terminated population, however contamination of a small amount of alcohol-terminated population, which is thought to ionize under similar conditions as the aldehyde-terminated polymer, could be responsible for a loss in resolution, explaining the difference in isotope intensity patterns. ^{1}H NMR spectroscopy of the same sample led to the observation of a sharp signal at δ 9.49, which is proposed to correlate with the aldehyde chain-end. In addition to these observations, addition of 10 equivalents of L-LA to **L^{tBu}Zr(BH$_4$)** in dry CDCl$_3$ within a Young's NMR tube gave rise to

only one significant peak in the $^{11}B\{^{1}H\}$ NMR spectrum at δ 25.6 after 24 hrs. This can be attributed to liberated BH_3 from the mechanism shown in Scheme 3.5, resulting in aldehyde-terminated polymer.[19]
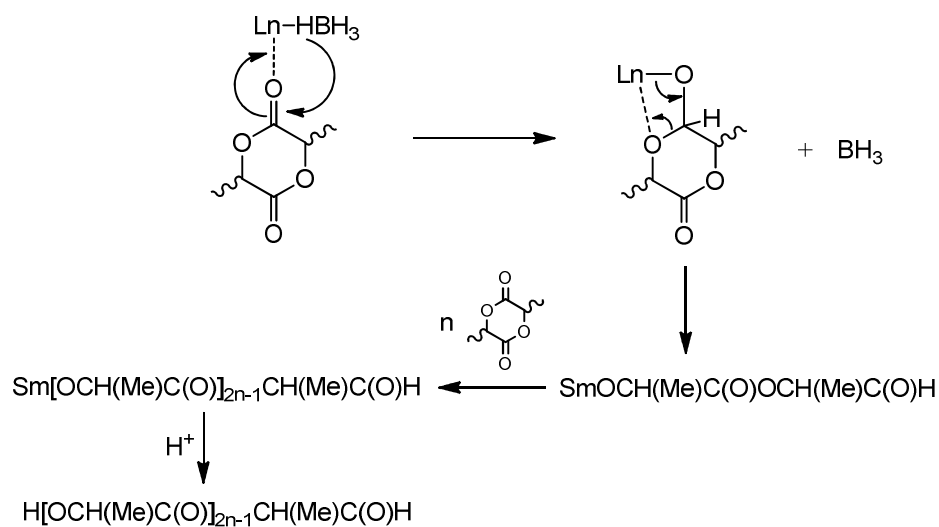
Scheme 3.5: ROP of LA using rare earth borohydride initiators: alternative mechanism proposed by Mountford and co-workers.[18]
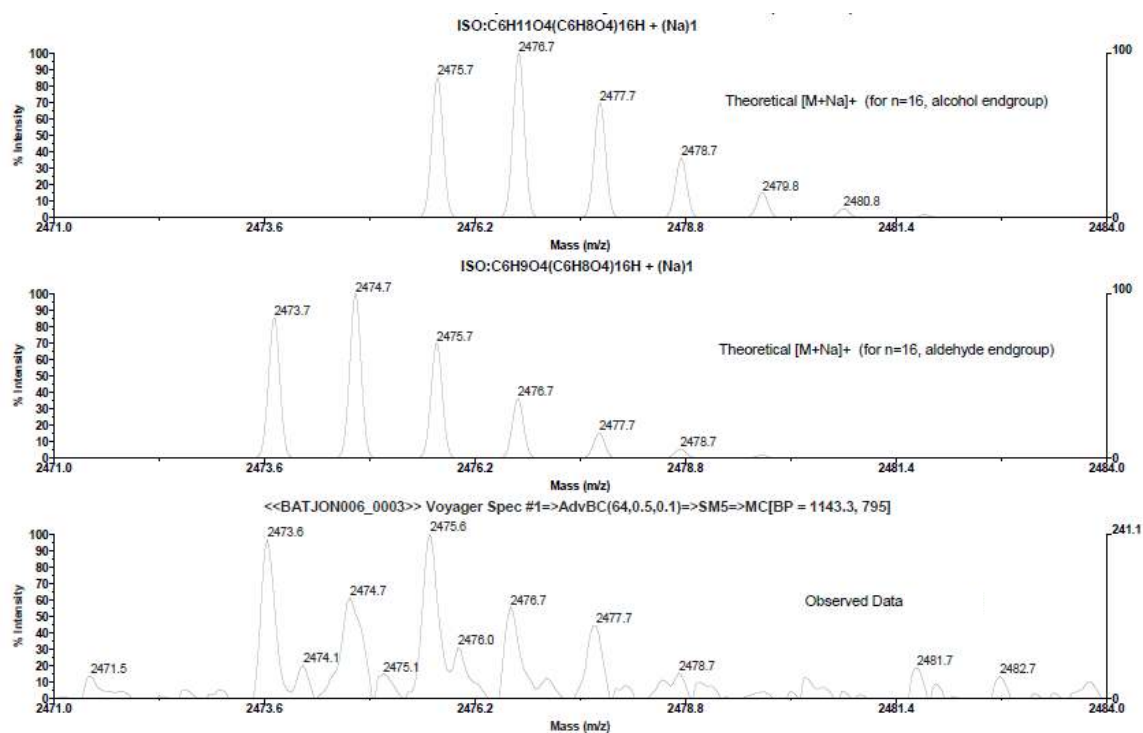
Figure 3.4: MALDI-ToF mass spectra of PLLA synthesised with $L^{tBu}Zr(BH_4)$. Calculated data for alcohol terminated polymer (top) and aldehyde terminated polymer (middle), and expanded experimental spectrum (bottom).

3.4.2. Group 4 amide initiators

3.4.2.1.　Solvent-free ROP

The zirconium amide complexes $L^{tBu}Zr(NR_2)$ (R = Me, Et) were also shown to be highly active in the melt, although the steric implications of the amine substituents appears to influence activity, as after 5 minutes in the melt, conversion was shown to decrease with increasing substituent size. The rate of initiation (k_{init}) appears to be slow in comparision to the rate of propagation (k_{prop}) for this series of amide initiators, as molecular weights much higher than calculated values were observed, although the resulting PDIs are reasonably low. Heterotactic selectivity was observed for both complexes, although the degree of stereocontrol is lower than is observed with the isopropoxide analogues and appears to decrease as sterics of the amine substituents increase.

| Complex	Time	Conv. (%)	M_n	M_w	PDI	P_s
$L^{tBu}Zr(NMe_2)$	5 min	97	103950	121300	1.17	0.83
$L^{tBu}Zr(NEt_2)$	5 min	82	82750	103950	1.26	0.71

Table 3.5: Solvent-free ROP of *rac*-LA by amide initiators. 2.0 g of *rac*-LA in the absence of solvent at 130 °C, [LA]/[cat] = 300. M_w, M_n and PDI determined by GPC in THF, relative to polystyrene standards.

3.4.2.2.　Solution ROP

Determination of end-group. In the case of amide initiator $L^{tBu}ZrNEt_2$, short chain PLLA (M_n = 9950, PDI = 1.17) (toluene, 100 °C, 2 hrs) was found, by MALDI-ToF mass spectrometry, to possess a diethyl amide group at one chain end, and the commonly observed hydroxyl group at the opposite chain end, a result of quenching of the reaction with methanol. The presence of a dialkyl amide chain end in PLA is a desirable feature,[20] but difficult to achieve. Metal complexes containing amide (NR_2) initiating groups are often considered non-ideal, resulting in poor molecular weight control and even macrocyclic PLA.[6, 21] An alternative approach is the use of amines as co-initiators within a polymerisation, as was reported with tin(II) octanoate in 2005,[22] and more recently with dicationic and zwitterionic rare earth complexes.[23] However, to the best of our knowledge, $L^{tBu}Zr(NEt_2)$ is the first reported ROP initiator to yield amide-terminated heterotactically enriched PLA without the use of an amine co-initiator.
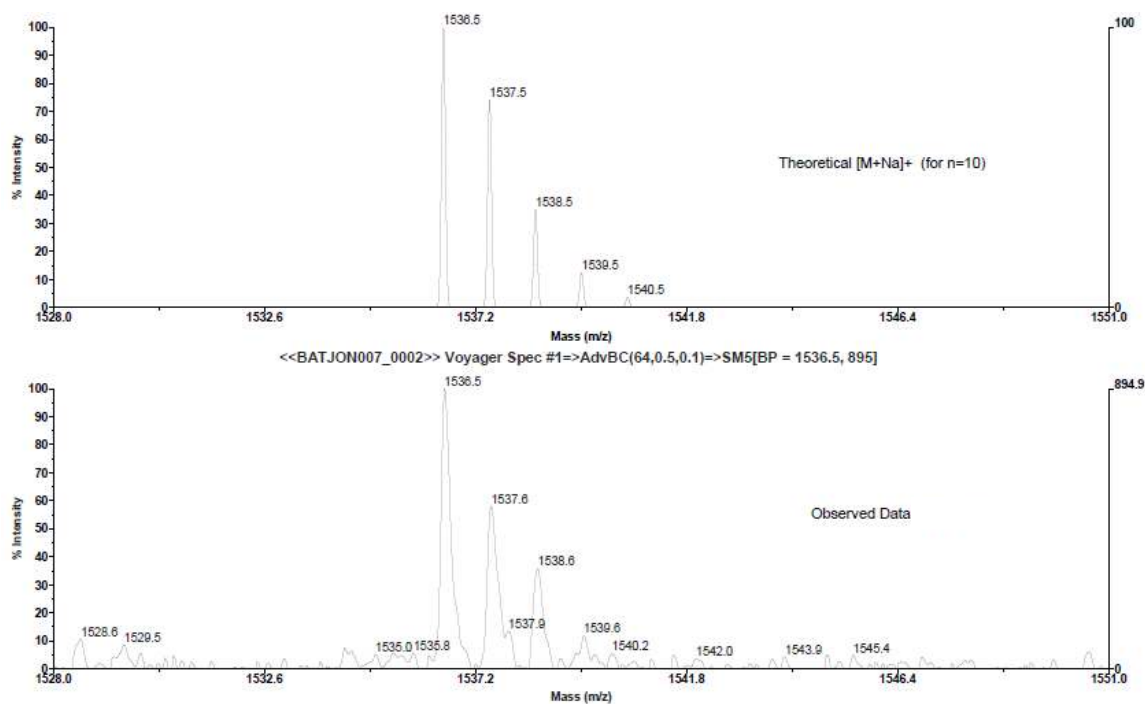
Figure 3.5: MALDI-ToF mass spectra of PLLA synthesised with $L^{tBu}Zr(NEt_2)$. Calculated data for amine terminated polymer (top) and expanded experimental spectrum (bottom).

3.4.3. Kinetic studies

A series of comparative kinetic investigations were carried out to determine what effect substitution of the initiating group would have on the relative rates of ROP exhibited by these initiators. These studies were carried out on the NMR scale in d_8-toluene at 333 K as the Zr amide complexes, $L^{tBu}Zr(NR_2)$, were found to be unstable in $CDCl_3$ over longer time scales.

Inspection of the semilogarithmic plots (Figure 3.6) of the investigated initiators shows no major difference between the rates of ROP of *rac*-LA between $L^{tBu}Zr(O^iPr)$ and $L^{tBu}Zr(BH_4)$, and the calculated values of k_{app} for these initiators are similar (Table 3.6). This is to be expected as, after the initial monomer coordination and ring-opening step, the rate-determining propagating species will be similar in nature (Figure 3.7). The near-overlay of the semilogarithmic plots for $L^{tBu}Zr(O^iPr)$ and $L^{tBu}Zr(BH_4)$ indicate these initiators exhibit similar, fast initiation rates, resulting in an absence of significant initiation period. In contrast, the semilogarithmic plots for $L^{tBu}Zr(NMe_2)$ and $L^{tBu}Zr(NEt_2)$ appear to be shifted to the right, indicative of a significant initiation period. The smaller values of k_{app} calculated for $L^{tBu}Zr(NR_2)$, in comparison to $L^{tBu}Zr(O^iPr)$ and $L^{tBu}Zr(BH_4)$, can be explained by the relative instabilities of the amine complexes. During the slower initiation process, a proportion of the amine initiator will degrade, resulting in a lower concentration of active catalyst. In addition to a decreased rate of ROP, the amine initiators have been shown to produce polymer of molecular weight consistent with a

107

smaller concentration of active initiator. The more stable of the two amine initiators, $L^{tBu}Zr(NEt_2)$, exhibits a value of k_{app} closer to $L^{tBu}Zr(O^iPr)$, as less initiator undergoes degradation.
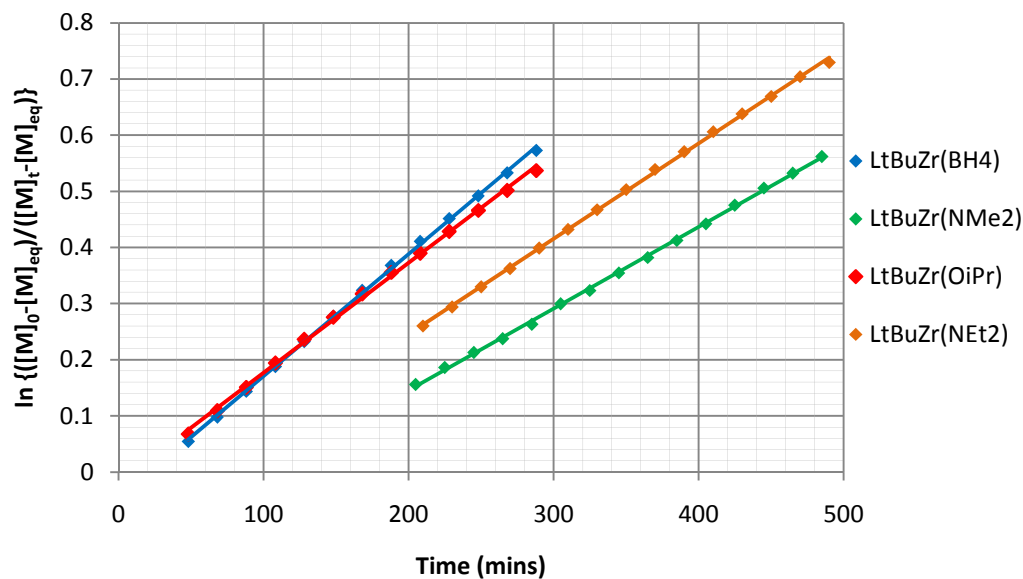
Figure 3.6: Semilogarithmic plots for ROP of *rac*-LA in d_8-toluene at 333 K.

Initiator	k_{app} (min^{-1})	Equation	R^2
$L^{tBu}Zr(O^iPr)$	2.0×10^{-3}	y = 0.0020x − 0.0191	0.9998
$L^{tBu}Zr(BH_4)$	2.2×10^{-3}	y = 0.0022x − 0.0467	0.9964
$L^{tBu}Zr(NMe_2)$	1.5×10^{-3}	y = 0.0015x − 0.1454	0.9951
$L^{tBu}Zr(NEt_2)$	1.7×10^{-3}	y = 0.0017x − 0.0949	0.9828

Table 3.6: Apparent rate constants (k_{app}) for ROP of *rac*-LA in d_8-toluene at 333 K. Calculated error < 10 %.
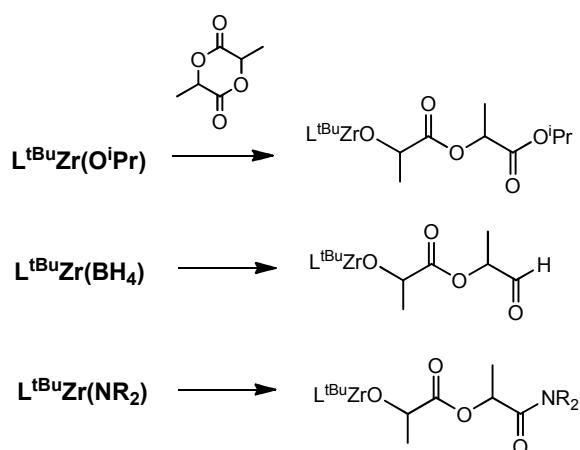
Figure 3.7: Propagation species

3.5. Summary

Within this chapter, several Group 4 amine tris(phenolate) complexes featuring initiating groups other than the previously explored isopropoxide moiety, were synthesised and investigated for their potential as initiators for the ROP of *rac*-LA.

The series of borohydride initiators, **L^{tBu}Ti(BH$_4$)**, **L^{tBu}Zr(BH$_4$)** and **L^{tBu}Hf(BH$_4$)**, synthesised directly from the isopropoxide analogues, were shown to undertake the well-controlled ROP of *rac*-LA, exhibiting a strong heterotactic selectivity in the case of Zr and Hf complexes. Kinetic studies of **L^{tBu}Zr(BH$_4$)** indicate that no significant initiation period results from the use of the borohydride group, and following the initial insertion, ROP progresses at a comparable rate to that observed by **L^{tBu}Zr(O^{i}Pr)**. MALDI-ToF analysis of short-chain PLA synthesised using **L^{tBu}Zr(BH$_4$)** indicated a major series of polymer chains terminated by an aldehyde group, and a minor series alcohol-terminated polymer chains. Although these have yet to be separated, the potential applications for both are wide-reaching: the reactive aldehyde group would allow a variety of moieties to be grafted onto the chain-end via standard organic procedures, and an –OH terminated polymer could be used as a macroinitiator in the synthesis of block co-polymers (Chapter 4).

By contrast, the amide initiators, **L^{tBu}Zr(NMe$_2$)** and **L^{tBu}Zr(NEt$_2$)**, were shown to result in PLA with molecular weights far higher than calculated values. Kinetic studies showed a significant initiation period present when these initiators were used for the ROP of *rac*-LA, and in addition, the sensitive nature of these complexes was shown lead to initiator degradation, resulting in smaller values of k$_{app}$ for the amide systems. Excitingly though, **L^{tBu}Zr(NMe$_2$)** and **L^{tBu}Zr(NEt$_2$)** not only exhibit a strong heterotactic selectivity, but also result in amide-terminated PLA chains (another highly desirable end-group for various forward syntheses), a combination of which to our knowledge has not been previously reported. In the context of this thesis, the highly reactive **L^{tBu}Zr(NMe$_2$)** and **L^{tBu}Zr(NEt$_2$)** were synthesised as potential reinitiators of pre-existing –OH terminated short-chain polymers, and will be discussed in further detail in the subsequent chapter.

3.6. References

1.   Dechy-Cabaret, O.; Martin-Vaca, B.; Bourissou, D., *Chem. Rev.* **2004,** *104* (12), 6147-6176.
2.   Kim, Y.; Verkade, J. G., *Organometallics* **2002,** *21* (12), 2395-2399.
3.   Kim, Y.; Jnaneshwara, G. K.; Verkade, J. G., *Inorg. Chem.* **2003,** *42* (5), 1437-1447.
4.   Chamberlain, B. M.; Cheng, M.; Moore, D. R.; Ovitt, T. M.; Lobkovsky, E. B.; Coates, G. W., *J. Am. Chem. Soc.* **2001,** *123* (14), 3229-3238.
5.   Amgoune, A.; Thomas, C. M.; Roisnel, T.; Carpentier, J. F., *Chem.--Eur. J.* **2006,** *12* (1), 169-179.
6.   Chisholm, M. H.; Delbridge, E. E., *New J. Chem.* **2003,** *27* (8), 1167-1176.
7.   Guillaume, S. M.; Schappacher, M.; Soum, A., *Macromolecules* **2003,** *36* (1), 54-60.

8.   Palard, I.; Soum, A.; Guillaume, S. M., *Chem.--Eur. J.* **2004,** *10* (16), 4054-4062.

9.   Palard, I.; Soum, A.; Guillaume, S. M., *Macromolecules* **2005,** *38* (16), 6888-6894.

10.   Palard, I.; Schappacher, M.; Soum, A.; Guillaume, S. M., *Polym. Int.* **2006,** *55* (10), 1132-1137.

11.   Barros, N.; Mountford, P.; Guillaume, S. M.; Maron, L., *Chem.--Eur. J.* **2008,** *14* (18), 5507-5518.

12.   Bonnet, F.; Cowley, A. R.; Mountford, P., *Inorg. Chem.* **2005,** *44* (24), 9046-9055.

13.   Johnson, A. L.; Davidson, M. G.; Mahon, M. F., *Dalton Trans.* **2007,** (46), 5405-5411.

14.   Iggo, J. A., *NMR Spectroscopy in Inorganic Chemistry*. Oxford University Press: Oxford, U.K., 1999.

15.   Bull, S. D.; Davidson, M. G.; Johnson, A. L.; Robinson, D.; Mahon, M. F., *Chem. Commun.* **2003,** (14), 1750-1751.

16.   Chmura, A. J.; Chuck, C. J.; Davidson, M. G.; Jones, M. D.; Lunn, M. D.; Bull, S. D.; Mahon, M. F., *Angew. Chem., Int. Ed.* **2007,** *46* (13), 2280-2283.

17.   Chmura, A. J.; Davidson, M. G.; Frankis, C. J.; Jones, M. D.; Lunn, M. D., *Chem. Commun.* **2008,** (11), 1293-1295.

18.   Dyer, H. E. New Lanthanide Complexes as Polymerisation Catalysts. University of Oxford, Oxford, United Kingdom, 2009.

19.   Noth, H.; Wrackmeyer, B., *Nuclear magnetic resonance spectroscopy of Boron compounds*. Springer-Verlag: 1978.

20.   Dove, A. P., *Chem. Commun.* **2008,** (48), 6446-6470.

21.   Ma, H. Y.; Okuda, J., *Macromolecules* **2005,** *38* (7), 2665-2673.

22.   Kowalski, A.; Libiszowski, J.; Biela, T.; Cypryk, M.; Duda, A.; Penczek, S., *Macromolecules* **2005,** *38* (20), 8170-8176.

23.   Clark, L.; Cushion, M. G.; Dyer, H. E.; Schwarz, A. D.; Duchateau, R.; Mountford, P., *Chem. Commun.* **2010,** *46* (2), 273-275.

Chapter 4

Synthesis of block polymers

4. Synthesis of block polymers

4.1 Preamble

The well-controlled and stereospecific nature exhibited in ROP of LA by initiators of the type **L^{R}ZrX** lends itself to the synthesis of multi-block polymers. Traditionally the monomer required for each block needs to be added sequentially and only when the preceeding block is complete, leading to a lengthy multi-step synthesis (Scheme 4.1(i)).[1-2] Within this chapter, two alternative methods of block polymer synthesis will be discussed. The first utilises the remarkable kinetic properties resulting from the high heterotactic selectivity exhibited by **L^{tBu}Zr(O^{i}Pr)** in such a way that mixtures of D- and L-LA can result in a series of di-stereoblock polymers (Scheme 4.1(ii)). A delay in the addition of the second monomer to this system has also been shown to allow the synthesis of tri-stereoblock PLA. The second alternative synthesis involves the reinitiation of pre-existing short-chain PLA or poly(ethylene glycol) (PEG) (known as the 'macroinitiator') using the more reactive initiator **L^{tBu}Zr(NR$_2$)** to produce a number of di-stereoblock PLA polymers, as well as di- and tri-block PEG-PLA copolymers (Scheme 4.1(iii)). Excitingly, a combination of both the synthetic procedures (ii) and (iii), allows for a one-pot, one step synthetic route to a penta-block polymer and has potential for the facile synthesis of even more complex systems.

i) Sequential polymerisation

ii) Stereo-specific polymerisation

iii) Macroinitiation
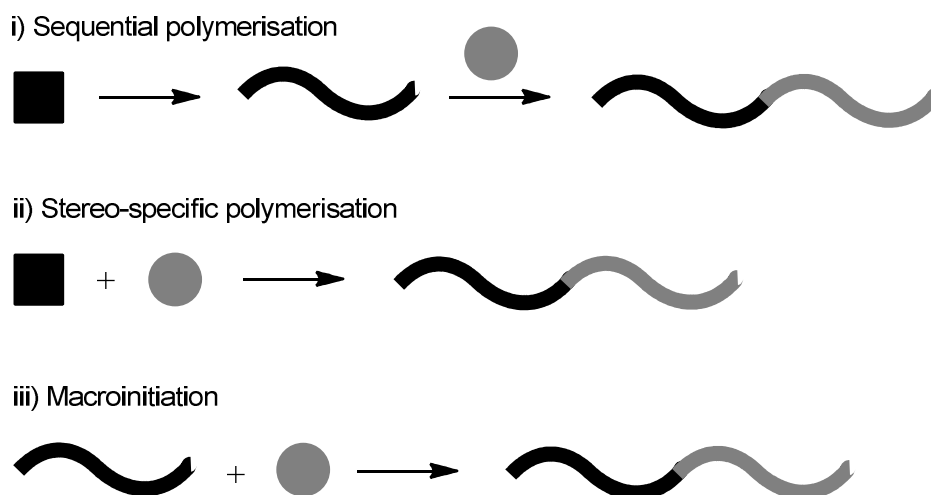
Scheme 4.1: Synthesis of di-block polymers via stereospecific polymerisation and macroinitiation.

4.2. Stereospecific polymerisation

4.2.1. Di-stereoblock PLA polymers

The observed kinetic differences between the ROP of *rac*, L- and D-LA by **L^{tBu}Zr(O^{i}Pr)** can be exploited to provide a convenient pathway to the synthesis of PLA stereoblock polymers. The initiator **L^{tBu}Zr(O^{i}Pr)** can be added to an inequivalent mixture of L- and D-LA, and will initially form a heterotactic PLA (P*het*LA) block as equal amounts of L- and D-LA are quickly consumed.

At the point at which none of the minor LA component remains, the rate of polymerisation decreases as an isotactic PLA (P*iso*LA) block is formed from the remaining major LA component (Scheme 4.2). In practice, a small quantity of enantionmerically pure LA can be added to bulk *rac*-LA to achieve the desired ratio. This simple one-pot synthesis can be tailored to create di-stereoblock PLA of varying block length and a series of materials have been synthesised in this manner (Table 4.1).
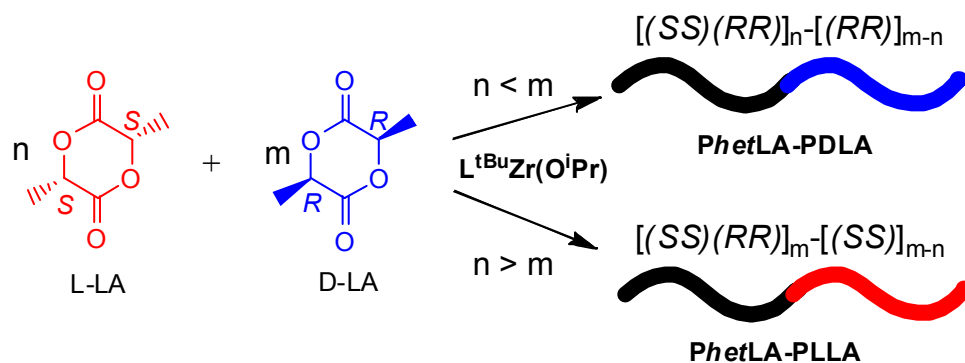
Scheme 4.2: Synthesis of PLA di-stereoblock polymers

The synthesis of a 2:1 P*het*LA-PLLA di-stereoblock was preliminarily undertaken in dichloromethane solution at room temperature over the course of several days. This allowed frequent sampling and monitoring of the reactions by homonuclear decoupled ^{1}H NMR spectroscopy and GPC. Initially, peaks corresponding to the *isi* and *sis* tetrads were observed, indicative of heterotactic bias, but as the reaction proceeded, the growth of the peak corresponding to the *iii* tetrad was noted, due to isotactic enhancement (Figure 4.1). Calculated values of P_s from these spectra were therefore seen to decrease and start to approach 0.5, as the initial domination of heterotactic tetrads decreases. GPC traces of the samples remain monomodal, while showing an increase in molecular weight with conversion and no appreciable increase in PDI, indicating a di-block structure (Figure 4.2).
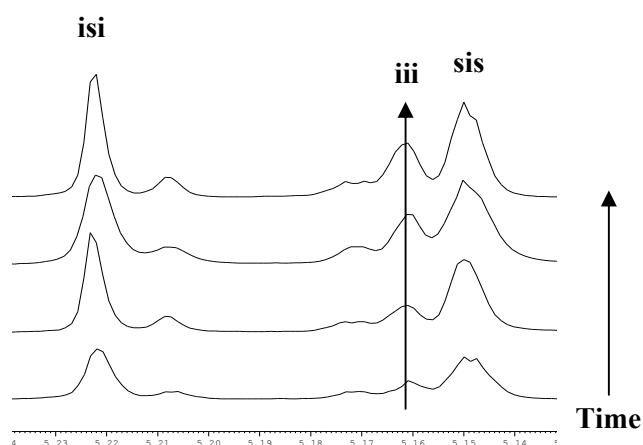
Figure 4.1: Homonuclear decoupled spectra from synthesis of 2:1 P*het*LA-PLLA di-stereoblock.
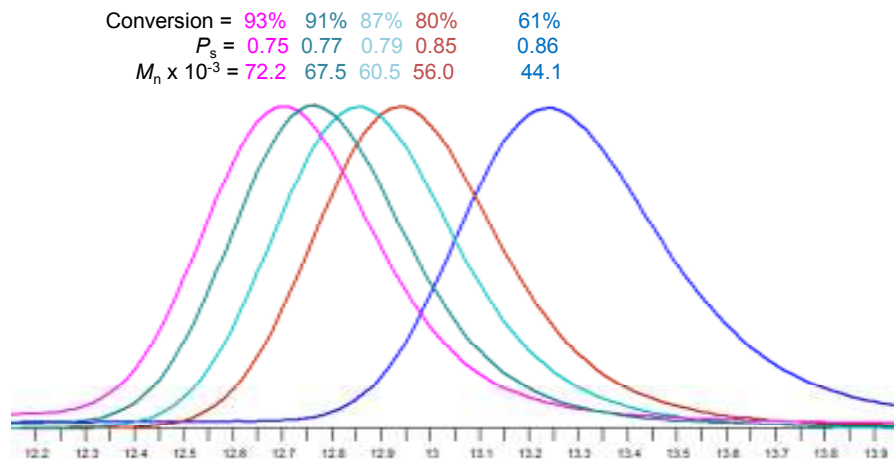
Figure 4.2: GPC traces from synthesis of 2:1 P*het*LA-PLLA di-stereoblock.

Differential scanning calorimetry (DSC) was used to investigate the architecture of the di-stereoblock polymers synthesised and the thermal properties are consistent with those proposed. Highly heterotactic PLA, although highly stereoregular, is not crystalline enough to exhibit visible melting exotherms (T_m) in a DSC themogram.[3] However, the majority of the synthesised materials had enough isotactic character within their chains to produce regions of crystallinity. It was therefore possible to observe, not only the glass transition temperature (T_g) of these materials, but also the melting points (T_m) in the second and first heating cycles respectively.
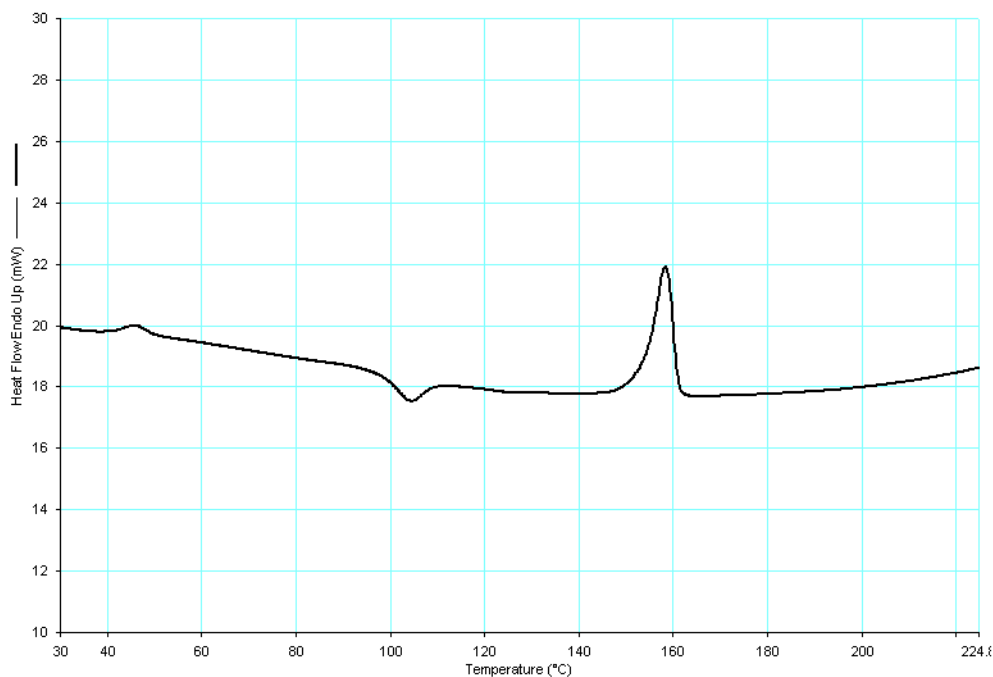
Figure 4.3: Example DSC thermogram: 1:1 P*het*LA-PLLA, 1st heating cycle.
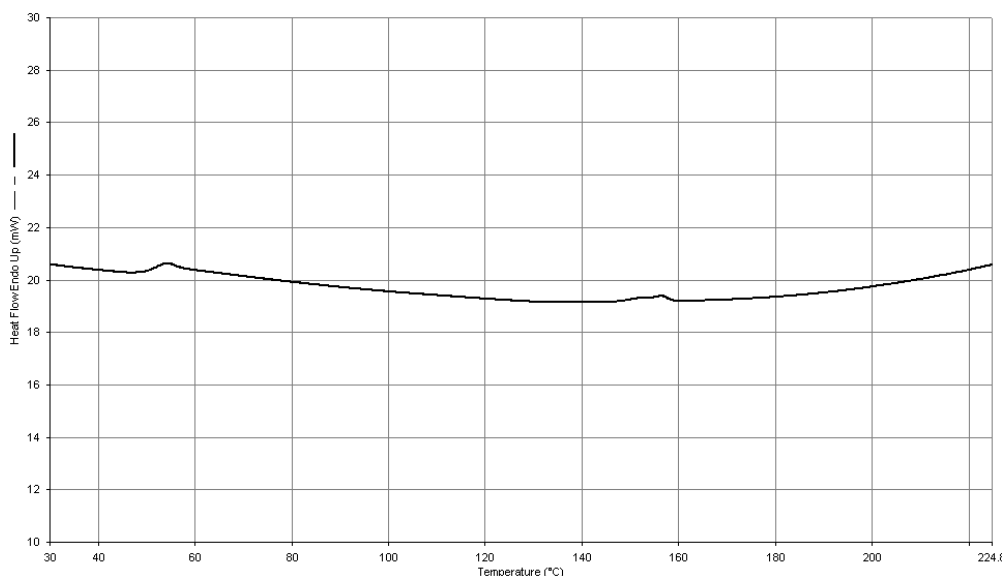
Figure 4.4: Example DSC thermogram: 1:3 P*het*LA-PLLA, 2nd heating cycle.

Di-stereoblock polymers synthesised in this one-step manner are summarised in Table 4.1, along with their corresponding DSC data. A general trend for lower values of T_g is seen as the ratio of P*het*LA to P*iso*LA increases. This agrees with published literature T_g values of 55-60 °C[4] for isotactic PLA and <45 °C[5] for heterotactic PLA, and follows trends reported by Kricheldorf and co-workers within systems which include long 'soft' segments and short 'hard' segments,[6] in this case P*het*LA and P*iso*LA respectively. The observation of only one T_g for each of these materials indicates the presence of only one phase, the nature of which appears to be crystalline in the 1:1 and 3:1 materials (Entries 1a – 2b), but amorphous in the 6:1 material (Entries 3a, 3b), indicated by the lack of observed T_m. In addition to these observations, the highest values of T_m were observed for 1:1 materials where the isotactic block length matches the heterotactic block length, but were seen to decrease as the heterotactic block lengthens.

Entry	Polymer (A-B)	M_n	PDI	T_g (2nd heat)	T_m (1st heat)	P_s
1a	1:1 P*het*LA-PLLA	44600	1.07	48	119	0.67
1b	1:1 P*het*LA-PDLA	44850	1.07	48	119	0.66
2a	3:1 P*het*LA-PLLA	33950	1.07	42	112	0.72
2b	3:1 P*het*LA-PDLA	34400	1.09	43	105	0.71
3a	6:1 P*het*LA-PLLA	68050	1.07	40	-	0.86
3b	6:1 P*het*LA-PDLA	64900	1.07	40	-	0.82

Table 4.1: PLA di-stereoblock polymers, one-step synthesis: molecular weights and DSC data. L[tBu]Zr(O[i]Pr), CH$_2$Cl$_2$, 25 °C, 6 days.

To illustrate the effectiveness of the one-step method, selected di-stereoblock PLA materials were also synthesised using a sequential two-step synthesis (Table 4.2).[1] In these cases, ROP of *rac*-LA into P*het*LA was primarily monitored by ^{1}H NMR spectroscopy, and enantiomerically pure D- or L-LA was only added after > 95% conversion of *rac*-LA had been achieved. Once again,

observed values of T_m were shown to increase with increasing isotactic block length, however comparisons between 1:1 and 3:1 P*het*LA-P*iso*LA di-stereoblock polymers synthesised using one-step and two-step methods show a significant decrease in T_m values by ~ 30 °C for those formed in a one-step manner. This indicates that a degree of 'tapering' occurs between the heterotactic and isotactic segments of materials synthesised in a one-step method, as availability of *rac*-LA drops and erroneous insertion of two identical monomer units becomes more likely. In the two-step method of synthesis, addition of the enantiomerically pure monomer only after > 95% means the 'tapered' segment in these materials can be considered insignificant. This is shown schematically in Scheme 4.3.

Entry	Polymer (A-B)	M_n	PDI	T_g (2nd heat)	T_m (1st heat)	P_s
4a	1:3 P*het*LA-PLLA	44000	1.09	49	161	0.50
4b	1:3 P*het*LA-PDLA	43000	1.08	50	160	0.48
5a	1:1 P*het*LA-PLLA	43100	1.11	49	154	0.64
5b	1:1 P*het*LA-PDLA	42650	1.11	46	149	0.64
6a	3:1 P*het*LA-PLLA	37550	1.05	48	138	0.74
6b	3:1 P*het*LA-PDLA	38050	1.05	40	133	0.74

Table 4.2: PLA di-stereoblock polymers, two-step synthesis: molecular weights and DSC data. **L^{tBu}Zr(O^{i}Pr)**, CH$_2$Cl$_2$, 25 °C, 6 days.
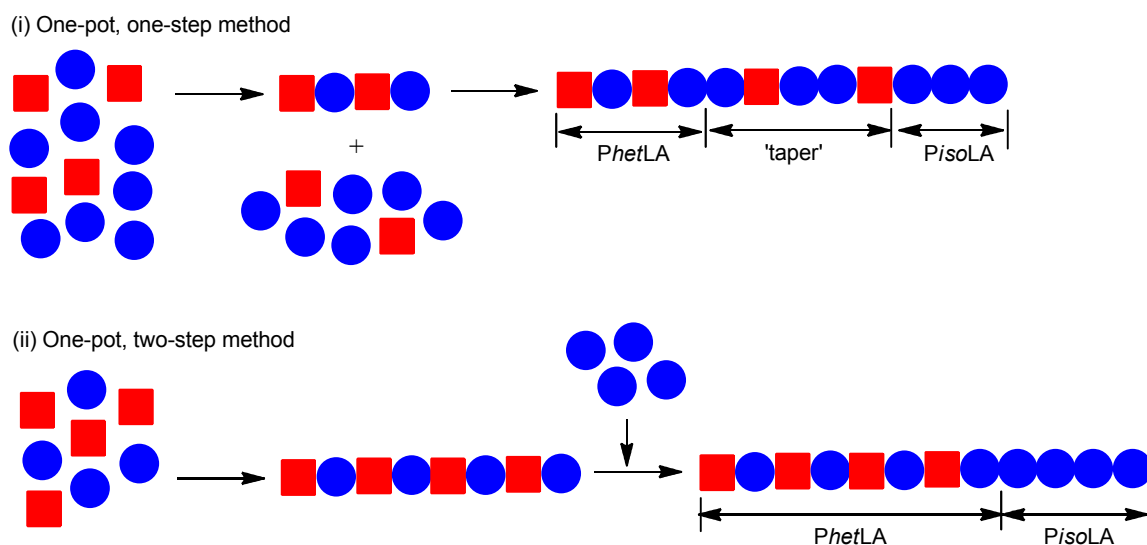
Scheme 4.3: Schematic diagram illustrating the presence of 'tapering' within a one-pot, one-step synthesis.

Synthesis of the four materials listed below was carried out under the industrially preferred bulk conditions in a one-step manner (Table 4.3). As the polymerisation proceeds at an extremely quick rate, the reaction could not be monitored, but all analyses were carried out on the isolated polymers. DSC analysis showed a significant difference in T_g values between these materials, again corresponding to the amount of isotactic character present. However, T_m values could only be obtained from materials consisting of equal heterotactic and isotactic chain segments, indicating crystalline regions were only formed in these materials. Interestingly, higher values of

116

T_m were observed for 1:1 materials synthesised by the one-step melt method (Table 4.3, Entries 7a, 7b) than were observed for the same materials synthesised by the one-step solution method (Table 4.1, Entries 1a, 1b), which could be attributed to the larger molecular weights of these materials. Analysis of these materials by homonuclear decoupled ^{1}H NMR spectroscopy showed prominent peaks corresponding to the *iii*, *isi* and *sis* tetrads, and resulted in values of P_s consistent with those obtained via solution syntheses.

Entry	Polymer (A-B)	M_n	PDI	T_g (2nd heat)	T_m (1st heat)	P_s
7a[b]	1:1 P*het*LA-PLLA	57800	1.19	50	124	0.61
7b[b]	1:1 P*het*LA-PDLA	78500	1.30	48	130	0.60
8a[b]	3:1 P*het*LA-PLLA	63450	1.34	37	-	0.74
8b[b]	3:1 P*het*LA-PDLA	51700	1.29	33	-	0.74

Table 4. 3: PLA di-stereoblock polymers, one-step synthesis: molecular weights and DSC data. L^{tBu}Zr(O^{i}Pr), Solvent-free conditions, 130 °C.

As a comparative study, melt polymerisation of the 1:1 and 3:1 mixtures of *rac*- and L-LA were also carried out using **L^{Me}Ti(O^{i}Pr)**, an initiator which exhibits no stereocontrol and undertakes ROP of *rac*- and L-LA at the same rate.[7] This allows us to compare the homodecoupled spectra of randomly isotactically-enriched atactic PLA with the sequential addition seen to be occurring in the **L^{tBu}Zr(O^{i}Pr)** initiated systems. In the 3:1 case, the spectrum looks similar to what we would expect for atactic addition (Chapter 2, Figure 2.23(a), page 80), but with a slightly more prominent *iii* tetrad. This is shown in Figure 4.5, with 3:1 P*het*LA:PLLA synthesised using **L^{tBu}Zr(O^{i}Pr)** (Table 4.3, Entry 8a), for comparison. DSC analysis of both the 1:1 and 3:1 materials synthesised using **L^{Me}Ti(O^{i}Pr)** was undertaken, and the absence of a visible T_m in either case indicates that the additional *iii* tetrads are distributed randomly throughout the polymer chain rather than occurring in a block, and thus the materials are amorphous in character.
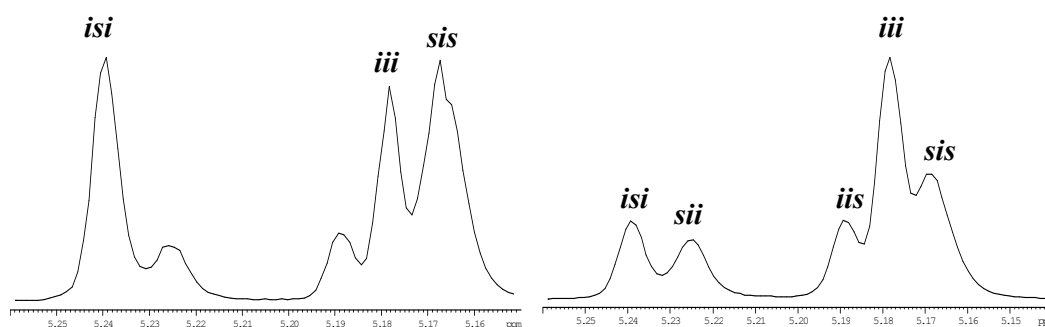
Figure 4.5: Homonuclear decoupled ^{1}H NMR spectra polymers resulting from ROP of 3:1 *rac*-LA:L-LA mixture using L^{tBu}Zr(O^{i}Pr) (Table 4.3, Entry 8a) (left) and L^{Me}Ti(O^{i}Pr) (right).

4.2.2.1. Stereocomplexation of di-stereoblock PLA

In each case, both enantiomeric forms of the polymers were synthesised (i.e. P*het*LA-PLLA and P*het*LA-PDLA) so that their propensity to undergo stereocomplexation could be investigated. The corresponding polymers were first dissolved in dichloromethane and allowed to stir together for a brief period. The solvent was then slowly evaporated under a flow of argon over the course of 20 hrs, as was described by Kricheldorf and co-workers,[6] to allow maximum interactions to take place between the isotactic sections of the chains. Analysis of the resulting materials was then carried out by DSC to obtain values of T_g and T_m, which could be compared to those of the individual polymers before mixing. The stereocomplexed materials were subsequently reprecipitated from dichloromethane and analysed again by DSC, to determine the sensitivity of the stereocomplexation process.

Entry	Polymer (P*het*LA:P*iso*LA)	Stereocomplex (evap[a])		Stereocomplex (reppt[b])	
		T_g (2nd heat)	T_m (1st heat)	T_g (2nd heat)	T_m (1st heat)
1c	1:1 **sc** (1-step, solution)	47	187	51	190
2c	3:1 **sc** (1-step, solution)	48	172	39	169
3c	6:1 **sc** (1-step, solution)	47	-	46	-
4c	1:3 **sc** (2-step, solution)	40	225	40	232
5c	1:1 **sc** (2-step, solution)	45	170	47	179
6c	3:1 **sc** (2-step, solution)	41	207	44	209
7c	1:1 **sc** (1-step, melt)	37	176	48	172
8c	3:1 **sc** (1-step, melt)	35	-	n/a	-

Table 4.4: Stereocomplexed PLA di-stereoblock polymers: DSC data. Stereocomplexes synthesised by: (a) slow evaporation of CH_2Cl_2 under Ar; (b) reprecipitation from CH_2Cl_2 with hexanes.

The similarity in the values of T_g and T_m obtained from these materials lead to the conclusion that reprecipitation creates a comparable degree of stereocomplexation to slow evaporation of the solvent. Only one endothermic peak was present in the DSC thermograms, evidence that all crystalline regions in these materials are due to stereocomplexation; that is, no contribution is made by interactions between isotactic chain segments of the same stereochemical nature.[8] In the majority of cases where the T_m could be observed, it was found to occur at approximately 50 - 70 ºC above the T_m of the respective individual polymers.[9] The one exception was 1:1 **sc**P*het*LA-P*iso*LA (Table 4.4, Entry 5c) synthesised via two-step method in solution, where stereocomplexation of the di-stereoblock materials results in a T_m increase of only 20 – 30 °C. As such, the observed T_m of 1:1 **sc**P*het*LA-P*iso*LA (Entry 5c) is significantly lower than that of 3:1 **sc**P*het*LA-P*iso*LA (Entry 6c), synthesised in the same manner. The observation of a similar result on repeating the analysis indicates a defect in the material, possibly due to degradation, and shall be considered anomalous. The absence of a visible T_m in 6:1 **sc**P*het*LA-P*iso*LA is in agreement with previous reports by Feijen and co-workers that a polymer must contain at least

20% PLLA and PDLA by weight for crystallisation due to stereocomplexation to occur.[10-11] Tsuji has previously reported an increase of T_g to 65-72 ºC[12] on stereocomplexation of PLA, but such high values were not observed here. There is an increase in the T_g's of the 6:1 materials, which, in the absence of visible T_m's, indicates stereocomplexation may still be taking place.

4.2.3. Tri-stereoblock PLA polymers

The difference in reactivity of *rac*- and L- (or D-) LA can be further exploited to prepare stereoblock polymers in an alternative fashion. If, for example, D-LA is added to partially polymerised L-LA after a known period of time, a tri-stereoblock polymer is easily synthesised (Scheme 4.4). The addition of the opposite LA enantiomer, forming racemic LA, allows the fast synthesis of heterotactic PLA, until only one enantiomer remains. If an identical amount of the opposite enantiomer is added (n = m), a PLLA-P*het*LA-PDLA tri-stereoblock can be synthesised, but addition of a much smaller amount (m < n-DP), coupled with careful timing of the addition, will lead to symmetrical PLLA-P*het*LA-PLLA and PDLA-P*het*LA-PDLA tri-stereoblocks.
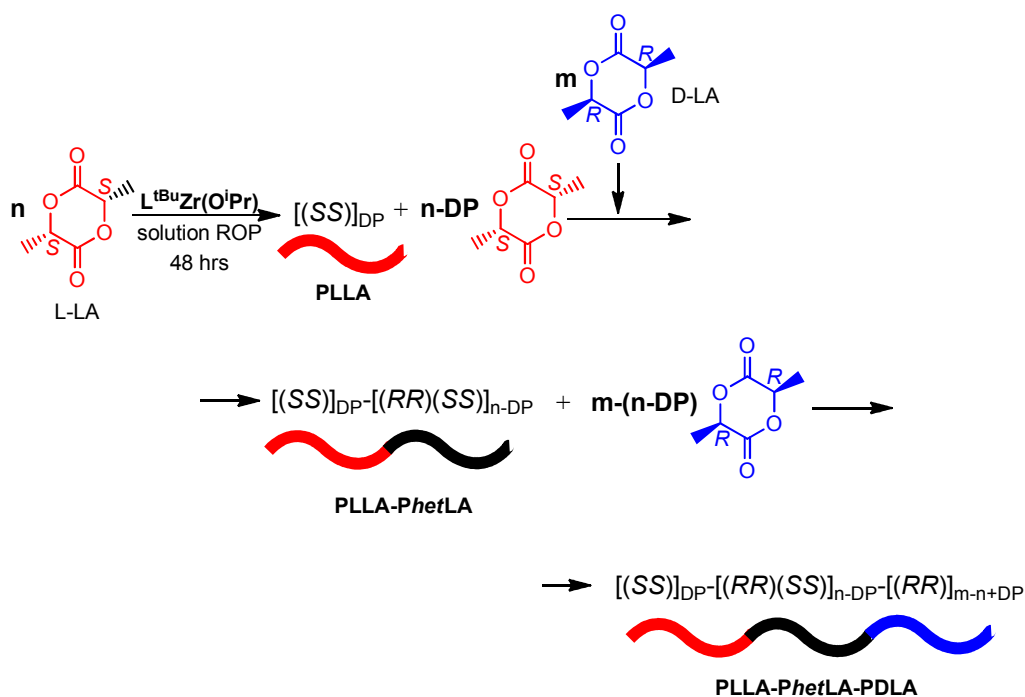
Scheme 4.4: Synthesis of unsymmetrical PLA tri-stereoblock.

This reaction can be monitored over time by ^{1}H NMR and the conversion graph in Figure 4.6 clearly illustrates the central heterotactic block of the chain being synthesised at a much faster rate than the isotactic blocks. A semilogarithmic graph of this data gives similar apparent rate constants, k_{app}, for synthesis of the isotactic sections (k_{app} PDLA = 2 x 10^{-4} min^{-1}, k_{app} PLLA = 4 x 10^{-4} min^{-1}), but gives a value 8 times higher for the synthesis of the heterotactic section (k_{app} P*het*LA = 3.2 x 10^{-3} min^{-1}) (Figure 4.7). This is broadly consistent with the values of k_{app} obtained from the kinetic studies discussed in Chapter 2 (page 83). A number of points do not fit

the linear rates associated with either the ROP of *rac*-LA or enantiomerically pure D- or L-LA. These are shown in green in Figure 4.7 and arise from the 'tapering' effect described in the Section 4.2.1. This will undoubtedly have a complex effect on the rates of ROP involved in the tri-stereoblock synthesis.
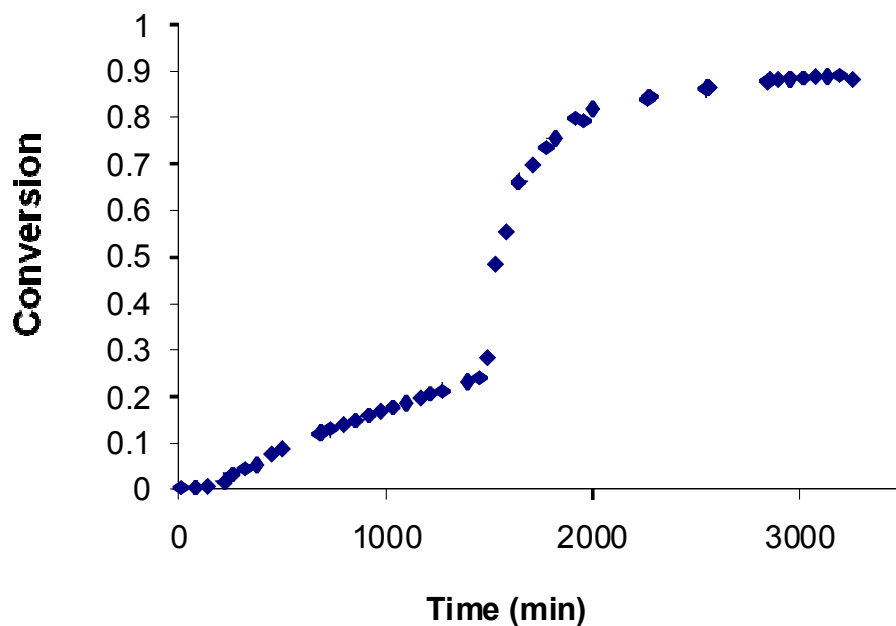
Figure 4.6: Plot of time (min) vs conversion (%) for tri-stereoblock synthesis (Table 4.5, Entry 1).
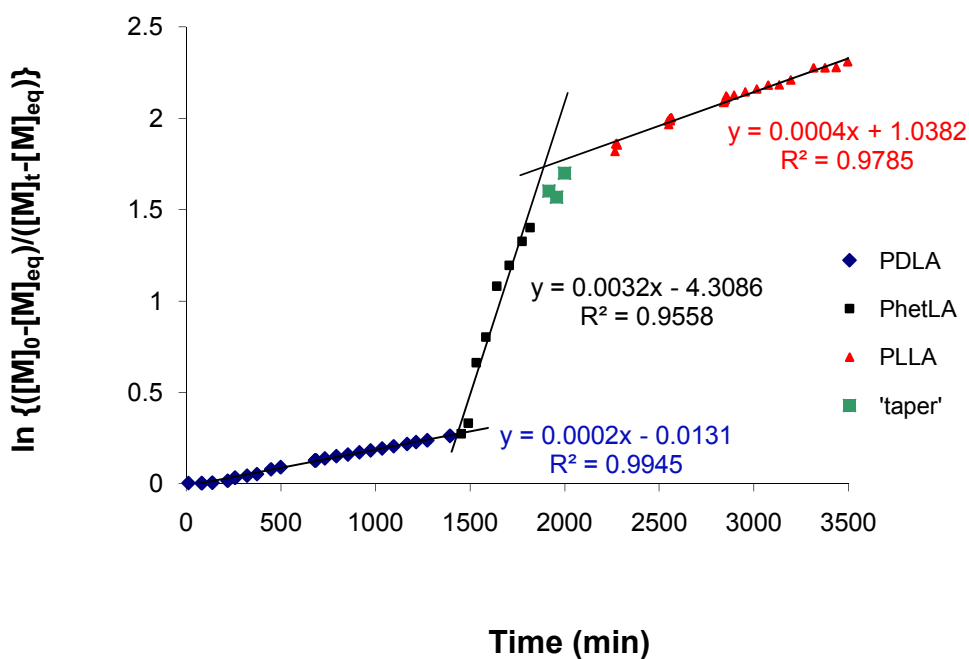
Figure 4.7: Semi-logarithmic plot of conversion data for tri-stereoblock synthesis (Table 4.5, Entry 1).

120

As well as the unsymmetrical PDLA-P*het*LA-PLLA tri-stereoblock, the symmetrical analogues, PLLA-P*het*LA-PLLA and PDLA-P*het*LA-PDLA were also synthesised using this method, consisting of broadly similar block lengths and total molecular weights. These materials are summarised, along with their thermal properties in Table 4.5.

Entry	Polymer (A-B-A/A-B-C)	DP	M_n	T_g (2nd heat)	T_c (2nd heat)	T_m (1st heat)
1	PDLA-P*het*LA-PLLA	25	55800	39	91	189
2	PLLA-P*het*LA-PLLA	21	42600	47	-	128
3	PDLA-P*het*LA-PDLA	24	39050	47	-	129
4	**sc**[PLLA-P*het*LA-PDLA + PDLA-P*het*LA-PDLA]	As above	As above	39	99	198

Table 4.5: Synthesised PLA tri-stereoblock polymers: molecular weights and DSC data.

4.2.3.1.   Stereocomplexation of tri-stereoblock PLA

Once again, the propensity of these materials to form stereocomplexes was investigated, and DSC was once again used to measure the physical properties of these materials (Table 4.5; Figure 4.8). Polymers with identical isotactic end blocks (Entries 2, 3) exhibited relatively low values of T_m, but a 1:1 mixture of the two resulted in a 70 ºC increase in T_m, which can be attributed to stereocomplexation.[9] Similarly, the unsymmetrical tri-stereoblock (Entry 1) displays a T_m of 190 ºC. In this case stereocomplexation could be occurring both inter- and intramolecularly.[13]
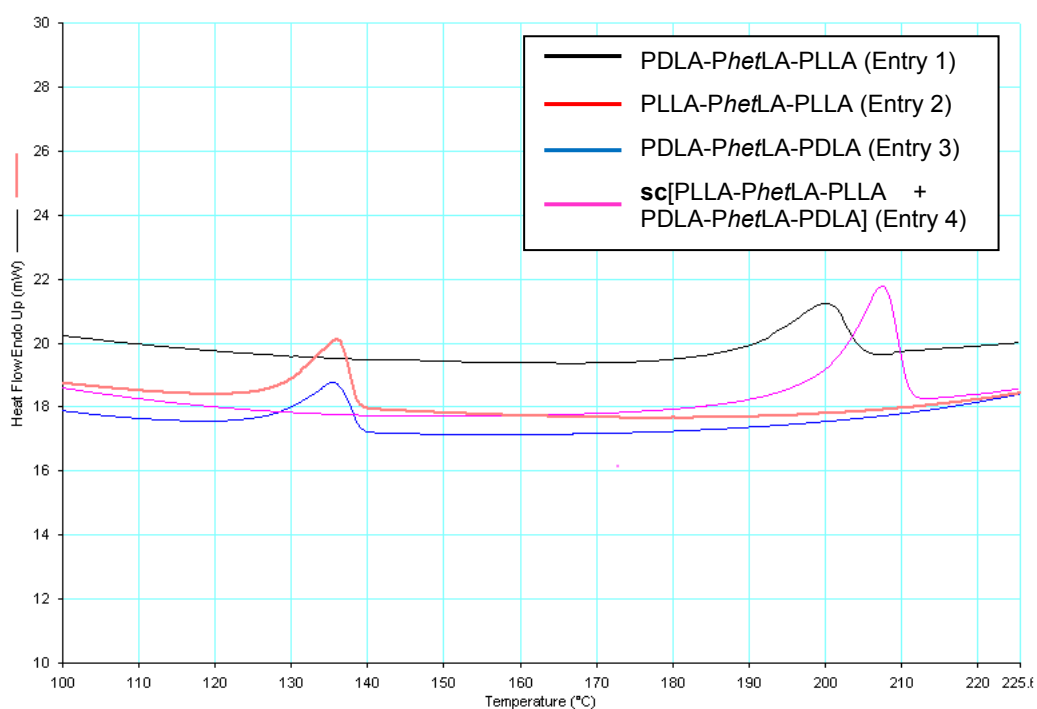
Figure 4.8: DSC thermograms of synthesised tri-stereoblock polymers, 1st heating cycle. Entry nos refer to Table 4.5.

4.3. Macroinitiation of short-chain polymers

An alternative synthetic route to multi-block polymers is to reinitiate the end of an exisiting short-chain polymer, and use this as the first block in the desired material.[1] Many commercially useful polyethers and polyesters are –OH terminated, including the PLA synthesised by the Zr and Hf initiators described in this thesis. However, the isopropoxide initiator $L^{tBu}Zr(O^{i}Pr)$ was investigated and discovered not to facilitate the reinitiation of an –OH terminated polymer. Attention was then turned to the more reactive amide initiator $L^{tBu}Zr(NR_2)$ (R = Me, Et), the synthesis of which has been previously discussed in Chapter 3. These complexes have been shown to reinitiate –OH terminated PLA and poly(ethylene glycol) (PEG), and allow the subsequent stereocontrolled growth of PLA with a range of architectures.

4.3.1. Synthesis of di-stereoblock PLA via Macroinitiation

The quenching of $L^{tBu}Zr(O^{i}Pr)$ initiated chains by the addition of methanol results in PLA terminated by an isopropoxide group at one end and a hydroxyl group at the other.[14] Initial studies showed that the amide initiator $L^{tBu}Zr(NMe_2)$ could be used to reinitiate pre-existing PLA chains of this type and significant chain growth was observed from monomodal GPC traces (Table 4.6). In such cases as these, the terminal isopropyl group inhibits chain growth, and so only di-block polymers could be synthesised in this manner.

Entry	Macroinitiator	M_n macroinitiator	Monomer	Co-polymer	M_n product
1	^{i}PrO-P*het*LA-OH	13550	D-LA	P*het*LA-PDLA	19200
2	^{i}PrO-PDLA-OH	22000	*rac*-LA	PDLA-P*het*LA	29850

Table 4.6: Di- and tri-stereoblock PLA synthesised by reinitiation using $L^{tBu}ZrNR_2$.

4.3.2. Synthesis of PEG-PLA block polymers

In contrast to isotactic PLA, PEG can be considered a very 'soft' polymeric material and is highly soluble in water. The convenient synthesis of PLA-PEG co-polymers that display characteristic properties from both materials is therefore desirable in various applications, including the controlled release of drug therapies. Commonly, both ends of a PEG chain are terminated with an –OH end group, so initial studies were undertaken using methoxy poly(ethylene glycol) to simplify characterisation of the macroinitiation process. Preliminary investigations showed significant chain growth of L-, D- and *rac*-LA, however reinitiation with *rac*-LA initially led to a lack of stereocontrol in the PLA block. This was attributed to the PEG macroinitiator being wet, and the subsequent drying of PEG macroinitiators with molecular sieves and recrystallisation resulted in the expected heterotactic selectivity.
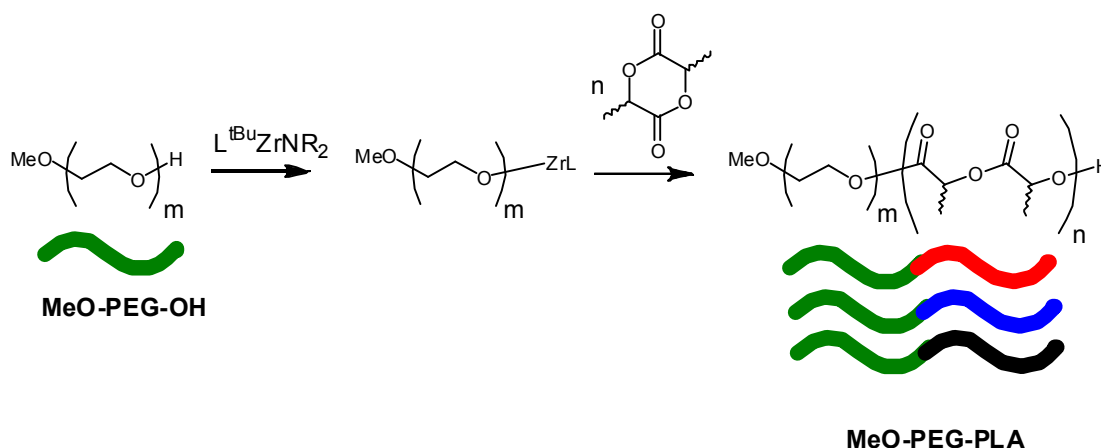
Scheme 4.5: Proposed reinitiation of methoxy PEG using L^{tBu}Zr(NR$_2$) resulting in various stereochemical forms of MeO-PEG-PLA. Red = PLLA; blue = PDLA; black = P*het*LA.

An NMR study was undertaken to prove the reinitiation was proceeding as expected. Methoxy PEG (M_n = 550) was stirred together with **L^{tBu}ZrNMe$_2$** in toluene at room temperature for 2 hours. The solvent was then removed and analysis of the reaction mixture undertaken by ^{1}H NMR spectroscopy. Comparison of the spectrum with that of methoxy PEG shows a shift in the position of the peak corresponding to the methoxy group, and also an absence of peaks that could be assigned to a dimethyl amide group. This confirms the nature of the initiator-coordinated PEG chain (Scheme 4.5).

In the reinitiation of double –OH terminated PEG, two equivalents of the amide initiator were added to allow reinitiation of both chain ends, which were expected to facilitate the synthesis of symmetrical tri-block polymers. Once again, a ^{1}H NMR study was carried out on a short-chain HO-PEG-OH initiator (M_n = 400) to confirm the mechanism of reinitiation. Initially, one equivalent of **L^{tBu}ZrNMe$_2$** was stirred with the polymer and, after two hours the solvent was removed, and ^{1}H NMR analysis showed no peaks that could correspond to the dimethyl amine initiator. However, terminating –OH groups were still observed, included in a broad peak at δ 2.88. This broad signal also encompasses the fluxional methylene protons of the zirconium-ligand system, and after taking these into account, an OH to PEG ratio of approximately 1:30 is observed. For comparison, the original PEG material displayed an -OH to PEG ratio of approximately 1:20, indicating a drop in the average number of terminating –OH groups per chain. Addition of a second equivalent of reinitiator, **L^{tBu}ZrNEt$_2$** in this instance, resulted in a decrease in this ratio to approximately 1:50, indicating only a small number of PEG chains are still bound by a terminal –OH. Again, no peaks were observed corresponding to the dialkyl amine group, which will be cleaved from the Zr complex in the reinitiation process and removed from the system under vacuum. Also, only one set of aryl and alkyl peaks corresponding to the ligand system are observed, indicating the **L^{tBu}Zr** system occupies only one environment i.e.

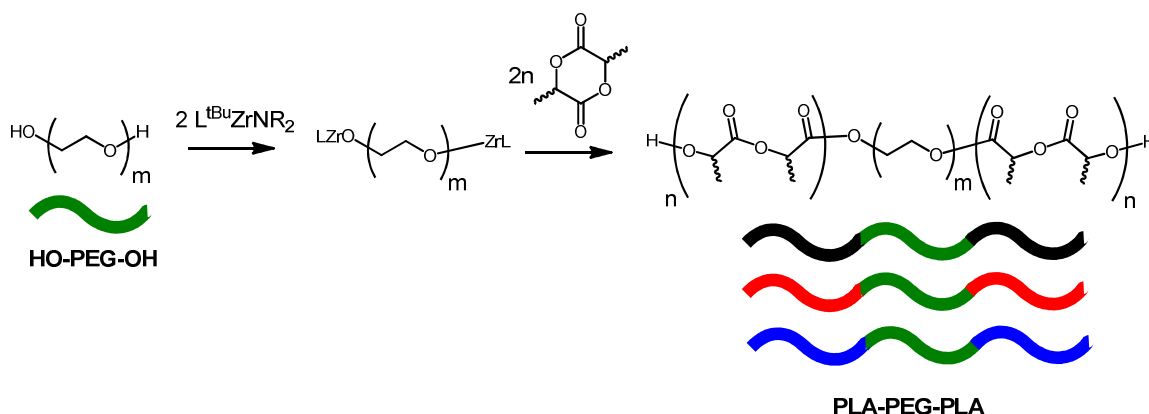bound to the PEG chain ends. L-LA was added to the macroinitiation sequentially and PLA chain growth was observed.

Scheme 4.6: Proposed reinitiation of PEG by L^{tBu}Zr(NR$_2$) resulting in various stereochemical forms of PLA-PEG-PLA. Red = PLLA; blue = PDLA; black = P*het*LA.

Having confirmed the validity of the approach, di- and tri-block PLA-PEG co-polymers were synthesised using longer chain PEG (Table 4.7). In an adapted method, the PEG macroinitiators were stirred together with **L^{tBu}ZrNR$_2$** in toluene at 100 °C, to which a toluene solution of either *rac*-, L- or D-LA, also heated to 100 °C to allow dissolution of the monomer, was added. Analysis of the polymers by ^{1}H NMR Spectroscopy, GPC and MALDI-ToF mass spectrometry confirmed the di- and tri-block nature of these copolymers, however there is poor correlation between the theoretical and observed molecular weights of the polymers. The synthesis of PEG-PLA di-block polymers from MeO-PEG-OH appears to consistently result in molecular weights lower than expected (Entries 1-3), while the synthesis of PLA-PEG-PLA tri-block polymers from HO-PEG-OH results in higher molecular weights than expected (Entries 5,6).

Entry	Macroinitiator	M_n	Monomer	Conv. (%)	Co-polymer	M_n Theo.	M_n Obs.
1	MeO-PEG-OH	5500	*rac*-LA[a]	80	MeO-PEG-P*het*LA	21500	11800
2	MeO-PEG-OH	5500	L-LA[a]	82	MeO-PEG-PLLA	21900	11300
3	MeO-PEG-OH	5500	D-LA[a]	89	MeO-PEG-PDLA	23300	16700
4	HO-PEG-OH	9600	*rac*-LA[b]	91	P*het*LA-PEG-P*het*LA	24150	19650
5	HO-PEG-OH	9600	L-LA[b]	> 95	PLLA-PEG-PLLA	25600	32300
6	HO-PEG-OH	9600	D-LA[b]	> 95	PDLA-PEG-PDLA	25600	32650

Table 4.7: PEG-PLA di-blocks and PLA-PEG-PLA tri-blocks synthesised by reinitiation using L^{tBu}ZrNR$_2$: GPC data. [a] PEG:init:LA = 1:1:139, [b] PEG:init:LA = 1:2:110.

The di- and tri-block polymers synthesised in this manner were tested for their propensity to undergo stereocomplexation with the enantiomeric opposite chain. Once again, the two respective polymers were reprecipitated from dichloromethane and examined using DSC; the results are summarised in Table 4.8. Once again, there is a substantial increase in T_m of 70 - 80 °C between the homopolymers and the mixtures, indicating that strong stereocomplexation is

occurring between the chains. Additionally, no melting endotherms were observed that would indicate homocrystallisation of enantiomerically identical PEG-P*iso*LA chains. In the case of the PEG-P*iso*LA di-block polymers, these results indicate that the process of stereocomplexation is tolerant to a degree of mis-matching in the P*iso*LA block length. These polymers are directly comparable to the range of ABA tri-block polymers reported by Kricheldorf and co-workers, consisting of 'hard' PLLA or PDLA 'A' blocks and a 'soft' central 'B' block.[6] Especially worthy of comparison are the reported tri-blocks PLLA-PEG-PLLA (Entry 7), PDLA-PEG-PDLA (Entry 8) and the respective stereocomplex (Entry 9). The block lengths in Kricheldorf's tri-blocks are approximately half what they are in the tri-blocks reported here, and interestingly display higher values of T_m, both in the homopolymers and the stereocomplex, as a result. Although the ratio of PEG:P*iso*LA is roughly the same in these materials, it is clear that a longer PEG block has a detrimental effect on the polymer thermal properties.

Entry	Polymer	M_w PEG block	M_w P*iso*LA block(s)	T_m polymer (1st heat)	T_m stereocomplex (1st heat)	Ref.
1	PEG-PLLA	5500[a]	5800[a]	139		This work
2	PEG-PDLA	5500[a]	11200[a]	156		"
3	**sc**PEG-P*iso*LA				214	"
4	PLLA-PEG-PLLA	9600[a]	11350[a]	122		"
5	PDLA-PEG-PDLA	9600[a]	11550[a]	121		"
6	**sc**P*iso*LA-PEG-P*iso*LA				189	"
7	PLLA-PEG-PLLA	4600	6120[b]	165		[6]
8	PDLA-PEG-PDLA	4600	6120[b]	161		"
9	**sc**P*iso*LA-PEG-P*iso*LA				220	"

Table 4.8: PEG-P*iso*LA di-blocks and P*iso*LA-PEG-P*iso*LA tri-blocks, synthesised by reinitiation using L^{tBu}Zr(NR$_2$) (1-6) or Sn(Oct)$_2$ (7-9)[6], and their stereocomplexes: molecular weights (calculated by (a) GPC or (b) conversion) and thermal properties.

4.4. Combining the synthetic tools

With these two approaches to block polymer synthesis in hand, a combined technique can be used to undertake the one-pot synthesis of more complex multi-block polymeric materials. Initially, a short-chain MeO-PEG-OH macroinitiator ($M_n = 5500$) was treated with a **L^{tBu}Zr(NR$_2$)** reinitiator. But instead of adding one form of monomer, a 1:1 mixture of *rac*- and L-LA was added to the reaction. A sample was taken every 20 minutes over a reaction time of 4 hrs and monitored by GPC and NMR. It was observed that over the course of the reaction, P_s decreased from ~0.8 to ~0.7 as the chain grew, without any increase in PDI that would indicate increased transesterification. The tri-block polymer MeO-PEG-P*het*LA-PLLA ($M_n = 11550$, PDI = 1.20, P_s = 0.69) was therefore synthesised in a one-pot manner (Scheme 4.7).
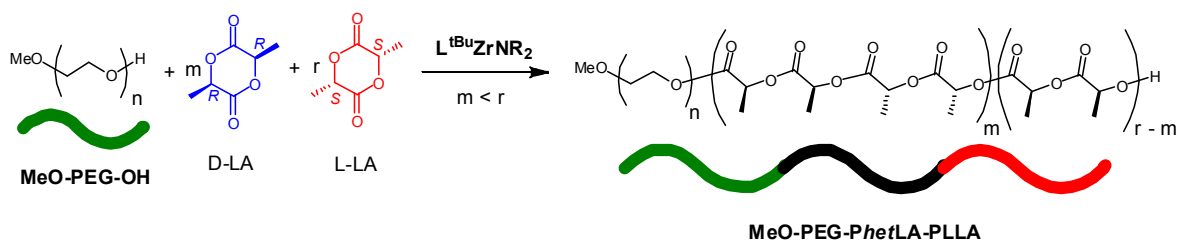
Scheme 4.7: Synthesis of PEG-P*het*LA-PLLA tri-block polymer

If short-chain HO-PEG-OH (M_n = 9600) is used instead as the macroinitiator, and the same procedure is undertaken, a symmetrical penta-block PEG-PLA co-polymer can be synthesised in a simple one-pot manner, as identical P*het*LA-P*iso*LA chains grow from either end of the macroinitiator (Scheme 4.8). The relative lengths of the heterotactic and isotactic segments can be easily controlled by varying the relative amounts of *rac-* and enantiomerically pure LA added to the reaction mixture. As such, four penta-block materials were synthesised with P*iso*LA:P*het*LA:PEG:P*het*LA:P*iso*LA ratios of approximately 1:1:2:1:1 and 2:1:2:1:2 (Table 4.9).
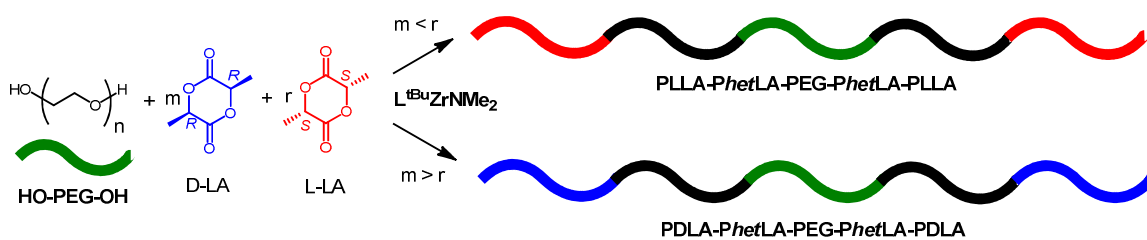
Scheme 4.8: Synthesis of P*iso*LA-P*het*LA-PEG-P*het*LA-P*iso*LA penta-block polymers.

Thermal analysis by DSC of materials 1a and 1b (Table 4.9), with short isotactic PLA blocks, resulted in no observable T_m, presumably due to the high content of amorphous PEG and non-crystalline P*het*LA in these polymers. Stereocomplexation of these materials was carried out as described previously, but still no T_m was observed. On the other hand, materials 2a and 2b, in which the isotactic block length has been doubled, display a number of peaks in their thermograms (Figure 4.9). As would be expected, on stereocomplexation of the homopolymers, the observed T_m of PLA was seen to increase by around 60 °C. Interestingly, the stereocomplex T_m peak area is considerably larger than those of the homopolymers, explained by the strength of stereocomplexation interactions compared to homocrystallisation.[8]

Entry	Polymer	PEG/ *rac*-LA/ L-(or D-)LA	Conv. (%)[c]	M_n PEG block[a]	M_n P*het*LA blocks (theor.)[b]	M_n P*iso*LA blocks (theor.)[b]	Total M_n (theor.)	Total M_n (obs.)[a]	PDI[a]	T_m PLA[d]	T_m area (mJ)[d]
1a	PLLA-P*het*LA-PEG-P*het*LA-PLLA	1/58/58	89	9600	4150	3700	24450	23050	1.06	-	-
1b	PDLA-P*het*LA-PEG-P*het*LA-PDLA	1/58/58	92	9600	4150	3850	24950	28100	1.07	-	-
1c	**sc**[1a+1b]									-	-
2a	PLLA-P*het*LA-PEG-P*het*LA-PLLA	1/58/116	> 95	9600	4150	8300	34600	33950	1.07	107	3.3
2b	PDLA-P*het*LA-PEG-P*het*LA-PLLA	1/58/116	> 95	9600	4150	8300	34600	34400	1.09	113	3.8
2c	**sc**[2a+2b]									163	64.2

Table 4.9: Synthesised P*iso*LA-P*het*LA-PEG-P*het*LA-P*iso*LA penta-block polymers: [a]M_n and PDI calculated by GPC. [b]M_n calculated by monomer molar ratio and conversion. [c]Conversion calculated by ^{1}H NMR spectroscopy. [d]T_m and T_m peak area calculated from DSC thermograms.
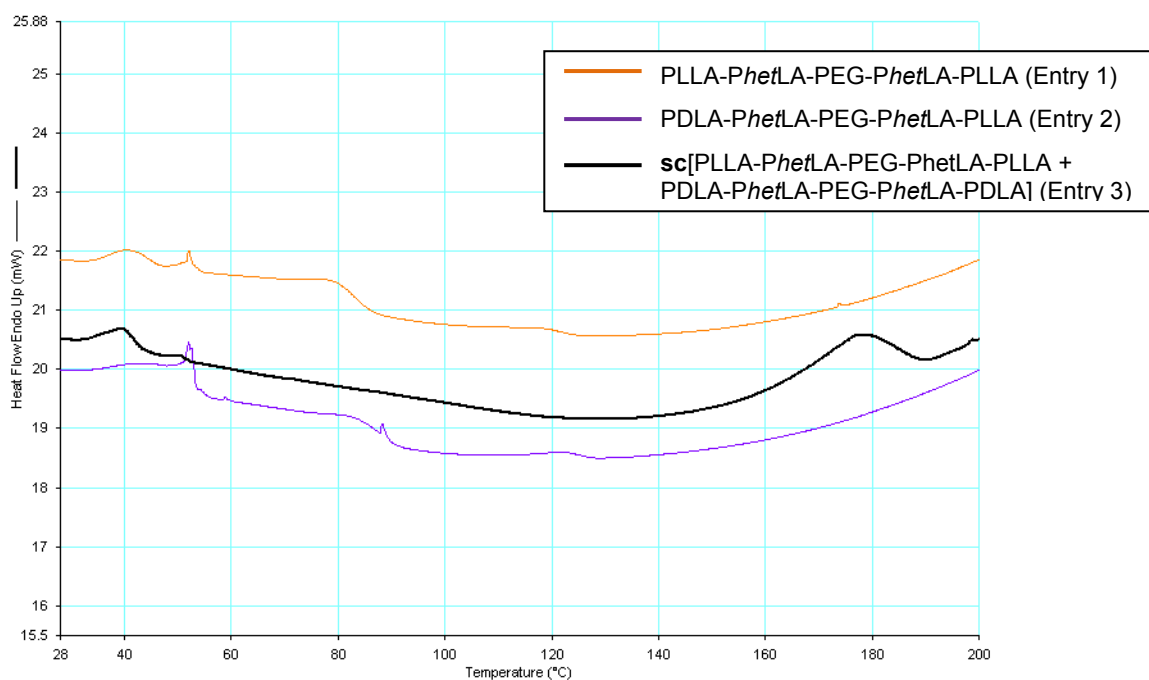
Figure 4.9: DSC thermograms of selected penta-stereoblock polymers, 1st heating cycle. Entry numbers refer to Table 4.10.

4.5. Summary and conclusions

The high level of stereocontrol exhibited by the **L^{tBu}ZrX** class of compounds, in conjunction with the living nature of polymerisations intitated by them, has been utilised in a number of simple, one-pot syntheses resulting in a series of PLA di- and tri-stereoblock polymers and PEG-PLA di- and tri-block polymers. These results highlight an unusual utility for heterotactic selective initiations, which have previously been a largely academic curiosity. In a similar manner, PLA multi-block polymer chains can also be grafted onto pre-existing PEG chains, using **L^{tBu}ZrNR$_2$**, and complex penta-block polymers have been synthesised.

PEG-PLA di- and tri-block polymers, similar to those synthesised here, have been previously reported to undergo micelle self-assembly, driven by the stereocomplexation of isotactic PLLA and PDLA blocks.[15-18] A significant further area of research arising from the results reported here would be the investigation of self-assembly in P*iso*LA-P*het*LA di- and tri-stereoblock polymers. As has been the case with PEG-PLA block polymers, such investigations would most likely initially yield spherical micelles, however, variation in ratio of P*iso*LA:P*het*LA or PLLA:PDLA could lead to a series of micelle morphologies, including cylinders and 'scarf-like' structures, such as those reported by Manners and co-workers in the case of polyferrocenyldimethylsilane block copolymers.[19-20]

128

4.6 References

1.   Hadjichristidis, N.; Pispas, S.; Floudas, G. A., *Block Copolymers: Synthetic Strategies, Physical Properties, and Applications*. Wiley: Hoboken, New Jersey, 2003.
2.   Muller, A. H. E.; Matyjaszewski, K., *Controlled and Living Polymerisations: From Mechanisms to Applications*. Wiley: Weinham, Germany, 2009.
3.   Dove, A. P., *Chem. Commun.* **2008,** (48), 6446-6470.
4.   Lou, X. D.; Detrembleur, C.; Jerome, R., *Macromol. Rapid Commun.* **2003,** *24* (2), 161-172.
5.   Nakano, K.; Kosaka, N.; Hiyama, T.; Nozaki, K. In *Metal-catalyzed synthesis of stereoregular polyketones, polyesters, and polycarbonates*, Dalton Discussion on Organometallic Chemistry and Catalysis, York, England, Sep 09-11; York, England, 2003; pp 4039-4050.
6.   Kricheldorf, H. R.; Rost, S.; Wutz, C.; Domb, A., *Macromolecules* **2005,** *38* (16), 7018-7025.
7.   Gendler, S.; Segal, S.; Goldberg, I.; Goldschmidt, Z.; Kol, M., *Inorg. Chem.* **2006,** *45* (12), 4783-4790.
8.   Fukushima, K.; Kimura, Y., *Polym. Int.* **2006,** *55* (6), 626-642.
9.   Ikada, Y.; Jamshidi, K.; Tsuji, H.; Hyon, S. H., *Macromolecules* **1987,** *20* (4), 904-906.
10.   Stevels, W. M.; Ankone, M. J. K.; Dijkstra, P. J.; Feijen, J., *Macromol. Chem. Phys.* **1995,** *196* (11), 3687-3694.
11.   Stevels, W. M.; Ankone, M. J. K.; Dijkstra, P. J.; Feijen, J., *Macromol. Symp.* **1996,** *102*, 107-113.
12.   Tsuji, H., *Macromol. Biosci.* **2005,** *5* (7), 569-597.
13.   Gu, Q.; Song, R.; Shen, D. Y., *Polym. Bull.* **2000,** *44* (5-6), 533-538.
14.   Chmura, A. J.; Davidson, M. G.; Frankis, C. J.; Jones, M. D.; Lunn, M. D., *Chem. Commun.* **2008,** (11), 1293-1295.
15.   Fujiwara, T.; Mukose, T.; Yamaoka, T.; Yamane, H.; Sakurai, S.; Kimura, Y., *Macromol. Biosci.* **2001,** *1* (5), 204-208.
16.   Mukose, T.; Fujiwara, T.; Nakano, J.; Taniguchi, I.; Miyamoto, M.; Kimura, Y.; Teraoka, I.; Lee, C. W., *Macromol. Biosci.* **2004,** *4* (3), 361-367.
17.   Riley, T.; Stolnik, S.; Heald, C. R.; Xiong, C. D.; Garnett, M. C.; Illum, L.; Davis, S. S.; Purkiss, S. C.; Barlow, R. J.; Gellert, P. R., *Langmuir* **2001,** *17* (11), 3168-3174.
18.   Kang, N.; Perron, M. E.; Prud'homme, R. E.; Zhang, Y. B.; Gaucher, G.; Leroux, J. C., *Nano Lett.* **2005,** *5* (2), 315-319.
19.   Wang, X. S.; Guerin, G.; Wang, H.; Wang, Y. S.; Manners, I.; Winnik, M. A., *Science* **2007,** *317* (5838), 644-647.
20.   Shen, L.; Wang, H.; Guerin, G.; Wu, C.; Manners, I.; Winnik, M. A., *Macromolecules* **2008,** *41* (12), 4380-4389.

Chapter 5

Rare earth complexes of amine tris(phenolates) as ROP initiators

5. Rare earth complexes of amine tris(phenolates) as ROP initiators

5.1. Preamble

As discussed in Chapter 1 of this thesis, the use of rare earth metals in the synthesis of ROP initiators has received great attention over the last decade, primarily due to their high reactivity.[1] However, many of the rare earth metals exhibit large ionic radii, and advanced ligand design is still required to overcome a high propensity to form multinuclear complexes.[2] In a number of instances, activity has been reported to decrease along the lanthanide period and also on ascending Group 3, as the ionic radii of the elements decreases. However, inversely, both molecular weight control and stereocontrol have been shown to *increase* with decreasing ionic radius, attributed to enhanced control offered by a sterically more crowded metal centre. In terms of stereocontrol, several reports have noted a high solvent dependency, in which ROP of *rac*-LA carried out in THF would result in significantly higher heterotactic selectivity than in toluene. However, unlike recent advancements in Group 4 initiators, the activity of rare earth metals in the solvent-free ROP of LA has rarely been reported.[3-5]

Following recent reports by Mountford and co-workers of the reaction of amine bis(phenolate) ligands with trivalent rare earth metals resulting in the series of zwitterionic complexes,[6-7] it was proposed that the coordination of amine tris(phenolate) ligands to rare earth metals would result in a series of mono- and bis-ligated complexes, depending on the steric demands of the ligand system. In the case of H_3L^{tBu}, the coordination of one ligand in a zwitterionic manner could potentially allow a single monodentate ligand to remain bound to the metal centre, which could then act as an initiator for the ROP of LA.

5.2. Synthesis of rare earth complexes

Following the recent interest in lanthanide complexes as potential initiators for ROP of cyclic esters, the ligands H_3L^{Me} and H_3L^{tBu} were reacted with various trivalent rare earth metals. The resulting novel complexes are summarised in Scheme 5.1, and can be grouped into three types, each of which will be discussed in turn: isopropanol-coordinated mono-ligated complexes $\{L^{tBu}Sc(IPA), L^{tBu}Y(IPA)_3, L^{tBu}Nd(IPA)_3, L^{tBu}Sm(IPA)_3, L^{tBu}Yb(IPA)_3\}$, dinuclear complexes $\{[L^{tBu}Nd(IPA)]_2, [L^{tBu}Gd]_2(\mu\text{-}H_2O)\}$ and zwitterionic bis-ligated complexes $\{[HL^{Me}]_2Ce, [HL^{Me}][H_2L^{Me}]Sc, [HL^{Me}][H_2L^{Me}]Sm\}$.
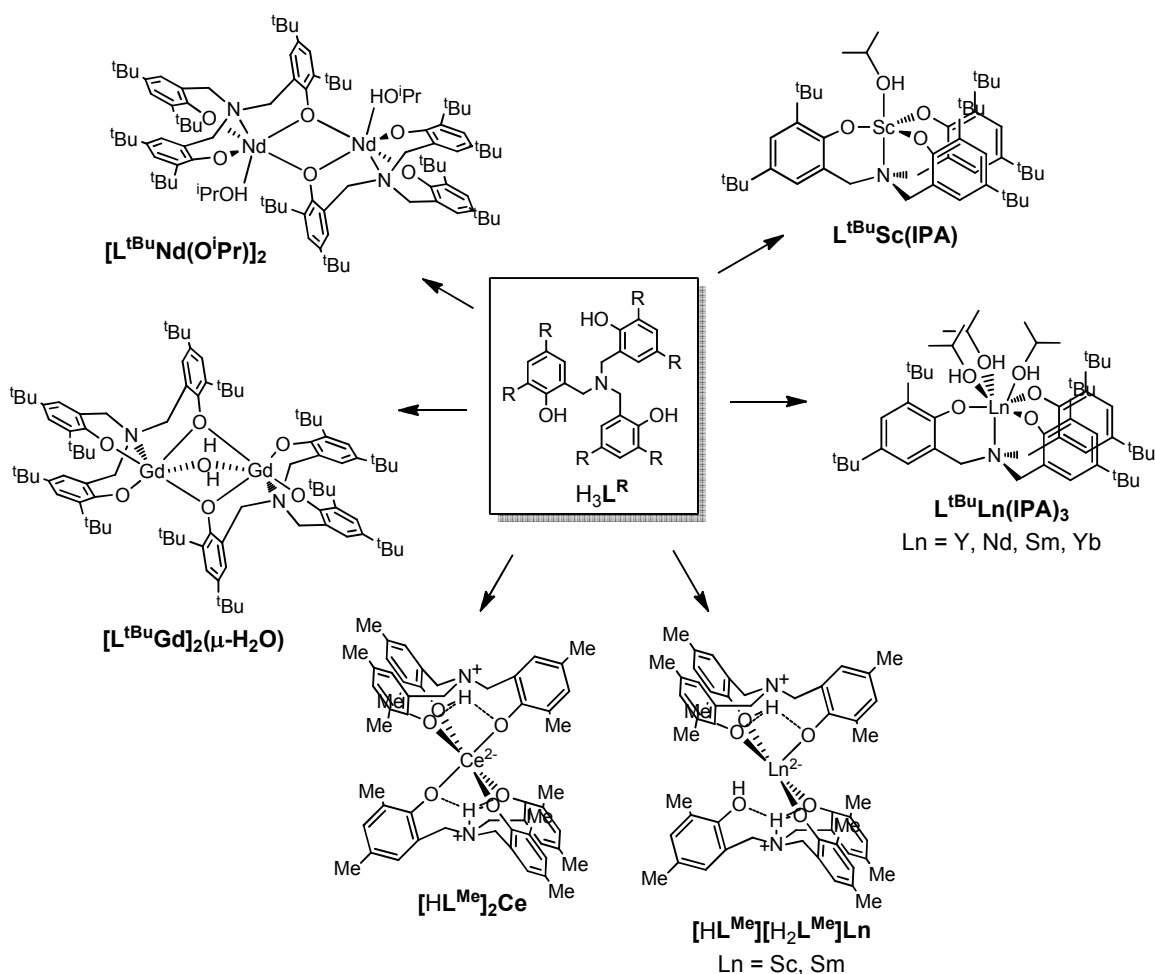
Scheme 5.1: Novel rare earth complexes reported within this chapter.

5.2.1. Synthesis of isopropanol coordinated rare earth metal complexes

The ligand H_3L^{tBu} was reacted with several rare earth isopropoxides, resulting in a series of isopropanol coordinated complexes, the number of coordinated molecules of isopropanol dependent on the size of the metal. In the case of Sc(III), the complex $L^{tBu}Sc(IPA)$ was isolated (Figure 5.1), but in the cases of Y(III), Nd(III), Sm(III) and Yb(III), a series of tris-isopropanol coordinated complexes were observed and will be discussed in due course. The reaction was also attempted with Ce(IV) under various conditions but no reaction was observed.

In this first instance, analysis of the ^1H NMR spectrum clearly shows the presence of a coordinated isopropanol. A distinctive multiplet, observed at δ 4.86 and a clear doublet at δ 3.72, were shown to be cross-coupled in the 2D ^1H COSY spectrum, and correspond to the methine and alcoholic protons of the coordinated group respectively, confirming this ligand is not isopropoxide in nature (Figure 5.2). The methylene protons of this complex were observed as two broad singlets at δ 2.92 and δ 4.11 at room temperature, indicating that fluxionality between the *P* and *M* enantiomers of this complex would occur at temperatures above, but close to, room temperature. This behaviour is unlike that of titanium, scandium's neighbour in the periodic

table, as fluxionality was only observed in the titanium analogue, $\textbf{L}^{\textbf{tBu}}\textbf{Ti(O}^{\textbf{i}}\textbf{Pr)}$, at temperatures approaching 386 K. However, examination of the respective ionic radii of the metals involved, reveal that Sc(III) (74.5 pm) is closer in size to Zr(IV) (72 pm) and Hf(IV) (71 pm) than Ti(IV) (60.5 pm)[8], and so a closer similarity in behaviour to $\textbf{L}^{\textbf{tBu}}\textbf{Zr(O}^{\textbf{i}}\textbf{Pr)}$ and $\textbf{L}^{\textbf{tBu}}\textbf{Hf(O}^{\textbf{i}}\textbf{Pr)}$ is to be expected.

Figure 5.1: Structure of $\textbf{L}^{\textbf{tBu}}\textbf{Sc(IPA)}$ as determined by X-ray crystallography. With the exception of H4, all hydrogen atoms have been omitted for clarity.
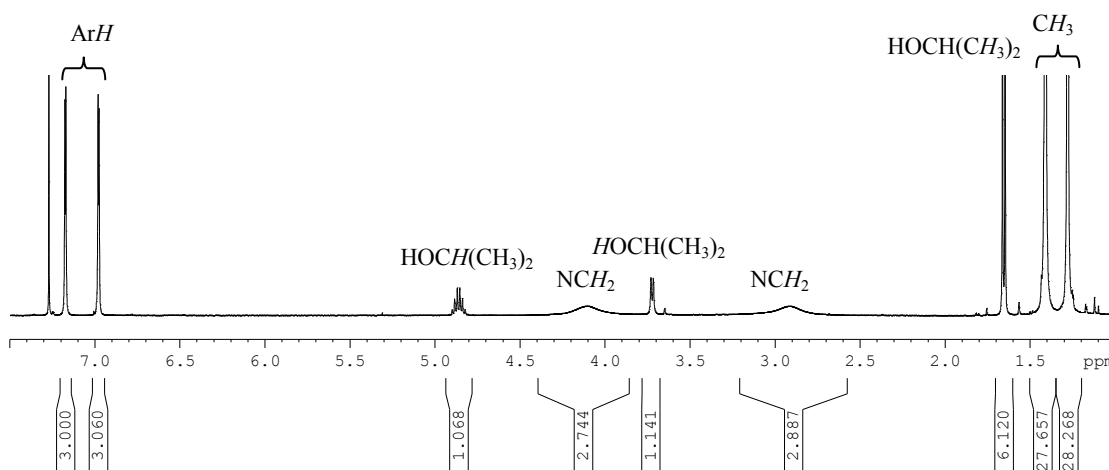
Figure 5.2: ^{1}H NMR spectrum of $\textbf{L}^{\textbf{tBu}}\textbf{Sc(IPA)}$.

X-ray crystallographic analysis was carried out on the colourless crystals of $\textbf{L}^{\textbf{tBu}}\textbf{Sc(IPA)}$ grown from a hexane/toluene mixture. Disorder in the isopropanol ligand was observed and modelled, resulting in Sc(1)-O(4)-C(4) bond angles of 124.9(5)° and 142.3(9)°. The similarity in ionic radii of Sc(III) and Hf(IV) leads to a natural comparison between the structures of $\textbf{L}^{\textbf{tBu}}\textbf{Sc(IPA)}$ and

133

L^{tBu}Hf(O^{i}Pr), especially with respect to the different coordination modes of the isopropoxide groups, and selected key structural parameters are summarised in Table 5.1. As would be expected the weaker coordination of an isopropanol group results in a longer M-O bond length in **L^{tBu}Sc(IPA)** than is seen in **L^{tBu}Hf(O^{i}Pr)**. This would allow more electron density at the metal centre to become involved in the M-N bond, and so this bond is seen to be considerably shorter in **L^{tBu}Sc(IPA)** than has been previously reported in **L^{tBu}Hf(O^{i}Pr)** and in scandium amine bis(phenolate) complexes reported by Mountford and co-workers.[9] Similarity in the ionic radii of Sc(III) and Hf(III) lead to no discernable difference in the average M-O(phenolate) bond length between **L^{tBu}Sc(IPA)** and **L^{tBu}Hf(O^{i}Pr)**, however this bond was found to be significantly shorter than that previously reported in Okuda's 1,ω-dithiaalkanediyl-bridged bis(phenolato) ligated scandium complex.[10]

	L^{tBu}Sc(IPA)	L^{tBu}Hf(O^{i}Pr)
M-O(O^{i}Pr/IPA) (Å)	2.190(6)/2.200(14)	1.920(2)
M-N (Å)	2.274(2)	2.406(2)
M-O1 (Å)	1.905(3)	1.949(3)
M-O2 (Å)	1.964(6)	1.944(3)
M-O3 (Å)	1.991(3)	1.999(3)
M-(O1,O2,O3)^a (Å)	0.129	0.300
M-O-C (°)	124.9(5)/142.3(9)	177.6

Table 5.1: Structural parameters of L^{tBu}Sc(IPA) and L^{tBu}Hf(O^{i}Pr). ^{a}(O1,O2,O3) represents the plane defined by the atoms O1, O2 and O3.

Reaction of the ligand H$_3$**L^{tBu}** with the larger rare earth metals Y(III) (90 pm)[8], Nd(III) (99.5 pm), Sm(III) (96.4 pm) and Yb(III) (85.8 pm)[11] resulted in a series of tris-isopropanol coordinated rare earth metal complexes (Figure 5.3), the characterisation of which relied heavily on X-ray crystallography due to the paramagnetic nature of Nd(III), Yb(III), and to a lesser extent Sm(III). However, analysis of the ^{1}H NMR spectrum of **L^{tBu}Y(IPA)$_3$** was possible and shows fluxionality of the complex at room temperature, with broad signals observed for the methylene protons of the ligand as well as the alcoholic and methine protons of the isopropanol molecules.

All four reported complexes of this nature were found to be isomorphous and were observed to crystallise in the highly symmetric cubic space group P_a-3. Inspection of structural parameters of these complexes showed a clear correlation between the increase in ionic radius of the rare earth metal and M-N, M-O(IPA) and M-O(phenolate) bond lengths (Table 5.2). Also seen to increase with ionic radius was the distance which the metal centre is removed out of the (O1,O2,O3) plane. Disorder was observed over the isopropyl groups in **L^{tBu}Sm(IPA)$_3$** and **L^{tBu}Nd(IPA)$_3$**, and over the whole isopropanol ligand in **L^{tBu}Y(IPA)$_3$**, however the M-O-C bond angle within the isopropanol groups was not shown to exceed 154.7(8)°.
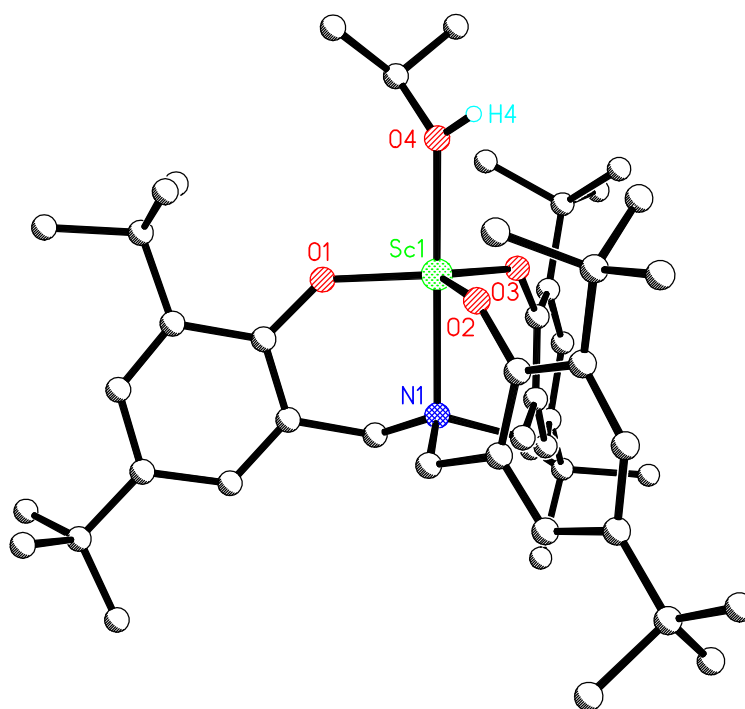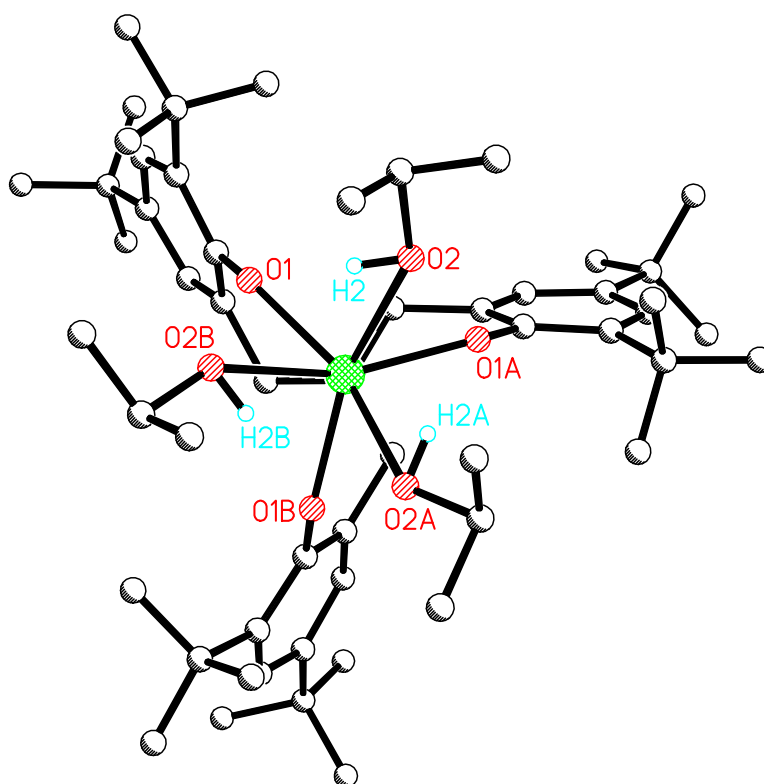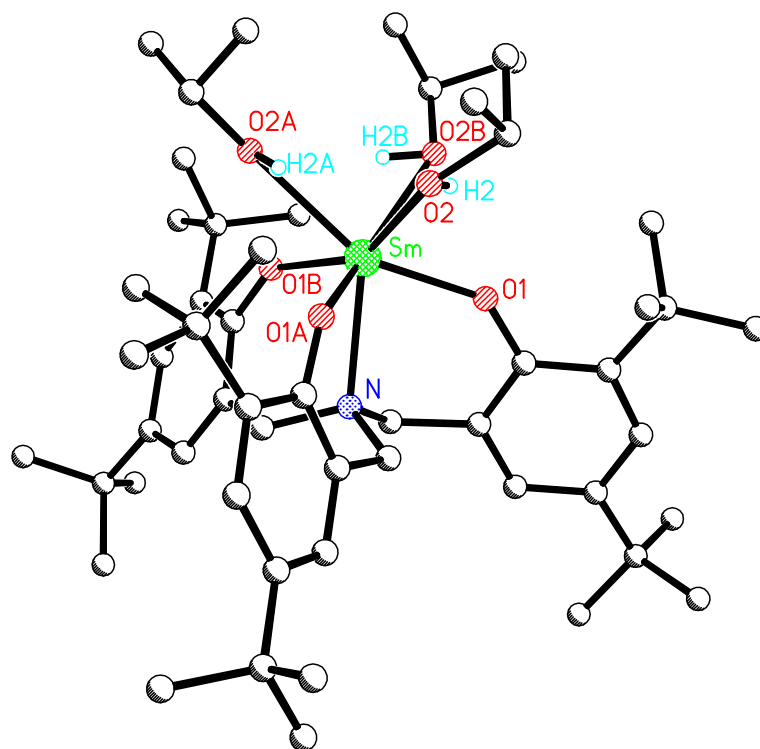
Figure 5.3: Structure of L^{tBu}Sm(IPA)₃ as determined by X-ray crystallography. With the exception of H1, H2 and H3, all hydrogen atoms have been omitted for clarity.

The long M-O(IPA) bond lengths are similar to those reported within a series of isopropanol coordinated Y and Nd cluster compounds, published by Mathur, Veith et al.[12-15] Coupled with the free location and refinement of the alcoholic protons, these long M-O(IPA) bond lengths confirm the isopropanol nature of these ligands. In the case of $\mathbf{L^{tBu}Y(IPA)_3}$, the Y-N bond (2.424(5) Å) was found to be significantly shorter than the analogous bond in several yttrium amine bis(phenolate) complexes reported by Carpentier,[16] Lui,[17] and Mountford,[9] but the Y-O(phenolate) bond (2.190(3) Å) was found to be significantly longer than has been previously observed.

	$\mathbf{L^{tBu}Yb(IPA)_3}$	$\mathbf{L^{tBu}Y(IPA)_3}$	$\mathbf{L^{tBu}Sm(IPA)_3}$	$\mathbf{L^{tBu}Nd(IPA)_3}$
M(III) radius (pm)	85.8	90.0	96.4	99.5
M-O(IPA) (Å)	2.385(3)	2.407(8)	2.525(3)	2.553(2)
M-N (Å)	2.378(4)	2.424(5)	2.487(5)	2.531(4)
M-O(phenolate) (Å)	2.164(2)	2.190(3)	2.241(3)	2.271(2)
M-(O1,O2,O3)^a (Å)	0.495	0.536	0.592	0.625
M-O-C (°)	140.8(2)	151.3(8)/154.7(8)	150.0(9)	142.1(2)

Table 5.2: Structural parameters of the tris-isopropanol coordinated rare earth complexes. ^{a}(O1,O2,O3) represents the plane defined by the atoms O1, O2 and O3.

5.2.2. Synthesis of rare earth dinuclear complexes

Dissolution of $\mathbf{L^{tBu}Nd(IPA)_3}$ in hexane by heating, followed by recrystallisation, resulted in the isolation of the dinuclear complex $\mathbf{[L^{tBu}Nd(IPA)]_2}$, in which two molecules of isopropanol are lost and one phenolate group from each ligand bridges the two metal centres. This indicates that the isopropanol groups are bound relatively weakly in complexes of this type.
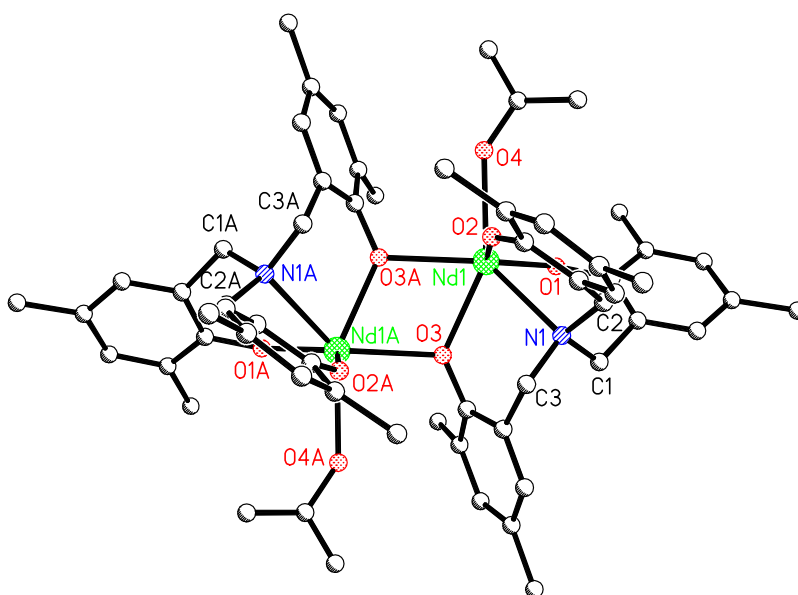
Figure 5.4: Structure of [L^{tBu}Nd(IPA)]$_2$ as determined by X-ray crystallography. Hydrogen atoms and tertiary butyl methyl groups have been omitted for clarity. Selected bond lengths [Å]: Nd(1)-O(1) 2.2216(17), Nd(1)-O(2) 2.1980(18), Nd(1)-O(3) 2.3855(17), Nd(1)-O(3A) 2.4739(16), Nd(1)-O4 2.547(2), Nd(1)-N(1) 2.571(2).

Inspection of selected bond lengths from **[L^{tBu}Nd(IPA)]$_2$** found the Nd-O(μ-phenolate) bonds of the dinuclear complex to be significantly longer than the M-O(phenolate) bonds of the mononuclear complex **L^{tBu}Nd(IPA)$_3$**, which were themselves found to be significantly longer than the non-bridging Nd-O(phenolate) bonds of **[L^{tBu}Nd(IPA)]$_2$**. Once again, the long Nd-O(IPA) bond length confirms the isopropanol nature of these ligands

Reaction of the ligand H$_3$**L^{tBu}** with Gd{N[SiMe$_3$]$_2$}$_3$ was also attempted, resulting in the isolation of the water-bridged dinuclear complex **[L^{tBu}Gd]$_2$(H$_2$O)** from hexane after standing for four weeks. One phenolate group from each ligand was again seen to bridge the metal centres, however in this case a bridging oxygen atom was also located. Assuming Gd(III), two possible extreme structures can be proposed (Figure 5.5): one in which the bridging oxygen is actually part of a water molecule, and a second oxo-bridged structure, in which the bridging ligand arms remain phenolic in nature.
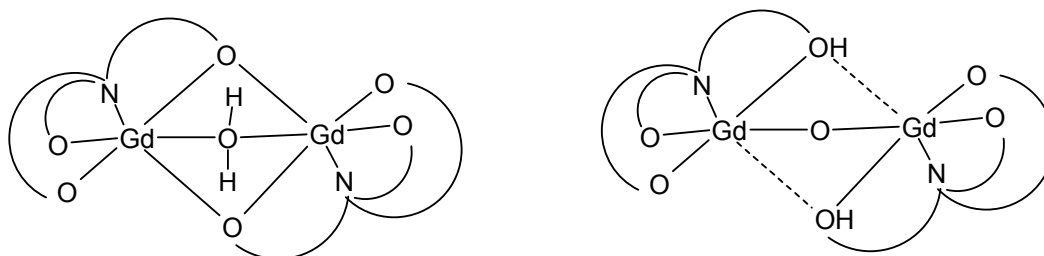
Figure 5.5: Possible binding modes of the Gd dinuclear complex.

The H atoms in question could not be located but examination of the Gd(1)-O(7)-Gd(2) bridge gives an unusually small bond angle of 83.87(14)° and long bond lengths of Gd(1)-O(7) 2.767(5) Å and Gd(2)-O(7) 2.699(5) Å. A search of the Cambridge Structural Database showed that previous reports of μ-H$_2$O groups are more common than μ-O in Gd multi-metal complexes, with only one report of the latter by Evans and co-workers who described a much larger Gd-O-Gd bond angle of 173.64(17)° and shorter symmetrical Gd-O bond lengths of 2.118(3) Å.[18] On the other hand a μ-H$_2$O Gd multi-metal complex reported by Plakatouras and co-workers exhibited a Gd(1)-O-Gd(2) angle of 89.1(3)° and symmetrical Gd-O bond lengths of 2.620(8) Å.[19] This evidence would suggest that the bridging oxygen belongs to a μ-H$_2$O group, however, in order to confirm this structure, further analysis of the crystals by neutron diffraction would be required to locate the hydrogen atoms.
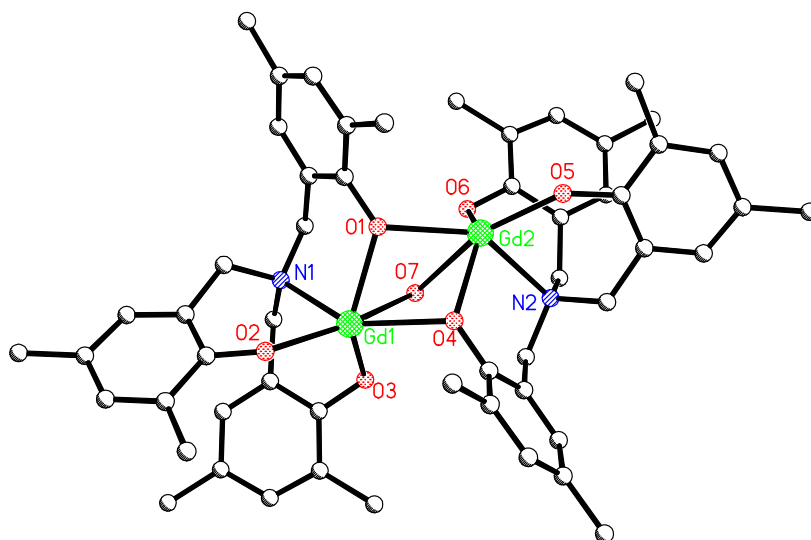
Figure 5.6: Structure of [L^tBuGd]₂(H₂O) as determined by X-ray crystallography. Hydrogen atoms and tertiary butyl metyl groups have been omitted for clarity. Selected bond lengths [Å] and angles [°]: Gd(1)-O(1) 2.295(3), Gd(1)-O(2) 2.150(3), Gd(1)-O(3) 2.181(3), Gd(1)-O(4) 2.411(3), Gd(1)-O(7) 2.767(5), Gd(1)-N(1) 2.461(4), Gd(1)-O(7)-Gd(2) 101.57(12).

5.2.2. Synthesis of zwitterionic rare earth complexes

The sterically less hindered ligand H₃**L^Me** was also reacted with a variety of rare earth isopropoxides, but always resulted in a zwitterionic complex, in which two tris(phenolate) ligands are bound to a central metal atom, although the exact nature of this ligand binding was found to depend on the oxidation state of the metal. Reaction of H₃**L^Me** with Ce(IV) resulted in the complex **[HL^Me]₂Ce** (Figure 5.7), found to be structurally identical to the previously reported complex **[HL^Me]₂Zr**,[20] and **[HL^Me]₂Hf**, reported in Chapter 2.

^{1}H NMR spectroscopy of **[HL^Me]₂Ce** clearly shows the N-H protons at 11.37 ppm and the methylene protons as two broad resonances at room temperature, which were resolved as doublets at δ 3.29 and δ 3.32 at 238 K. Despite the similarity in fluxionality of **[HL^Me]₂Hf** and **[HL^Me]₂Ce**, there are some pronounced differences in their X-ray structures (Table 5.3), due to the increase in ionic radii on moving from Group 4 metals to Ce(IV) (87 pm)[21]. These are similar to observations made by Raymond and co-workers with regards to the molecular structures of tetrakis(catecholateo)hafnate(IV) and –cerate(IV),[22] although in this case M-O(phenolate) bond lengths in both structures (Hf: 2.220(3), 2.194(3) Å; Ce: 2.362(4), 2.357(4) Å) were found to be significantly longer than those reported in **[HL^Me]₂Hf** and **[HL^Me]₂Ce**. However, the tetrakis(catecholateo)cerate(IV) structure appears to be an exceptional case, as the M-O(phenolate) bond lengths in **[HL^Me]₂Ce** are in fact comparable to a number of amine bis(phenolate)[23-24] and Schiff base[25-26] ligated cerium complexes.

Figure 5.7: Structure of [HL^Me]₂Ce as determined by X-ray crystallography. With the exception of H1 and H1A, all hydrogen atoms have been omitted for clarity.

	[HL^Me]₂Hf	**[HL^Me]₂Ce**
M-O1	2.042(2)	2.207(2)
M-O2	2.046(2)	2.216(2)
M-O3	2.037(2)	2.213(2)
N-H⋯O1	2.872(4)	2.892(3)
N-H⋯O2	2.906(4)	2.846(3)
N-H⋯O3	2.830(4)	3.020(3)
M-(O1,O2,O3) plane	1.241	1.396

Table 5.3: Structural parameters of [HL^Me]₂Hf and [HL^Me]₂Ce (Å). (O1,O2,O3) represents the plane defined by O1, O2 and O3.

Reaction of H_3L^{Me} with Sc(III), Y(III) and Sm(III) each resulted in a structure where two ligand systems are bound to one metal centre, but here binding only occurs formally through five M-O(phenolate) bonds (Figure 5.5). The sixth M-O(phenolate) interaction was shown to be significantly longer in the X-ray structures of **[HL^Me][H₂L^Me]Sc** and **[HL^Me][H₂L^Me]Sm**, indicating this bond is in fact a phenol⋯metal interaction, although the H atom itself could not be freely located in either structure. There is little difference in the M-O1 bond lengths, corresponding to the unbound phenol groups, between the Sc and Sm analogues, while the remaining M-O(phenolate) bonds are significantly shorter in **[HL^Me][H₂L^Me]Sc** than in **[HL^Me][H₂L^Me]Sm**. This is in keeping with their respective ionic radii and the influence of *f*

orbitals in the bonding interactions of **[HL^{Me}][H$_2$L^{Me}]Sm**. The asymmetry of the M-O(phenolate) bonding interactions resulted in larger distances between the metal and (O1,O2,O3) plane than were observed between the metal and (O4,O5,O6) plane. Unlike the symmetrical complexes **[HL^{Me}]$_2$M**, the longer M-O(1) bonds tilts the (O1,O2,O3) plane considerably in **[HL^{Me}][H$_2$L^{Me}]Sc** and **[HL^{Me}][H$_2$L^{Me}]Sm**. The bonding nature of each phenolate group also has an observable effect on the respective N-H···O hydrogen bond interaction, which was found to be significantly weaker in cases where the phenolate group was unbound. Examination of the structural parameters of **[HL^{Me}][H$_2$L^{Me}]Sm** reveal two longer M-O(phenolate) bonds, Sm-O(1) and Sm-O(5). Bearing in mind that due to a phase transition, the crystal structure of **[HL^{Me}][H$_2$L^{Me}]Sm** was determined at 200 K, it is feasible that the alcoholic proton of the unbound group is shared between two adjacent phenolate groups.
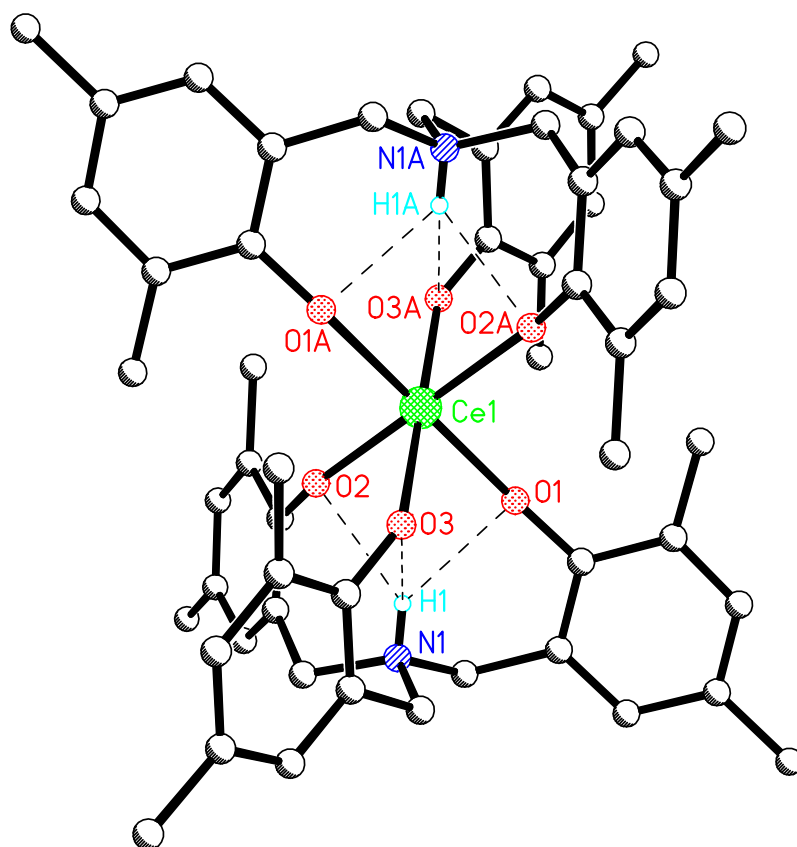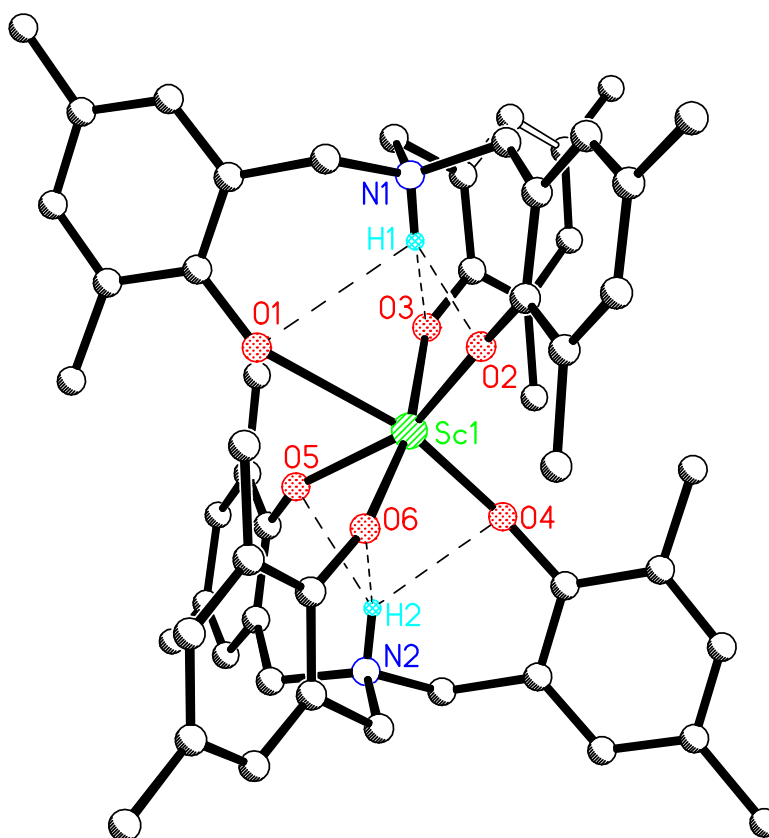

Figure 5.8: Structure of [HL^{Me}][H$_2$L^{Me}]Sc as determined by X-ray crystallography. With the exception of H1 and H2, all hydrogen atoms have been omitted for clarity.

	[HL^{Me}][H₂L^{Me}]Sc		[HL^{Me}][H₂L^{Me}]Sm
	Sc1	**Sc2**	
M-O1	2.481(2)	2.539(2)	2.562(4)
M-O2	2.000(2)	1.984(2)	2.232(4)
M-O3	2.058(2)	2.049(2)	2.221(4)
M-(O1,O2,O3)	1.298	1.467	1.548
M-O4	1.961(2)	1.961(2)	2.219(4)
M-O5	2.100(2)	2.147(2)	2.412(4)
M-O6	2.060(2)	2.028(2)	2.239(4)
M-(O4,O5,O6)	1.151	0.981	1.440
N1-H1···O1	3.208(4)	3.082(4)	3.096(6)
N1-H1···O2	2.717(3)	2.891(4)	2.816(6)
N1-H1···O3	2.294(4)	2.704(4)	2.821(6)
N2-H2···O4	2.957(4)	2.909(4)	2.884(6)
N2-H2···O5	2.882(3)	3.019(4)	3.142(6)
N2-H2···O6	2.808(4)	2.755(4)	2.771(6)

Table 5.4: Structural parameters of [HL^{Me}][H₂L^{Me}]Sc and [HL^{Me}][H₂L^{Me}]Sm. (X,Y,Z) represents the plane defined by the atoms X, Y and Z.

Just as is seen in the symmetrical complexes of the type **[HL^{Me}]₂M**, each of the tris(phenolate) ligands in **[HL^{Me}][H₂L^{Me}]Sc** are coordinated in a heteroditopic manner;[27] that is, one ligand takes on a *P* conformation on binding, while the other ligand takes on an *M* conformation. This results in all six ligand arms appearing to point in the same direction when the complex is viewed from the top down (Figure 5.6). Interestingly, inspection of **[HL^{Me}][H₂L^{Me}]Sm** found the tris(phenolate) ligands to be bound in a homoditopic manner, resulting in an alternative complex structure in which, when coordinated, the arms of the two ligands point in opposite directions (Figure 5.7). Such a structure results in a shorter O1···O5 distance (Sm: 2.465 Å; Sc: 2.561 Å (av)), allowing for a possible O1-H···O5 H-bonding interaction.

^{1}H NMR spectroscopic analysis of **[HL^{Me}][H₂L^{Me}]Sc** and **[HL^{Me}][H₂L^{Me}]Y** showed high fluxionality at room temperature with only one broad resonance observed for the methylene and N-H protons, but cooling of the sample to 238 K led to the observation of two sets of shifts. As was the case for **[HL^{Me}]₂Hf**, the axial signal is further split by the N-H proton, as dictated by the Karplus-Conroy curve,[28] and two overlaying doublets are observed. This behaviour was not observed for **[HL^{Me}][H₂L^{Me}]Sm**, where multiple signals were observed at room temperature, but heating of the sample led to a spectrum similar to those showing the fluxionality of the Sc and Y analogues. It has been proposed that this difference in behaviour may be due to the O1-H···O5 H-bonding interaction mentioned above, arising from the close proximity of the oxygen atoms within **[HL^{Me}][H₂L^{Me}]Sm**, and resulting in a significantly longer Sm-O5 bond, in addition to a long Sm-O1 bond length.
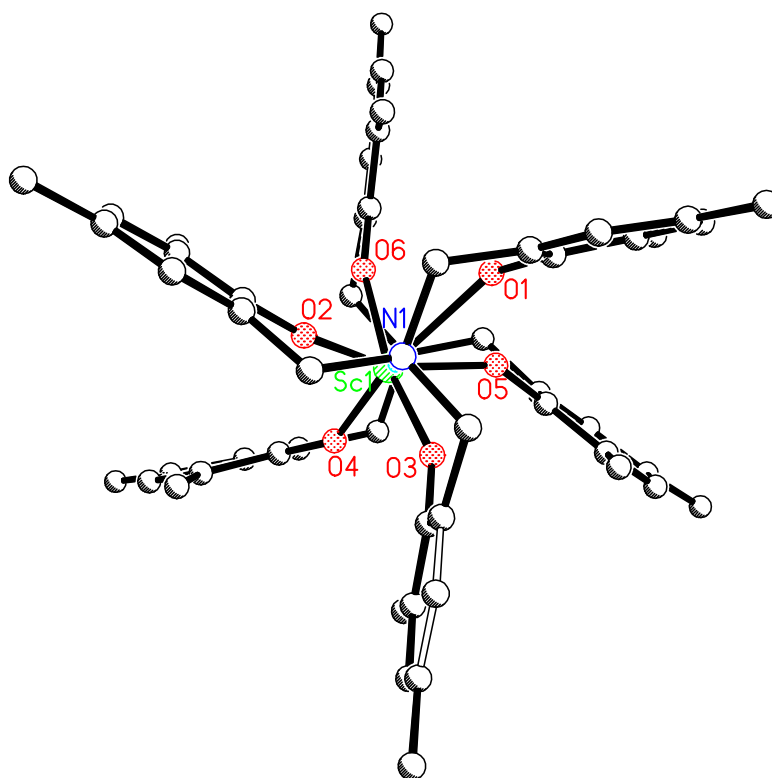
Figure 5. 9: Top-down view of [HL^{Me}][H₂L^{Me}]Sc.
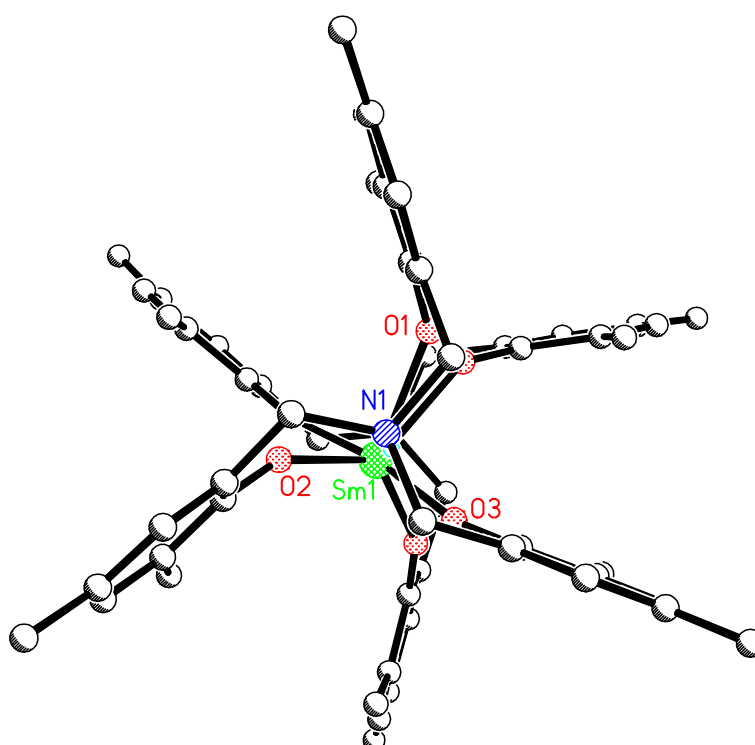
Figure 5.10: Top-down view of [HL^{Me}][H₂L^{Me}]Sm.

5.3. Rare earth metal complexes as initiators

5.3.1. Isopropanol and dinuclear complexes

5.3.1.1. Solvent-free ROP

All synthesised isopropanol and dinuclear rare earth complexes were shown to initiate the ROP of *rac*-LA under solvent-free conditions, and in the cases where ^{1}H homonuclear decoupled NMR experiments could be carried out, displayed a slight heterotactic bias. However, within the series of tris-isopropanol coordinated complexes, isolated yield and molecular weight was observed to decrease dramatically across the lanthanide period. This is at odds with previous reports of ROP of *rac*-LA using one component rare earth initiators under solvent-free conditions, in which high molecular weights were observed.[3] It is thought that the availability of electrons in *f* orbitals for monomer binding, coupled with an excess of isopropanol within the system, may in fact hinder the propagation step of polymerisation, to be discussed in due course. Interestingly, a far higher degree of polymerisation control was observed when the dinuclear complexes $[\mathbf{L^{tBu}Nd(IPA)}]_2$ and $[\mathbf{L^{tBu}Gd]_2(H_2O)}$ were used as initiators, presumably due to the presence of fewer active sites.

Entry	Complex	Time	Yield (%)	M_n	M_w	PDI	P_s
1	$\mathbf{L^{tBu}Sc(IPA)}$	16 hr	55	72050	141950	1.97	0.66
2	$\mathbf{L^{tBu}Y(IPA)_3}$	10 min	56	29950	55100	1.84	0.69
3	$\mathbf{L^{tBu}Nd(IPA)_3}$	16 hr	9	7400	12750	1.72	-
4	$\mathbf{L^{tBu}Sm(IPA)_3}$	5 min	6	8800	11000	1.25	0.62
5	$\mathbf{L^{tBu}Yb(IPA)_3}$	5 min	~0	950	1300	1.39	-
6	$\mathbf{[L^{tBu}Nd(IPA)]_2}$	10 min	78	25800	51450	1.99	-
7	$\mathbf{[L^{tBu}Gd]_2(H_2O)}$	10 min	67	44900	76600	1.71	-

Table 5.5: ROP of *rac*-LA. 1.0 - 2.0 g of *rac*-LA in the absence of solvent at 130 °C, [LA]/[cat] = 300. M_w, M_n and PDI determined by GPC in THF, relative to polystyrene standards.

5.3.1.2. Solution ROP

ROP of *rac*- and L-LA was successfully undertaken using $\mathbf{L^{tBu}Sc(IPA)}$ in toluene at 100 °C over the course of several hours, resulting in polymers with narrow polydispersities (Table 5.7). Reduction in the [M]/[I] ratio resulted in a reduction in polymer weight, indicating controlled polymerisation despite the absence of a formal initiating group. A small but significant heterotactic enrichment was observed in the ROP of *rac*-LA.

Entry	Complex	Monomer	[M]/[I]	Time	Conv (%)	M_n	PDI	P_s
1	$\mathbf{L^{tBu}Sc(IPA)}$	*rac*-LA	100	4 hr	87	21750	1.04	0.66
2	$\mathbf{L^{tBu}Sc(IPA)}$	L-LA	50	4 hr	> 95	16600	1.04	-
3	$\mathbf{L^{tBu}Sc(IPA)}$	L-LA	10	2 hr	> 95	2500	1.09	-

Table 5.6: ROP of LA. 0.144 g – 1.44 g of LA in toluene solutions 100 °C. M_w, M_n and PDI determined by GPC in THF, relative to polystyrene standards.

End-group analysis was carried out on PLLA synthesised using **L^{tBu}Sc(IPA)** by MALDI-ToF mass spectrometry (Table 5.7; Entry 2) and ^{1}H NMR spectroscopy (Table 5.7; Entry 3), and found to be isopropoxide in nature. The methine proton of the terminal isopropoxide group can be clearly seen as a septet at δ 4.35 in the ^{1}H NMR spectrum (Figure 5.12).
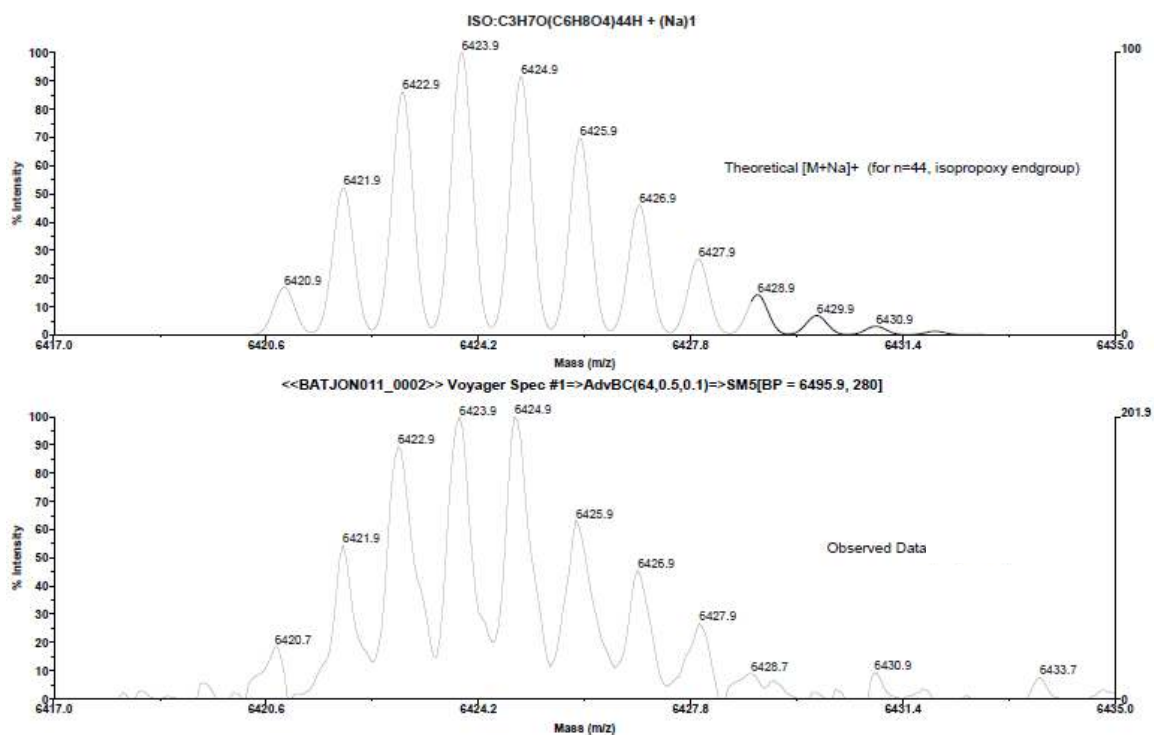
Figure 5.11: MALDI-ToF mass spectra of PLLA synthesised using L^{tBu}Sc(IPA). Calculated data for isopropoxide terminated polymer (top) and expanded experimental spectrum (bottom).
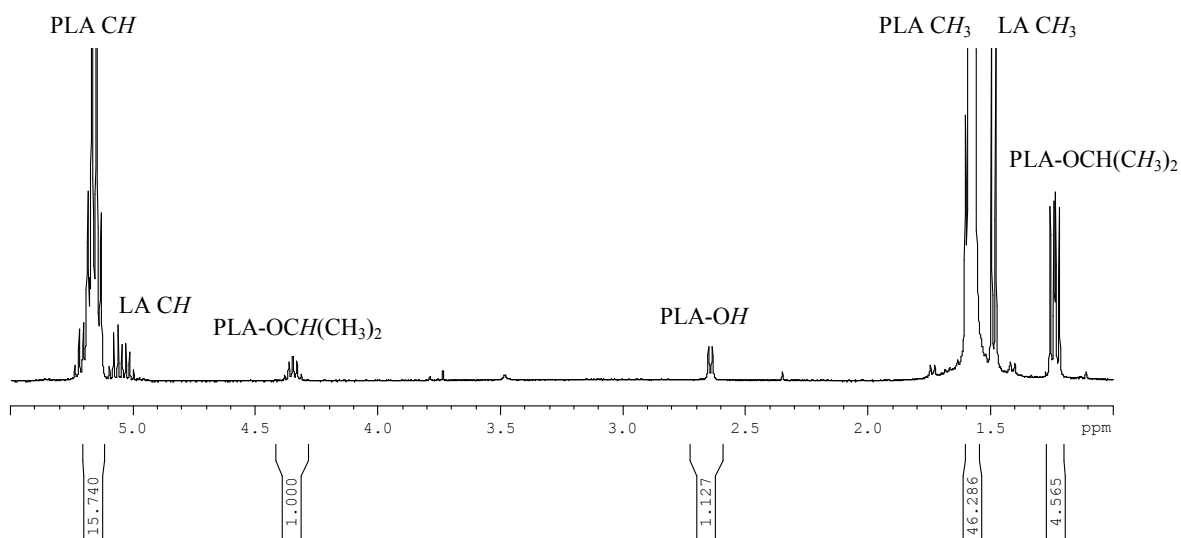
Figure 5.12: ^{1}H NMR spectrum of short-chain PLLA synthesised using L^{tBu}Sc(IPA).

144

5.3.1.3.   Determination of mechanism

An isopropoxide end-group to the polymer, indicates an initiation mechanism that proceeds by the isopropanol group acting as a co-initiator. After the initiating step, the polymerisation is then able to proceed in a living manner, resulting in good molecular weight control and an isopropoxide end-group.
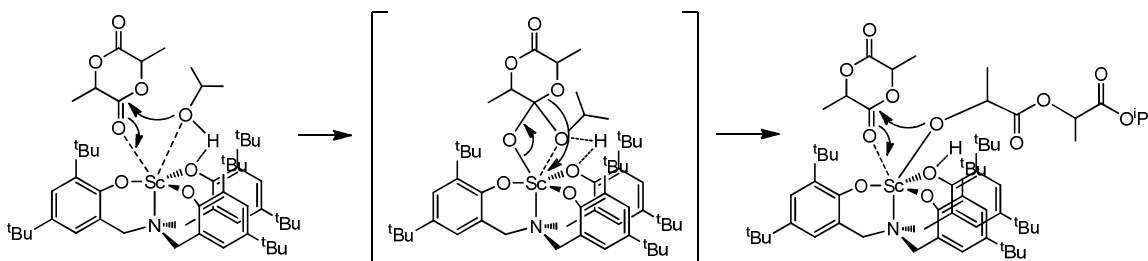
Figure 5.13: Proposed initiation and propagation steps in ROP of LA by L^{tBu}Sc(IPA).

It is therefore reasonable to believe that the tris-isopropanol coordinated complexes initiate the ROP of LA in a similar manner, however increased isopropanol molar ratio may lead to the growth of multiple polymer chains from each metal centre. This would result in low molecular weight of the resulting polymer, or oligomers in the case of **L^{tBu}Yb(IPA)$_3$**, and difficulties in isolating such low molecular weight polymer may explain the low yields obtained from the solvent-free ROP of *rac*-LA using these initiators. This explanation also takes into account the noteworthy difference in resulting polymer from **L^{tBu}Y(IPA)$_3$** and **L^{tBu}Yb(IPA)$_3$** despite the similarity in ionic radius (Yb: 85.8 pm; Y: 90.0 pm). The difference in activity between the two Nd complexes, **L^{tBu}Nd(IPA)$_3$** and **[L^{tBu}Nd(IPA)]$_2$** can therefore be simply explained in terms of available co-initiator: in the dinuclear complex, only one molecule of isopropanol is present Nd metal and so high molecular weights and yields were observed.

5.3.2. Zwitterionic complexes

All zwitterionic rare earth complexes were shown to undertake the ROP of *rac*-LA under solvent-free conditions, however no appreciable polymerisation was observed in toluene solution at 100 °C and only oligomers were observed.

5.3.2.1.   Solvent-free ROP

The solvent-free ROP of *rac*-LA by the zwitterionic rare earth complexes **[HL^{Me}]$_2$Ce**, **[HL^{Me}][H$_2$L^{Me}]Sc**, **[HL^{Me}][H$_2$L^{Me}]Y** and **[HL^{Me}][H$_2$L^{Me}]Sm** resulted in high conversions and isolated yields, but relatively high values of PDI and no observed stereoselectivity. In line with the ROP behaviour of its Group 4 analogues, **[HL^{Me}]$_2$Ce** required a much longer reaction time to reach high conversions of LA than the heteroleptic M^{3+} zwitterionic complexes. However, at high conversions, **[HL^{Me}]$_2$Ce** resulted in polymers of reasonable molecular weights, whereas **[HL^{Me}]$_2$Zr** and **[HL^{Me}]$_2$Hf** led to polymers with very high molecular weights due to a slow

145

initiation step in the ROP process (Section 2.5.2). On the other hand, ROP by the M^{3+} heteroleptic initiators $[HL^{Me}][H_2L^{Me}]Sc$, $[HL^{Me}][H_2L^{Me}]Y$ and $[HL^{Me}][H_2L^{Me}]Sm$ all reached high conversions in 10-30 minutes, while also achieving polymer molecular weights close to expected values.

Complex	Time	Conv. (%)	Yield (%)	M_n	M_w	PDI	P_s
$[HL^{Me}]_2Ce$	20 hr	92	72	31650	60000	1.89	0.48
$[HL^{Me}][H_2L^{Me}]Sc$	30 min	92	66	42000	52900	1.26	0.56
$[HL^{Me}][H_2L^{Me}]Y$	15 min	97	57	18200	25950	1.53	0.52
$[HL^{Me}][H_2L^{Me}]Sm$	10 min	99	86	45092	80850	1.79	0.50

Table 5.7: ROP of *rac*-LA. 1.0 - 2.0 g of *rac*-LA in the absence of solvent at 130 °C, [LA]/[cat] = 300. M_w, M_n and PDI determined by GPC in THF, relative to polystyrene standards.

5.3.2.2. Proposed mechanisms

It is thought $[HL^{Me}]_2Ce$ initiates the ROP of LA in a similar process to its Group 4 analogues, $[HL^{Me}]_2Zr$ and $[HL^{Me}]_2Hf$. However, the increased ionic radius and *f* electron availability in Ce^{4+} may aid the coordination of monomer and co-initiator to the metal centre. This would increase the value of k_{init} with respect to k_{prop}, resulting in a higher degree of molecular weight control.
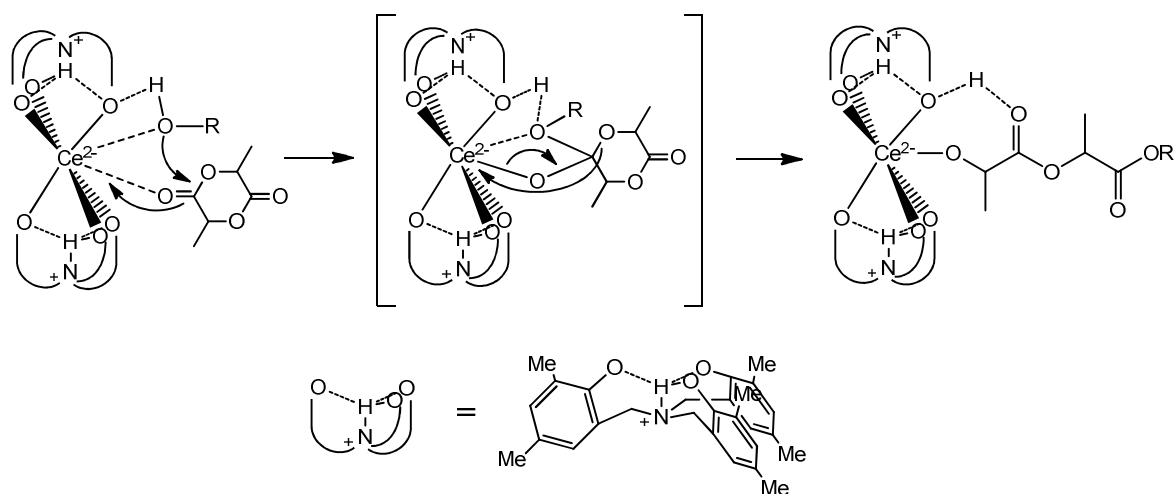
Figure 5.14: Proposed initiation step in ROP of LA by $[HL^{Me}]_2Ce$.

In the case of the heteroleptic M^{3+} zwitterionic complexes, $[HL^{Me}][H_2L^{Me}]Sc$, $[HL^{Me}][H_2L^{Me}]Y$ and $[HL^{Me}][H_2L^{Me}]Sm$, it is thought that the unbound phenolate group may act as an internal co-initiator, meaning k_{init} depends on the coordination of the monomer only. The macrocycle formed by the ring-opened LA and the zwitterionic complex could potentially hinder the approach of further monomers and decrease k_{prop}, so that $k_{init} > k_{prop}$, leading to polymer molecular weights close to theoretical values. It is thought that termination of the polymerisation by the addition of

MeOH would cleave the polymer from the zwitterionic complex, resulting in linear polymer chains.
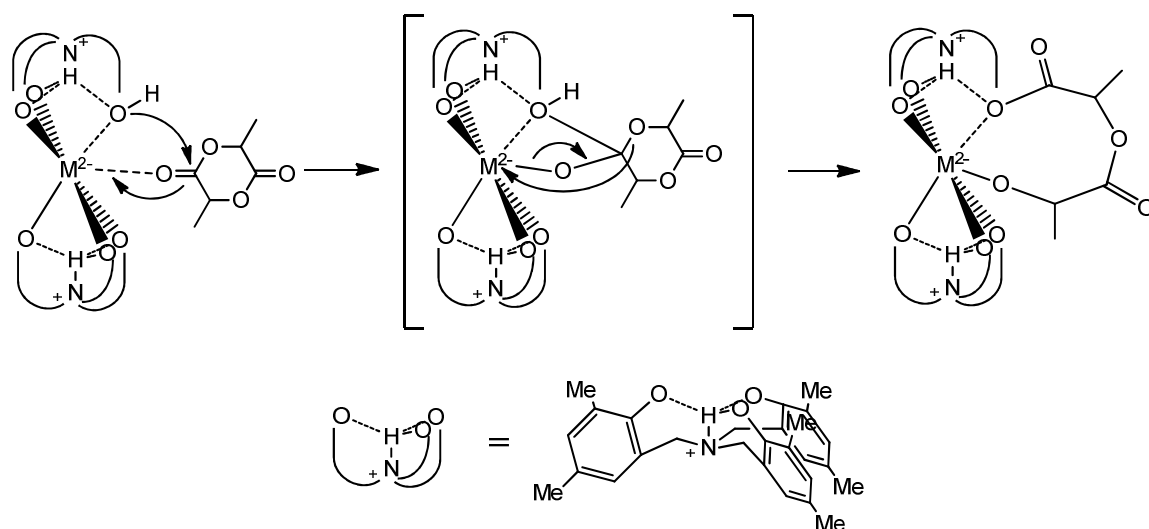
Figure 5.15: Proposed initiation step in ROP of LA by [HL^{Me}][H$_2$L^{Me}]Sc, [HL^{Me}][H$_2$L^{Me}]Y and [HL^{Me}][H$_2$L^{Me}]Sm.

5.4. Summary

Recent interest in rare earth metals as initiators for the ROP of LA led us to investigate the potential of a series of amine tris(phenolate) complexes. Variation of the ligand sterics led to two main complex structures: mono-ligand isopropanol coordinated and bis-ligand zwitterionic complexes, the difference in structure proving influential in the respective proposed mechanisms of ROP.

The Group 3 isopropanol coordinated complexes **L^{tBu}Sc(IPA)** and **L^{tBu}Y(IPA)$_3$** were shown to initiate well-controlled ROP of *rac*-LA, resulting in high molecular weight PLA with a significant heterotactic enhancement. The living nature of polymerisation initiated by **L^{tBu}Sc(IPA)** was confirmed by the presence of an isopropoxide polymer end-group, indicating a coordination insertion mechanism, in which the coordinated IPA acts as an internal co-initiator, similar to the activated monomer mechanism proposed in the case of Sn(Oct)$_2$.[1] However, analogous isopropanol complexes containing the lanthanide metals, **L^{tBu}Nd(IPA)$_3$**, **L^{tBu}Sm(IPA)$_3$** and **L^{tBu}Yb(IPA)$_3$**, were shown to produce only short-chain PLA or oligomers.

However, in the case of the zwitterionic complex **[HL^{Me}]$_2$Ce**, it has been proposed that the increased reactivity brought about by the availability of *f* electrons allow for a faster initiation step than was observed for the Group 4 analogues, resulting in a better controlled polymerisation and PLA with molecular weights close to calculated values. Interestingly, the protonated ligand arm observed in zwitterionic complexes featuring M^{3+}, **[HL^{Me}][H$_2$L^{Me}]Sc, [HL^{Me}][H$_2$L^{Me}]Y** and

[HL^{Me}][H₂L^{Me}]Sm, is thought to play a crucial role in the ROP of *rac*-LA by these complexes, acting as a co-initiator, which again activates and promotes the ring-opening of the coordinated monomer. The resulting PLA was shown to possess molecular weights close to calculated values and high conversions were observed on relatively short timescales (10 – 30 min), although only atactic PLA was isolated.

5.4. References

1.   Albertsson, A. C.; Varma, I. K., *Biomacromolecules* **2003,** *4* (6), 1466-1486.
2.   Kawaguchi, H.; Matsuo, T., *J. Organomet. Chem.* **2004,** *689* (24), 4228-4243.
3.   Sun, J. Q.; Wu, L. T., *Chin. J. Polym. Sci.* **1996,** *14* (4), 324-329.
4.   Kohn, R. D.; Pan, Z. D.; Sun, J. Q.; Liang, C. F., *Catal. Commun.* **2003,** *4* (1), 33-37.
5.   Zhu, X. L.; Wu, G.; Qiu, Z. C.; Zhou, Y.; Gong, J.; Yang, K. K.; Wang, Y. Z., *J. Polym. Sci., Part A: Polym. Chem.* **2008,** *46* (15), 5214-5222.
6.   Dyer, H. E.; Huijser, S.; Schwarz, A. D.; Wang, C.; Duchateau, R.; Mountford, P., *Dalton Trans.* **2008,** (1), 32-35.
7.   Clark, L.; Cushion, M. G.; Dyer, H. E.; Schwarz, A. D.; Duchateau, R.; Mountford, P., *Chem. Commun.* **2010,** *46* (2), 273-275.
8.   Jones, C. J., *d- and f- Block Chemistry*. The Royal Society of Chemistry: Cambridge, U.K., 2001; p 175.
9.   Boyd, C. L.; Toupance, T.; Tyrrell, B. R.; Ward, B. D.; Wilson, C. R.; Cowley, A. R.; Mountford, P., *Organometallics* **2005,** *24* (2), 309-330.
10.   Ma, H. Y.; Spaniol, T. P.; Okuda, J., *Dalton Trans.* **2003,** (24), 4770-4780.
11.   Gerloch, M.; Constable, E. C., *Transition Metal Chemistry: the valence shell in d-block chemistry*. VCH Verlagsgesellschaft, Weinheim
VCH Publishers, New York: 1994.
12.   Veith, M.; Mathur, S.; Lecerf, N.; Bartz, K.; Heintz, M.; Huch, V., *Chem. Mater.* **2000,** *12* (2), 271-+.
13.   Mathur, S.; Veith, M.; Shen, H.; Hufner, S.; Jilavi, M. H., *Chem. Mater.* **2002,** *14* (2), 568-582.
14.   Mathur, S.; Shen, H.; Rapalaviciute, R.; Kareiva, A.; Donia, N., *J. Mater. Chem.* **2004,** *14* (21), 3259-3265.
15.   Mathur, S.; Veith, M.; Rapalaviciute, R.; Shen, H.; Goya, G. F.; Martins, W. L.; Berquo, T. S., *Chem. Mater.* **2004,** *16* (10), 1906-1913.
16.   Cai, C. X.; Amgoune, A.; Lehmann, C. W.; Carpentier, J. F., *Chem. Commun.* **2004,** (3), 330-331.
17.   Liu, X. L.; Shang, X. M.; Tang, T.; Hu, N. H.; Pei, F. K.; Cui, D. M.; Chen, X. S.; Jing, X. B., *Organometallics* **2007,** *26* (10), 2747-2757.
18.   Evans, W. J.; Davis, B. L.; Nyce, G. W.; Perotti, J. M.; Ziller, J. W., *J. Organomet. Chem.* **2003,** *677* (1-2), 89-95.
19.   Plakatouras, J. C.; Baxter, I.; Hursthouse, M. B.; Malik, K. M. A.; McAleese, J.; Drake, S. R., *J. Chem. Soc., Chem. Commun.* **1994,** (21), 2455-2456.
20.   Davidson, M. G.; Doherty, C. L.; Johnson, A. L.; Mahon, M. F., *Chem. Commun.* **2003,** (15), 1832-1833.
21.   Cotton, F. A., *Advanced Inorganic Chemistry: A comprehensive text*. Third ed.; John Wiley & Sons, Inc.: 1972.
22.   Sofen, S. R.; Cooper, S. R.; Raymond, K. N., *Inorg. Chem.* **1979,** *18* (6), 1611-1616.
23.   Liu, Y. F.; Xia, H. T.; Wang, D. Q.; Yang, S. P., *Acta Crystallogr., Sect. E: Struct. Rep. Online* **2007,** *63*, M484-M486.
24.   Yang, S. P.; Han, L. J.; Wang, D. Q.; Wang, B., *Acta Crystallogr., Sect. E: Struct. Rep. Online* **2007,** *63*, M2777-U1351.
25.   Broderick, E. M.; Diaconescu, P. L., *Inorg. Chem.* **2009,** *48* (11), 4701-4706.

26.   Szlyk, E.; Wojtczak, A.; Dobrzanska, L.; Barwiolek, M., *Polyhedron* **2008,** *27* (2), 765-776.
27.   Licini, G.; Mba, M.; Zonta, C., *Dalton Trans.* **2009,** (27), 5265-5277.
28.   Gunther, H., *NMR Spectroscopy - An Introduction*. John Wiley & Sons, Ltd.: 1980.

Chapter 6

Experimental

6. Experimental

6.1. General considerations

All manipulations involving metal complexes were carried out under an atmosphere of dry argon using standard Schlenk and glove-box techniques. Solvents were purified by an MBraun SPS solvent system. $Ce(O^iPr)_4(HO^iPr)$ and $Hf(O^iPr)_4(HO^iPr)$ were purchased from Strem and used without further purification. $Sc(O^iPr)_3$, $Ti(O^iPr)_4$, 25% wt. solution $Y(O^iPr)_3$, $Zr(O^iPr)_4(HO^iPr)$, $Nd(O^iPr)_3$, $Sm(O^iPr)_3$, $Gd[N(SiMe_3)_2]$ and $Yb(O^iPr)_3$ were purchased from Aldrich, and with the exception of $Ti(O^iPr)_4$, used without further purification. $Ti(O^iPr)_4$ was vacuum distilled prior to use. Solution ^1H and ^{13}C NMR experiments were performed at ambient temperature unless otherwise stated using a Bruker Advance-300, Bruker DRX400 or Bruker DRX500 MHz FT-NMR spectrometer with samples dissolved in $CDCl_3$ or CD_2Cl_2. Wilmad 5 mm NMR tubes were used for ligand characterisation, while NMR tubes fitted with Young's taps were used for metal complexes. All chemical shifts are quoted as δ values in ppm relative to residual protio solvent resonances; all coupling constants are given in Hertz.

Accurate Mass Spectrometry was carried out by the EPSRC National Mass Spectrometry Service Centre at the University of Wales, Swansea for $H_3\mathbf{L^{Br}}$, and for all other cases a micrOTOFQ electrospray quadrupole time-of-flight (ESI-QTOF) mass spectrometer (Bruker Daltonik GmbH, Bremen, Germany) was used; this was coupled to a syringe driver (Hamilton, Bonaduz, Switzerland) situated inside a glove box (MBraun, Garching, Germany) under Argon. An opening through the side of the glove box allows for the PEEK tubing from the syringe pump to pass through to the mass spectrometer without any interaction with air or moisture. The sample was infused at a rate of 10 uL/min. The instrument was calibrated using a range of sodium formate clusters to achieve accurate mass. The observed mass and isotope pattern perfectly matched the corresponding theoretical values as calculated from the expected elemental formula.

With one exception, X-ray crystallographic analyses were carried out using a Bruker Nonius Kappa X-ray diffractometer in-house at the Bath Chemical Crystallographic Unit. X-ray crystallographic analysis of $\mathbf{L^{tBu}Hf(BH_4)}$ was carried out using a Bruker Apex II diffractometer at Daresbury Laboratories.

6.2. Synthetic Procedures

6.2.1. Synthesis of ligands

Preparation of $H_3\mathbf{L^{Me}}$**:** Prepared as previously described in the literature (see Section 2.1).[1] **^1H NMR** ($CDCl_3$, 400.13 MHz, 298 K) 2.19 (s, 9H CH_3), 2.21 (s, 9H CH_3), 3.62 (s, 6H CH_2), 6.38 (br s, 3H OH), 6.73 (d, ^4J(H-H) = 1.5 Hz, 3H ArH), 6.85 (d, ^4J(H-H) = 1.5 Hz, 3H ArH). **$^{13}C\{^1H\}$**

NMR (100.62 MHz, CDCl$_3$, 298 K) 16.2 (*CH$_3$*), 20.7 (*CH$_3$*), 56.9 (N*CH$_2$*), 122.2 (*C*), 124.9 (*C*), 129.2 (*C*), 129.5 (*CH*), 131.6 (*CH*), 151.5 (*C*).

Preparation of H$_3$**L**^{tBu}: Prepared as previously described in the literature (see Section 2.1).[1] **^{1}H NMR** (CDCl$_3$, 400.13 MHz, 298 K) 1.28 (s, 27H C*H$_3$*), 1.41 (s, 27H C*H$_3$*), 3.65 (s, 6H C*H$_2$*), 6.98 (d, ^{4}J(H-H) = 2.4 Hz, 3H Ar*H*), 7.24 (d, ^{4}J(H-H) = 2.4 Hz, 3H Ar*H*). **^{13}C{^{1}H} NMR** (100.62 MHz, CDCl$_3$, 298 K) 30.0 (*CH$_3$*), 32.0 (*CH$_3$*), 34.5 (*C*(CH$_3$)), 35.2 (*C*(CH$_3$)), 56.9 (N*CH$_2$*), 122.1 (*C*), 124.3 (*CH*), 125.9 (*CH*), 136.8 (*C*), 142.4 (*C*), 151.8 (*C*).

Preparation of H$_3$**L**^{Np}: 2,4-Di-tert-amylphenol (18.8 g, 80 mmol), hexamethylenetetramine (0.92 g, 6.6 mmol) and 37% formaldehyde aqueous solution (2.3 ml, 28 mmol) were heated together with stirring at 130 °C for 72 hrs, with additional equivalents of phenol (6.3 g, 26.7 mmol) added after 24 and 48 hrs. The ligand was isolated via fractional crystallization of the crude from ethanol. Anal: Calc. for C$_{51}$H$_{81}$N$_1$O$_3$ C: 81.0%; H: 10.7%; N: 1.85%. Found C: 81.2%; H: 10.8%; N: 1.76%. Mass Spec: Calc for [M+H]+: 756.6295. Found: 756.6261. **^{1}H NMR** (CDCl$_3$, 500.13 MHz, 298 K) 0.63 (t, ^{3}J(H-H) = 7.5 Hz, 9H CH$_2$C*H$_3$*), 0.65 (t, ^{3}J(H-H) = 7.4 Hz, 9H CH$_2$C*H$_3$*), 1.24 (s, 18H CC*H$_3$*), 1.34 (s, 18H CC*H$_3$*), 1.57 (q, ^{3}J(H-H) = 7.4 Hz, 6H C*H$_2$*CH$_3$), 1.86 (q, ^{3}J(H-H) = 7.5 Hz, 6H C*H$_2$*CH$_3$), 3.60 (s, 6H C*H$_2$*), 6.36 (br s, 3H O*H*), 6.92 (d, ^{4}J(H-H) = 2.3 Hz, 3H Ar*H*), 7.11 (d, ^{4}J(H-H) = 2.4 Hz, 3H Ar*H*). **^{13}C{^{1}H} NMR** (CDCl$_3$, 125.76 MHz, 298 K) 9.52 (*CH$_3$* neopentyl), 9.89 (*CH$_3$* neopentyl), 28.1 (*CH$_3$* neopentyl), 28.9 (*CH$_3$* neopentyl), 33.4 (*CH$_2$* neopentyl), 37.4 (*CH$_3$* neopentyl), 37.7 (*C* neopentyl), 38.9 (*C* neopentyl), 56.8 (N*CH$_2$*), 121.8 (*C*), 126.6 (*CH*), 126.6 (*CH*), 134.9 (*C*), 140.5 (*C*), 151.7 (*C*).

Preparation of H$_3$**L**^{Cl}·**HMTA:** 2,4-Diclorophenol (8.0 g, 49 mmol) and hexamethylenetetramine (2.4 g, 17 mmol) were melted and stirred at 115 °C for 2.5 hrs, after which time additional phenol was added (2.0 g, 12 mmol) and the reaction was heated for a further hour. Hot ethanol was added to the reaction mixture and the stirring was continued until the oil was dissolved completely, and some solid started to form. The stirring was stopped and the solid was allowed to precipitate overnight. The solid was filtered, and the filtrate evaporated to give an oil, which was triturated with methanol to give the ligand precursor. Recrystallisation from ethyl acetate gave colourless blocks. Anal: Calc for C$_{27}$H$_{27}$N$_5$O$_3$Cl$_6$ C: 47.5%; H: 4.00%; N: 10.3%. Found C: 47.4%; H: 3.89%; N: 10.2%. **^{1}H NMR** (400.13 MHz, CDCl$_3$, 298 K) 3.70 (s, 6H C*H$_2$*), 4.78 (s, 12H HMTA C*H$_2$*), 7.01 (d, ^{4}J(H-H) = 2.5Hz, 3H Ar*H*), 7.23 (d, ^{4}J(H-H) = 2.5 Hz, 3H Ar*H*). **^{13}C{^{1}H} NMR** (100.62 MHz, CDCl$_3$, 298 K) 55.909 (N*CH$_2$*), 74.83 (HMTA *CH$_2$*), 121.52 (*C*), 125.48 (*C*), 128.97 (*CH*), 129.41 (*CH*), 150.70 (*C*).

Preparation of H₃L^{Cl}: H₃L^{Cl}·**HMTA** was purified by column chromatography (silica gel, chloroform). Recrystallisation from chloroform gave the pure ligand as colourless plates. Anal: Calc for $C_{21}H_{15}N_1O_3Cl_6$ C: 46.5%; H: 2.79%; N: 2.58%. Found C: 46.0%; H: 2.60%; N: 2.58%. Mass Spec: Calc for [M+H]+: 539.9261. Found: 539.9222. **¹H NMR** (400.13 MHz, CDCl₃, 298 K) 3.73 (s, 6H CH_2), 7.03 (d, ^{4}J(H-H) = 2.4 Hz, 3H ArH), 7.25 (d, ^{4}J(H-H) = 2.4 Hz, 3H ArH). **¹³C{¹H} NMR** (100.62 MHz, CDCl₃, 298 K) 55.73 (NCH₂), 121.47 (C), 125.12 (C), 125.23 (C), 128.92 (CH), 129.48 (CH), 150.20 (C).

Preparation of H₃L^{Br}·HMTA: Analogous to preparation of H₃L^{Cl}·**HMTA** with 2,4-dibromophenol as starting material. Anal: Calc for $C_{27}H_{27}N_5O_3Br_6$ C: 34.1%; H: 2.85%; N: 7.38%. Found C: 33.4%; H: 2.62%; N: 5.79%. **¹H NMR** (400.13 MHz, CDCl₃, 298 K) 3.71 (s, 6H CH_2), 4.75 (s, 12H HMTA CH_2), 7.16 (d, ^{4}J(H-H) = 2.1 Hz, 3H ArH), 7.49 (d, ^{4}J(H-H) = 2.2 Hz, 3H ArH). **¹³C{¹H} NMR** (100.62 MHz, CDCl₃, 298 K) 56.18 (NCH₂), 75.03 (HMTA CH₂), 111.61 (C), 112.05 (C), 125.70 (C), 132.99 (CH), 134.46 (CH), 151.83 (C).

Preparation of H₃L^{Br}: H₃L^{Br}·**HMTA** was purified by column chromatography (silica gel, chloroform). Anal: Calc for $C_{21}H_{15}N_1O_3Br_6$ C: 31.2%; H: 1.87%; N: 1.73%. Found C: 30.0%; H: 1.76%; N: 1.60%. Mass Spec: Calc for [M+H]+: 803.6225. Found: 803.6222. **¹H NMR** (400.13 MHz, CDCl₃, 298 K) 3.72 (s, 6H CH_2), 7.17 (d, ^{4}J(H-H) = 2.2 Hz, 3H ArH), 7.50 (d, ^{4}J(H-H) = 2.3 Hz, 3H ArH). **¹³C{¹H} NMR** (100.62 MHz, CDCl₃, 298 K) 56.09 (NCH₂), 111.57 (C), 112.25 (C), 125.59 (C), 133.02 (CH), 134.42 (CH), 151.56 (C).

6.2.2. Synthesis of Group 4 complexes

Preparation of L^{Me}Ti(O^{i}Pr):[2] H₃L^{Me} (0.30 g, 0.72 mmol) was dissolved in diethyl ether (20 ml) to which 20 ml of Ti(O^{i}Pr)₄ (0.41 g, 0.43 ml, 1.44 mmol) diethyl ether solution was added. The solution was stirred for 2 hrs, after which time the solvent was removed under vacuum and product recrystallized from hexane, collected on a frit and dried. Yield = 40 %. Anal: Calc for $C_{30}H_{37}N_1O_4Ti_1$ C: 68.8 %; H: 7.12 %; N: 2.68 %. Found C: 67.8 %; H: 7.17 %; N: 2.52 %. **¹H NMR** (400.13 MHz, CDCl₃, 298 K) 1.52 (d, ^{3}J(H-H) = 6.2 Hz, 6H OCH(CH_3)₂), 2.21 (s, 9H CH₃), 2.23 (s, 9H CH₃), 2.82 (br s, 3H NCH_2), 3.97 (br s, 3H NCH_2), 5.20 (sept, ^{3}J(H-H) = 6.2 Hz, 1H OCH(CH₃)₂), 6.70 (d, ^{4}J(H-H) = 1.7 Hz, 3H ArH), 7.69 (d, ^{4}J(H-H) = 0.8 Hz, 3H ArH). **¹³C{¹H} NMR** (100.62 MHz, CDCl₃, 298 K) 16.57 (CH₃), 20.94 (CH₃), 25.98 (OCH(CH₃)₂), 58.91 (NCH₂), 79.80 (OCH(CH₃)₂), 123.94 (C), 124.63 (C), 127.76 (CH), 129.62 (C), 130.98 (CH), 169.95 (C).

Preparation of [HL^{Me}]₂Zr:[3] H₃L^{Me} (1.00 g, 2.38 mmol) was dissolved in toluene (20 ml) to which Zr(O^{i}Pr)₄·HO^{i}Pr was added (0.46 g, 1.19 mmol) with stirring at 298 K for 16 hours. The

resulting white precipitate was collected on a frit and dried in *vacuo*. Yield = 74 %. Anal: Calc for $C_{54}H_{62}N_2O_6Zr_1$ C: 69.9 %; H: 6.95 %; N: 3.02 %. Found C: 69.6 %; H: 6.73 %; N: 3.32 %. Mass Spec: Calc for [M-H]-: 923.3571. Found: 923.3590. **^{1}H NMR** (400.13 MHz, CDCl$_3$, 298 K) 1.95 (s, 9H C*H*$_3$), 2.18 (s, 9H C*H*$_3$), 3.31 (br s, 3H NC*H*$_2$), 4.74 (br s, 3H NC*H*$_2$), 6.66 (d, ^{4}J(H-H) = 2.0 Hz, 3H Ar*H*), 6.85 (d, ^{4}J(H-H) = 2.0 Hz, 3H Ar*H*), 11.83 (br s, 2H N*H*). **^{13}C{^{1}H} NMR** (100.62 MHz, CDCl$_3$, 298 K) 16.86 (*C*H$_3$), 20.72 (*C*H$_3$), 56.58 (N*C*H$_2$), 117.17 (*C*), 125.22 (*C*), 128.29 (*C*H), 129.94 (*C*), 33.08 (*C*H), 59.47 (*C*).

Preparation of [HL^{Me}]$_2$Hf: The ligand H$_3$L^{Me} (0.50 g, 1.19 mmol) was dissolved in toluene (10 ml) to which Hf(O^{i}Pr)$_4$·HO^{i}Pr was added (0.28 g, 0.60 mmol) with stirring at 298 K for 16 hours. The resulting white precipitate was collected on a frit and dried in vacuo. Yield = 65 %. Anal: Calc for $C_{54}H_{62}N_2O_6Hf_1$ C: 64.0 %; H: 6.17 %; N: 2.76 %. Found C: 64.0 %; H: 6.17 %; N: 2.76 %. Mass Spec: Calc for [M+H]+: 1015.4146. Found: 1015.4249. **^{1}H NMR** (400.13 MHz, CDCl$_3$, 298 K) 1.94 (s, 9H C*H*$_3$), 2.18 (s, 9H C*H*$_3$), 3.31 (br s, 3H NC*H*$_2$), 4.79 (br s, 3H NC*H*$_2$), 6.67 (d, ^{4}J(H-H) = 2.0 Hz, 3H Ar*H*), 6.85 (d, ^{4}J(H-H) = 2.2 Hz, 3H Ar*H*), 11.80 (br s, 2H N*H*). **^{13}C{^{1}H} NMR** (100.62 MHz, CDCl$_3$, 298 K) 16.48 (*C*H$_3$), 20.35 (*C*H$_3$), 56.17 (N*C*H$_2$), 117.06 (*C*), 124.89 (*C*), 127.95 (*C*H), 129.67 (*C*), 132.80 (*C*H), 159.27 (*C*).

Preparation of L^{tBu}Ti(O^{i}Pr):[4] H$_3$L^{tBu} (5.0 g, 7.4 mmol) was dried under vacuum in a Schlenk tube, and then dissolved in minimum toluene with stirring. Ti(O^{i}Pr)$_4$ (2.05 ml, 7.4 mmol) was then added dropwise by syringe to the stirred solution of H$_3$L^{tBu}. The solvent was removed under vacuum and the dry residue was recrystallised from toluene with heating. Yield = 40%. Anal: Calc for $C_{48}H_{76}N_1O_4Ti_1$ C: 74.3%; H: 9.48%; N: 1.80%. Found C: 74.3%; H: 9.47%; N: 1.91%. **^{1}H NMR** (400.13 MHz, CDCl$_3$, 298 K) 1.29 (s, 27H C*H*$_3$), 1.47 (s, 27H C*H*$_3$), 1.52 (d, ^{3}J(H-H) = 6.12 Hz, 6H OCH(C*H*$_3$)$_2$), 2.91 (d, ^{2}J(H-H) = 13.5 Hz, 3H NC*H*$_2$), 4.00 (d, ^{2}J(H-H) = 13.3 Hz, 3H NC*H*$_2$), 5.25 (sept, ^{3}J(H-H) = 6.04, 1H OC*H*(CH$_3$)$_2$), 6.98 (d, ^{4}J(H-H) = 2.4 Hz, 3H Ar*H*), 7.21 (d, ^{4}J(H-H) = 2.4 Hz, 3H Ar*H*). **^{13}C{^{1}H} NMR** (100.62 MHz, CDCl$_3$, 298 K) 26.58 (OCH(*C*H$_3$)$_2$), 29.62 (*C*H$_3$), 31.69 (*C*H$_3$), 34.32 (*C*), 35.03 (*C*), 58.99 (N*C*H$_2$), 79.45 (O*C*H(CH$_3$)$_2$), 122.91 (*C*H), 124.05 (*C*H), 124.26 (*C*) 135.11 (*C*) 142.19 (*C*) 160.44 (*C*).

Preparation of L^{tBu}Zr(O^{i}Pr):[5] H$_3$L^{tBu} (2.00 g, 2.97 mmol) was dried under vacuum in a Schlenk tube, and then dissolved in toluene (20 ml) with stirring. Zr(O^{i}Pr)$_4$·HO^{i}Pr (1.15 g, 2.97 mmol) was then added and the reaction was left to stir at 298 K for 2 hours, after which time the solvent was removed under vacuum. The dry residue was recrystallised from toluene with heating and collected on a frit. Yield = 71 %. Anal: Calc for $C_{48}H_{76}N_1O_4Zr_1$ C: 70.4%; H: 8.98%; N: 1.71%. Found C: 70.8%; H: 9.50%; N: 1.26%. **^{1}H NMR** (400.13 MHz, CDCl$_3$, 298 K) 1.29 (s, 27H C*H*$_3$), 1.41 (d, ^{3}J(H-H) = 6.12 Hz, 6H OCH(C*H*$_3$)$_2$), 1.45 (s, 27H C*H*$_3$), 2.92 (br s, 3H NC*H*$_2$),

154

3.99 (br s, 3H NCH_2), 4.66 (sept, ^{3}J(H-H) = 6.0 Hz, 1H OCH(CH$_3$)$_2$), 7.00 (d, ^{4}J(H-H) = 2.5 Hz, 3H ArH), 7.23 (d, ^{4}J(H-H) = 2.5 Hz, 3H ArH). ^{13}C{^{1}H} NMR (100.62 MHz, CDCl$_3$, 258 K) 27.19 (OCH(CH$_3$)$_2$), 29.36 (CH$_3$), 31.60 (CH$_3$), 34.14 (C), 34.88 (C), 59.45 (NCH$_2$), 72.49 (OCH(CH$_3$)$_2$), 123.41 (CH), 123.67 (C), 124.74 (CH), 135.69 (C), 141.01 (C), 157.11 (C).

Preparation of L^{tBu}Hf(O^{i}Pr):[5] H$_3$L^{tBu} (1 g, 1.5 mmol) was dried under vacuum in a Schlenk tube, and then dissolved in toluene (20 ml) with stirring. Hf(O^{i}Pr)$_4$·HO^{i}Pr (0.91 g, 1.5 mmol) was then added and the reaction was left to stir at 298 K for 2 hours, after which time the solvent was removed under vacuum. The dry residue was recrystallised from toluene with heating and collected on a frit. Yield = 95%. Anal: Calc for C$_{48}$H$_{76}$N$_1$O$_4$Hf$_1$ C: 63.6%; H: 8.12%; N: 1.54%. Found C: 63.3%; H: 8.44%; N: 1.76%. **^{1}H NMR** (400.13 MHz, CDCl$_3$, 298 K) 1.29 (s, 27H CH_3), 1.40 (d, ^{3}J(H-H) = 5.9 Hz, 6H OCH(CH_3)$_2$), 1.45 (s, 27H CH_3), 2.95 (br s, 3H NCH_2), 4.03 (br s, 3H NCH_2), 4.74 (sept, ^{3}J(H-H) = 6.2, 1H OCH(CH$_3$)$_2$), 6.98 (d, ^{4}J(H-H) = 2.4 Hz, 3H ArH), 7.27 (d, ^{4}J(H-H) = 2.2 Hz, 3H ArH). **^{13}C{^{1}H} NMR** (100.62 MHz, CDCl$_3$, 298 K) 27.45 (OCH(CH$_3$)$_2$), 29.59 (CH$_3$), 31.72 (CH$_3$), 34.22 (C), 34.95 (C), 59.48 (NCH$_2$), 72.35 (OCH(CH$_3$)$_2$), 123.57 (C), 123.67 (CH), 124.64 (CH), 136.76 (C), 141.51 (C), 157.22 (C).

Preparation of L^{Np}Ti(O^{i}Pr): H$_3$L^{Np} (0.30 g, 0.40 mmol) was dissolved in toluene (20 ml) to which Ti(O^{i}Pr)$_4$ (0.11 g, 0.12 ml, 0.40 mmol) was added. The solution was stirred for 2 hrs, after which time the solvent was removed in vacuo and product recrystallized from hexane, collected on a frit and dried. Yield = Mass Spec: Calc for [M+Cl]-: 894.5652. Found: 894.5674. **^{1}H NMR** (400.13 MHz, CDCl$_3$, 298 K) 0.57 (t, ^{3}J(H-H) = 7.5 Hz, 9H CH$_2$CH_3), 0.65 (t, ^{3}J(H-H) = 7.4 Hz, 9H CH$_2$CH_3), 1.24 (d, ^{5}J(H-H) = 2.9 Hz, 18H CCH_3), 1.38 (d, ^{5}J(H-H) = 5.6 Hz, 18H CCH_3), 1.49 (d, ^{3}J(H-H) = 6.1 Hz, 6H OCH(CH_3)$_2$), 1.57 (q, ^{3}J(H-H) = 7.4 Hz, 3H CH_2CH$_3$), 1.57 (q, ^{3}J(H-H) = 7.5 Hz, 3H CH_2CH$_3$) (overlaying quartets), 1.99 (m, 6H CH_2CH$_3$), 2.11 (m, 6H CH_2CH$_3$), 2.83 (d, ^{2}J(H-H) = 13.3 Hz, 3H NCH_2), 3.92 (d, ^{2}J(H-H) = 13.1 Hz, 3H NCH_2), 5.20 (sept, ^{3}J(H-H) = 6.1 Hz, 1H OCH(CH$_3$)$_2$), 6.90 (d, ^{4}J(H-H) = 2.4 Hz, 3H ArH), 7.06 (d, ^{4}J(H-H) = 2.4 Hz, 3H ArH). **^{13}C{^{1}H} NMR** (100.62 MHz, CDCl$_3$, 298 K) 9.56 (CH$_3$ Np), 9.92 (CH$_3$ Np), 26.8 (OCH(CH$_3$)$_2$), 28.0 (CH$_3$ Np), 28.3 (CH$_3$ Np), 29.0 (CH$_3$ Np), 33.4 (CH$_2$ Np), 37.5 (CH$_3$ Np), 37.8 (C Np), 38.9 (C Np), 59.33 (NCH$_2$), 79.75 (OCH(CH$_3$)$_2$), 124.4 (C), 125.1 (CH), 125.3 (CH), 133.7 (C), 140.7 (C), 160.9 (C).

Preparation of L^{Np}Zr(O^{i}Pr).IPA: Zr(O^{i}Pr)$_4$·^{i}PrOH (0.30 g, 0.78 mmol) was dissolved in toluene (20 ml) to which the ligand H$_3$L^{Np} (0.59 g, 0.78 mmol) was added. The solution was stirred for 2 hrs, after which time the solvent was removed in vacuo. Yield = 24%. Mass Spec: Calc for [M-IPA+Cl]-: 936.5220. Found: 936.5230. **^{1}H NMR** (400.13 MHz, CDCl$_3$, 298 K) 0.61 (t, ^{3}J(H-H) = 7.5 Hz, 9H CH$_2$CH_3), 0.65 (t, ^{3}J(H-H) = 7.5 Hz, 9H CH$_2$CH_3), 0.99 (d, ^{3}J(H-H) = 6.2 Hz, 6H

HOCH(CH_3)$_2$), 1.24 (s, 18H CCH_3), 1.37 (d, ^{3}J(H-H) = 6.2 Hz, 6H OCH(CH_3)$_2$), 1.39 (s, 18H CCH_3), 1.57 (q, ^{3}J(H-H) = 7.4 Hz, 6H CH_2CH$_3$), 1.99 (q, ^{3}J(H-H) = 7.4 Hz, 6H CH_2CH$_3$), 3.44 (v br s, 6H NCH_2), 4.00 (br m, 1H HOCH(CH$_3$)$_2$), 4.61 (sept, ^{3}J(H-H) = 6.1, 1H OCH(CH$_3$)$_2$), 6.89 (d, ^{4}J(H-H) = 2.4 Hz, 3H ArH), 7.09 (d, ^{4}J(H-H) = 2.4 Hz, 3H ArH). **^{13}C{^{1}H} NMR** (100.62 MHz, CDCl$_3$, 298 K) 9.58 (CH_3 Np), 9.97 (CH_3 Np), 24.7 (HOCH(CH_3)$_2$), 27.6 (OCH(CH_3)$_2$), 28.1 (CH_3 Np), 29.0 (CH_3 Np), 33.5 (CH_2 Np), 37.5 (CH_3 Np), 37.6 (C Np), 38.9 (C Np), 60.5 (NCH$_2$), 68.8 (HOCH(CH$_3$)$_2$), 72.5 (OCH(CH$_3$)$_2$), 124.4 (C), 126.0 (CH), 126.0 (CH), 134.7 (C), 138.8 (C), 157.5 (C).

Preparation of L^{Np}Hf(O^{i}Pr).IPA: Hf(O^{i}Pr)$_4$.^{i}PrOH (0.30 g, 0.63 mmol) was dissolved in toluene (20 ml) to which the ligand H$_3$L^{Np} (0.48 g, 0.63 mmol) was added. The solution was stirred for 2 hrs, after which time the solvent was removed in vacuo. Yield = 32%. Anal: Calc for C$_{57}$H$_{93}$N$_1$O$_5$Hf C: 65.1%; H: 8.92%; N: 1.33%. Found: C: 65.1%; H: 8.83%; N: 1.27%. Mass Spec: Calc for [M-IPA+Cl]-: 1026.5624. Found: 1026.5712. **^{1}H NMR** (400.13 MHz, CDCl$_3$, 298 K) 0.62 (t, ^{3}J(H-H) = 7.5 Hz, 9H CH$_2$CH_3), 0.65 (t, ^{3}J(H-H) = 7.3 Hz, 9H CH$_2$CH_3), 0.99 (d, ^{3}J(H-H) = 6.2 Hz, 6H HOCH(CH_3)$_2$), 1.24 (s, 18H CCH_3), 1.35 (d, ^{3}J(H-H) = 5.5 Hz, 6H OCH(CH_3)$_2$), 1.37 (s, 18H CCH_3), 1.57 (q, ^{3}J(H-H) = 7.4 Hz, 6H CH_2CH$_3$), 2.00 (q, ^{3}J(H-H) = 7.4 Hz, 6H CH_2CH$_3$), 3.49 (v br s, 6H CH$_2$), 4.02 (br m, 1H HOCH(CH$_3$)$_2$), 4.68 (sept, ^{3}J(H-H) = 6.0, 1H HOCH(CH$_3$)$_2$), 6.87 (d, ^{4}J(H-H) = 2.4 Hz, 3H ArH), 7.11 (d, ^{4}J(H-H) = 2.4 Hz, 3H ArH). **^{13}C{^{1}H} NMR** (100.62 MHz, CDCl$_3$, 298 K) 9.59 (CH_3 Np), 9.98 (CH_3 Np), 24.7 (HOCH(CH_3)$_2$), 27.8 (OCH(CH_3)$_2$), 28.4 (CH_3 Np), 29.1 (CH_3 Np), 33.4 (CH_2 Np), 37.6 (CH_3 Np), 37.6 (C Np), 38.8 (C Np), 60.9 (NCH$_2$), 69.0 (HOCH(CH$_3$)$_2$), 72.1 (OCH(CH$_3$)$_2$), 124.4 (C), 125.9 (CH), 126.1 (CH), 135.4 (C), 138.5 (C), 157.4 (C).

Preparation of L^{Np}Hf(O^{i}Pr): L^{Np}Hf(O^{i}Pr)·IPA (0.3 g, 0.29 mmol) was heated to 180 °C over 2 hrs. Anal: Calc for C$_{54}$H$_{85}$N$_1$O$_4$Hf C: 65.5%; H: 8.65%; N: 1.41%. Found: C: 64.3%; H: 8.39%; N: 1.22%. **^{1}H NMR** (400.13 MHz, CDCl$_3$, 298 K) 0.62 (t, ^{3}J(H-H) = 7.5 Hz, 9H CH$_2$CH_3), 0.65 (t, ^{3}J(H-H) = 7.3 Hz, 9H CH$_2$CH_3), 1.24 (s, 18H CCH_3), 1.35 (d, ^{3}J(H-H) = 5.5 Hz, 6H OCH(CH_3)$_2$), 1.37 (s, 18H CCH_3), 1.58 (q, ^{3}J(H-H) = 7.4 Hz, 6H CH_2CH$_3$), 2.00 (br s, 6H CH_2CH$_3$), 2.98 (v br s, 3H CH$_2$), 4.14 (v br s, 3H CH$_2$), 4.71 (sept, ^{3}J(H-H) = 6.1, 1H HOCH(CH$_3$)$_2$), 6.90 (d, ^{4}J(H-H) = 2.3 Hz, 3H ArH), 7.13 (d, ^{4}J(H-H) = 2.4 Hz, 3H ArH). **^{13}C{^{1}H} NMR** (100.62 MHz, CDCl$_3$, 298 K) 9.57 (CH_3 Np), 9.98 (CH_3 Np), 27.7 (OCH(CH_3)$_2$), 28.1 (CH_3 Np), 29.0 (CH_3 Np), 33.6 (CH_2 Np), 37.5 (CH_3 Np), 37.7 (C Np), 38.9 (C Np), 59.9 (NCH$_2$), 72.6 (OCH(CH$_3$)$_2$), 123.8 (C), 125.7 (CH), 126.2 (CH), 135.4 (C), 139.8 (C), 157.5 (C).

Preparation of L^{Cl}Ti$_2$(O^{i}Pr)$_5$: H$_3$L^{Cl} (0.39 g, 0.72 mmol) was dissolved in diethyl ether (20 ml) to which 20 ml of Ti(O^{i}Pr)$_4$ (0.41 g, 0.43 ml, 1.44 mmol) diethyl ether solution was added. The

solution was stirred for 2 hrs, after which time the solvent was removed in *vacuo* and reaction products washed with hexane. Small orange block crystals were isolated from the washings after several days, collected on a frit and dried in vacuo. Anal: Calc for $C_{36}H_{47}N_1O_8Cl_6Ti_2$ C: 46.5%; H: 5.05%; N: 1.51%. Found: C: 43.9%; H: 4.60%; N: 1.47%. **^{1}H NMR** (400.13 MHz, CDCl$_3$, 258K) 0.99 (d, ^{3}J(H-H) = 6.1 Hz, 9H OCH(CH_3)$_2$), 1.09 (d, ^{3}J(H-H) = 6.0 Hz, 9H OCH(CH_3)$_2$), 1.32 (d, ^{3}J(H-H) = 6.0 Hz, 6H OCH(CH_3)$_2$), 1.37 (d, ^{3}J(H-H) = 6.1 Hz, 3H μ-OCH(CH_3)$_2$), 1.48 (d, ^{3}J(H-H) = 6.1 Hz, 3H μ-OCH(CH_3)$_2$), 2.76 (d, ^{2}J(H-H) = 13.5 Hz, 1H NCH_2), 3.03 (d, ^{2}J(H-H) = 13.1 Hz, 1H NCH_2), 3.27 (d, ^{2}J(H-H) = 14.0 Hz, 1H NCH_2), 3.89 (d, ^{2}J(H-H) = 13.3 Hz, 1H NCH_2), 3.98 (d, ^{2}J(H-H) = 12.7 Hz, 1H NCH_2), 4.55 (m, 3H OCH(CH$_3$)$_2$), 4.66 (d, ^{2}J(H-H) = 13.7 Hz, 1H NCH_2), 4.93 (m, 1H OCH(CH$_3$)$_2$), 5.53 (m, 1H OCH(CH$_3$)$_2$), 6.32 (d, ^{4}J(H-H) = 2.3 Hz, 1H ArH), 6.73 (d, ^{4}J(H-H) = 2.4 Hz, 1H ArH), 6.94 (d, ^{4}J(H-H) = 2.5 Hz, 1H ArH), 6.98 (d, ^{4}J(H-H) = 2.4 Hz, 1H ArH), 7.07 (d, ^{4}J(H-H) = 2.4 Hz, 1H ArH), 7.31 (d, ^{4}J(H-H) = 2.5 Hz,1H ArH). **^{13}C{^{1}H} NMR** (100.62 MHz, CDCl$_3$, 258K) 22.81 (OCH(CH_3)$_2$), 23.50 (OCH(CH_3)$_2$), 24.50 (OCH(CH_3)$_2$), 24.85 (OCH(CH_3)$_2$), 25.96 (OCH(CH_3)$_2$), 26.09 (OCH(CH_3)$_2$), 60.31 (NCH_2), 61.98 (NCH_2), 63.35 (NCH_2), 76.00 (OCH(CH$_3$)$_2$), 79.06 (OCH(CH$_3$)$_2$), 83.91 (OCH(CH$_3$)$_2$), 111.03 (C), 122.34 (C), 107.18 (C), 122.53 (C), 123.08 (C), 124.89 (C), 125.33 (C), 126.18 (CH), 126.95 (C), 127.30 (CH), 127.33 (CH), 127.67 (C), 128.46 (C), 128.80 (CH), 128.82 (CH), 129.02 (CH), 155.31 (C), 156.14 (C).

Preparation of L$^{Cl}_2$Ti$_3$(O^{i}Pr)$_4$: H$_3$L^{Cl} (0.19 g, 0.34 mmol) was dissolved in toluene (10 ml) to which Ti(O^{i}Pr)4 (0.10 ml, 0.34 mmol) was added drop-wise with stirring at 298 K. After 16 hours, a yellow precipitate was observed, which was collected on a frit and was found to be a mixture of products by NMR analysis. On standing for 4 days, the filtrate yielded large yellow block crystals, which were collected on a frit and dried in vacuo. Anal: Calc for $C_{54}H_{52}N_2O_{10}Cl_{12}Ti_3$ C: 44.0%; H: 3.56%; N: 1.90%. Found C: 44.1%; H: 3.95%; N: 1.78%. **^{1}H NMR** (400.13 MHz, CDCl$_3$, 298 K) 0.68 (d, ^{3}J(H-H) = 6.2 Hz, 6H OCH(CH_3)$_2$), 0.90 (d, ^{3}J(H-H) = 6.2 Hz, 6H OCH(CH_3)$_2$) 1.39 (d, ^{3}J(H-H) = 6.1 Hz, 6H OCH(CH_3)$_2$) 1.56 (d, ^{3}J(H-H) = 6.2 Hz, 6H OCH(CH_3)$_2$) 2.85 (d, ^{2}J(H-H) = 14.4 Hz, 2H NCH_2) 3.16 (d, ^{2}J(H-H) = 13.7 Hz, 2H NCH_2) 3.17 (d, ^{2}J(H-H) = 12.8 Hz, 2H NCH_2) 3.73 (d, ^{2}J(H-H) = 14.1 Hz, 2H NCH_2) 4.55 (sept, ^{3}J(H-H) = 6.2 Hz, 2H OCH(CH$_3$)$_2$) 4.98 (d, ^{2}J(H-H) = 12.8 Hz, 2H NCH_2) 5.77 (sept, ^{3}J(H-H) = 6.2 Hz, 2H OCH(CH$_3$)$_2$) 6.06 (d, ^{2}J(H-H) = 13.6 Hz, 2H NCH_2) 6.58 (d, ^{4}J(H-H) = 2.4 Hz, 2H ArH) 6.78 (d, ^{4}J(H-H) = 2.5 Hz, 2H ArH) 6.95 (d, ^{4}J(H-H) = 2.5 Hz, 2H ArH) 7.01 (m, 4H, ArH) 7.12 (d, ^{4}J(H-H) = 2.5 Hz, 2H, ArH). **^{13}C{^{1}H} NMR** (100.62 MHz, CDCl$_3$, 298 K) 24.80 (OCH(CH_3)$_2$), 25.06 (OCH(CH_3)$_2$), 25.60 (OCH(CH_3)$_2$), 25.71 (OCH(CH_3)$_2$), 60.04 (NCH_2), 62.80 (NCH_2), 64.23 (NCH_2), 83.37 (OCH(CH$_3$)$_2$), 84.49 (OCH(CH$_3$)$_2$), 121.53 (C), 121.95 (C), 122.86 (C), 124.16 (C), 125.96 (C), 126.51 (CH), 127.26 (C), 128.14 (CH), 128.42 (C), 128.61 (CH), 128.72 (CH), 129.90 (CH), 130.15 (CH), 156.18 (C), 156.44 (C), 156.93 (C).

Preparation of [HL^{Cl}]$_2$Zr: Zr(O^{i}Pr)$_4$·^{i}PrOH (0.40 g, 1.0 mmol) was dissolved in diethyl ether (20 ml) to which the ligand H$_3$L^{Cl} (0.57 g, 1.0 mmol) was added. The solution was stirred for 3 hrs, after which time the solvent was removed in *vacuo* and reaction products washed with toluene. Colourless block crystals were isolated from the washings after several weeks, collected on a frit and dried in *vacuo*. Mass Spec: Calc for [M-H]-: 1162.7016. Found: 1162.688

Preparation of L^{tBu}Ti(BH$_4$): L^{tBu}Ti(O^{i}Pr) (1.85 g, 2.38 mmol) was dissolved with stirring in minimum toluene and cooled to 0 °C before addtion of 1M solution of BH$_3$·THF in THF (4.76 ml, 4.76 mmol) drop-wise. The reaction was allowed to return to room temperature and left stirring overnight. The solvent was then removed under vacuum and the dry residue was recrystallised from toluene, and the orange crystalline form collected on a frit. Yield = 58 %. Anal. Calc for C$_{45}$H$_{70}$B$_1$N$_1$O$_3$Ti$_1$ C: 73.9%; H: 9.64%; N: 1.91%. Found C: 72.6%; H: 9.22%; N: 1.65%. **^{1}H NMR** (300.22 MHz, CDCl$_3$, 298 K) 1.29 (s, 27H CH_3), 1.40 (s, 27H CH_3), 1.62-2.31 (br m, 3H BH_3-Ti), 3.15 (d, ^{2}J(H-H) = 14.2 Hz, 3H NCH_2), 4.14 (d, ^{2}J(H-H) = 14.0 Hz, 3H NCH_2), 7.00 (d, ^{4}J(H-H) = 2.2 Hz, 3H ArH), 7.24 (d, ^{4}J(H-H) = 2.3 Hz, 3H ArH) **^{13}C{^{1}H} NMR** (75.49 MHz, CDCl$_3$, 298 K) 29.89 (CH_3), 31.95 (CH_3), 34.85 (C), 35.15 (C), 59.03 (NCH_2), 123.46 (CH), 123.84 (CH), 124.16 (CH), 135.95 (C), 144.32 (C), 161.42 (C) **^{11}B{^{1}H} NMR** (96 MHz, CDCl$_3$, 298 K) −17.1 (s).

Preparation of L^{tBu}Zr(BH$_4$): L^{tBu}Zr(O^{i}Pr) (0.55 g, 0.67 mmol) was dissolved with stirring in minimum toluene and cooled to 0 °C before addtion of 1M solution of BH$_3$·THF in THF (1.34 ml, 1.34 mmol) drop-wise. The reaction was allowed to return to room temperature and left stirring overnight. The solvent was then removed under vacuum and the dry residue was recrystallised from toluene, and the colourless crystalline form collected on a frit. Yield = 63%. Anal. Calc for C$_{45}$H$_{70}$B$_1$N$_1$O$_3$Zr$_1$ C: 69.7%; H: 9.10%; N: 1.81%. Found C: 67.2%; H: 8.98%; N: 2.03%. **^{1}H NMR** (400.13 MHz, CDCl$_3$, 298 K) 1.29 (s, 27H CH_3), 1.40 (s, 27H CH_3), 1.62-2.31 (br m, 3H BH_3-Zr), 3.15 (d, ^{2}J(H-H) = 14.2 Hz, 3H NCH_2), 4.14 (d, ^{2}J(H-H) = 14.0 Hz, 3H, NCH_2), 7.00 (d, ^{4}J(H-H) = 2.2 Hz, 3H ArH), 7.24 (d, ^{4}J(H-H) = 2.3 Hz, 3H, ArH) **^{13}C{^{1}H} NMR** (100.62 MHz, CDCl$_3$, 298 K) 29.55 (CH_3), 31.63 (CH_3), 34.35 (C), 34.85 (C), 59.11 (NCH_2), 122.68 (C), 124.06 (CH), 124.48 (CH), 136.48 (C), 142.87 (C), 157.12 (C) **^{11}B{^{1}H} NMR** (96 MHz, CDCl$_3$, 298 K) -18.5 (s).

Preparation of L^{tBu}Hf(BH$_4$): L^{tBu}Hf(O^{i}Pr) (0.50 g, 0.55 mmol) was dissolved with stirring in minimum toluene and cooled to 0 °C before addtion of 1M solution of BH$_3$·THF in THF (1.10 ml, 1.10 mmol) drop-wise. The reaction was allowed to return to room temperature and left stirring overnight. The solvent was then removed under vacuum and the dry residue was recrystallised

from toluene, and the colourless crystalline form collected on a frit. Yield = 74%. Anal. Calc for C$_{45}$H$_{70}$B$_1$N$_1$O$_3$Hf$_1$ C: 62.7%; H: 8.18%; N: 1.62%. Found C: 60.5%; H: 7.77%; N: 1.66%. **^{1}H NMR** (300.22 MHz, CDCl$_3$, 298 K) 1.28 (s, 27H C*H*$_3$), 1.41 (s, 27H C*H*$_3$), 1.61-2.31 (br m, 3H B*H*$_3$-Hf), 3.11 (d, ^{2}J(H-H) = 13.9 Hz, 3H NC*H*$_2$), 4.09 (d, ^{2}J(H-H) = 13.8 Hz, 3H NC*H*$_2$), 6.99 (d, ^{4}J(H-H) = 2.4 Hz, 3H Ar*H*), 7.29 (d, ^{4}J(H-H) = 2.4 Hz, 3H Ar*H*) **^{13}C{^{1}H} NMR** (75.49 MHz, CDCl$_3$, 298 K) 29.90 (*C*H$_3$), 32.01 (*C*H$_3$), 34.68 (*C*), 35.15 (*C*), 59.47 (N*C*H$_2$), 122.90 (*C*), 124.51 (*C*H), 124.64 (*C*H), 137.54 (*C*), 143.02 (*C*), 157.22 (*C*) **^{11}B{^{1}H} NMR** (96 MHz, CDCl$_3$, 298 K) −20.52 (s).

Preparation of L^{tBu}Zr(NMe$_2$): A solution of H$_3$L^{tBu} (1.44 g, 2.15 mmol) in toluene (20 ml) was added drop-wise to a solution of Zr(NMe$_2$)$_4$ (0.57 g, 2.15 mmol) in toluene (10 ml) and allowed to stir at room temperature for 2 hrs. The solvent was then removed under high vacuum and the residue washed with hexane. The product was then recrystallised from toluene. Yield = 18%. Anal: Calc for C$_{47}$H$_{72}$N$_2$O$_3$Zr$_1$ C: 70.2%, H: 9.02 %, N: 3.48 %. Found: C: 70.6%, H: 8.98%, N: 3.06%. **^{1}H NMR** (400.13 MHz, CDCl$_3$, 238 K) 1.26 (s, 27H C*H*$_3$), 1.41 (s, 27H C*H*$_3$), 2.92 (d, ^{2}J(H-H) = 13.2 Hz, 3H NC*H*$_2$), 3.28 (s, 6H, N(C*H*$_3$)$_2$), 3.90 (d, ^{2}J(H-H) = 13.2Hz, 3H NC*H*$_2$), 6.98 (s, 3H Ar*H*), 7.20 (s, 3H Ar*H*) **^{13}C{^{1}H} NMR** (100.62 MHz, CDCl$_3$, 238 K) 29.72 (*C*H$_3$), 31.91 (*C*H$_3$), 34.51 (*C*), 35.21 (*C*), 42.90 (N(*C*H$_3$)$_2$), 59.08 (N*C*H$_2$), 123.86 (*C*), 124.11 (*C*H), 125.21 (*C*H), 135.94 (*C*), 141.54 (*C*), 157.67 (*C*).

Preparation of L^{tBu}Zr(NEt$_2$): A solution of H$_3$L^{tBu} (1.00 g, 1.49 mmol) in toluene (20 ml) was added drop-wise to Zr(NEt$_2$)$_4$ (0.55 ml, 1.49 mmol) and allowed to stir at room temperature for 2 hrs. The white precipitate was filtered, washed with hexane and dried in *vacuo*. Yield = 38%. Anal: Calc for C$_{49}$H$_{76}$N$_2$O$_3$Zr$_1$ C: 70.7%; H: 9.20%; N: 3.37%. Found C: 70.5%; H: 9.18%; N: 3.36%. **^{1}H NMR** (500.13 MHz, CDCl$_3$, 278 K) 1.17 (t, ^{3}J(H-H) = 7.0 Hz, 6H N(CH$_2$C*H*$_3$)$_2$), 1.28 (s, 27H C*H*$_3$), 1.45 (s, 27H CH$_3$), 2.89 (d, ^{2}J(H-H) = 13.2 Hz, 3H NC*H*$_2$), 3.81 (m, ^{3}J(H-H) = 7.0 Hz, 4H N(C*H*$_2$CH$_3$)$_2$), 3.93 (d, ^{2}J(H-H) = 13.2 Hz, 3H NC*H*$_2$), 6.98 (d, ^{4}J(H-H) = 2.2 Hz, 3H Ar*H*), 7.23 (d, ^{4}J(H-H) = 2.4 Hz, 3H Ar*H*). **^{13}C{^{1}H} NMR** (125.76 MHz, CDCl$_3$, 298 K) 15.05 (N(CH$_2$*C*H$_3$)$_2$), 29.75 (*C*H$_3$), 31.67 (*C*H$_3$), 34.23 (*C*), 34.98 (*C*), 41.01 (N(*C*H$_2$CH$_3$)$_2$), 59.15 (N*C*H$_2$), 123.47 (*C*H), 124.03 (C), 124.89 (*C*H), 135.96 (*C*), 141.56 (*C*), 157.76 (*C*).

6.2.3. Synthesis of rare earth complexes

Preparation of [HL^{Me}]$_2$Ce: H$_3$L^{Me} (0.27 g, 0.64 mmol) was dissolved in dichloromethane (20 ml) to which Ce(O^{i}Pr)$_4$(HO^{i}Pr) (0.14 g, 0.32 mmol) was added and allowed to stir at 298 K for 16 hours. The resulting brown precipitate was collected on a frit and dried in *vacuo*. Yield = 26 %. Mass Spec: Calc for [M-H]-: 973.3589. Found: 973.3614. **^{1}H NMR** (400.13 MHz, CDCl$_3$, 238 K) 2.17 (s, 18H C*H*$_3$), 2.24 (s, 18H C*H*$_3$), 3.29 (d, ^{2}J(H-H) = 10.0 Hz, 3H NC*H*$_2$), 3.32 (d, ^{2}J(H-H)

159

= 10.0 Hz, 3H NCH_2), 4.85 (d, ^{2}J(H-H) = 11.5 Hz, 6H NCH_2), 6.70 (s, 6H ArH), 6.91 (s, 6H ArH), 11.37 (br d, 2H NH) ^{13}C{^{1}H} NMR (100.62 MHz, CDCl$_3$, 298 K) 16.71 (CH_3), 20.30 (CH_3), 56.56 (NCH_2), 116.06 (C), 125.41 (C), 127.63 (CH), 129.35 (C), 132.14 (CH), 166.14 (C).

Preparation of [HL^{Me}][H$_2$L^{Me}]Sc: H$_3$L^{Me} (1.28 g, 3.05 mmol) was dissolved in toluene (20 ml) to which Sc(O^{i}Pr)$_3$ (0.34 g, 1.53 mmol) was added and allowed to stir at 298 K for 16 hours. The resulting white precipitate was collected on a frit and dried in *vacuo*. Yield = 37%. Anal: Calc for C$_{54}$H$_{63}$N$_2$O$_6$Sc$_1$ C: 73.5%; H: 7.42%; N: 3.17%. Found C: 72.5%; H: 7.13%; N: 3.05%. **^{1}H NMR** (400.13 MHz, CDCl$_3$, 218 K) 1.93 (s, 18H CH_3), 2.17 (s, 18H CH_3), 3.34 (m, ^{2}J(H-H) = 11.6 Hz, 6H NCH_2), 4.73 (d, ^{2}J(H-H) = 12.9 Hz, 6H NCH_2), 6.70 (s, 6H ArH), 6.86 (s, 6H ArH), 10.37 (br s, 1H NH), 10.86 (br s, 1H NH) ^{13}C{^{1}H} NMR (100.62 MHz, CDCl$_3$, 238 K) 16.65 (CH_3), 20.36 (CH_3), 56.94 (NCH_2), 116.37 (C), 124.42 (C), 128.06 (CH), 128.23 (C), 132.41 (CH), 158.19 (C).

Preparation of [HL^{Me}][H$_2$L^{Me}]Y: H$_3$L^{Me} (0.84 g, 2.0 mmol) was dissolved in toluene (20 ml) to which 25% wt. solution of Y(O^{i}Pr)$_3$ (1.10 ml, 1.0 mmol) was added and allowed to stir at 298 K for 3 hours. The resulting white precipitate was collected on a frit and dried in *vacuo*. Yield = 52%. Anal: Calc for C$_{54}$H$_{63}$N$_2$O$_6$Y$_1$ C: 70.0%; H: 7.07%; N: 3.02%. Found C: 71.0%; H: 6.90%; N: 2.53%. **^{1}H NMR** (400.13 MHz, CDCl$_3$, 238 K) 1.97 (s, 18H CH_3), 2.19 (s, 18H CH_3), 3.31 (br s, 6H NCH_2), 4.72 (br s, 6H, NCH_2), 6.71 (s, 6H ArH), 6.89 (s, 6H ArH), 12.06 (br s, 2H NH). ^{13}C{^{1}H} NMR (100.62 MHz, CDCl$_3$, 238 K) 16.98 (CH_3), 20.36 (CH_3), 56.16 (NCH_2), 116.13 (C), 124.21 (C), 127.65 (C), 128.46 (CH), 132.16 (CH), 158.33 (C).

Preperation of [HL^{Me}][H$_2$L^{Me}]Sm: H$_3$L^{Me} (0.99 g, 2.36 mmol) was dissolved in dichloromethane (20 ml) to which Sm(O^{i}Pr)$_3$ (0.39 g, 1.18 mmol) was added and allowed to stir at 298 K for 1 hour. The resulting off-white precipitate was collected on a frit and dried in *vacuo*. Yield = 56 %. Anal: Calc for C$_{54}$H$_{63}$N$_2$O$_6$Sm$_1$ C: 65.6%; H: 6.63%; N: 2.83%. Found C: 68.3%; H: 6.66%; N: 2.02%. **^{1}H NMR** (400.13 MHz, CDCl$_3$, 328 K) -0.79 (br s, 18H CH_3), 2.30 (br s, 18H CH_3), 6.45 (br s, 6H ArH), 6.63 (br s, 12H NCH_2), 7.57 (br s, 6H ArH), 13.11 (br d, 2H NH). ^{13}C{^{1}H} NMR (100.62 MHz, CDCl$_3$, 328 K) 14.88 (CH_3), 20.53 (CH_3), 64.71 (NCH_2), 118.96 (C), 124.88 (C), 126.09 (C), 129.72 (CH), 132.33 (CH), 157.93 (C).

Preparation of L^{tBu}Sc(IPA): H$_3$L^{tBu} (2.0 g, 2.98 mmol) was dissolved in hexane (20 ml) to which Sc(O^{i}Pr)$_3$ (0.66 g, 2.98 mmol) was added and allowed to stir for 30 minutes at room temperature. The solvent was removed under high vacuum   and the product recrystallised from a hexane and toluene mix. The crystals were filtered and dried in *vacuo*. Yield = 58%. Anal: Calc for C$_{48}$H$_{74}$N$_1$O$_4$Sc$_1$ C: 74.5%; H: 9.64%; N: 1.81%. Found C: 73.8%; H: 9.50%; N: 1.68%. **^{1}H**

NMR (400.13 MHz, CDCl$_3$, 298 K) 1.20 (s, 27H CH_3), 1.41 (s, 27H CH_3), 1.66 (d, ^{3}J(H-H) = 6.12 Hz, 6H HOCH(CH_3)$_2$), 2.92 (br s, 3H CH_2), 3.72 (d, 1H HOCH(CH$_3$)$_2$), 4.11 (br s, 3H CH_2), 4.86 (m, ^{3}J(H-H) = 6.2 Hz, 1H HOCH(CH$_3$)$_2$), 6.98 (d, ^{4}J(H-H) = 2.7 Hz, 3H ArH) 7.17 (d, ^{4}J(H-H) = 2.4 Hz, 3H ArH). ^{13}C{^{1}H} **NMR** (100.62 MHz, CDCl$_3$, 298 K) 24.75 (HOCH(CH$_3$)$_2$), 29.61 (CH$_3$), 31.76 (CH$_3$), 34.04 (C), 34.90 (C), 59.81 (NCH$_2$), 71.11 (HOCH(CH$_3$)$_2$), 123.27 (CH), 123.88 (C), 124.97 (CH), 134.70 (C), 138.77 (C), 159.00 (C).

Preparation of L^{tBu}Y(IPA)$_3$: H$_3$L^{tBu} (1.10 g, 1.6 mmol) was dissolved in hexane (20 ml) to which a 25 % wt. solution of Y(O^{i}Pr)$_3$ (1.75 ml, 1.6 mmol) was added and allowed to stir for 30 minutes at room temperature. The solvent was removed under high vacuum and the product recrystallised from hexane. The crystals were filtered and dried in vacuo. Yield = 46 %. Anal: Calc for C$_{54}$H$_{90}$N$_1$O$_6$Y$_1$ C: 69.1%; H: 9.67%; N: 1.49%. Found C: 69.0%; H: 9.30%; N: 1.57%. ^{1}**H NMR** (400.13 MHz, CDCl$_3$, 298 K) 1.26 (s, 27H CH_3), 1.34 (d, ^{3}J(H-H) = 6.08 Hz, 18H HOCH(CH_3)$_2$), 1.39 (s, 27H CH_3), 3.47 (br s, 6H NCH_2), 3.57 (br s, 3H HOCH(CH$_3$)$_2$), 4.39 (br m, 3H HOCH(CH$_3$)$_2$), 6.91 (d, ^{4}J(H-H) = 2.4 Hz, 3H ArH), 7.14 (d, ^{4}J(H-H) = 2.4 Hz, ArH). ^{13}C{^{1}H} **NMR** (100.62 MHz, CDCl$_3$, 298 K) 25.03 (HOCH(CH$_3$)$_2$), 30.03 (CH$_3$), 31.85 (CH$_3$), 60.57 (NCH$_2$), 68.23 (HOCH(CH$_3$)$_2$), 123.28 (CH), 124.28 (C), 125.68 (CH), 134.48 (C), 136.80 (C), 159.98 (C).

Preparation of L^{tBu}Nd(IPA)$_3$: H$_3$L^{tBu} (0.52 g, 0.78 mmol) was dissolved in hexane (20 ml) to which Nd(O^{i}Pr)$_3$ (0.25 g, 0.78 mmol) was added and allowed to stir for 30 minutes at room temperature. The solvent was removed under high vacuum and the product recrystallised from hexane. The small, pale blue crystals were filtered and dried in *vacuo*. Yield = 3%. Anal: Calc for C$_{54}$H$_{90}$N$_1$O$_6$Nd$_1$ C: 65.3%; H: 9.13%; N: 1.41%. Found C: 63.6%; H: 8.40%; N: 1.42%.

Preparation of L^{tBu}Sm(IPA)$_3$: H$_3$L^{tBu} (0.51 g, 0.76 mmol) was dissolved in hexane (20 ml) to which Sm(O^{i}Pr)$_3$ (0.25 g, 0.76 mmol) was added and allowed to stir for 30 minutes at room temperature. The solvent was removed under high vacuum and the product recrystallised from hexane. The crystals were filtered and dried in *vacuo*. Yield = 23%. Anal: Calc for C$_{54}$H$_{90}$N$_1$O$_6$Sm$_1$ C: 64.9%; H: 9.07%; N: 1.40%. Found C: 64.3%; H: 8.85%; N: 1.47%. ^{1}**H NMR** (400.13 MHz, d_8-tol, 318 K) -0.98 (br s, 8H, HOCH(CH_3)$_2$), -0.12 (br s, 8H, HOCH(CH_3)$_2$), 0.68 (br s, 9H, CH_3), 1.15 (br s, 9H, CH_3), 1.31 (s, 27H, CH_3), 1.87 (s, 9H, CH_3), 2.56 (br s, 6H, NCH_2), 3.00 (br s, 3H, HOCH(CH$_3$)$_2$), 3.83 (br s, 3H, HOCH(CH$_3$)$_2$), 6.73 (br s, 1H, ArH), 6.85 (br s, 1H, ArH), 7.28 (br s, 2H, ArH), 8.03 (br s, 1H, ArH), 8.29 (br s, 1H, ArH).

Preparation of L^{tBu}Yb(IPA)$_3$: H$_3$L^{tBu} (0.48 g, 0.71 mmol) was dissolved in hexane (20 ml) to which Yb(O^{i}Pr)$_3$ (0.25 g, 0.71 mmol) was added and allowed to stir for 30 minutes at room

temperature. The solvent was removed under high vacuum and the product recrystallised from hexane. The crystals were filtered and dried in *vacuo*. Yield = 13%. Anal: Calc for $C_{54}H_{90}N_1O_6Yb_1$ C: 63.4%; H: 8.87%; N: 1.37%. Found C: 63.0%; H: 8.67%; N: 1.49%.

Preparation of [L^tBu^Nd(IPA)]₂: H_3L^{tBu} (0.52 g, 0.78 mmol) was dissolved in hexane (20 ml) to which Nd(O^iPr^)₃ (0.25 g, 0.78 mmol) was added and allowed to stir for 30 minutes at room temperature. The solvent was removed under high vacuum and redissolved in fresh hexane with heating. The Schlenk was left to stand at –15 °C, but subsequent precipitations from the solution were repeatedly redissolved back into hexane with heating. After two weeks large green crystals were observed to drop out of the dark green solution, which were filtered and dried in *vacuo*. Yield = 5%. Anal: Calc for $C_{96}H_{148}N_2O_8Nd_1$ C: 66.0%; H: 8.54%; N: 1.60%. Found C: 65.3%; H: 8.45%; N: 1.60%.

Preparation of [L^tBu^Gd]₂(H₂O): $Gd[N(SiMe_3)_2]_3$ (0.25 g, 0.39 mmol) was dissolved in toluene (20 ml) to which the ligand (0.26 g, 0.39 mmol) was added. The solution was stirred overnight, after which time the solvent was removed in *vacuo* and the reaction products dissolved in minimum hexane. Green block crystals were isolated after four weeks, collected on a frit and dried.

6.3.   Polymerisations – General considerations

L- and D-LA monomers, obtained from Purac, and *rac*-LA, purchased from Aldrich, were all recrystallised from toluene and sublimed prior to use. PEG and methoxy PEG macroinitiators, purchased from Aldrich, were dried over 4Å molecular sieves and recrystallised from toluene prior to use. All metal initiators were prepared as described previously in this chapter. Monomer conversions were calculated from the relative intensities of monomer and polymer signals *via* ^{1}H NMR spectroscopy (page 79). Polymer microstructure was determined using homonuclear decoupled ^{1}H NMR spectroscopy where P_s is calculated from the relative intensity of [*sis*]. In the case of *rac*-LA, [*sis*] = ∫(*sis*)/[∫(*sis*)+∫(*sii*)+∫(*iis*)+∫(*iii*)+∫(*isi*)]; in the case of *meso*-LA, [*sis*] = ∫(*sis*)/[∫(*sis*)+∫(*sss+iss+ssi+isi*)] (page 80), as discussed in Chapters 1 and 2.

Gel Permeation Chromatography (GPC) was carried out on resulting polymers using a Polymer Laboratories PL-GPC 50 integrated system using a PLgel 5 µm MIXED-D 300 x 7.5 mm column at 35 °C, THF solvent (flow rate, 1.0 mL/min). The polydispersity index (PDI) was determined from M_w/M_n, where M_n is the number-average molecular weight and M_w the weight-average molecular weight. The polymers were referenced to 10 narrow molecular weight polystyrene standards with a range of M_w 580 - 6035000 Da.

Thermal analyses were performed using Differential Scanning Calorimetry (DSC; Perkin-Elmer Pyris 1) using nitrogen as the purge gas and calibrated using indium standards (T_m 156.6). The reported melting temperature (T_m) was obtained from the peak onset obtained from a first heating cycle of the materials, as when observed, T_m values were consistently observed in first heating cycles. The glass transition temperature (T_g) was taken as the midpoint of the transition determined for the second heating cycle. In each case the sample was heated at a rate of 10 °C/min from -20 °C to 220 °C, in the case of homopolymeric materials, and -20 °C to 250 °C, in the case of stereocomplexed materials.

When possible, polymer end-group analysis was carried out using MALDI-ToF mass spectrometry by the EPSRC National Mass Spectrometry Centre at the University of Wales, Swansea.

6.4.   Polymerisations – Typical syntheses

Bulk polymerisation: Typically, *rac*-LA (2.0 g) and the initiator **L^{tBu}Zr(O^{i}Pr)** (0.038 g) were stirred together at 130 °C in a thick-walled Young's vessel. When the reaction medium became too viscous to stir (10 mins), the polymerisation was allowed to cool and quenched with MeOH (0.5 ml). The resulting solid was dissolved in CH$_2$Cl$_2$ (10 ml), which was then removed in *vacuo* and conversion determined by ^{1}H NMR spectroscopy (conv = 90 %). Any unreacted monomer was removed by washing with copious amounts of methanol.

Solution polymerisation (high temp): Toluene (20 ml) was added to a mixture of *rac*-LA (1.44 g) and initiator **L^{tBu}Zr(O^{i}Pr)** (0.082 g) in a Schlenk tube. Using Schlenk line techniques, the mixture was heated to 100 °C for 2-4 hrs with stirring, after which time MeOH (0.5 mL) was added to quench the polymerisation. An aliquot is taken from the reaction liquor to determine conversion, and the resultant polymer is precipitated by the addition of *n*-hexane (100 mL).

Solution polymerisation (room temp): Typically, *rac*-LA (1.918 g) was initially stirred at room temperature in CDCl$_3$ (20 mL) within an inert-atmosphere glovebox, to which the initiator **L^{tBu}Zr(O^{i}Pr)** (0.11 g) was added. Aliquots of 0.1 mL were removed at intervals of 120 min and made up to 0.5 mL with CDCl$_3$ in an NMR tube, together with a drop of D$_2$O to quench the reaction. Conversion was calculated using 1H NMR spectroscopy. When conversion reached > 95%, the polymerisation was deemed complete, MeOH (0.5 mL) added to quench the reaction and the resultant polymer precipitated by the addition of *n*-hexane.

Solution polymerisation (NMR scale, high temp): Typically, d_8-toluene (1 mL) was added to *rac*-LA (0.02 g) in a Young's NMR tube, to which 0.14M d_8-toluene solution of **L^{tBu}Zr(O^{i}Pr)** (0.1 mL) was added. The sample was immediately placed on an NMR spectrometer and heated to 333 K. Using an automation programme, NMR spectra were taken of the sample every 20 minutes for 12 hours. Following this initial period, the sample was left at room temperature until > 95% conversion had been reached, at which point the resultant polymer was precipitated by the addition of MeOH.

Solution polymerisation (NMR scale, room temp): Typically, *rac*-LA (0.096 g) and the initiator **L^{tBu}Zr(O^{i}Pr)** (0.0055 g) were dissolved in CDCl$_3$ (1.0 mL) in a Young's NMR tube, which was immediately placed on an NMR spectrometer programmed to run the sample every 60 – 120 mins. When conversion reached > 95 %, the polymerisation was deemed complete, and the solvent removed in *vacuo*. The resultant polymer was washed with MeOH to remove any unreacted monomer.

One-step solution synthesis of di-stereoblock PLA (1:6 PLLA-P*het*LA): *rac*-LA (3.0 g) and L-LA (0.5 g) were dissolved in CH$_2$Cl$_2$ (30 mL), to which the initiator **L^{tBu}Zr(O^{i}Pr)** (0.057 g) was added. The polymerisation was left to stir at room temperature for a number of days, samples were taken periodically and conversion determined by ^{1}H NMR spectroscopy. When > 95 % had been achieved, polymerisation was quenched with MeOH (0.5 ml) and reprecipitated from toluene with MeOH.

Two-step solution synthesis of di-block stereoblock PLA (1:1 PLLA-P*het*LA): *rac*-LA (0.5 g) was dissolved in CH$_2$Cl$_2$ (10 mL) to which the initiator **L^{tBu}Zr(O^{i}Pr)** (0.02 g) was added and left to stir in an inert-atmosphere glovebox at room temperature for 48 hrs. After this time, polymerisation of *rac*-LA was shown to be complete (> 95 %), and L-LA (0.5g) was added to the reaction and left to stir for 8 days. The solvent was removed in *vacuo* and the resultant polymer reprecipitated from toluene with MeOH.

One-step bulk synthesis of di-block stereoblock PLA (1:1 PLLA-P*het*LA): *rac*-LA (1.0 g), L-LA (1.0 g) and the initiator **L^{tBu}Zr(O^{i}Pr)** (0.038 g) were stirred together at 130 °C in a thick-walled Young's vessel. When the reaction medium became too viscous to stir (10 mins), the polymerisation was allowed to cool and quenched with MeOH (0.5 ml). The resulting solid was dissolved in CH$_2$Cl$_2$ (10 ml), which was then removed in vacuo and conversion determined by ^{1}H NMR spectroscopy (90%). Any unreacted monomer was removed by washing with copious amounts of methanol.

Synthesis of symmetrical tri-stereoblock PLA (1:6:1 PLLA-P*het*LA-PLLA): L-LA (0.12 g) and the initiator **L^tBuZr(O^iPr)** (0.0055 g) were dissolved in CDCl₃ (1.2 ml). After 19 hrs, conversion had reached 20%, and D-LA (0.072 g) was added to the polymerisation. Conversion and tacticty was monitored periodically via ¹H NMR spectroscopy, until > 90 % conversion had been reached after 11 days. The solvent was removed in *vacuo*.

Synthesis of unsymmetrical tri-stereoblock PLA (1:6:1 PLLA-P*het*LA-PDLA): L-LA (0.096 g) and the initiator **L^tBuZr(O^iPr)** (0.0055 g) were dissolved in CDCl₃ (1 ml). After 24 hrs, conversion had reached 25 %, and D-LA (0.096 g) was added to the polymerisation. Conversion and tacticity was monitored periodically via ¹H NMR spectroscopy, until > 95 % conversion had been reached after 4 days. The solvent was removed in *vacuo*.

Synthesis of di-stereoblock PLA via macroinitiation (P*het*LA-PDLA): Pre-prepared P*het*LA (M_w = 13550) (0.32 g) and the initiator **L^tBuZr(NMe₂)** (0.018 g) were dissolved in toluene (5 ml) at 100 °C, to which D-LA (0.658 g) in toluene (5 ml) at 100° C was added via a syringe. After 3 hrs, the polymer was reprecipitated with *n*-hexane. Monomer conversion (as calculated by comparison of polymer molecular weights) = 20 %.

Synthesis of PEG-PLA di-block polymers via macroinitiation (PEG-PLLA): Methoxy PEG (M_w = 5500) (0.5 g) and the initiator **L^tBuZr(NMe₂)** (0.08 g) were dissolved in toluene (10 ml) at 100 °C, to which L-LA (2.0g) in toluene (10 ml) at 100° C was added via a syringe. After 18 hrs, an aliquot of the reaction medium was taken to determine monomer conversion (80 %) via ¹H NMR spectroscopy, and the polymer was reprecipitated with *n*-hexane.

Synthesis of PLA-PEG-PLA tri-block polymers via macroinitiation (PLLA-PEG-PLLA): PEG (M_w = 9600) (0.25 g) and the initiator **L^tBuZr(NEt₂)** (0.052 g) were dissolved in toluene (5 ml) at 100 °C, to which L-LA (2.0g) in toluene (5 ml) at 100° C was added via a syringe. After 3 hrs, an aliquot of the reaction medium was taken to determine monomer conversion via ¹H NMR spectroscopy, and the polymer was reprecipitated with *n*-hexane.

Synthesis of PEG-P*het*LA-PisoPLA tri-block polymers (PEG-P*het*LA-PLLA): Methoxy PEG (M_w = 5500) (0.5 g) and the initiator **L^tBuZr(NMe₂)** (0.08 g) were dissolved in toluene (10 ml) at 100 °C, to which a mixture of *rac*-LA (1.0 g) and L-LA (1.0g) in toluene (10 ml) at 100° C was added via a syringe. Aliquots were taken from the reaction medium every 20 mins, and analysed via ¹H NMR spectroscopy to determine monomer conversion (72 %) and tacticity. After 4 hrs, reaction medium was reduced to minimum volume and the polymer precipitated with *n*-hexane.

Synthesis of P*iso*PLA-P*het*LA-PEG-P*het*LA-P*iso*LA penta-block polymers (PLLA-P*het*LA-PEG-P*het*LA-PLLA): PEG (M_w = 9600) (0.25 g) and the initiator **L$^{\text{tBu}}$Zr(NEt$_2$)** (0.052 g) were dissolved in toluene (5 ml) at 100 °C, to which a mixture of *rac*-LA (0.25 g) and L-LA (0.25 g) in toluene (5 ml) at 100° C was added via a syringe. After 2 hrs, an aliquot of the reaction medium was taken to determine monomer conversion (89 %) via ^{1}H NMR spectroscopy, and the polymer was reprecipitated with *n*-hexane.

6.4.1. Synthesis of stereocomplexes

Formation of stereocomplexes: Enantiomeric pairs of di-block or tri-block stereoblock or co-polymers (i.e. PEG-PLLA and PEG-PDLA) can be mixed together in equal quantites resulting in stereocomplexes. Typically, 0.2 g of each polymer is dissolved in dichloromethane (approx 5 ml). These solutions are then mixed together and allowed to stir at room temperature for 10 mins. Isolation of the stereocomplex material can be achieved either by reprecipitation with methanol, in the case of PLA stereoblocks, or hexane, in the case of PEG-PLA co-polymers. Alternatively, the dichloromethane can be allowed to slowly evaporate over a period of 16 – 20 hrs under a steady flow of argon gas.[6]

6.5.   Refererences

1.   Kol, M.; Shamis, M.; Goldberg, I.; Goldschmidt, Z.; Alfi, S.; Hayut-Salant, E., *Inorg. Chem. Commun.* **2001,** *4* (4), 177-179.
2.   Kim, Y.; Verkade, J. G., *Organometallics* **2002,** *21* (12), 2395-2399.
3.   Davidson, M. G.; Doherty, C. L.; Johnson, A. L.; Mahon, M. F., *Chem. Commun.* **2003,** (15), 1832-1833.
4.   Gendler, S.; Segal, S.; Goldberg, I.; Goldschmidt, Z.; Kol, M., *Inorg. Chem.* **2006,** *45* (12), 4783-4790.
5.   Chmura, A. J.; Davidson, M. G.; Frankis, C. J.; Jones, M. D.; Lunn, M. D., *Chem. Commun.* **2008,** (11), 1293-1295.
6.   Kricheldorf, H. R.; Rost, S.; Wutz, C.; Domb, A., *Macromolecules* **2005,** *38* (16), 7018-7025.

Appendix

X-ray Crystal Structure Data

Appendix – X-ray Crystal Structure Data

H_3L^{Np}

Identification code	k07mgd06
Empirical formula	C51 H81 N O3
Formula weight	756.17
Temperature	150(2) K
Wavelength	0.71073 A
Crystal system, space group	Monoclinic, $P2_1/c$
Unit cell dimensions	a = 18.3660(2) A alpha = 90 deg.
	b = 9.1620(1) A beta = 104.92 deg.
	c = 29.2350(3) A gamma = 90 deg.
Volume	4753.52(9) A^3
Z, Calculated density	4, 1.057 Mg/m^3
Absorption coefficient	0.063 mm^-1
F(000)	1672
Crystal size	0.25 x 0.25 x 0.13 mm
Theta range for data collection	3.59 to 27.50 deg.
Limiting indices	-23<=h<=23, -11<=k<=11, -37<=l<=37
Reflections collected / unique	64569 / 10821 [R(int) = 0.0547]
Completeness to theta = 27.50	99.3 %
Absorption correction	None
Max. and min. transmission	0.9921 and 0.9843
Refinement method	Full-matrix least-squares on F^2
Data / restraints / parameters	10821 / 0 / 557
Goodness-of-fit on F^2	1.029
Final R indices [I>2sigma(I)]	R1 = 0.0493, wR2 = 0.1196
R indices (all data)	R1 = 0.0757, wR2 = 0.1344
Largest diff. peak and hole	0.420 and -0.259 e.A^-3

H$_3$L^{Cl}·HMTA

Identification code	h06mgd24
Empirical formula	C27 H27 Cl6 N5 O3
Formula weight	682.24
Temperature	150(2) K
Wavelength	0.71073 A
Crystal system, space group	Monoclinic, $P2_1/c$
Unit cell dimensions	a = 9.9100(3) A alpha = 90 deg.
	b = 17.8750(6) A beta = 93.292(2) deg.
	c = 16.9380(6) A gamma = 90 deg.
Volume	2995.47(17) A^3
Z, Calculated density	4, 1.513 Mg/m^3
Absorption coefficient	0.613 mm^-1
F(000)	1400
Crystal size	0.50 x 0.30 x 0.30 mm
Theta range for data collection	3.98 to 27.48 deg.
Limiting indices	-12<=h<=11, -23<=k<=23, -21<=l<=21
Reflections collected / unique	33827 / 6812 [R(int) = 0.0821]
Completeness to theta = 27.48	99.4 %
Absorption correction	None
Max. and min. transmission	0.8375 and 0.7492
Refinement method	Full-matrix least-squares on F^2
Data / restraints / parameters	6812 / 0 / 373
Goodness-of-fit on F^2	1.026
Final R indices [I>2sigma(I)]	R1 = 0.0433, wR2 = 0.0925
R indices (all data)	R1 = 0.0808, wR2 = 0.1073
Largest diff. peak and hole	0.286 and -0.658 e.A^-3

H₃L^{**Cl**}

Identification code	k07mgd04
Empirical formula	C22 H16 Cl9 N O3
Formula weight	661.41
Temperature	150(2) K
Wavelength	0.71073 A
Crystal system, space group	Monoclinic, $P2_1/a$
Unit cell dimensions	a = 14.01800(10) A alpha = 90 deg.
	b = 14.04200(10) A beta = 100.64 deg.
	c = 27.4030(3) A gamma = 90 deg.
Volume	5301.27(8) A^3
Z, Calculated density	8, 1.657 Mg/m^3
Absorption coefficient	0.978 mm^-1
F(000)	2656
Crystal size	0.30 x 0.10 x 0.05 mm
Theta range for data collection	3.56 to 27.47 deg.
Limiting indices	-18<=h<=18, -18<=k<=18, -35<=l<=34
Reflections collected / unique	76449 / 12090 [R(int) = 0.0539]
Completeness to theta = 27.47	99.6 %
Absorption correction	None
Refinement method	Full-matrix least-squares on F^2
Data / restraints / parameters	12090 / 0 / 649
Goodness-of-fit on F^2	1.136
Final R indices [I>2sigma(I)]	R1 = 0.0651, wR2 = 0.1448
R indices (all data)	R1 = 0.0796, wR2 = 0.1507
Largest diff. peak and hole	0.874 and -1.240 e.A^-3

H₃L^{Br}·HMTA

H₃L^{Br}·HMTA

Identification code	k06mgd28
Empirical formula	C27 H27 Br6 N5 O3
Formula weight	949.00
Temperature	150(2) K
Wavelength	0.71073 A
Crystal system, space group	monoclinic, $P2_1/c$
Unit cell dimensions	a = 9.932(2) A alpha = 90 deg.
	b = 18.266(3) A beta = 94.053(1) deg.
	c = 17.322(4) A gamma = 90 deg.
Volume	3134.66(11) A^3
Z, Calculated density	4, 2.011 Mg/m^3
Absorption coefficient	7.723 mm^-1
F(000)	1832
Crystal size	0.20 x 0.10 x 0.05 mm
Theta range for data collection	3.71 to 25.00 deg.
Limiting indices	-11<=h<=11, -21<=k<=21, -20<=l<=20
Reflections collected / unique	32634 / 5478 [R(int) = 0.1034]
Completeness to theta = 25.00	99.2 %
Absorption correction	multi-scan
Max. and min. transmission	0.6987 and 0.3073
Refinement method	Full-matrix least-squares on F^2
Data / restraints / parameters	5478 / 1 / 379
Goodness-of-fit on F^2	1.072
Final R indices [I>2sigma(I)]	R1 = 0.0418, wR2 = 0.0955
R indices (all data)	R1 = 0.0631, wR2 = 0.1076
Largest diff. peak and hole	0.726 and -1.070 e.A^-3

[HL^{Me}]₂Hf

Identification code	h07mgd08
Empirical formula	C75 H86 Hf N2 O6
Formula weight	1289.95
Temperature	150(2) K
Wavelength	0.71073 Å
Crystal system	Triclinic
Space group	*P*-1
Unit cell dimensions	a = 11.3140(3)Å alpha = 81.7490(10)°
	b = 11.7480(3)Å beta = 83.5620(10)°
	c = 12.8720(4)Å gamma = 73.5700(10)°
Volume	1619.44(8) Å^3
Z	1
Density (calculated)	1.323 Mg/m^3
Absorption coefficient	1.664 mm^{-1}
F(000)	670
Crystal size	0.20 x 0.10 x 0.10 mm^3
Theta range for data collection	3.60 to 27.60°.
Index ranges	-14<=h<=14, -15<=k<=15, -16<=l<=16
Reflections collected	35973
Independent reflections	7406 [R(int) = 0.0908]
Completeness to theta = 27.60°	98.8 %
Max. and min. transmission	0.8512 and 0.7319
Refinement method	Full-matrix least-squares on F^2
Data / restraints / parameters	7406 / 0 / 402
Goodness-of-fit on F^2	1.013
Final R indices [I>2sigma(I)]	R1 = 0.0473, wR2 = 0.0897
R indices (all data)	R1 = 0.0684, wR2 = 0.0961
Largest diff. peak and hole	0.804 and -1.046 e.Å^{-3}

L^{Np}Ti(OⁱPr)

Identification code	k07mgd23
Empirical formula	C54 H85 N O4 Ti
Formula weight	860.13
Temperature	150(2) K
Wavelength	0.71073 A
Crystal system, space group	Monoclinic, $P2_1/n$
Unit cell dimensions	a = 10.8100(1)A alpha = 90 deg.
	b = 23.8760(3)A beta = 104.669(1) deg.
	c = 21.0500(2)A gamma = 90 deg.
Volume	5255.91(10) A^3
Z, Calculated density	4, 1.087 Mg/m^3
Absorption coefficient	0.204 mm^-1
F(000)	1880
Crystal size	0.10 x 0.10 x 0.10 mm
Theta range for data collection	3.52 to 27.49 deg.
Limiting indices	-14<=h<=14, -30<=k<=30, -27<=l<=27
Reflections collected / unique	90576 / 12002 [R(int) = 0.0971]
Completeness to theta = 27.49	99.7 %
Absorption correction	None
Max. and min. transmission	0.9799 and 0.9799
Refinement method	Full-matrix least-squares on F^2
Data / restraints / parameters	12002 / 0 / 770
Goodness-of-fit on F^2	1.099
Final R indices [I>2sigma(I)]	R1 = 0.1276, wR2 = 0.2969
R indices (all data)	R1 = 0.1645, wR2 = 0.3172
Extinction coefficient	0.0095(14)
Largest diff. peak and hole	0.896 and -0.517 e.A^-3

L^{Cl}Ti$_2$(O^{i}Pr)$_5$

Identification code	k07mgd01
Empirical formula	C18 H23.50 Cl3 N0.50 O4 Ti
Formula weight	465.12
Temperature	150(2) K
Wavelength	0.71073 A
Crystal system, space group	Triclinic, *P*-1
Unit cell dimensions	a = 9.770(1) A alpha = 76.32 deg. b = 11.558(1) A beta = 83.338(1) deg. c = 20.748(3) A gamma = 69.582(1) deg.
Volume	2131.95(4) A^3
Z, Calculated density	4, 1.449 Mg/m^3
Absorption coefficient	0.798 mm^-1
F(000)	960
Crystal size	0.20 x 0.15 x 0.10 mm
Theta range for data collection	3.63 to 27.49 deg.
Limiting indices	-12<=h<=12, -15<=k<=14, -26<=l<=26
Reflections collected / unique	40732 / 9717 [R(int) = 0.0519]
Completeness to theta = 27.49	99.4 %
Absorption correction	None
Max. and min. transmission	0.9244 and 0.8566
Refinement method	Full-matrix least-squares on F^2
Data / restraints / parameters	9717 / 0 / 488
Goodness-of-fit on F^2	1.016
Final R indices [I>2sigma(I)]	R1 = 0.0340, wR2 = 0.0872
R indices (all data)	R1 = 0.0421, wR2 = 0.0942
Largest diff. peak and hole	0.385 and -0.474 e.A^-3

L$^{Cl}_2$Ti$_3$(O^{i}Pr)$_4$

Identification code	k07mgd24
Empirical formula	C60 H66 Cl12 N2 O11 Ti3
Formula weight	1560.25
Temperature	150(2) K
Wavelength	0.71073 A
Crystal system, space group	Monoclinic, $P2_1/n$
Unit cell dimensions	a = 19.3200(4)A alpha = 90 deg.
	b = 15.8750(4)A beta = 101.919(1) deg.
	c = 22.0660(4)A gamma = 90 deg.
Volume	6621.8(2) A^3
Z, Calculated density	4, 1.565 Mg/m^3
Absorption coefficient	0.897 mm^-1
F(000)	3192
Crystal size	0.50 x 0.50 x 0.30 mm
Theta range for data collection	3.01 to 25.04 deg.
Limiting indices	-23<=h<=22, -18<=k<=18, -26<=l<=26
Reflections collected / unique	54176 / 11400 [R(int) = 0.1315]
Completeness to theta = 25.04	97.3 %
Absorption correction	None
Max. and min. transmission	0.7747 and 0.6627
Refinement method	Full-matrix least-squares on F^2
Data / restraints / parameters	11400 / 2 / 793
Goodness-of-fit on F^2	1.607
Final R indices [I>2sigma(I)]	R1 = 0.1520, wR2 = 0.3821
R indices (all data)	R1 = 0.1832, wR2 = 0.4138
Largest diff. peak and hole	3.971 and -1.092 e.A^-3

[HL^{Cl}]₂Zr

Identification code	k07mgd15
Empirical formula	C31.50 H24.50 Cl6 N O3 Zr0.50
Formula weight	723.33
Temperature	150(2) K
Wavelength	0.71073 A
Crystal system, space group	Monoclinic, *C*2/c
Unit cell dimensions	a = 14.4810(1) A alpha = 90 deg.
	b = 18.2100(2) A beta = 102.04 deg.
	c = 24.3040(2) A gamma = 90 deg.
Volume	6268.05(10) A^3
Z, Calculated density	8, 1.533 Mg/m^3
Absorption coefficient	0.740 mm^-1
F(000)	2932
Crystal size	0.28 x 0.28 x 0.15 mm
Theta range for data collection	3.60 to 30.04 deg.
Limiting indices	-20<=h<=20, -25<=k<=25, -33<=l<=34
Reflections collected / unique	57074 / 9153 [R(int) = 0.0485]
Completeness to theta = 30.04	99.6 %
Absorption correction	None
Max. and min. transmission	0.8971 and 0.8224
Refinement method	Full-matrix least-squares on F^2
Data / restraints / parameters	9153 / 0 / 382
Goodness-of-fit on F^2	1.041
Final R indices [I>2sigma(I)]	R1 = 0.0352, wR2 = 0.0817
R indices (all data)	R1 = 0.0503, wR2 = 0.0900
Largest diff. peak and hole	0.895 and -0.618 e.A^-3

L^{tBu}Ti(BH$_4$)

Identification code	h08mgd01
Empirical formula	C52 H78 B N O3 Ti
Formula weight	823.86
Temperature	150(2) K
Wavelength	0.71073 Å
Crystal system	Triclinic
Space group	*P*-1
Unit cell dimensions	a = 13.1430(5)Å alpha = 88.737(2)°.
	b = 13.4980(5)Å beta = 68.533(2)°.
	c = 16.1430(9)Å gamma = 73.731(2)°.
Volume	2548.0(2) Å^3
Z	2
Density (calculated)	1.074 Mg/m^3
Absorption coefficient	0.206 mm^{-1}
F(000)	896
Crystal size	0.30 x 0.15 x 0.10 mm^3
Theta range for data collection	3.53 to 24.23°.
Index ranges	-15<=h<=15, -15<=k<=15, -18<=l<=18
Reflections collected	17090
Independent reflections	8001 [R(int) = 0.0796]
Completeness to theta = 24.23°	97.3 %
Max. and min. transmission	0.9796 and 0.9407
Refinement method	Full-matrix least-squares on F^2
Data / restraints / parameters	8001 / 0 / 586
Goodness-of-fit on F^2	1.035
Final R indices [I>2sigma(I)]	R1 = 0.0607, wR2 = 0.1263
R indices (all data)	R1 = 0.1136, wR2 = 0.1526
Largest diff. peak and hole	0.270 and -0.288 e.Å^{-3}

L^{tBu}Hf(BH$_4$)

Identification code	bath603
Empirical formula	C21.50 H32 B0.50 Hf0.50 N0.50 O1.50
Formula weight	416.13
Temperature	150(2) K
Wavelength	0.71073 A
Crystal system, space group	Monoclinic, $P2_1/m$
Unit cell dimensions	a = 10.706 A alpha = 90 deg.
	b = 19.059 A beta = 99.87 deg.
	c = 10.983 A gamma = 90 deg.
Volume	2207.9 A^3
Z, Calculated density	4, 1.252 Mg/m^3
Absorption coefficient	2.397 mm^-1
F(000)	860
Crystal size	0.10 x 0.05 x 0.05 mm
Theta range for data collection	2.68 to 30.52 deg.
Limiting indices	-15<=h<=15, -26<=k<=26, -15<=l<=14
Reflections collected / unique	25396 / 6885 [R(int) = 0.0352]
Completeness to theta = 30.52	99.4 %
Absorption correction	None
Max. and min. transmission	0.8896 and 0.7956
Refinement method	Full-matrix least-squares on F^2
Data / restraints / parameters	6885 / 3 / 347
Goodness-of-fit on F^2	0.928
Final R indices [I>2sigma(I)]	R1 = 0.0343, wR2 = 0.1115
R indices (all data)	R1 = 0.0404, wR2 = 0.1171
Largest diff. peak and hole	1.782 and -1.105 e.A^-3

L^{tBu}Zr(NMe₂)

Identification code	h08mgd13
Empirical formula	C50.50 H75.50 N2 O3 Zr
Formula weight	849.85
Temperature	150(2) K
Wavelength	0.71073 A
Crystal system, space group	Triclinic, P-1
Unit cell dimensions	a = 11.1590(5)A alpha = 74.769(3) deg.
	b = 12.9660(5)A beta = 75.813(2) deg.
	c = 18.5450(9)A gamma = 72.037(2) deg.
Volume	2423.12(19) A^3
Z, Calculated density	2, 1.165 Mg/m^3
Absorption coefficient	0.267 mm^-1
F(000)	913
Crystal size	0.20 x 0.20 x 0.20 mm
Theta range for data collection	5.49 to 26.79 deg.
Limiting indices	-14<=h<=14, -16<=k<=16, -23<=l<=23
Reflections collected / unique	24246 / 10033 [R(int) = 0.1060]
Completeness to theta = 26.79	97.0 %
Absorption correction	None
Max. and min. transmission	0.9485 and 0.9485
Refinement method	Full-matrix least-squares on F^2
Data / restraints / parameters	10033 / 0 / 661
Goodness-of-fit on F^2	1.039
Final R indices [I>2sigma(I)]	R1 = 0.0605, wR2 = 0.1496
R indices (all data)	R1 = 0.0878, wR2 = 0.1732
Largest diff. peak and hole	0.555 and -0.500 e.A^-3

[HL^{Me}]₂Ce

Identification code	k07mgd25
Empirical formula	C75 H86 Ce N2 O6
Formula weight	1251.58
Temperature	150(2) K
Wavelength	0.71073 A
Crystal system, space group	Triclinic, *P*-1
Unit cell dimensions	a = 11.4990(4)A alpha = 85.558(2) deg.
	b = 11.7270(5)A beta = 84.566(2) deg.
	c = 12.7630(6)A gamma = 72.267(2) deg.
Volume	1629.79(12) A^3
Z, Calculated density	1, 1.275 Mg/m^3
Absorption coefficient	0.752 mm^-1
F(000)	656
Crystal size	0.10 x 0.10 x 0.10 mm
Theta range for data collection	5.50 to 27.51 deg.
Limiting indices	-14<=h<=14, -15<=k<=15, -16<=l<=16
Reflections collected / unique	17880 / 7385 [R(int) = 0.0532]
Completeness to theta = 27.51	98.3 %
Absorption correction	None
Max. and min. transmission	0.9286 and 0.9286
Refinement method	Full-matrix least-squares on F^2
Data / restraints / parameters	7385 / 0 / 394
Goodness-of-fit on F^2	1.040
Final R indices [I>2sigma(I)]	R1 = 0.0509, wR2 = 0.1170
R indices (all data)	R1 = 0.0604, wR2 = 0.1236
Largest diff. peak and hole	1.041 and -0.848 e.A^-3

[HL^{Me}][H₂L^{Me}]Sc

Identification code	k09mgd07
Empirical formula	C164.82 H173.05 N3.78 O11.33 Sc1.74
Formula weight	2466.04
Temperature	150(2) K
Wavelength	0.71073 A
Crystal system, space group	Monoclinic, *P*2₁
Unit cell dimensions	a = 21.3700(2) A alpha = 90 deg. b = 15.7520(1) A beta = 98.84 deg. c = 22.9250(2) A gamma = 90 deg.
Volume	7625.35(11) A^3
Z, Calculated density	2, 1.074 Mg/m^3
Absorption coefficient	0.135 mm^-1
F(000)	2631
Crystal size	0.38 x 0.30 x 0.25 mm
Theta range for data collection	2.99 to 27.49 deg.
Limiting indices	-27<=h<=27, -20<=k<=20, -29<=l<=29
Reflections collected / unique	136288 / 34228 [R(int) = 0.0762]
Completeness to theta = 27.49	96.2 %
Absorption correction	None
Max. and min. transmission	0.9670 and 0.9504
Refinement method	Full-matrix least-squares on F^2
Data / restraints / parameters	34228 / 1 / 2168
Goodness-of-fit on F^2	0.995
Final R indices [I>2sigma(I)]	R1 = 0.0684, wR2 = 0.1568
R indices (all data)	R1 = 0.1171, wR2 = 0.1841
Absolute structure parameter	0.49(2)
Extinction coefficient	0.0030(3)
Largest diff. peak and hole	1.205 and -0.409 e.A^-3

[HL^Me][H2L^Me]Sm

Identification code	h10mgd02
Empirical formula	C66.60 H76.40 N2 O6 Sm
Formula weight	1151.25
Temperature	200(2) K
Wavelength	0.71073 A
Crystal system, space group	Monoclinic, $P2_1/c$
Unit cell dimensions	a = 14.2030(4)A alpha = 90 deg.
	b = 25.2920(7)A beta = 92.313(1) deg.
	c = 16.5970(3)A gamma = 90 deg.
Volume	5957.2(3) A^3
Z, Calculated density	4, 1.284 Mg/m^3
Absorption coefficient	1.037 mm^-1
F(000)	2400
Crystal size	0.40 x 0.10 x 0.10 mm
Theta range for data collection	3.53 to 25.04 deg.
Limiting indices	-16<=h<=16, -30<=k<=30, -19<=l<=19
Reflections collected / unique	90394 / 10464 [R(int) = 0.1357]
Completeness to theta = 25.04	99.4 %
Absorption correction	None
Max. and min. transmission	0.9034 and 0.6817
Refinement method	Full-matrix least-squares on F^2
Data / restraints / parameters	10464 / 12 / 674
Goodness-of-fit on F^2	1.080
Final R indices [I>2sigma(I)]	R1 = 0.0542, wR2 = 0.1059
R indices (all data)	R1 = 0.0998, wR2 = 0.1224
Largest diff. peak and hole	0.632 and -0.702 e.A^-3

L^{tBu}Sc(IPA)

Identification code	k08mgd12
Empirical formula	C48 H74 N O4 Sc
Formula weight	774.04
Temperature	150(2) K
Wavelength	0.71073 A
Crystal system, space group	Orthorhombic, *P*cab
Unit cell dimensions	a = 12.9750(2) A alpha = 90 deg.
	b = 26.5250(4) A beta = 90 deg.
	c = 26.7130(5) A gamma = 90 deg.
Volume	9193.6(3) A^3
Z, Calculated density	8, 1.118 Mg/m^3
Absorption coefficient	0.201 mm^-1
F(000)	3376
Crystal size	0.35 x 0.30 x 0.12 mm
Theta range for data collection	3.45 to 24.10 deg.
Limiting indices	-14<=h<=14, -30<=k<=30, -30<=l<=30
Reflections collected / unique	63895 / 7262 [R(int) = 0.0805]
Completeness to theta = 24.10	99.4 %
Absorption correction	None
Max. and min. transmission	0.9763 and 0.9330
Refinement method	Full-matrix least-squares on F^2
Data / restraints / parameters	7262 / 0 / 779
Goodness-of-fit on F^2	1.098
Final R indices [I>2sigma(I)]	R1 = 0.0505, wR2 = 0.1161
R indices (all data)	R1 = 0.0724, wR2 = 0.1280
Largest diff. peak and hole	0.170 and -0.357 e.A^-3

L^tBuY(IPA)₃

Identification code	k08mgd16
Empirical formula	C60 H104 N O6 Y
Formula weight	1024.35
Temperature	150(2) K
Wavelength	0.71073 A
Crystal system, space group	Cubic, *Pa*-3
Unit cell dimensions	a = 24.4010(2) A alpha = 90 deg. b = 24.4010(2) A beta = 90 deg. c = 24.4010(2) A gamma = 90 deg.
Volume	14528.6(2) A^3
Z, Calculated density	8, 0.937 Mg/m^3
Absorption coefficient	0.841 mm^-1
F(000)	4464
Crystal size	0.25 x 0.20 x 0.20 mm
Theta range for data collection	3.64 to 25.31 deg.
Limiting indices	-28<=h<=29, -29<=k<=29, -27<=l<=29
Reflections collected / unique	143501 / 4406 [R(int) = 0.1509]
Completeness to theta = 25.31	99.4 %
Max. and min. transmission	0.8499 and 0.8173
Refinement method	Full-matrix least-squares on F^2
Data / restraints / parameters	4406 / 9 / 227
Goodness-of-fit on F^2	1.072
Final R indices [I>2sigma(I)]	R1 = 0.0709, wR2 = 0.1957
R indices (all data)	R1 = 0.0979, wR2 = 0.2222
Largest diff. peak and hole	0.876 and -0.485 e.A^-3

L^{tBu}Nd(IPA)₃

Identification code	k08mgd11
Empirical formula	C60 H104 N Nd O6
Formula weight	1079.68
Temperature	150(2) K
Wavelength	0.71073 A
Crystal system, space group	Cubic, *Pa*-3
Unit cell dimensions	a = 24.4640(2) A alpha = 90 deg. b = 24.4640(2) A beta = 90 deg. c = 24.4640(2) A gamma = 90 deg.
Volume	14641.4(2) A^3
Z, Calculated density	8, 0.980 Mg/m^3
Absorption coefficient	0.747 mm^-1
F(000)	4632
Crystal size	0.1 x 0.1 x 0.1 mm
Theta range for data collection	3.53 to 27.48 deg.
Limiting indices	-31<=h<=31, -31<=k<=31, -31<=l<=31
Reflections collected / unique	178348 / 5569 [R(int) = 0.0882]
Completeness to theta = 27.48	99.5 %
Refinement method	Full-matrix least-squares on F^2
Data / restraints / parameters	5569 / 10 / 240
Goodness-of-fit on F^2	1.107
Final R indices [I>2sigma(I)]	R1 = 0.0435, wR2 = 0.1186
R indices (all data)	R1 = 0.0623, wR2 = 0.1358
Largest diff. peak and hole	1.034 and -0.477 e.A^-3

L^{tBu}Sm(IPA)₃

Identification code	k08mgd3
Empirical formula	C60 H101 N O6 Sm
Formula weight	1082.77
Temperature	150(2) K
Wavelength	0.71073 A
Crystal system, space group	Cubic, *Pa*-3
Unit cell dimensions	a = 24.4210(2) A alpha = 90 deg.
	b = 24.4210(2) A beta = 90 deg.
	c = 24.4210(2) A gamma = 90 deg.
Volume	14564.3(2) A^3
Z, Calculated density	8, 0.988 Mg/m^3
Absorption coefficient	0.844 mm^-1
F(000)	4624
Crystal size	0.1 x 0.1 x 0.13 mm
Theta range for data collection	3.54 to 27.47 deg.
Limiting indices	-31<=h<=31, -31<=k<=31, -31<=l<=31
Reflections collected / unique	253615 / 5538 [R(int) = 0.1154]
Completeness to theta = 27.47	99.3 %
Refinement method	Full-matrix least-squares on F^2
Data / restraints / parameters	5538 / 8 / 246
Goodness-of-fit on F^2	1.121
Final R indices [I>2sigma(I)]	R1 = 0.0477, wR2 = 0.1151
R indices (all data)	R1 = 0.0857, wR2 = 0.1437
Largest diff. peak and hole	1.276 and -0.757 e.A^-3

L^{tBu}Yb(IPA)$_3$

Identification code	k08mgd05
Empirical formula	C60 H104 N O6 Yb
Formula weight	1108.48
Temperature	150(2) K
Wavelength	0.71073 A
Crystal system, space group	Cubic, Pa-3
Unit cell dimensions	a = 24.3789(1) A alpha = 90 deg. b = 24.3789(1) A beta = 90 deg. c = 24.3789(1) A gamma = 90 deg.
Volume	14489.13(10) A^3
Z, Calculated density	8, 1.016 Mg/m^3
Absorption coefficient	1.329 mm^-1
F(000)	4712
Crystal size	0.1 x 0.1 x 0.1 mm
Theta range for data collection	3.55 to 27.48 deg.
Limiting indices	-24<=h<=31, -31<=k<=31, -31<=l<=31
Reflections collected / unique	235850 / 5530 [R(int) = 0.0466]
Completeness to theta = 27.48	99.5 %
Refinement method	Full-matrix least-squares on F^2
Data / restraints / parameters	5530 / 9 / 220
Goodness-of-fit on F^2	1.183
Final R indices [I>2sigma(I)]	R1 = 0.0377, wR2 = 0.0945
R indices (all data)	R1 = 0.0562, wR2 = 0.1158
Largest diff. peak and hole	1.301 and -0.652 e.A^

[L^{tBu}Nd(IPA)]$_2$

Identification code	k08mgd13
Empirical formula	C54 H87 N Nd O4
Formula weight	958.49
Temperature	150(2) K
Wavelength	0.71073 A
Crystal system, space group	Orthorhombic, Pbcn
Unit cell dimensions	a = 17.5050(1) A alpha = 90 deg.
	b = 24.5800(2) A beta = 90 deg.
	c = 24.9230(2) A gamma = 90 deg.
Volume	10723.69(14) A^3
Z, Calculated density	8, 1.187 Mg/m^3
Absorption coefficient	1.009 mm^-1
F(000)	4080
Crystal size	0.20 x 0.10 x 0.10 mm
Theta range for data collection	2.96 to 27.48 deg.
Limiting indices	-22<=h<=22, -31<=k<=31, -32<=l<=32
Reflections collected / unique	168641 / 12283 [R(int) = 0.0781]
Completeness to theta = 27.48	99.8 %
Absorption correction	None
Max. and min. transmission	0.9058 and 0.8237
Refinement method	Full-matrix least-squares on F^2
Data / restraints / parameters	12283 / 0 / 689
Goodness-of-fit on F^2	1.061
Final R indices [I>2sigma(I)]	R1 = 0.0342, wR2 = 0.0751
R indices (all data)	R1 = 0.0543, wR2 = 0.0848
Largest diff. peak and hole	1.086 and -0.850 e.A^-3

[L^tBuGd]₂(H₂O)

Identification code	k07mgd19
Empirical formula	C94.96 H143.57 Cl0 Gd2 N2 O6.83
Formula weight	1736.92
Temperature	150(2) K
Wavelength	0.71073 A
Crystal system, space group	Monoclinic, $P2_1/c$
Unit cell dimensions	a = 14.2010(1) A alpha = 90 deg.
	b = 23.0140(2) A beta = 100.90 deg.
	c = 29.0010(4) A gamma = 90 deg.
Volume	9307.04(17) A^3
Z, Calculated density	4, 1.240 Mg/m^3
Absorption coefficient	1.463 mm^-1
F(000)	3640
Crystal size	0.10 x 0.05 x 0.05 mm
Theta range for data collection	3.54 to 22.50 deg.
Limiting indices	-15<=h<=15, -24<=k<=24, -31<=l<=31
Reflections collected / unique	125384 / 12111 [R(int) = 0.1283]
Completeness to theta = 22.50	99.6 %
Absorption correction	None
Max. and min. transmission	0.9304 and 0.8675
Refinement method	Full-matrix least-squares on F^2
Data / restraints / parameters	12111 / 0 / 1034
Goodness-of-fit on F^2	1.065
Final R indices [I>2sigma(I)]	R1 = 0.0378, wR2 = 0.0640
R indices (all data)	R1 = 0.0633, wR2 = 0.0710
Largest diff. peak and hole	0.396 and -0.464 e.A^-3